Author:
Davy, Matthew J

Title:
Development of Pure Shift NMR Spectroscopy Techniques Through Novel Acquisition Schemes

Development of Pure Shift NMR Spectroscopy Techniques Through Novel Acquisition Schemes

Matthew James Davy

A dissertation submitted to the University of Bristol in accordance with the requirements for award of the degree of Doctor of Philosophy in the Faculty of Science.

June 2021

Abstract

Modern NMR Spectroscopy relies not just upon sophisticated hardware but also upon complex pulse sequences that often trade sensitivity for selectivity or vice versa. Pure shift NMR Spectroscopy allows collection of broadband homodecoupled spectra, but such techniques cause losses in sensitivity. The MSE (Multiple Spin Echo) pure shift methodology in this thesis provides a sensitivity increase of around 10% for pure shift spectra acquired using the "Zangger Sterk" refocussing technique, though this varies substantially based on experimental parameters and the molecule under study. This is achieved without introducing significant artefacts or line broadening. The repeated refocussing of the MSE method also offers significant advantages with regard to pulse miscalibration. However, even in optimal cases MSE pure shift provides less absolute signal-to-noise than the PSYCHE approach (which it is incompatible with). It does, however, represent an enticing "something for nothing" approach to signal acquisition which may have implications for other NMR techniques where acquisition is limited to short data chunks.

In contrast, the SHARPER experiment trades selectivity for sensitivity in reaction monitoring methods. The originally reported SHARPER experiment provides a significant boost in signal-to-noise and magnetic field inhomogeneity compensation, but only one resonance at a time can be studied and the frequency of this resonance must remain stationary throughout the experiment.

The mobile-SHARPER and MR-SHARPER (Multiple Resonance SHARPER) methodologies presented here alleviate the extreme selectivity by allowing significant frequency changes to occur with no loss in spectral quality and multiple signals to be recorded simultaneously. The methodology used to do so is demonstrated on up to three signals, though in principle could be further extended. Adding such capability to SHARPER is ideal for its role as a sequence for chemical reaction monitoring as it allows simultaneous monitoring of signals relating to products, reactants and intermediates.

Acknowledgements

First and foremost, I am sincerely grateful to Professor Craig Butts for all his help and guidance throughout the course of my PhD. I could not have asked for a better supervisor and under his direction have turned from someone who simply uses NMR as a tool to someone who is starting to truly understand, appreciate and exploit it.

I would also like to thank Paul Lawrence, Thomas Leman and Samantha Ferrins – the NMR Technicians past and present for their help when one of the menagerie of spectrometers we have at Bristol was being uncooperative. This has been an absolute blessing during my PhD as it provided an easy, if unsubtle, way to work around the subtle differences between Bruker, Jeol and Varian spectrometers.

I'd like to thank all present and former members of the Butts Research group for all their advice and assistance over the past few years. Special thanks go to Claire Dickson and Zahra Al-Aasmi, where without the many useful discussions we have had some of the SHARPER work in this thesis might never have been fully realised.

Thanks also goes to Natalie Pridmore, of Bristol's X-Ray group, who provided invaluable writing advice throughout the years on abstracts, posters and indeed this thesis. In the special circumstances of the past year Natalie and Ismail Adem of Site Services deserve special mention for keeping me productive and in good spirits as they came to represent an enormous fraction of my in-person interaction as everyone's world shrunk. Significant thanks also go to my mother, for her tireless help in proofreading this thesis in the final stages.

The EPSRC and C4X Discoveries, especially Charles Blundell and Martin Watson, are also acknowledged for having provided funding for this PhD through the NPIF scheme.

Author’s Declaration

I declare that the work in this dissertation was carried out in accordance with the requirements of the University's Regulations and Code of Practice for Research Degree Programmes and that it has not been submitted for any other academic award. Except where indicated by specific reference in the text, the work is the candidate's own work. Work done in collaboration with, or with the assistance of, others, is indicated as such. Any views expressed in the dissertation are those of the author.

SIGNED: Matthew Davy DATE: 08/06/2021

Contents

Abstract 2
Acknowledgements 3
Author's Declaration 4
Abbreviations 8
1 Introduction 9
2 Enhancing Sensitivity in Pure Shift NMR 12
2.1 Introduction – Removal of Homocoupling 12
2.1.1 Selective Inversion Elements for Broadband Decoupling 16
2.1.1.1 BIRD 16
2.1.1.2 Zangger Sterk 18
2.1.1.3 PSYCHE 20
2.1.2 Pure Shift NMR Acquisition Schemes 21
2.1.2.1 Real Time Pure Shift 22
2.1.2.2 Interferogram Pure Shift 24
2.2 Refocussed Interferogram Theory 26
2.3 Testing Refocussed Interferograms in ^{13}C Spectra 28
2.4 Refocussed Interferogram 30
2.5 Pseudo Real Time Pure Shift 35
2.6 Multiple Spin Echo Pure Shift 41
2.6.1 MSE Theory and Pulse Sequence 41
2.6.2 Initial Results 47
2.6.3 Pulse Miscalibration Compensation 52
2.6.4 MSE Pure Shift Results with Differing Selective Pulses 59
2.6.5 Comparison with PSYCHE 64
2.7 Conclusion 66
2.8 Future Work 67
3 Off-Resonance SHARPER 68
3.1 Introduction 68
3.1.1 Reaction Monitoring by NMR Spectroscopy 68
3.1.2 SHARPER 71
3.2 Experimental Off-Resonance SHARPER 76
3.2.1 Theory for Off-Resonance SHARPER 76
3.2.2 Experimental Off-Resonance SHARPER 78
3.2.3 Incomplete Rotations 82

3.2.4 Effects of Variation of Chunk Duration 87
4 Multiple Resonance SHARPER 91
4.1 Theory for MR-SHARPER 91
4.2 Practical Determination of Timings 94
4.3 Retention of SHARPER Properties 99
4.4 Quantitative Integration for MR-SHARPER 102
4.5 Three Resonance MR-SHARPER 107
5 Mobile-SHARPER 110
5.1 Estimation of Resonance Frequency 110
5.2 Mobile-SHARPER Macro 112
5.3 Initial Experiments on a Stationary Resonance 114
5.4 Mobile-SHARPER on a Resonance with a Changing Frequency 119
5.5 Experimental Factors Affecting Optimum Transmitter Offset 121
5.5.1 Initial Pulse Flip Angle 121
5.5.2 Delta Duration 123
5.5.3 Shimming 124
5.5.4 Theoretical Model for Effects on Optimum Transmitter Offset 128
5.6 Mobile-MR-SHARPER 135
5.6.1 Mobile-MR-SHARPER Macro 135
5.6.2 Mobile-MR-SHARPER on Resonances with Changing Frequencies 137
6 Conclusion – Improvements to SHARPER 141
7 Experimental 143
7.1 NMR Samples Used 143
7.2 NMR Data Acquisition 143
7.3 NMR Data Processing 144
7.4 Calculations and Scripts 144
8 Appendix 145
8.1 MSE Pure Shift 145
8.1.1 MSE Pure Shift Pulse Sequence (Varian) 145
8.1.2 MSE Pure Shift Reconstruction Scripts 148
8.2 Signal-to-Noise for Individual Peaks Using MSE Pure Shift 149
8.3 Signal-to-Noise for Individual Peaks Using PSYCHE 152
8.4 Strychnine Assignment, T_1 and T_2 Values 153
8.5 SHARPER 154
8.5.1 SHARPER Pulse Sequence (Bruker) 154

8.5.2 Offsets Used for Off-Resonance SHARPER 155
8.5.3 MR-SHARPER Script (One Frequency) 158
8.5.4 MR-SHARPER Script (Two Frequencies) 160
8.5.5 MR-SHARPER Script for Evaluation 162
8.5.6 Random Frequencies for Comparison of NMR Spectrometers 164
8.5.7 Mobile-SHARPER Scripts 174
8.5.8 Mobile-MR-SHARPER Scripts 179
8.5.9 Dwell Times available on a Varian, with OpenVNMRJ 4.2 in µs 187
8.5.10 Dwell Times on a Bruker with Topspin 3.6.1 and an AVIII HD in µs 188
9 References 190

Abbreviations

BIRD	Bilinear Rotational Decoupling
COSY	Correlation Spectroscopy
CPMG	Carr-Purcell-Meiboom-Gill
DEET	N,N-Diethyl-meta-toluamide
DOSY	Diffusion Ordered NMR Spectroscopy
DPFGSE	Double Pulsed Field Gradient Spin Echo
EXACT	Extended Acquisition Time
FID	Free Induction Decay
GSTAB	Gradient Stabilisation
HSQC	Heteronuclear Single Quantum Coherence
INADEQUATE	Incredible Natural Abundance Double Quantum Transfer
MAS	Magic Angle Spinning
MR-SHARPER	Multiple Resonance SHARPER
MSE	Multiple Spin Echo
NMR	Nuclear Magnetic Resonance
NOAH	NMR by Ordered Acquisition using ^{1}H Detection
NOE	Nuclear Overhauser Effect
NOESY	Nuclear Overhauser Effect Spectroscopy
NUS	Non-Uniform Sampling
PSYCHE	Pure Shift Yielded by Chirp Excitation
SHARPER	Sensitive Homogenous and Resolved Peaks in Real time
SNR	Signal-to-noise Ratio
TOCSY	Total Correlation Spectroscopy
TSE	Triple Spin Echo
UPSIF	Ultrahigh Resolution Pure Shifts in Inhomogeneous Fields
ZF	Zero Filling
ZS	Zangger Sterk

1 Introduction

Modern Nuclear Magnetic Resonance (NMR) spectroscopy is an important and powerful technique for the elucidation of molecular structures. Significant advances in the technique have been made since 1945, arguably the start of the experimental field of NMR spectroscopy, when Purcell et al. observed an NMR signal from a full kilogram block of Paraffin.[1] Perhaps the largest single leap forward was the introduction of the Fourier transform to NMR spectroscopy, coming about in 1966.[2] This replaced the older "continuous wave" method of slowly sweeping the radiofrequency with a short intense radiofrequency pulse. This allowed simultaneous excitation of all nuclei within a sample to produce an FID (free induction decay), substantially reducing experiment time. As this FID will contain *every* frequency in the spectrum the time domain data is often so convoluted as to be near impenetrable. By means of Fourier transformation, the time domain FID can be converted into a more easily interpreted frequency domain NMR spectrum.

Hardware innovations over the past seven decades have increased sensitivity substantially, including the development of ever stronger superconducting magnets in order to increase the strength of the NMR signal from a given sample. Even then the signals are typically very weak but cryogenic cooling of probes to reduce electrical contributions to noise and the miniaturisation of probes to place detection coils as close as possible to the sample both improve our ability to detect these signals.[3] Even after detection modern digital filtration schemes can improve our ability to discriminate between signals and noise whilst also providing increased data quality.[4] With all the advances in sensitivity from hardware, NMR can be routinely used on milligram and even microgram amounts of material[5] – a far cry from the original experiment where almost a kilogram of sample was used.[1]

Radio frequency pulse sequences have also changed a great deal since the inception of NMR, with the ability to glean much more information than just the chemical shift and couplings of a nucleus via simple pulse acquire experiments. Perhaps the largest revolution came with the advent of multidimensional NMR methods, where data becomes a function of multiple time domains – the directly measured one and additional incremented delays within the pulse sequence.[6] This allows investigation of a vast wealth of different molecular characteristics.[7] One of the earliest 2D techniques to find common usage was the COSY (Correlation Spectroscopy) experiment, which reports on scalar couplings between homonuclei[8] (typically ${}^{n}J_{HH}$), which allows easy and unambiguous determination of connectivity in a molecule. Development of 2D NMR has been well complemented by the aforementioned advances in sensitivity as they allow for detection of very weak NMR signals. For example NOE (Nuclear Overhauser Effect) enhancements, which report on

intermolecular distances[9,10] and those experiments based on $^{1}J_{CC}$ couplings at natural abundance, *e.g.* INADEQUATE[11] – arguably opening up the ultimate technique for determining connectivity in carbon rich molecules. One relatively recent and particularly notable information rich pulse sequence is the NOAH experiment, which consists of a nested set of NMR experiments where relaxation delays can be minimised, potentially allowing for full characterisation of molecular structure with only a single experiment.[12,13] The wealth of information that can be gained from such techniques, often combined with computational approaches, can allow very subtle insight into the behaviour of molecules in solution. For example, conformers with near negligible populations can be detected,[14] seemingly intractable stereochemical problems unravelled[15,16] and complex reaction systems elucidated.[17]

In Chapter 2, this thesis will explore the field of "pure shift" NMR spectroscopy, a technique developed to simplify the information presented in an NMR spectrum. The complexity of molecules that can be studied and the wealth of information that NMR can provide often causes overlap of resonances, making the extraction of information a scientist is truly interested in challenging. One solution has been to reduce the number of nuclei examined in a given experiment. Methods have been devised that allow examination of specific molecules,[18] spin systems,[19] even individual chemical environments.[20] Whilst such experiments are phenomenal assets sometimes it is useful to keep all nuclei in the spectrum but limit the information each produces. As far back as 1963, it was already considered desirable to remove all coupling information, leaving only chemical shift information.[21] The theory for removing heterocouplings from spectra[22,23] by repeatedly applying radiofrequency pulses to the non-measured nucleus has existed for more than five decades. Robust practical applications have existed for almost as long.[24,25,26] Achieving the removal of homocouplings from spectra proves to be substantially more challenging, as the coupled spins occupy the same frequency space. Many different approaches have been used over the years to try and achieve this.

Perhaps the most conceptually similar to heterodecoupling is the use of selective pulses targeting a particular chemical environment, or environments. Such methods entirely remove both couplings to and signals arising from the selected spins, though retain good sensitivity for those that remain.[27,28] 2D methods such as the 2D*J*,[29] anti-Z-COSY[30] and constant time approach[31,32] can provide broadband spectra, though as 2D methods they require inherently longer experimental times and potentially require nonstandard data processing.

A number of similar broad band methods of homodecoupling have been developed more recently, generally referred to as "pure shift" experiments. These work by splitting the spins

into an active and passive group – the signals from the active spins are acquired, whilst the passive spins are manipulated to refocus homocoupling between them. These methods provide good quality spectra and are incredibly versatile,[33,34] but pay a heavy cost in sensitivity for the selectivity of information they provide, potentially as much as 99%.[35] Partly, this loss in sensitivity is a necessary evil due to the aforementioned nature of the splitting of the spins into active and passive groups. However, it is compounded by the specialised acquisition schemes pure shift spectra are forced to use where acquisition has to be composed of short data chunks, each a fraction of the duration of typical NMR signals.[33] Chapter 2 details a modified pure shift acquisition scheme which attempts to claw back some of these losses in sensitivity, refocussing data chunks to allow their collection and noise averaging multiple times within a single scan of an FID.

Conversely to this, the SHARPER (Sensitive Homogenous and Resolved Peaks in Real time) NMR experiment trades selectivity for sensitivity, greatly increasing the intensity of a single resonance and collapsing multiplicity. Magnetic field inhomogeneity is also compensated for, giving a reduction in linewidth. Whilst the degree of enhancement offered varies signal-to-noise improvements of more than an order of magnitude are not uncommon.[36] The experiment's Achilles heel is that it operates on just one NMR signal at a time and it must be placed precisely on-resonance, and any change in frequency can greatly affect the quality of the resulting NMR spectra, introducing significant artefacts. This is often an issue in reaction monitoring applications where changes in the Larmor frequency of a given resonance are common, as reaction environments change over the course of the experiment (*e.g.* changes in pH or ionic strength). Chapter 3 explores the behaviour of the artefacts in SHARPER spectra when acquired off-resonance and demonstrates the conditions where high quality SHARPER spectra *can* be acquired off-resonance.

Chapter 4 then applies this knowledge in order to acquire SHARPER spectra with multiple resonances at the same time, be they on or off-resonance. This is achieved through use of sample and spectrometer specific timings, an approach dubbed MR-SHARPER (Multiple Resonance SHARPER). Chapter 5 demonstrates a method to analyse the artefacts in SHARPER spectra to determine the ideal transmitter offset. By means of a macro, mobile-SHARPER, this analysis can be carried out rapidly, allowing updates to the offset in real time to adjust for a constantly changing frequency. These two experiments hopefully make SHARPER more widely applicable, as multiple resonances can be studied and changes in the frequency of a resonance throughout a chemical reaction can be compensated for. These two variations on the original SHARPER experiment can be combined, though do complicate analysis when this is done, which is discussed at the end of Chapter 5.

2 Enhancing Sensitivity in Pure Shift NMR

2.1 Introduction – Removal of Homocoupling

Pure shift NMR is a group of experimental techniques used to remove homocoupling from NMR spectra, yielding broadband spectra with only chemical shift information present – with an example spectrum shown in Figure 1. As only a single signal is present in the spectrum per chemical environment regions that are normally heavily overlapped due to homocoupling become well resolved. This allows for easier interpretation of the spectrum and allows easy determination of multiplet centres to aid in assignment, further selective NMR experiments or spin simulations.

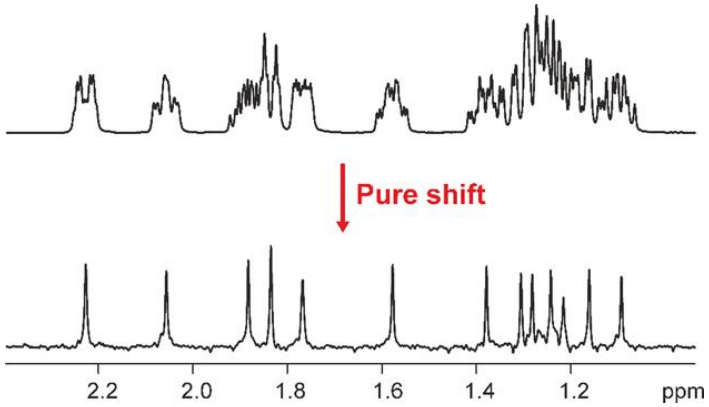

Figure 1: 1D ^{1}H spectrum (top) and a pure shift spectrum (bottom) of estradiol. Adapted from (Foroozanadeh, M. 2014.[45])

The idea of removing homocouplings from a spectrum is not a new one – indeed this can be achieved with a 2D*J* NMR spectrum, one of the earliest 2D NMR experiments, dating back to 1976.[29] The 2D*J* spectrum displays chemical shift evolution in the direct dimension and coupling in the indirect dimension, a cartoon of which is shown in Figure 2. In principle this allows simple extraction of couplings from overlapped multiplets. For example, whilst extraction of coupling constants from the 1D ^{1}H spectra from the overlapped multiplet at 1.4 ppm poses a challenge these should be as trivial to extract from the 2D*J* as they would be for the simple doublet and triplet at 1.0 and 2.0 ppm.

If one wishes to create a one-dimensional spectrum with only chemical shift information from the 2D*J* (similar to the pure shift spectrum in Figure 1) one simply needs to take a projection of the 2D data.[37]

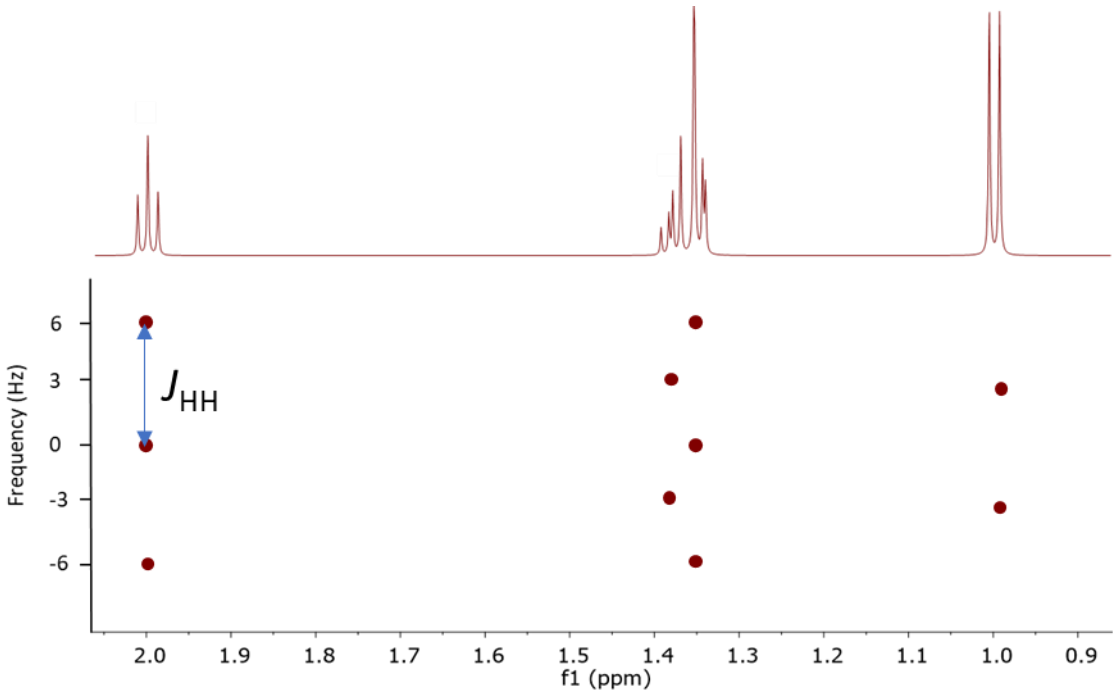

Figure 2: A cartoon of a 2DJ pure shift spectrum, along with an equivalent simulated 1D ^{1}H spectrum. A 45º tilt has been applied.

Unfortunately, 2D*J* experiments rarely produce such excellent results in practice. Partly this is because coupling evolution also occurs in the directly measured dimension. This means that the data measured is a convolution of chemical shift *and* coupling, as can be seen in Figure 3 before the 45º tilt operation. Whilst this problem is solved by the 45º tilt this has the consequence of significantly distorting the line shape.[38] If a projection is taken to give a 1D spectrum then linewidth will be limited by the number of increments run in the indirect dimension, meaning excessive experimental times may be required to provide a high-resolution spectrum.

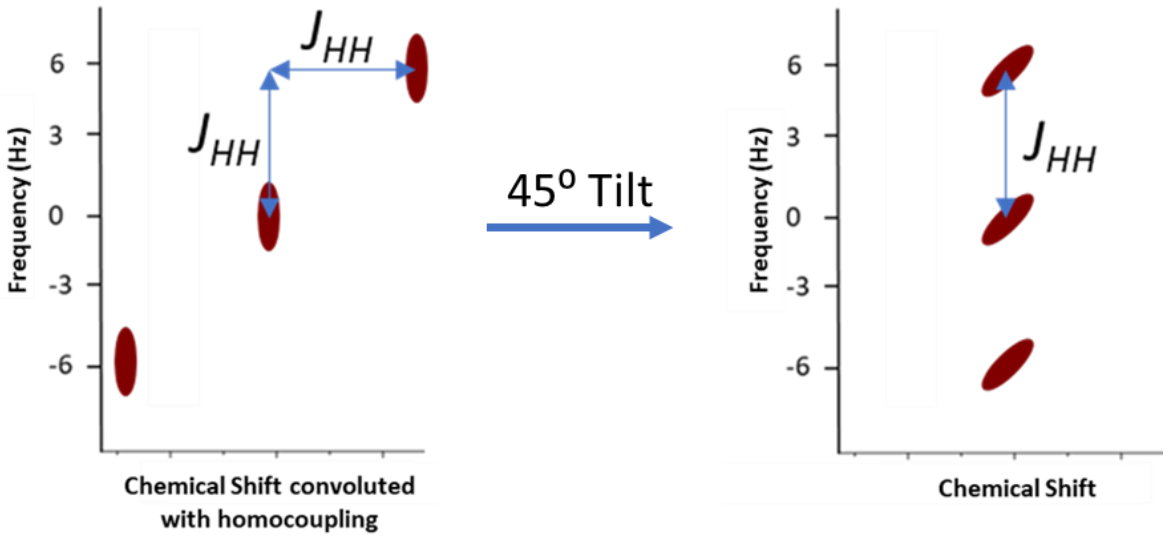

Figure 3: A cartoon of the line shapes of a triplet in a 2DJ spectrum before and after application of a 45º tilt.

Another drawback many older 2D*J* experiments have is that they produce “phase twist” line shapes, rather than absorption mode line shapes. This line shape, shown in Figure 4a is a convolution of both absorption and dispersion line shapes.[39] This dispersive component makes it significantly broader than a pure absorption mode line shape (Figure 4b), compromising both sensitivity and resolution.[40] Data processing schemes such as the “pseudo echo” can improve linewidth, but come at the cost of severe distortions in intensity.[41] These features ironically often render the 2D*J* spectra unsuitable for analysis of heavily overlapped regions of the spectra, which is exactly where they are required the most.

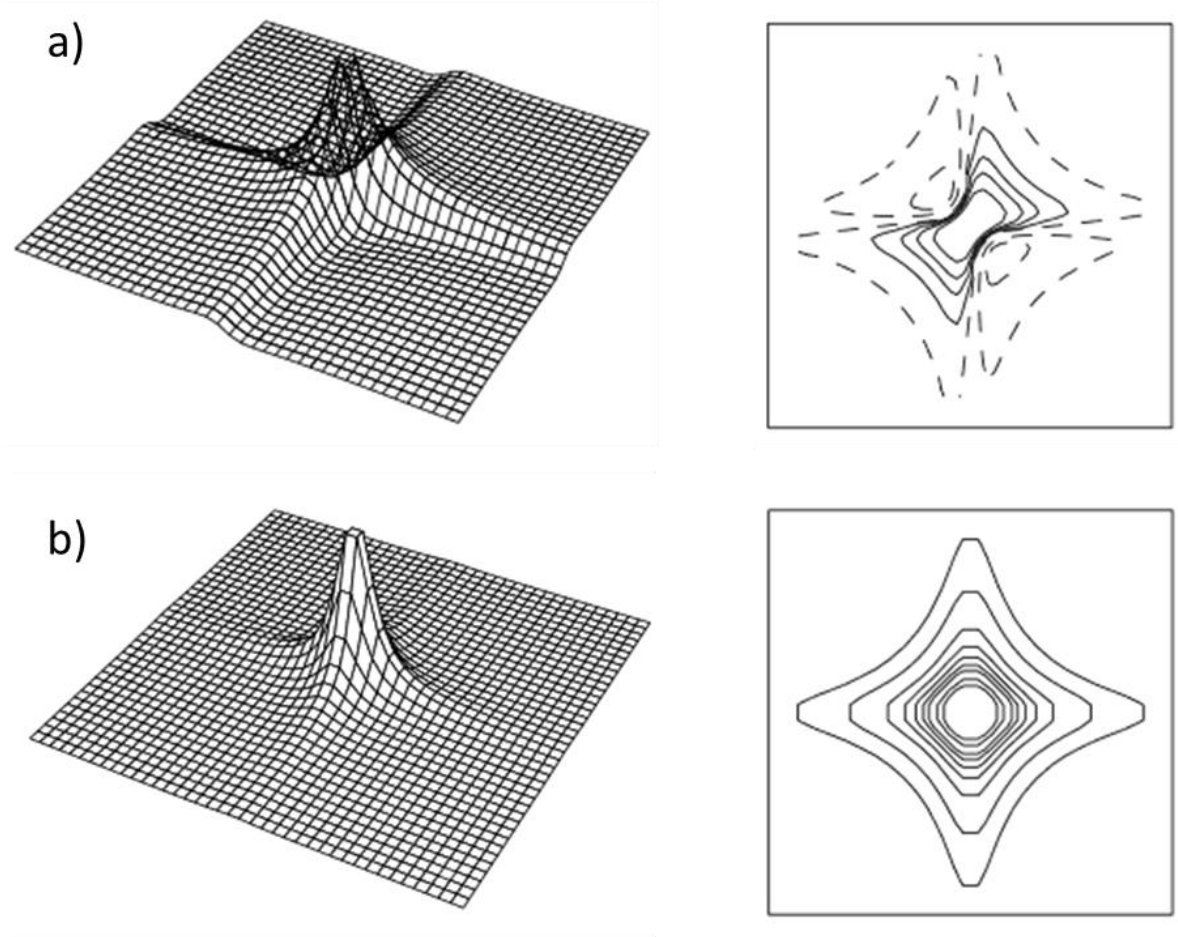

Figure 4: 3D view and a 2D contour plot of the (a) phase twist and (b) absorption mode line shapes found in 2D NMR spectra. (Adapted from Keeler, 2014.[39])

Other older methods exist to acquire NMR spectra without the effects of homocoupling, such as the constant time method. Here, couplings are allowed to undergo *exactly* the same amount of evolution in every increment of a 2D NMR spectrum, removing the effects of homocoupling.[31] However, depending on the choice of constant time period this may lead to coupling-dependent modulation of the intensities of NMR signals – up to and including their disappearance from the spectrum.[42]

Over the past decade there has been a great deal of interest in use of “pure shift” NMR methods to remove homocoupling from spectra, which lack the drawbacks of older methods.[33,43] These utilise a selective inversion element to discriminate between spins in otherwise identical chemical environments, as shown in Figure 5. The two groups can be thought of as “active” (red) and “passive” (black). These groups are manipulated to refocus any homocoupling between them, and all NMR acquisition is on the active spins. Assuming that the active spins are distributed such that no molecules exist where any two “active” spins are coupled to one another the result will be an NMR spectrum free of homocoupling. Of course, because the NMR signal now only arises from a subset of spins, signal is diminished and sensitivity will suffer. For example in Figure 5, signals would only be one third the intensity of a 1D ^{1}H spectrum. Some sensitivity loss is a necessary evil from homodecoupling in this fashion, though the exact magnitude of this loss depends upon the choice of selective inversion element. The different methods used to achieve selective inversion are detailed in the next Section.

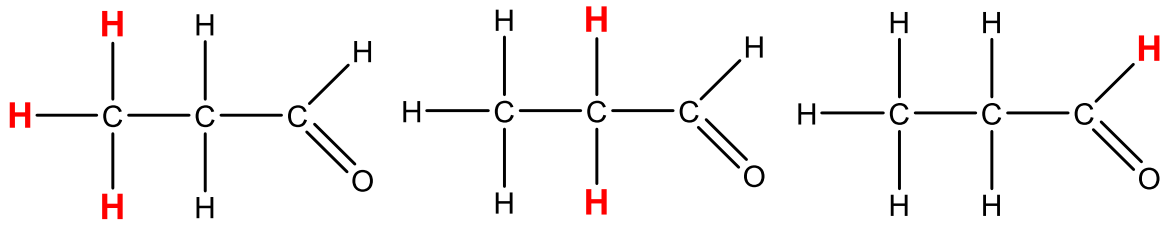

Figure 5: The effects of a selective inversion element, where the red and black ^{1}H spins can be discriminated between.

One significant advantage of using selective inversion elements for homodecoupling is their flexibility. Incorporation into existing NMR experiments has allowed for “pure shift” versions of the NOESY,[44] TOCSY[45] and DOSY[46] among others, providing a significant resolution advantage. Such selective inversion elements have even been incorporated into the 2D*J*, providing an experimental solution to the “phase twist” line shape and yielding high resolution spectra, far better suited to analysis of overlapping multiplets.[38,40,47] Refocussing of homocoupling by selective inversion elements has even been able to bypass the requirement for a 45º tilt in the 2D*J.* This is done by preventing evolution of coupling in the directly measured dimension, though this results in very long acquisition times.[38]

One drawback of pure shift NMR is that the selective inversion elements must be regularly applied so as to continually refocus $^{n}J_{HH}$ couplings throughout the FID. This necessitates specialised acquisition schemes, which cause further sensitivity losses, further compounding the losses due to the use of selective inversion elements. It is these acquisition schemes that this Chapter of the thesis tries to improve upon, retaining sensitivity as far as possible without sacrificing resolution.

2.1.1 Selective Inversion Elements for Broadband Decoupling

A core component of pure shift NMR techniques is the differentiation between “active” and “passive” spins, which are otherwise in the same chemical environments and thus have identical Larmor frequencies in a given magnetic field. Despite this difficulty there are a number of methods that can provide the required selectivity – each of which has advantages and disadvantages regarding flexibility, sensitivity losses and spectral quality.

2.1.1.1 BIRD

The earliest of the broadband selective inversion elements, dating to 1982, is BIRD (Bilinear Rotational Decoupling).[35] This technique differentiates between nuclei based on couplings to a sparse heteronucleus – typically ^{1}H and ^{13}C respectively. A vector model diagram of the operation of BIRD is shown in Figure 6. An initial 90° pulse places the magnetisation of both $^{1}H_{12C}$ and $^{1}H_{13C}$ in the XY plane. Couplings freely evolve for $1/2J_{CH}$ such that the $^{1}H_{13Ca}$ and $^{1}H_{13Cb}$ magnetisation lies 180° apart along X and -X and the $^{1}H_{12C}$ magnetisation lies along Y. At this point a 180° pulse is applied to both ^{1}H and ^{13}C. The pulse on ^{1}H inverts the magnetisation on ^{1}H nuclei, whilst the pulse on ^{13}C prevents the sense of $^{n}J_{CH}$ being reversed. After another $1/2J_{CH}$ of free evolution the $^{1}H_{13Ca}$ and $^{1}H_{13Cb}$ magnetisation will refocus 180° out of phase with the $^{1}H_{12C}$ magnetisation. A further 90° pulse on ^{1}H will then place the magnetisation into the Z and -Z axes – the overall effect of this sequence has been to invert the magnetisation of H_{12C} whilst having no net effect on $^{1}H_{13C}$.

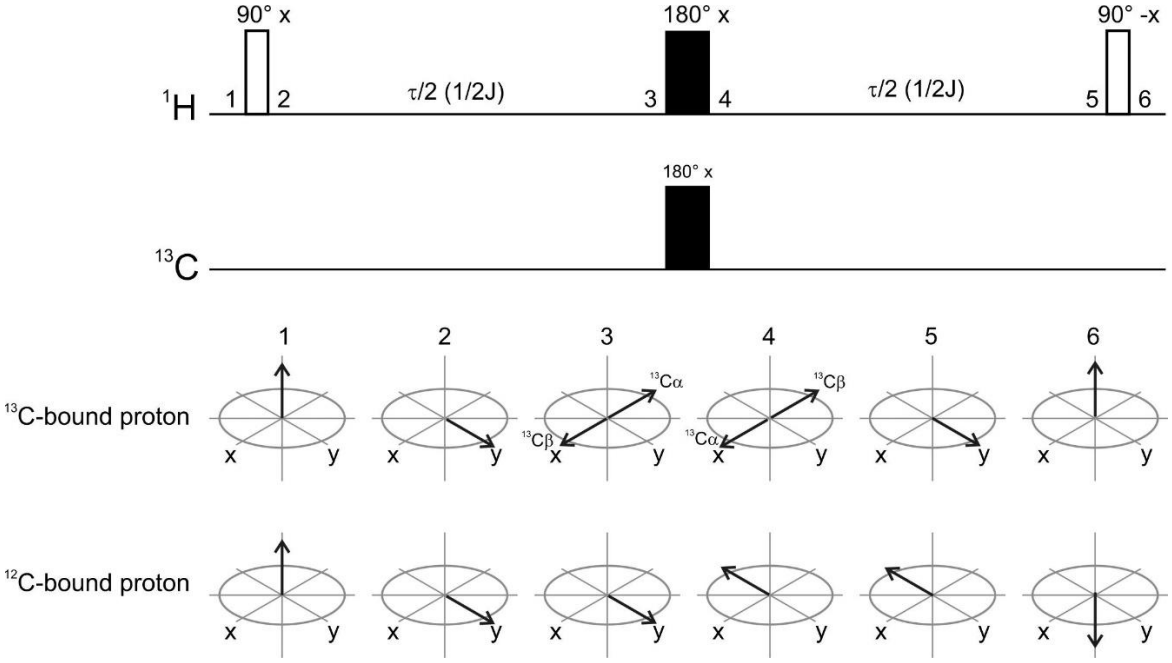

Figure 6: Pulse sequence and diagrams showing the operation of BIRD. (Adapted from Zangger, K. 2015.[42])

As ^{13}C is around one percent natural abundance $^{1}H_{12C}$ is manipulated to remove coupling to the active $^{1}H_{13C}$ spins which are unlikely to be coupled to one another, due to their low abundance. The obvious exception is geminal protons, which will always be attached to the same carbon, be it ^{12}C or ^{13}C. In these cases, BIRD will fail to decouple the protons from one another. This can be alleviated by use of the Perfect BIRD sequence but doing so dramatically increases the time required to refocus the coupling to the point it becomes unsuitable for certain acquisition schemes.[48]

This isotopic selectivity gives BIRD an enormous 99% sensitivity penalty for samples at natural abundance, as signal only arises from protons bonded to ^{13}C. However, it is particularly valuable when incorporated into experiments with the same isotopic selectivity, such as the HSQC spectrum. In such cases use of BIRD can actually lead to improvement in signal-to-noise ratio due to collapse of multiplicity.[34]

2.1.1.2 Zangger Sterk

Another method to differentiate between otherwise identical nuclei is by exploiting their different positions spatially in the sample. This was first described in 1996 by Zangger and Sterk.[49] Ordinarily, when a hard pulse on ^{1}H is applied to a sample, all ^{1}H spins will be affected. In the case of a 90º hard pulse, this will result in a signal from each chemical environment present, as Figure 7a. If a selective 90º pulse is applied then only spins with Larmor frequencies close to the frequency of the selective pulse will be excited – resulting in Figure 7b, where only one NMR signal is detected.

However, if a field gradient is applied the effective magnetic field experienced by any individual molecule will vary depending on its position within the sample. This causes chemical shifts to vary in a spatially dependent fashion. If a selective pulse is applied at the same time as a field gradient, different nuclei will have a Larmor frequency equal to the frequency of the selective pulse at different points in the sample. This causes a spectrum, as Figure 7c, where each NMR signal arises from a different group of nuclei in a different region of the sample. By using a 180º selective pulse, rather than a 90º selective pulse this can be exploited to achieve selective inversion.

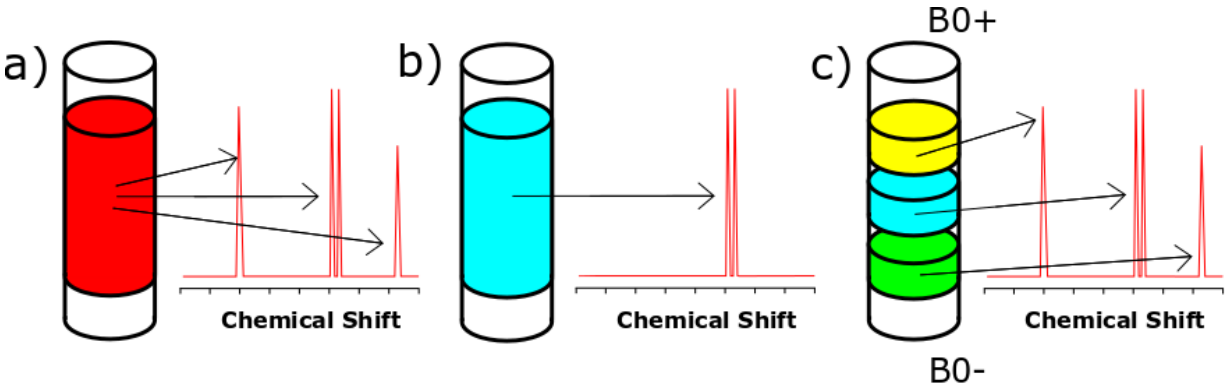

Figure 7: The results of applying a single 90° pulse using (a) a hard pulse, (b) a selective pulse or (c) a selective pulse applied at the same time as a magnetic field gradient.

Because signal only arises from within these slices the intensity of NMR signals for any given nucleus will be diminished, causing a drop in signal-to-noise. Perhaps the most obvious way to combat this is to increase the sizes of these slices, which can be done by using a weaker magnetic field gradient or a larger bandwidth selective pulse. However, this can cause issues if slices relating to coupled nuclei overlap, meaning they can no longer be discriminated between by this method. Exactly when this happens will be determined by the chemical shifts of the sample being observed. However, it does pose a problem with regard to strongly coupled systems where, by definition, the coupled nuclei have similar chemical shifts.

There have been several attempts to address this sensitivity problem. One example is multi slice excitation, where a shaped selective pulse is used that excites nuclei over multiple different frequency ranges. This means that the same chemical environments will be excited in multiple slices throughout the sample. This can substantially increase the number of "active" spins selected for, decreasing the sensitivity penalty.[50] However, the user must pay very careful attention to the chemical shifts in the sample and the pulse used. For example, with reference to Figure 8 if the blue and red bandwidths are excited simultaneously sensitivity is increased, as the non-coupled B and C spins are excited in the same slice. However, if the red and green bandwidths are excited the coupled spins, A and B, are excited in the same slice, so the selective inversion element will fail to distinguish between them (and any attempts at homodecoupling will fail).

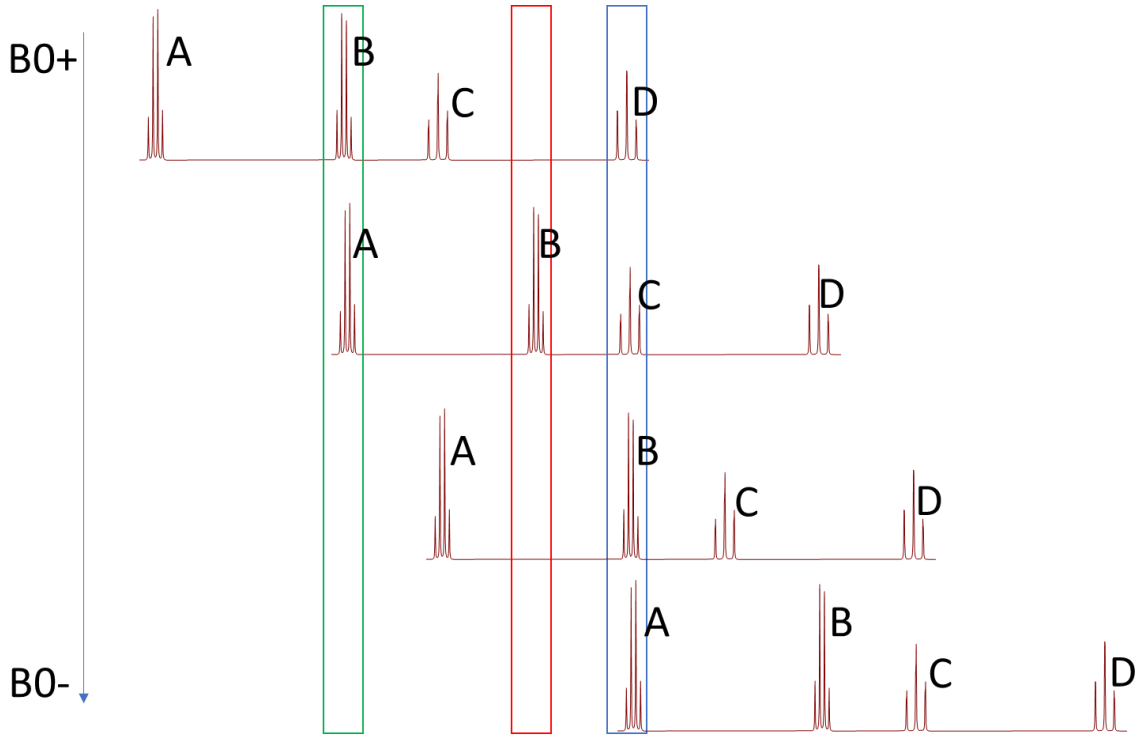

Figure 8: A diagram of a ^{1}H spectra with different potential excitation frequencies (coloured boxes) and four chemical environments. A is coupled to B and C is coupled to D. Not all possible slices are shown for brevity.

A related approach is to change the excitation frequency between scans – *i.e.* applying the green, red and blue excitations – with reference to Figure 8 in concurrent scans. This means that nuclei affected in one scan are allowed to relax during the next. This allows the relaxation delay between scans to be minimised or even eliminated entirely, allowing the maximum number of scans and thus sensitivity within a given experimental time.[51]

2.1.1.3 PSYCHE

PSYCHE (Pure Shift Yielded by CHIRP Excitation) is a relatively recent development in pure shift NMR which uses swept frequency CHIRP pulses in a swept field gradient to selectively invert an essentially random but statistically predictable population of spins. The proportion of spins inverted is equal to $\cos^2\beta$ where β is the flip angle used (and thus spins not inverted are proportional to $\sin^2\beta$).[52]

As β is increased and a higher percentage of spins selected the sensitivity penalty from using PSYCHE decreases, meaning more intense spectra. However, as the selection of spins is essentially random the chances of any two selected spins being coupled to each other also increases with β. In these cases artefacts will arise as the decoupling fails *in that particular molecule*, though it will work elsewhere in the sample. These two effects, producing either the desired homodecoupled NMR signals or artefacts scale differently, as illustrated by Figure 9.

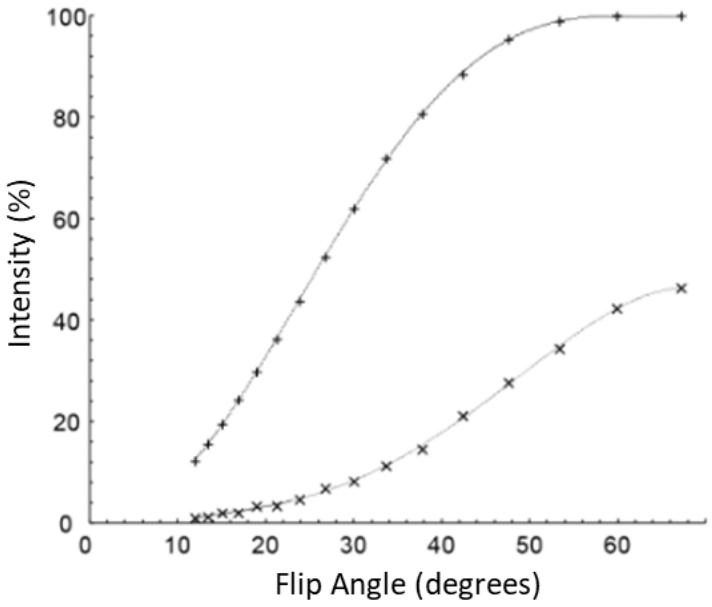

Figure 9: Graph showing the experimental intensities of pure shift signals (+) and recoupling artefacts (x) as a function of β. (Adapted from SI of Foroozandeh, M. et al. 2014.[53])

As the flip angle is a readily changeable parameter it can be freely adjusted in order to obtain high signal-to-noise spectra but with significant artefacts, low signal-to-noise but high-quality spectra, or anything in-between.

However, because the selection of spins in PSYCHE is essentially random the same set of spins cannot be repeatedly selected, an issue BIRD and “Zangger Sterk” methods do not share. This limits which pure shift acquisition schemes PSYCHE can be used with, with the common schemes discussed in the next Section.

2.1.2 Pure Shift NMR Acquisition Schemes

Traditional heterodecoupling is achieved by manipulating a non-measured set of spins to remove coupling to an actively measured set of spins. This can be achieved very simply as the measured and non-measured spins do not share the same frequency space.

Quite possibly the most common decoupled experiment is the $^{13}C\{^{1}H\}$, where protons are irradiated in order to remove $^{n}J_{CH}$ from the resulting NMR spectra, with a simple scheme shown in Figure 10. As mentioned, when dealing with heterocouplings, the two involved groups of spins occupy different frequency spaces so pulsing on one whilst acquiring on the other poses no significant issue. A vast array of decoupling schemes now exist ranging from continual irradiation schemes[54] to supercycles of hard pulses[55] through to adiabatic schemes.[56] All of these different methods have advantages and disadvantages with regard to bandwidth, duty cycle or spectral quality.[57] Ultimately, the aim of all decoupling schemes is to rapidly flip the non-measured nuclei between different spin states so that the nucleus being detected experiences an average of these states, leading to a spectrum devoid of that particular type of coupling. To a first approximation many of these can be thought of as continually applying 180º pulses to the non-measured nucleus with additional elements to compensate for pulse miscalibration and the physical limits of hard pulses with regard to bandwidth.[58]

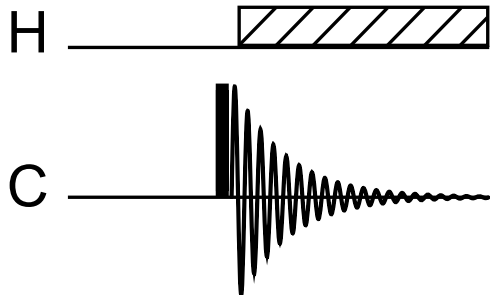

Figure 10: A 1D ^{13}C sequence with gated decoupling (dashed box).

This line of thinking can unfortunately not be directly applied to homodecoupling, because the nuclei involved *do* inhabit the same frequency space, making simultaneous pulsing and acquiring impossible. The approach that must be taken is to periodically pause acquisition in order to apply selective inversion elements, which will refocus the coupling between the active and passive spins. Technically, homocoupling is only refocused at a single point in time. However, because *J*-evolution is slow compared to chemical shift evolution data can be acquired in data chunks about 1/3*J* in length (10-20 ms for typical $^{3}J_{HH}$ couplings).[33] In order to measure a full-length NMR spectrum many of these data chunks must be acquired, each representing a different 10-20 ms of chemical shift evolution. This necessitates specialised data acquisition schemes, which are detailed below.

2.1.2.1 Real Time Pure Shift

Given that acquisition needs to be periodically halted to apply selective inversion elements the real time scheme is perhaps the most intuitive way to acquire a pure shift spectrum. Figure 11 shows a generalised diagram of the scheme, acquisition is periodically halted to allow application of a hard 180º pulse and a selective inversion element. The selective inversion element refocuses coupling between the active and passive spins, whilst the hard 180º pulse means any chemical shift evolution on the active spins that occurs while acquisition is paused will be refocussed, so chemical shift evolution is continuous in the recorded FID.[59,60]

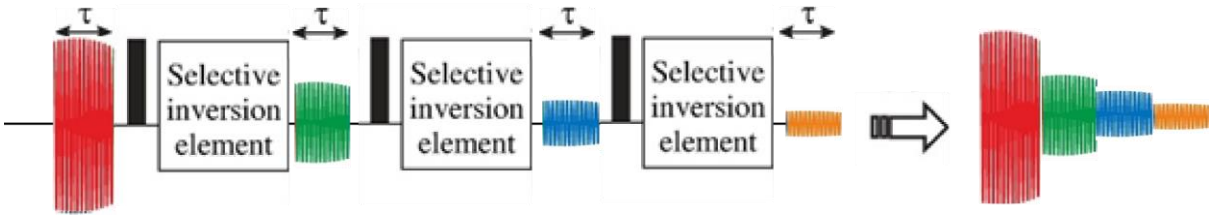

Figure 11: Generalised acquisition scheme for real time pure shift. (Adapted from Castañar, L. 2017. [33])

An attractive feature of this method is that data is acquired for the full length of time that NMR signals are detectable – around a full second for ^{1}H. However, a significant issue becomes apparent when considering the relative lengths of the selective inversion elements and acquisition periods. Many selective inversion elements (on the order of tens of ms) are of similar length, if not longer than the acquisition periods.[33] This allows a significant amount of relaxation to occur whilst both acquisition and chemical shift evolution are suspended, which makes accessing later periods of chemical shift evolution impossible. This significantly reduces the length of the final FID. After Fourier transformation this manifests as an increase in the linewidth of signals, potentially preventing the resolution of nearby chemical shifts.

Another issue this causes is that the relaxation in the FID is no longer continuous. This introduces slight steps in amplitude which result in artefacts to either side of the genuine peaks at frequencies related to the chunk duration. This may cause problems with analysis, such as when analysing a mixture of compounds with significantly different concentrations. In such a case it may be difficult to distinguish between artefacts relating to high intensity peaks and genuine low intensity peaks that relate to low concentration compounds. Methods do exist to minimise these artefacts. For example, by recording multiple real time pure shift spectra with a varied chunk duration the position of artefacts will vary in each spectrum, whilst the position of signals remains the same. Upon summation this will lead to a diminished signal-to-artefact ratio but requires a long minimum experimental time and can never entirely remove artefacts.[51]

This acquisition scheme also necessitates that the same group of active spins can be selected repeatedly within the same scan. Otherwise a continuous sense of chemical shift evolution could not be provided from data chunk to data chunk. This is not a problem for BIRD, as it operates via coupling to sparse heteronuclei. For “Zangger Sterk” based approaches a given molecule could conceivably move out of the “slice” it started the experiment in due to diffusion. However, this is not a significant problem in practice and real time “Zangger Sterk” experiments can give reliable quantitation.[51] However, the PSYCHE approach is unable to meet this requirement and is thus unsuitable for use with a real time pure shift acquisition scheme.

2.1.2.2 Interferogram Pure Shift

The interferogram pure shift approach allows the collection of a full-length pure shift FID (with regard to chemical shift evolution), offering the highest possible resolution after Fourier transformation. A generalised example scheme is shown in Figure 12. The same homocoupling refocussing motif as the real time scheme – a hard 180º pulse followed by a selective inversion element is used. This is flanked by a pair of incrementable delays, which allow coupling to be refocussed at different points of chemical shift evolution. A data chunk (around 10-20 ms) can be collected around this point, where the effects of homocoupling are negligible.

After many such increments are collected, each describing a different period of chemical shift evolution, they can be concatenated together yielding a full length, high resolution FID. Because of these incremented delays, the scheme is often referred to as a pseudo-2D experiment. The same approach can be used to generate higher dimensionality datasets, such as a final 2D-FID from a pseudo 3D dataset.[33]

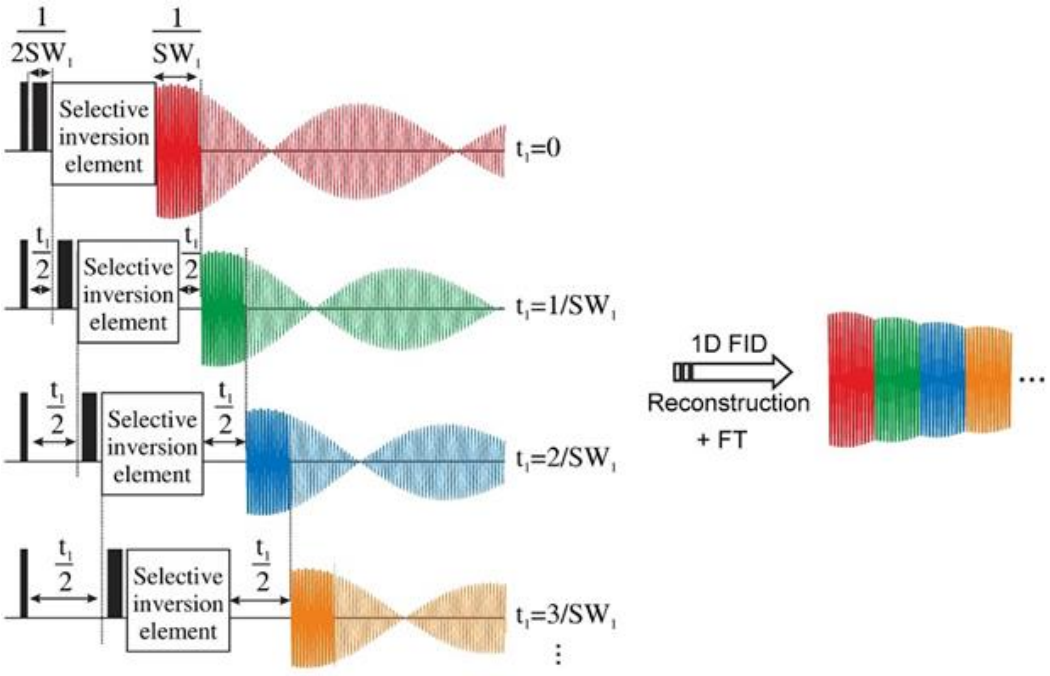

Figure 12: Generalised acquisition scheme for interferogram pure shift. (Adapted from Castañar, L. 2017.[33])

In addition to the increased resolution over spectra generated using the real time pure shift scheme the interferogram method typically results in reduced artefacts, though some sidebands are still present due to the small amount of $^{n}J_{HH}$ evolution that takes place within each data chunk. Methods do exist to eliminate these artefacts entirely, by altering the exact point within the data chunk at which homocoupling is refocussed. This results in alteration of the phases of sidebands relative to the genuine signals and allows them to be entirely

eliminated from the final spectrum.[61] However, this mandates an increase in the minimum experimental time of the interferogram scheme – which is already typically long.

For example, if a full one second FID is to be acquired it would require fifty 20 ms data chunks to be collected. As only a single data chunk is collected per increment this represents an absolute minimum of fifty scans.

Methods do exist that somewhat alleviate this by reducing the number of increments that need to be collected. For example, recording a small fraction of the increments and interpolating missing datapoints by iterative soft thresholding – largely analogous to NUS (Non-Uniform Sampling) on conventional 2D spectra. Such methods can allow significant time savings, requiring as little as 25% of the time for conventional experiments.[62] By incorporation of prior knowledge of the compound being studied, the high data quality of the pure shift interferogram can largely be retained.[63]

However, such methods do not directly address the limited amount of data collected per scan – only 10-20 ms of data can be acquired per increment, orders of magnitude less than the time a typical NMR signal is detectable for. This Chapter of the thesis seeks to address this – increasing the time within each increment that data can be acquired for in an interferogram.

2.2 Refocussed Interferogram Theory

Broadly speaking the choice between interferogram and real time pure shift is a trade-off between resolution losses and further sensitivity losses. An ideal pure shift acquisition scheme would allow optimal resolution whilst minimising sensitivity losses.

In this work, the concept of a Refocussed Interferogram is introduced, in which each data chunk collected in an interferogram experiment is repeatedly refocussed so that it can be acquired multiple times in a single increment. Figure 13 shows a generalised scheme to achieve this. Each of these periods of data refocusing and data collection is referred to as a refocussing cycle, and in principle can be repeated for as long as NMR signals are detectable. The first data chunk measured in every increment can then be concatenated together, yielding a full-length FID – essentially the output of a standard pure shift interferogram scheme. However, all the data chunks relating to a given number of refocussing cycles can also be concatenated together, producing additional full-length FIDs, though only a single additional FID is shown in Figure 13.

These FIDs will have uncorrelated noise and can thus be summed together, providing noise averaging in the same way as running multiple scans of the same experiment. However, the additional data chunks are collected during time when the NMR spectrometer would normally be idle – *i.e.* as part of the relaxation delay between increments.

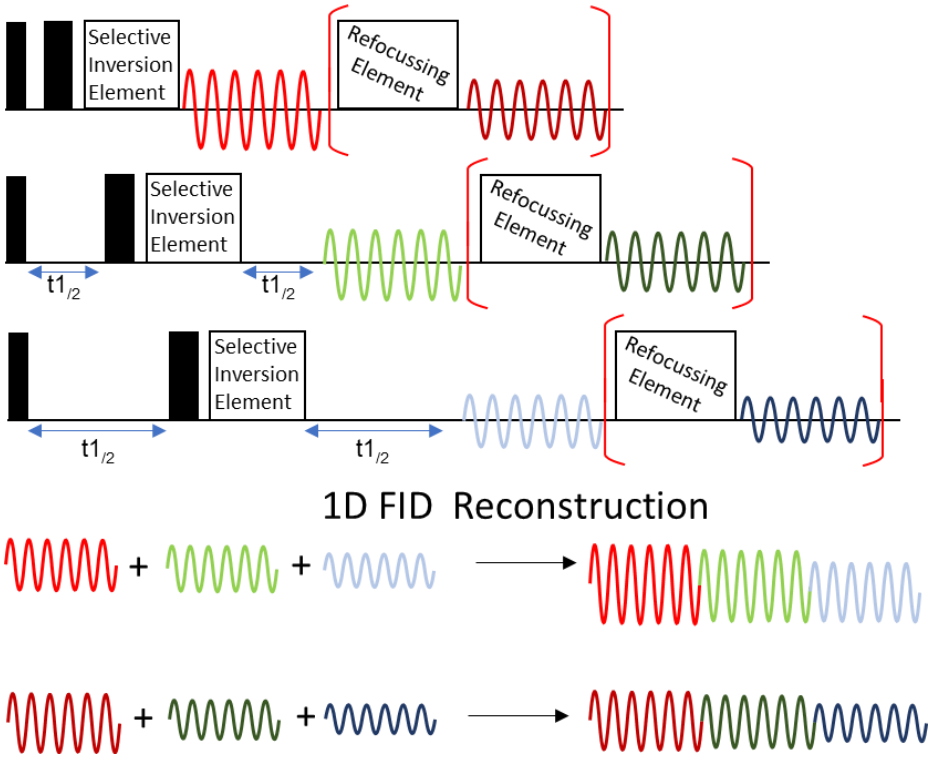

Figure 13: A generalised pure shift acquisition scheme, which attempts to combine some of the benefits of the real time and interferogram schemes. Narrow and wide black rectangles respectively indicate 90º and 180º hard pulses.

Superficially, the interspersion of acquisition with periods to refocus homocoupling is similar to the real time pure shift scheme. Indeed, it shares the same obvious advantage of being able to acquire useful data chunks where homocoupling has been refocussed for as long as an NMR signal is detectable. However, as in the interferogram scheme, later periods of chemical shift evolution are accessed through incremented delays. This should mean that resolution remains uncompromised. Of course, relaxation will still occur during the refocussing elements in the scheme. Thus, after each refocussing cycle signal intensity will drop, whilst noise remains constant. Therefore, the signal-to-noise ratio will fall in later refocussing cycles, so summing data acquired in such a way will lead to less signal-to-noise improvement than simply repeating scans. However, as the Refocussed Interferogram scheme does not require additional experimental time to collect this data it can be considered 'something for nothing' in terms of sampling signal intensity that would otherwise not be acquired.

When the multiple FIDs generated by the scheme are summed together the expected signal-to-noise ratio (SNR) in the final NMR spectrum is given by Equation 1.

$$Final\ SNR = \frac{\sum Signals}{Noise * \sqrt{nR}}$$

Equation 1: The final signal-to-noise ratio is dependent upon the sum of the recorded NMR signals and the total nR – number of refocussings incorporated.

Because the noise is random and uncorrelated it will increase by a multiple of the square root of the number of FIDs incorporated. Thus summing the initial pure shift FID (derived from the first data chunk in each increment) with the FID derived from one refocussing cycle will lead to a $\sqrt{2}$ (~1.41) increase in noise. However, the signals will sum directly as they are correlated. In an ideal case, where no signal was lost during refocussing summation would yield a twofold enhancement in signal intensity, and thus a $\sqrt{2}$ enhancement of signal-to-noise. However, signal-to-noise of the resulting spectrum will be enhanced as long as the signal after one refocussing cycle is greater than $\sqrt{2} - 1$ (~0.41) times the signal in the initial non-refocussed data in each increment. If signal intensity remains high after multiple refocussing cycles (*i.e.* in data chunks three, four etc.) significant enhancements in the final signal-to-noise ratio could be realised. As this refocussed acquisition requires no additional experimental time and no resolution is lost, this represents a direct improvement to the pure shift interferogram. However, if signal intensity rapidly decreases during refocussing cycles, such that the $\sqrt{2} - 1$ signal intensity threshold is rapidly reached then signal-to-noise may be diminished by summing the data. Whether or not refocussing of signals can be performed without significant reduction in intensity over typical relaxation periods will determine the efficacy of this proposed methodology on any given sample.

2.3 Testing Refocussed Interferograms in ^{13}C Spectra

The critical question regarding the proposed acquisition scheme is if it is possible to refocus the chemical shift evolution of an NMR signal quickly and efficiently enough to avoid significant losses in signal intensity, given the relaxation properties of samples typically used for pure shift. The answer to this determines if the Refocussed Interferogram scheme can provide any benefit to net signal-to-noise over a standard interferogram.

An initial proof of concept experiment was run on ^{13}C, with nuclear relaxation rates on the order of 1 s or under for most protonated carbons under standard experimental conditions. Since $^{n}J_{CC}$ couplings are not meaningfully present at natural abundance and $^{n}J_{CH}$ couplings can be trivially removed by heterodecoupling this represents an ideal test system to answer this question without the need to deal with homodecoupling.

Figure 14 shows a pulse sequence which repeatedly refocuses a given period of chemical shift evolution using hard 180º pulses. An initial delay, t1, allows selection of the period of chemical shift evolution to be repeated. On each scan four refocussing cycles are used, with each data chunk sequentially labelled “a” through to “e” for clarity of discussion.

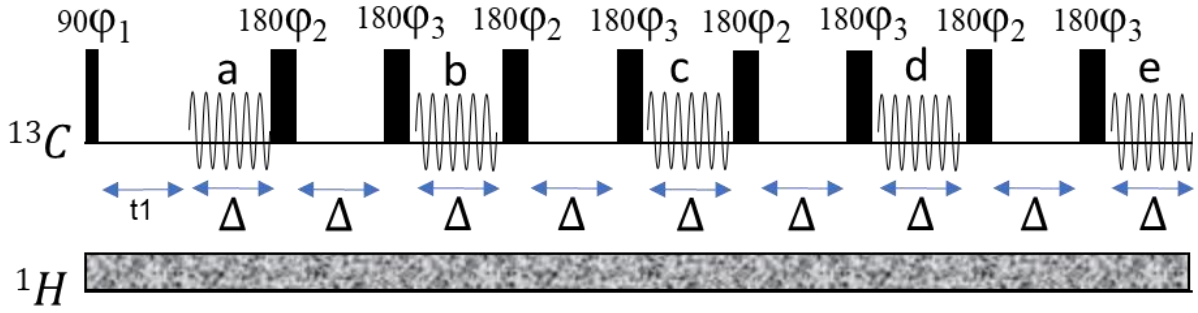

Figure 14: Pulse sequence for repeat acquisition of chemical shift from period t1 to t1 +Δ. Flip angles as indicated with phases: φ1 = X, φ2 = Y, φ3 = -Y. Hard decoupling is used to remove $^{n}J_{CH}$.

The above sequence was run on a sample of DEET with t1 set to 0 ms and Δ set to 30 ms. This is slightly longer than the durations of data chunks that could be expected during a pure shift interferogram experiment, and so mimics the additional relaxation that could be expected in selective inversion elements (with durations on the order of ms to tens of ms). These 30 ms data chunks were then summed and the average signal-to-noise for the eleven resonances measured, shown in Figure 15. The number of acquisition blocks incorporated indicates the number of data chunks added together in alphabetical order – just “a” then “a + b” through to “a + b + c + d + e.” This is compared to the results of a hypothetical increase in the number of scans – taking the signal-to-noise ratio of “a” and extrapolating by the square root of the number of scans.

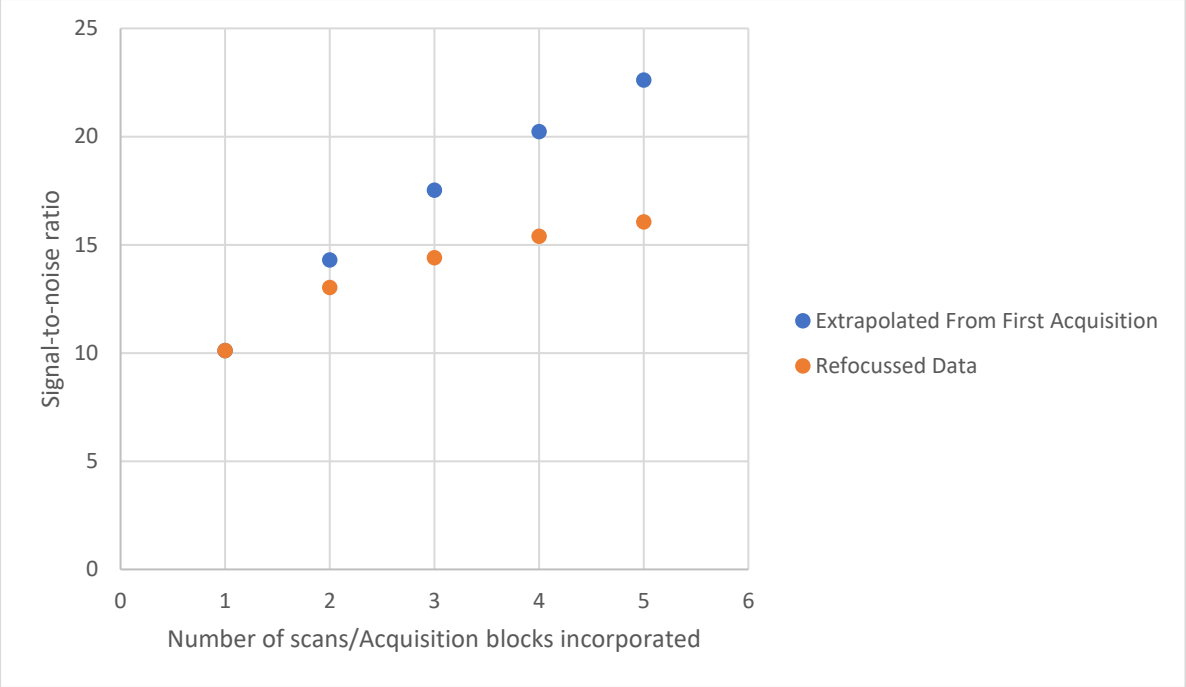

Figure 15: Comparison of signal-to-noise of a short (30 ms) ^{13}C acquisition with summations of refocussed data.

As can be seen the signal averaging of all five data chunks “a” through to “e” in a single scan allows us to achieve the same signal-to-noise ratio as between 2 to 3 standard scans of the same 30 ms period of chemical shift evolution. Also notable is that there are diminishing returns from the incorporation of latter data chunks, because the signal-to-noise ratio within each refocussed chunk continually drops – *i.e.* signal is weaker in data chunk “c” than in chunk “b”. Of course, this experiment in of itself is fundamentally pointless – the best option for signal-to-noise here would simply be acquisition of the full FID for the full duration of the NMR signals as in a normal $^{13}C\{^{1}H\}$ experiment. However it demonstrates that refocussing short (tens of ms) data chunks within a single scan can yield significant signal-to-noise benefits without an increase in experimental time.

2.4 Refocussed Interferogram

The experiments on ^{13}C have suggested that data chunks of the lengths typical for pure shift interferogram experiments can be refocussed to allow collection of the same period of chemical shift evolution multiple times within a scan, yielding signal-to-noise enhancement upon summation. However, these experiments only considered the refocusing of chemical shift evolution. We now move to apply this to pure shift experiments on ^{1}H, in which we must also refocus $^{n}J_{HH}$ between the active and passive spins. This can be done by replacing the hard 180º pulses in Figure 14 with the selective inversion elements already used by the pure shift sequence. Thus, the same groups of active and passive spins are repeatedly selected.

One way to achieve this refocussing is to use the "Zangger Sterk" approach – *i.e.* a selective pulse applied simultaneously to a field gradient. Figure 16 shows a schematic pulse sequence based on this approach, where Δ is the chunk duration. The two selective 180º pulses and delay have the same effect on the active spins with regard to chemical shift as the hard pulses in the ^{13}C experiment. As the selective pulses are not felt by the passive spins each pulse serves to invert the sense of the coupling evolution between the active and passive spins. As the delay, Δ, between the pulses is equal to the length of the data chunks then any *J* coupling evolution in the initial chunk of pure shift data is cancelled out during the delay. After the sense of the coupling evolution is restored by the second "Zangger Sterk" element the coupling and chemical shift evolution in the refocussed data collection should be identical to the initial data collection, with $^{n}J_{HH}$ passing through zero halfway through the data chunk in both cases. This scheme can be simply extended by repeating the same motif to collect as many additional refocussed data chunks as desired.

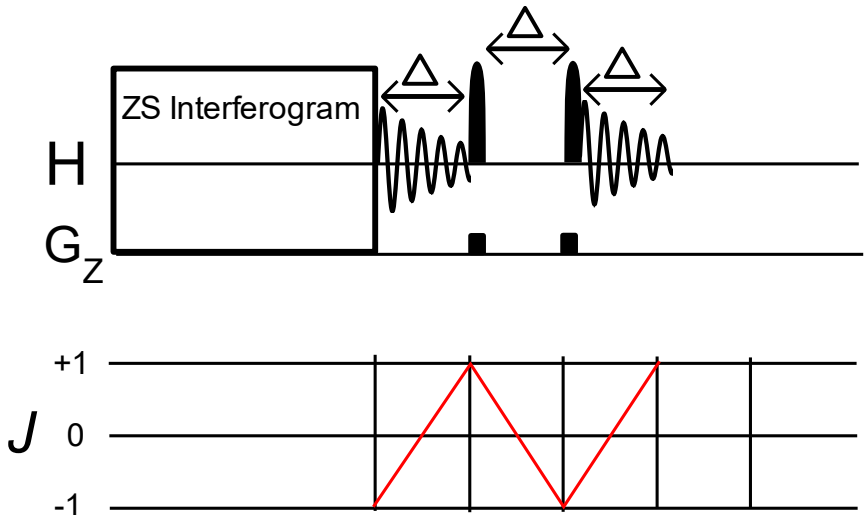

Figure 16: Schematic pulse sequence to refocus a "Zangger Sterk" Interferogram. Pulses are selective with a 180º flip angle. The initial data acquisition is standard for a "Zangger Sterk" Interferogram. Expected evolution of $^{n}J_{HH}$ during the data chunks is shown.

Figure 17 shows the pulse sequence used in this study. The part of the sequence outside of the brackets is a standard “Zangger Sterk” pure shift interferogram. After initial excitation by a 90º hard pulse (φ1) magnetisation is allowed to freely evolve for $t1_{/2}$ +Δ/4 in the XY plane, before dephasing with a field gradient (G1). Magnetisation is then inverted by the application of a 180º hard pulse (φ2) and signals further dephased by application of a second field gradient of equal but negative strength (to G1). After a further Δ/4 of free evolution a ZS element (φ3) is then applied. This inverts the sense of the coupling between the active and passive spins and changes the net chemical shift evolution on the active spins to $t1_{/2}$. Another field gradient (G3) then serves to rephase the active spins, whilst signals from the passive spins (which were unaffected by the ZS element) remain dephased. After another period of free evolution for $t1_{/2}$ net chemical shift evolution on the active spins is t1, whilst the coupling evolution between these spins is Δ/2. The initial data chunk thus describes chemical shift information from t1 to t1+Δ and includes coupling evolution from +Δ/2 to -Δ/2 (the value of Δ is chosen such that this is negligible).

The bracketed section of the pulse sequence is the refocussing cycle discussed earlier and can in principle be repeated several times if desired. Both ZS elements in the brackets are flanked by field gradients (G4 and G5), which serve to dephase any unwanted excitation of passive spins. Field gradients are of differing power levels in order to avoid unwanted accidental rephasing of signals.

At the start of the refocussing cycle, the chemical shift evolution of the active spins is t1+Δ, and net coupling evolution is at -Δ/2. The first ZS element serves to reverse the sense of coupling evolution and invert chemical shift evolution to -t1-Δ. After period Δ chemical shift evolution is expected to be -t1, with coupling evolution being +Δ/2. The second ZS element again inverts chemical shift evolution, to t1, and switches the sense of coupling evolution. Thus the refocussed data chunk in the brackets describes chemical shift evolution from t1 to t1+Δ and includes coupling evolution from +Δ/2 to -Δ/2, identical values to the first data chunk in the increment.

The first data chunk recorded in each increment can then be concatenated together in the same way as a conventional pure shift interferogram spectrum to provide an FID with continuous chemical shift evolution. Indeed, the results from Fourier transforming this should be the same as could be expected from a normal pure shift interferogram experiment using the “Zangger Sterk” approach. Data chunks from any given number of refocussing cycles can then be concatenated in the same way to provide additional refocussed FIDs. These FIDs should be identical to the one derived from data chunks before refocussing, barring amplitude losses due to relaxation.

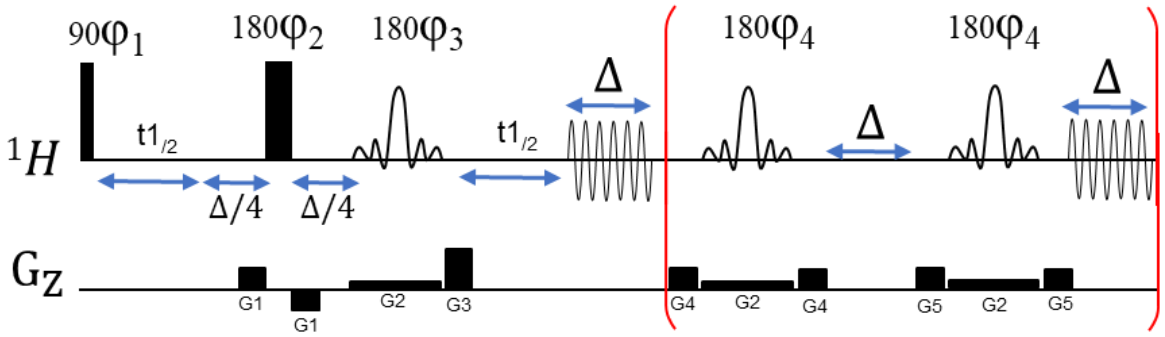

*Figure 17: Pulse sequence for refocusing the data chunk in each increment of a "Zangger Sterk" interferogram. The black rectangles indicate field gradients or hard pulses, with strength and sign as indicated. Rounded shapes represent selective pulses. G3 = 2*G1. Phases as follows: φ1 = x,y,-x,-y φ2 = x,x,x,x φ3 = x,x,y,y φ4 = x,x,y,y.*

This pulse sequence was then run on a sample of strychnine in $CDCl_3$ using 4 scans, 51 t1 increments and a 16 ms chunk duration. All field gradients other than G2 had a duration of 1 ms. The field gradient G2 was applied simultaneously to a Gaussian 180º selective pulse, lasting 9 ms. Only a single refocussing cycle was used, yielding two FIDs after processing – one equivalent to the normal output of a pure shift experiment, referred to as the non-refocussed data and the other composed solely of data chunks refocussed a single time, referred to as the refocused data.

When these are overlayed, Figure 18, the same signals are clearly present, with the same narrow linewidths in both cases. Signals have been adjusted to approximately the same intensity, making the greater noise contribution in the refocussed (blue) data evident.

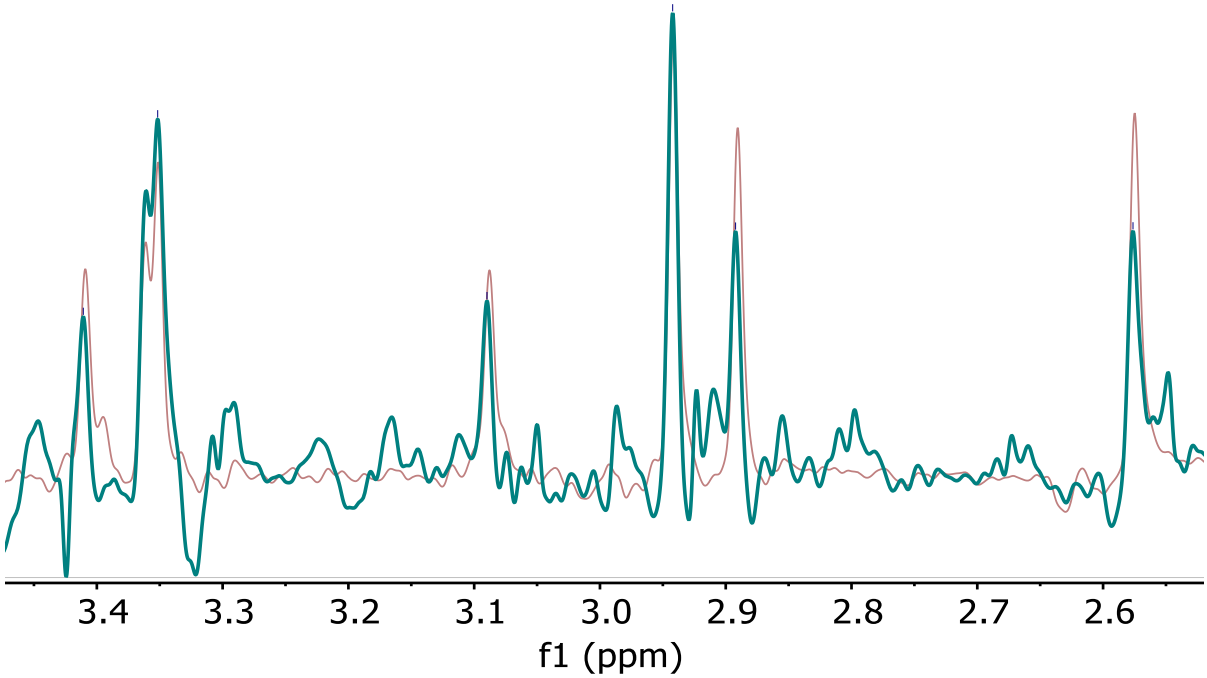

Figure 18: An overlapped region of the strychnine 1D ^1H spectrum showing the Fourier transforms of the non-refocussed data in red and a refocussed pure shift FID in blue, Gaussian 180º selective pulses used.

The non-refocussed data was then baseline corrected (1st order polynomial fit) and signal-to-noise measured for several resonances. This was then summed with the refocussed data and analysed again in the same fashion. The experiment was also conducted using rSNOB selective pulses for the Zangger Sterk element. A comparison of the signal-to-noise change for each resonance is shown in Figure 19. In both cases there is a minor improvement in the average signal-to-noise ratio (2.4% and 7.0% for Gaussian 180º and rSNOB respectively). However, there is also significant variation between resonances, with some having signal-to-noise ratios enhanced by more than 20%, whilst others show a decrease of up to around 7.0%. This means that some signals retain a greater proportion of their intensity after being refocussed than others. There is limited correlation between the two as to which signals are enhanced or diminished in the final summed spectrum.

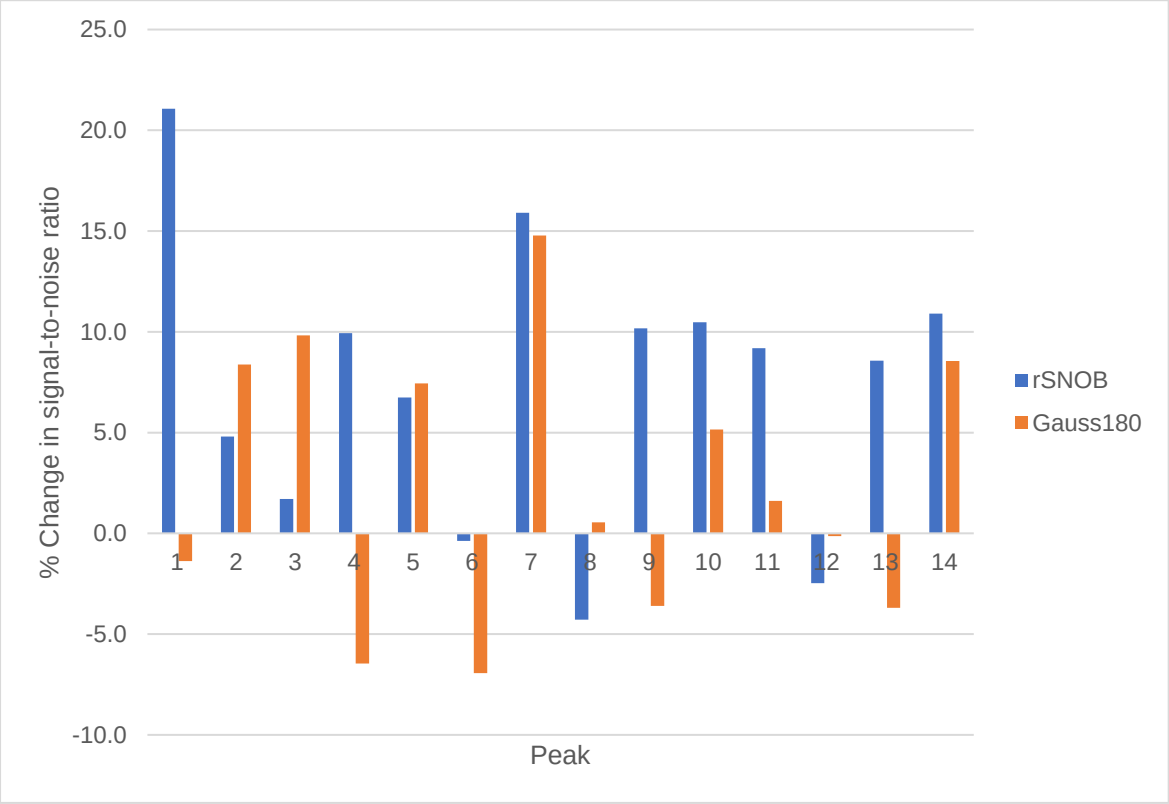

Figure 19: Signal-to-noise change between a standard pure shift interferogram and after its summation with the refocussed data.

The magnitude of the signal-to-noise ratio change for each peak was plotted against T_1 and T_2 values for strychnine – shown in Figure 20. No strong correlation is present, which suggests that T_1 and T_2 relaxation are not major drivers of the discrepancy seen between the differential enhancement of signals in strychnine. The main issue appears to lie with the selective inversion elements, and it may be that their repeated application exacerbates any imperfections in them. Thus, a method for refocussing pure shift data that requires fewer selective pulses is needed.

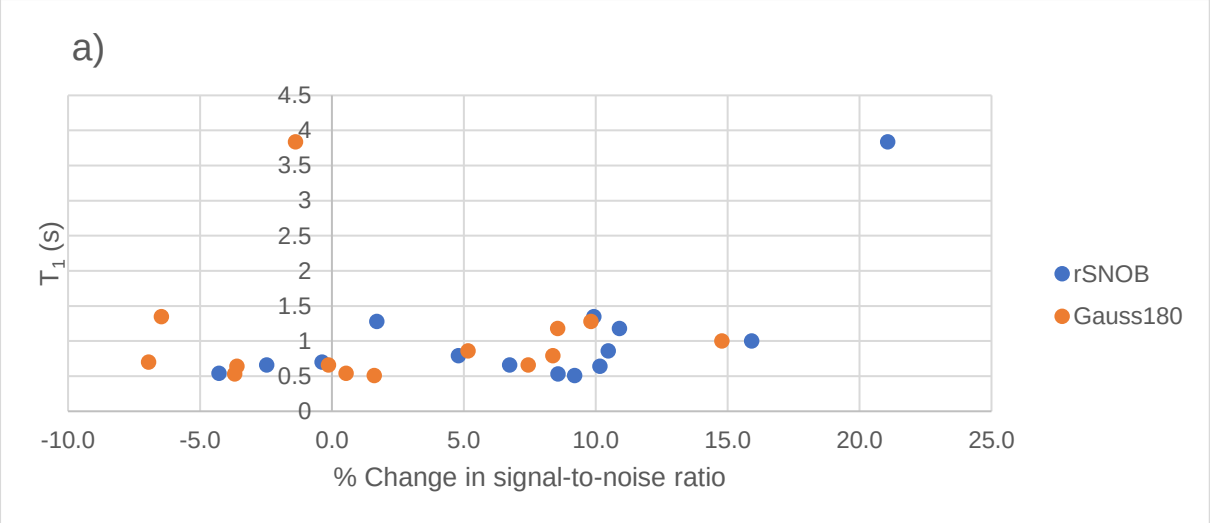

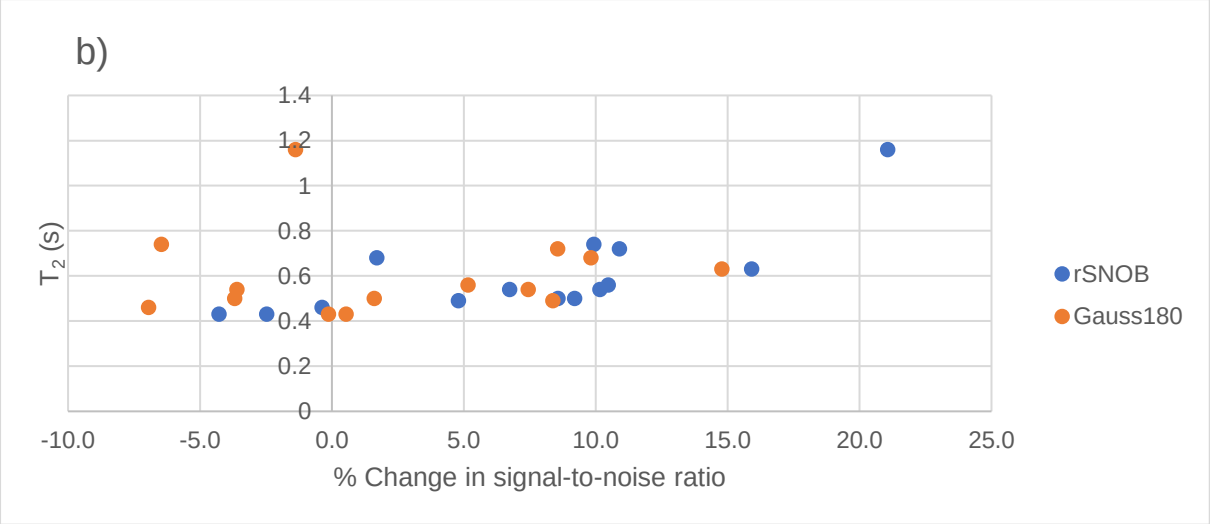

Figure 20: (a) T_1 and (b) T_2 values for strychnine plotted against the signal-to-noise ratio change of each resonance. (T_1 and T_2 values taken from existing work within the group.[64])

It is worth reiterating that the results of the standard pure shift experiment (the non-refocussed data) and the refocussed data are obtained from the same single increment and so no additional experimental time is required to collect the latter. Thus, a user could measure both, then simply Fourier transform both the summed and the separate FIDs to check which gave the most intense signals in a region of interest.

In any case, the signal enhancements from this pure shift Refocussed Interferogram method are modest compared to those observed for the proof of concept experiments on ^{13}C. Part of this may be that the refocussing elements themselves are significantly longer – the hard pulses used are on the order of microseconds whilst the selective pulses and field gradients used here are often of comparable length (9 ms for the Gaussian 180º and 18.5 ms for the rSNOB) to the data acquisition period being refocussed (tens of milliseconds). However, as differences are present between the Gaussian 180º and rSNOB data, it appears that imperfections in the selective pulses create additional complications.

2.5 Pseudo Real Time Pure Shift

In order to both reduce the total number of selective pulses applied and reduce the time taken to refocus the NMR signal an improved general scheme was designed, shown in Figure 21. The same core concept is kept – the useful data from a standard interferogram experiment is refocussed and so can be recorded multiple times within the same scan. However, this scheme does not attempt to refocus chemical shift evolution, only the effects of coupling. This can be achieved with a much shorter hard 180º pulse followed by a selective inversion element with minimal delay. This allowance of chemical shift evolution between chunks in the same increment is reminiscent of real time pure shift approaches and hence this scheme is dubbed the “Pseudo Real time” pure shift approach.

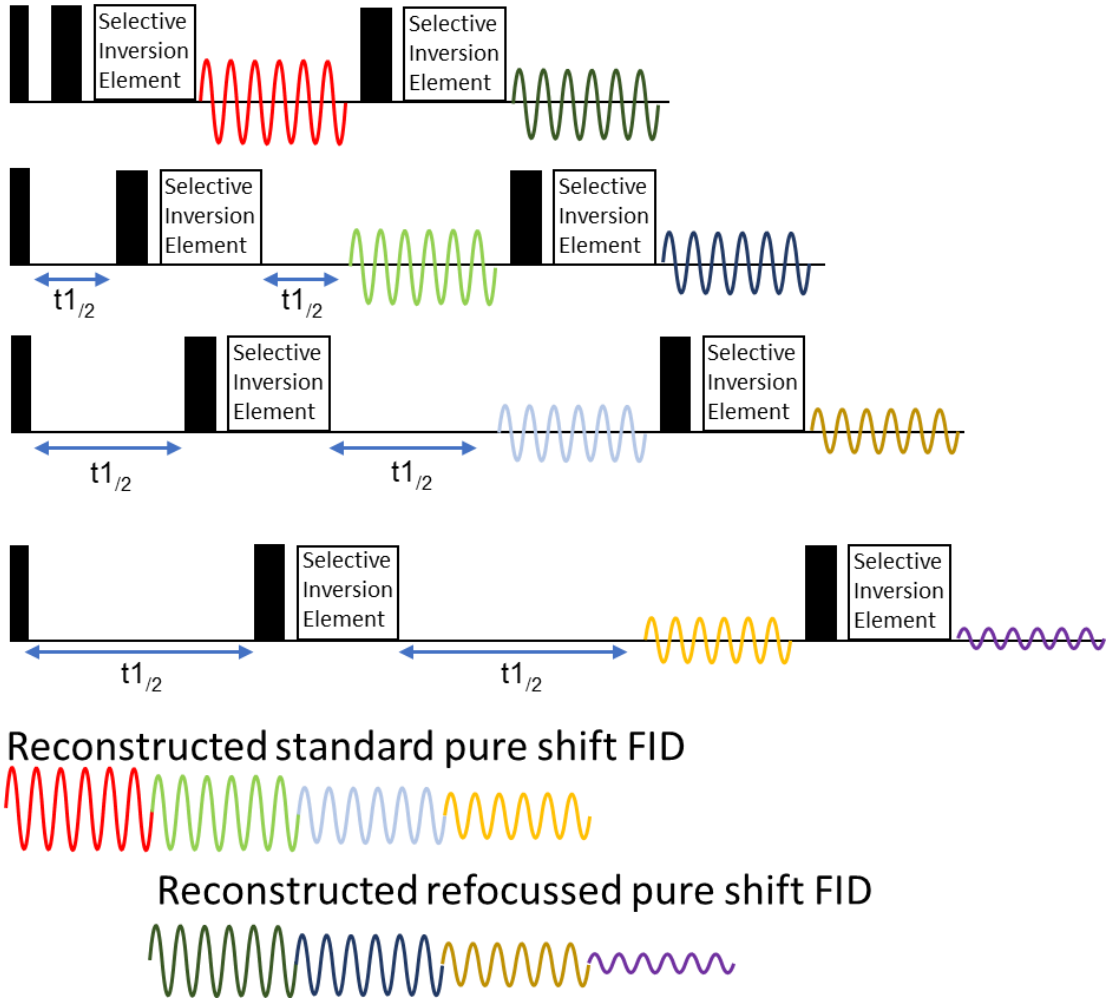

Figure 21: A generalised acquisition scheme for Pseudo Real Time pure shift. Different colours (in the order red, green, blue, yellow, purple) represent different periods of chemical shift evolution, whilst the darker shades of the colour have been J refocussed. Narrow and wide dark rectangles indicate 90º and 180º hard pulses respectively.

A significant potential issue with this scheme is that the first chunk of chemical shift evolution is not acquired twice – *i.e.* it is not re-acquired after refocussing in any subsequent increment (illustrated by the red chunk of data in Figure 21). After summing of the FIDs this will create a step-discontinuity in the amplitude of the signals between the first and subsequent chunks that will lead to artifacts in the resulting Fourier transform spectrum.

One simple solution to this 'first chunk' problem would be to simply delete the first chunk, however that will cause a substantial 1st order phase problem with the dataset which cannot be corrected without inducing significant baseline distortion. One could propose phasing both the initial and refocussed FIDs in magnitude mode before summing them – sidestepping the issue of phase altogether. However, this will give broader line shapes and thus a reduced signal-to-noise ratio – not ideal for a scheme intended to increase sensitivity.

Another solution would be to simply record the first chunk of chemical shift evolution again and simply append it to the start of second refocussed FID. This is shown diagrammatically in Figure 22, with the refocussed FID elements in red. This approach requires little additional experimental time – as it only requires recording a single additional increment. However, because the non-refocussed FID is expected to be more intense than the refocussed FID, due to the additional relaxation during refocussing elements this will cause a step-discontinuity in amplitude similar to the real time pure shift acquisition scheme. If refocussing more than once, this problem of missing data chunks gets worse as a summed FID derived from refocussing twice in each increment will be missing the first two periods of chemical shift evolution and have an even larger step-discontinuity in amplitude. However, it should be noted that the discontinuity only exists for the first data chunk in the FID (or a small number of data chunks) rather than between every single chunk in the FID, so the artefacts should be of lower intensity than for real time pure shift approaches.

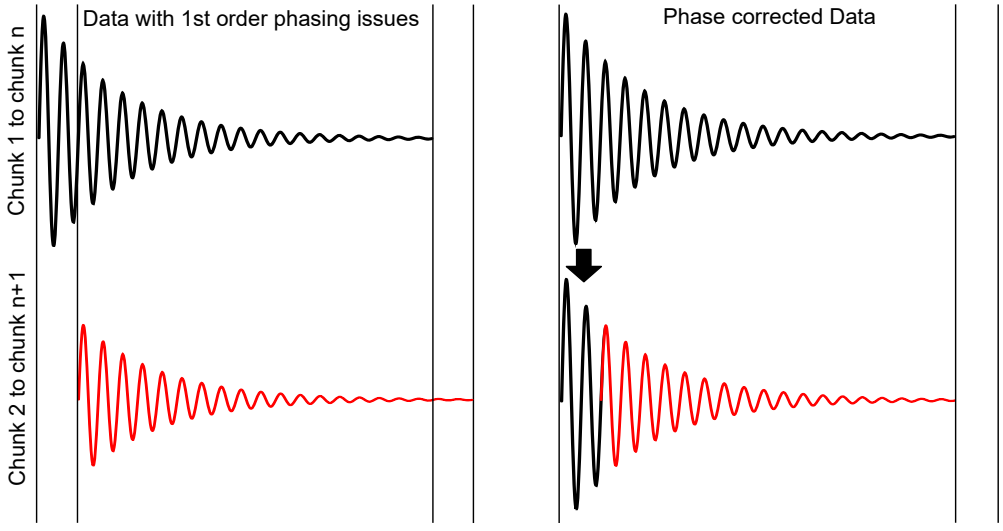

Figure 22: A reconstruction process to prevent 1st order phase issues in analysis of the refocussed FID.

It should also be noted that the “final” chunk of chemical shift evolution (purple, with reference to Figure 21), is also not re-acquired in a subsequent increment. However, in a full spectrum acquired with tens of increments, the final chunk can simply be discarded without significant detriment to the spectrum quality.

In the same way as the previous acquisition scheme this methodology is purely acquisition related and can be appended onto an existing pure shift interferogram scheme. This is shown in Figure 23, with delays for field gradient stabilisation and avoidance of ringdown also defined (GSTAB). These additional delays complicate refocussing the coupling *exactly* at the centre of the subsequent refocussed data chunk whilst maintaining continuous chemical shift evolution. After collection of the initial non-refocussed data chunk the coupling evolves for four GSTAB periods and the duration of three field gradient pulses before the sense of its evolution is inverted, after which it only evolves for two GSTAB periods and the duration of a single field gradient pulse before data collection is resumed. This means coupling evolution between the non-refocussed data and the refocussed data differs by the length of two GSTAB periods and a selective pulse. This is around 1-4 ms depending on the exact parameters of the experiment and a potential source of error with pure shift experiments where the value of Δ can be expected to be between 10 and 30 ms. This could potentially cause issues where the difference in coupling evolution modulates the phase of signals, causing imperfect addition in a phase-sensitive analysis. It is worth noting that this error cancels out in subsequent refocussing cycles such that the coupling evolution within the chunk would be expected to be identical between the original non-refocussed data chunk and the data chunk collected after two refocussing cycles.

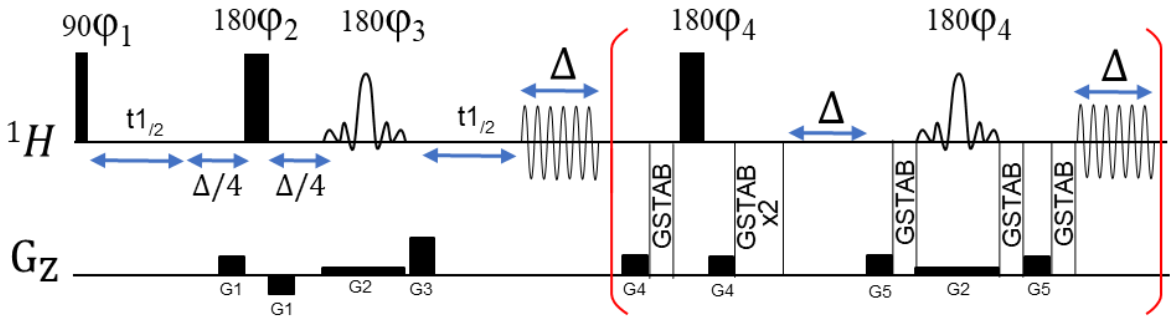

Figure 23: Pulse sequence for Pseudo Real time pure shift using “Zangger Sterk” elements. Rounded shapes represent selective 180º pulses, and narrow and wide black rectangles represent hard 90º and 180º pulses respectively. Phases as follows: φ1 = x,y,-x,-y φ2 = x,x,x,x φ3 = x,x,y,y φ4 = x,x,y,y

The pulse sequence above was tested on a sample of strychnine in $CDCl_3$. Similar parameters to the previous refocussed interferogram scheme were used (4 scans, 51 t1 increments and a 16 ms chunk duration). A Gaussian 180º pulse, lasting 9 ms was used for the selective inversion elements. However, field gradient stabilisation delays and field

gradient durations were both minimised (to 300 µs and 500 µs respectively). This reduces the time that potential coupling modulation can occur to 1.1 ms. Only a single refocussing cycle was used in each increment, allowing collection of non-refocussed data representative of a default “Zangger Sterk” pure shift interferogram experiment and data refocussed once (albeit missing the first chunk of chemical shift evolution). The first increment of the experiment was then repeated and the first data chunk from this repeat was appended to the start of the refocussed FID, as shown in Figure 22, to remove 1st order phase error. An overlay of the Fourier transformed spectra for these sub-FIDs is shown in Figure 24, demonstrating that no significant artefacts are introduced by the step-discontinuity in amplitude this process introduces.

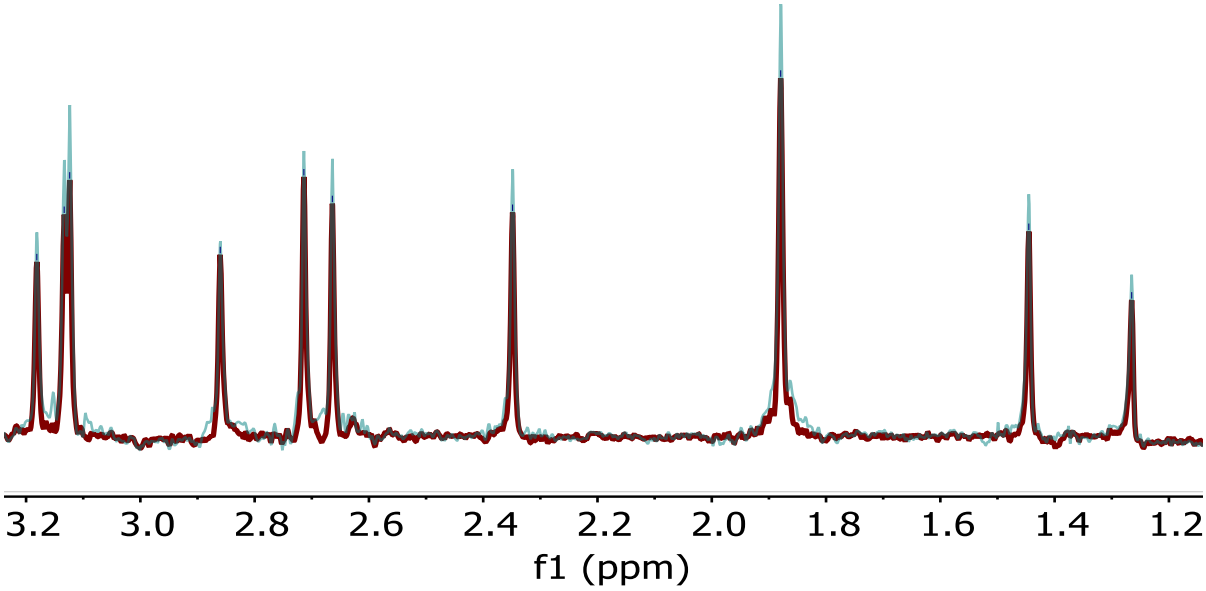

Figure 24: Overlay of a standard “Zangger Sterk” pure shift spectrum of a region of strychnine (shown in blue) with a phase corrected refocussed Pseudo Real time spectrum (shown in red).

Spectra were then baseline corrected (1st order polynomial) and peak picked. This process was also repeated after summation. The signal-to-noise ratio change, shown in Figure 25, is positive for every resonance measured. A significant range of enhancements are observed (between 1.9% and 26.9%), with an average 14.2% enhancement.

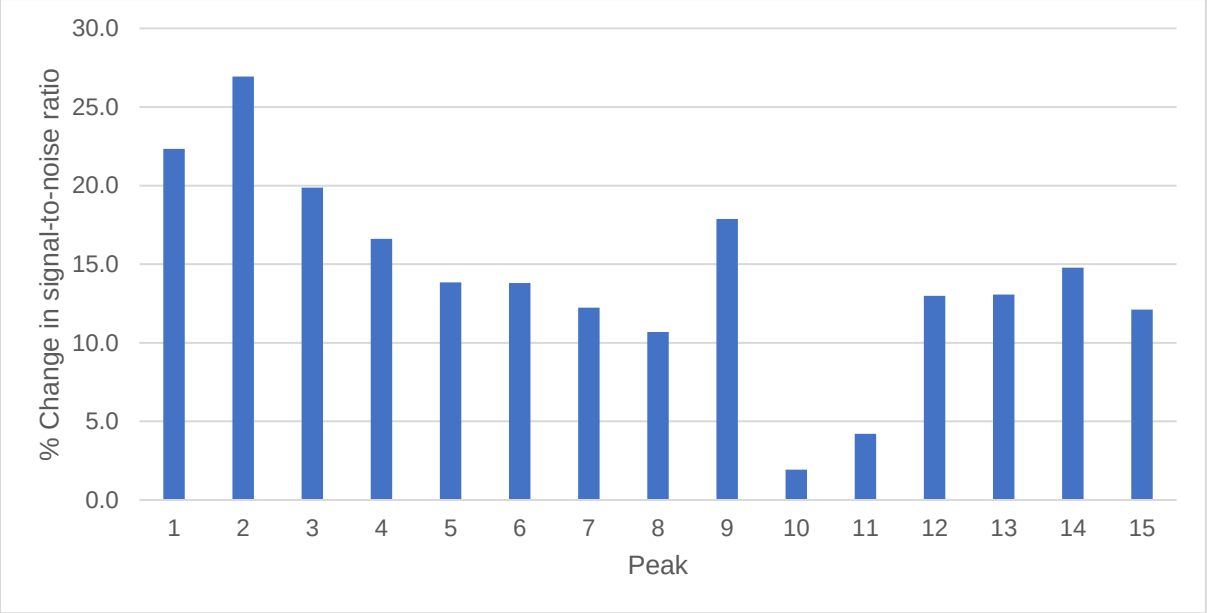

Figure 25: Signal-to-noise change of 15 resonances in strychnine when comparing the non-refocussed data with the sum of the non-refocussed and refocussed data.

This data was then reanalysed with magnitude mode processing rather than phase-sensitive analysis. Intriguingly, the results of this, Figure 26, show far greater signal-to-noise enhancements from summing the data than the phase-sensitive analysis. This may be because analysis in magnitude mode removes any phase modulation caused by residual coupling differences and thus better addition of the signals, leading to relatively more intense resonances in the final summed spectrum. In this case all resonances are enhanced by at least 15% but no additional experimental time is required. Roughly speaking this is equivalent to increasing the number of scans by 30% – giving the sensitivity that could be expected from a 13 scan experiment with only 10 scans. Remarkably, some resonances approach 41.42% enhancement – this is the theoretical maximum that would be reached when a signal suffered no loss in intensity during refocussing, and so was equally intense in both original and refocussed data. For these resonances the sensitivity gain is almost equivalent to doubling the number of scans – if these were of particular interest this represents an enormous amount of either additional sensitivity or potential saving in experimental time.

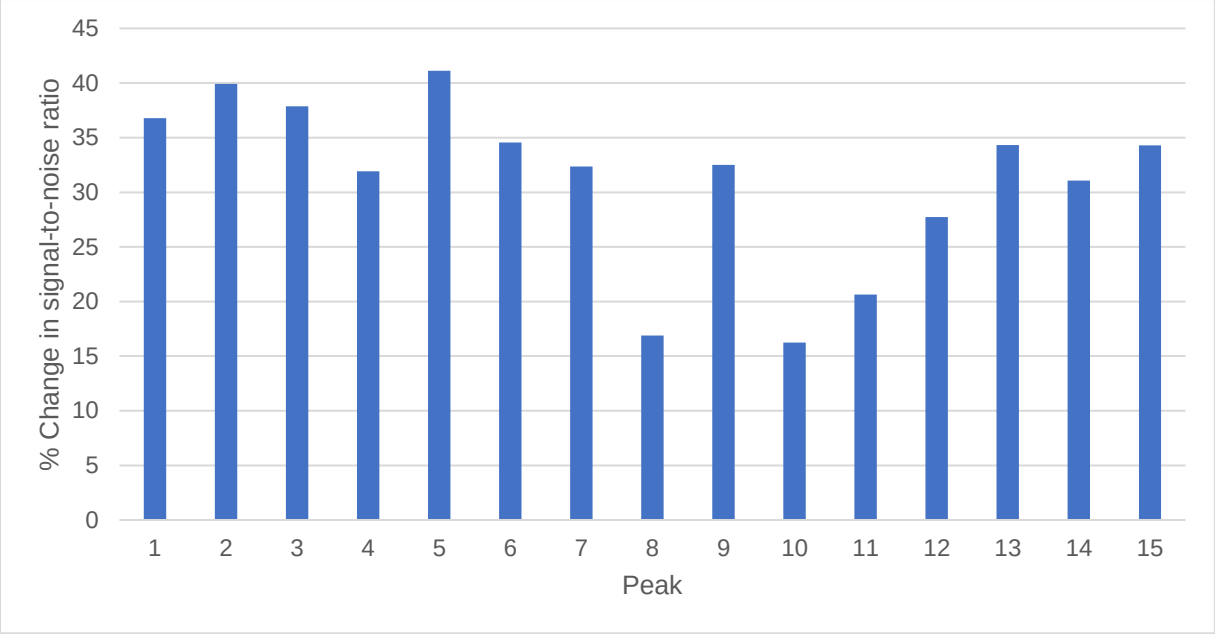

Figure 26: Signal-to-noise change of 15 resonances in strychnine when comparing the non-refocussed data with the sum of the non-refocussed and refocussed data, where data was Fourier transformed in magnitude mode before summation.

Whilst these results appear highly promising, as mentioned before, magnitude mode analysis leads to broad line shapes and diminished signal-to-noise compared to phase-sensitive analysis. This means there is no significant benefit to the summed Pseudo Real Time experiment (with magnitude processing) when compared to a standard interferogram experiment (which is phase-sensitive). However, if the results obtained from the magnitude mode comparisons can be replicated with a phase-sensitive variant of the experiment, they could represent significant enhancements in sensitivity and/or experimental time.

2.6 Multiple Spin Echo Pure Shift

The Pseudo Real time interferogram method described in the preceding Section, while achieving positive signal-to-noise enhancements of 1.9-26.9% in this test study, still performs substantially below the theoretical limit of noise averaging two data chunks (~41%). The primary reason for this is still likely inefficiencies in the refocusing elements, and particularly the need for the long refocussing period (Δ) between data chunks. In order to address this, a third iteration of refocussed pure shift interferograms, the MSE (Multiple Spin Echo) pure shift experiment was designed to refocus both chemical shift and coupling, but post processing data to allow acquisition of useful data during the refocussing period. This allows an absolute minimum of pulses and delays within the sequence.

2.6.1 MSE Theory and Pulse Sequence

The pulse sequence for the MSE pure shift sequence applied to the “Zangger Sterk” method of refocussing homocoupling is shown in Figure 27 (pulse sequence code in Appendix 8.1.1). Only a single selective inversion element is used to refocus the NMR signal, with no Δ delay period incorporated (essentially the data chunk is measured *during* the Δ period). This should minimise signal losses whilst refocussing the data, and thus yield the best possible signal-to-noise enhancement.

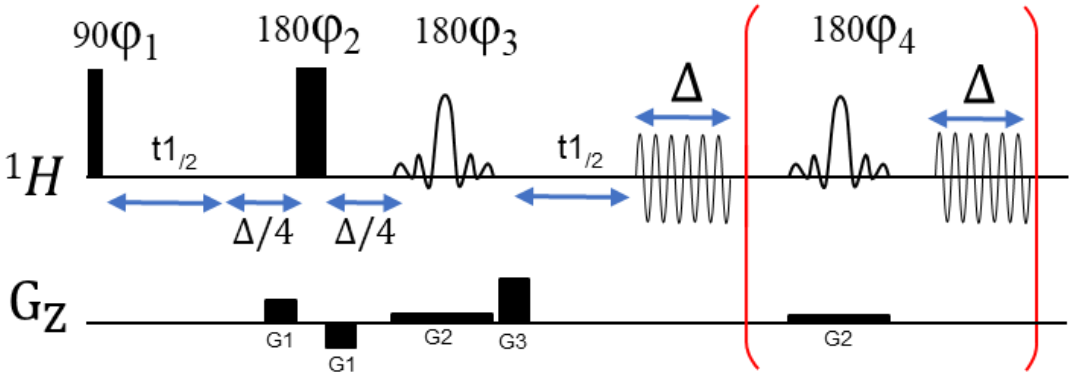

Figure 27: MSE pure shift pulse sequence. Hard pulses are represented by black rectangles, whilst selective pulses are represented by the rounded shapes. Δ indicates the chunk duration. Field gradients are of the indicated sign and strength. Flip angles as indicated, phases as follows φ1 = x,y,-x,-y φ2 = x,x,x,x φ3 = x,x,y,y φ4 = x,x,y,y.

However, by using only a single pulse for refocussing, every second (even numbered) data chunk is refocussed by an odd number of additional refocussing pulses. Thus, every even numbered data chunk represents the ascending portion of a spin echo period. By time reversing and taking the complex conjugate of every even numbered data chunk, these can be corrected to match the odd-numbered data chunks and produce an FID that Fourier transforms into a normal absorption mode spectrum. Such processing is not new,[65] and was proposed for use in solution state NMR in the 1970s to compensate for fast T_2* relaxation in $^{13}C\{^1H\}$ experiments.[66] More recently it has found use in singlet state NMR where relaxation properties are often extreme (with T_1 and T_2 values on the order of minutes to hours).[67] Similar data processing has also found application in solid state NMR to enable acquisition of high-resolution spectra – on the order of Hz – at very low MAS (Magic Angle Spinning) rates.[68]

To explain how the complex conjugation and time reversal are utilised to produce corrected data from the spin echoes it is useful to analyse the pulse sequence using the product operator formalism on a simplified model, Figure 28. As in the pulse sequences presented earlier, the chunk duration here is Δ. Prior to data acquisition and refocussing a variable amount of chemical shift evolution, equivalent to an integer multiple (*n*) of Δ, will have occurred dependent on which increment is being acquired. Effects of homocoupling are not considered, as they are assumed to have been perfectly refocussed during this period.

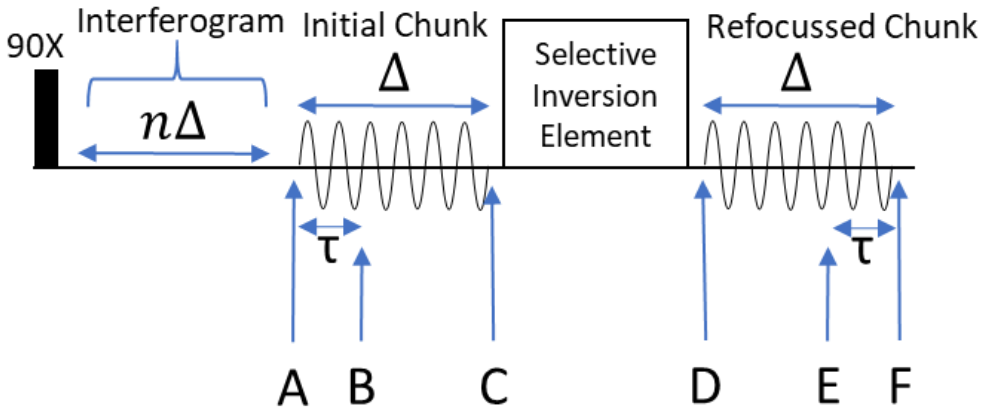

Figure 28: A simplified version of the MSE pure shift sequence and labels for the product operator analysis.

As the sequence starts with a 90_X^o pulse the chemical shift evolution for a frequency Ω at position (A) in Figure 28 can be described as:

$$sin(n\Delta\Omega)\, I_x - cos(n\Delta\Omega)\, I_y \qquad \textit{Equation 2}$$

At datapoint (B) after time τ, where $\tau \leq \Delta$, chemical shift evolution in the initial chunk can then be described by Equation 3.

$$sin(n\Delta\Omega + \tau\Omega)\, I_x - cos(n\Delta\Omega + \tau\Omega)\, I_y \qquad \textit{Equation 3}$$

At time (C) $\tau = \Delta$, so chemical shift evolution simplifies to:

$$sin((n+1)\Delta\Omega)\, I_x - cos((n+1)\Delta\Omega)\, I_y \qquad \textit{Equation 4}$$

The selective inversion element is assumed to operate as an instantaneous 180_X^o pulse. This means that at (D) chemical shift evolution can be described as:

$$sin((n+1)\Delta\Omega)\, I_x + cos((n+1)\Delta\Omega)\, I_y \qquad \textit{Equation 5}$$

At point (E), chemical shift has been allowed to freely evolve from (D) for a period of $(\Delta - \tau)$. Thus, the signal can be described as:

$$sin\big((n+1)\Delta\Omega\big)\cos(\Delta - \tau\Omega)I_x - \cos\left((n+1)\Delta\Omega\right)\ sin(\tau\Omega)\, I_x$$
$$+cos\ ((n+1)\Delta\Omega\,)cos(\tau\Omega)I_y + sin((n+1)\Delta\Omega)\, sin\ (\Delta - \tau\Omega)I_y$$

Using identities this can be simplified to:

$$\sin\big((n+1)\Delta\Omega - (\Delta - \tau)\Omega\big)\, I_x + \cos\big((n+1)\Delta\Omega - (\Delta - \tau)\Omega\big)\, I_y$$

Which expands to:

$$\sin(n\Delta\Omega + \Delta\Omega - \Delta\Omega + \tau\Omega)\, I_x + \cos(n\Delta\Omega + \Delta\Omega - \Delta\Omega + \tau\Omega)\, I_y$$

and cancels to:

$$sin(n\Delta\Omega + \tau\Omega)\, I_x + cos(n\Delta\Omega + \tau\Omega)\, I_y \qquad \textit{Equation 6}$$

At the end of the refocussed data chunk (F) $\Delta = \tau$, so Equation 6 simplifies to:

$$sin(n\Delta\Omega)\, I_x + cos(n\Delta\Omega)\, I_y \qquad \textit{Equation 7}$$

Notably Equations 3 and 6, describing chemical shift evolution at points B and E are identical, barring the sign of the cos term *i.e.* they are the complex conjugate of each other. However, the former describes the datapoint time τ after *start* of the data chunk whilst the latter describes the datapoint time τ before the *end* of the data chunk. Consequently, one simply needs to reverse the time order of datapoints after taking the complex conjugate of the second chunk and datapoint B and E will then map perfectly onto each other *i.e.* the chemical shift evolution at each sequential point in the two data chunks will be identical.

We then move to consider the effects of concatenating multiple increments of data, with a three-increment example in Figure 29, where each allows a defined number of multiples of Δ of chemical shift evolution prior to acquisition.

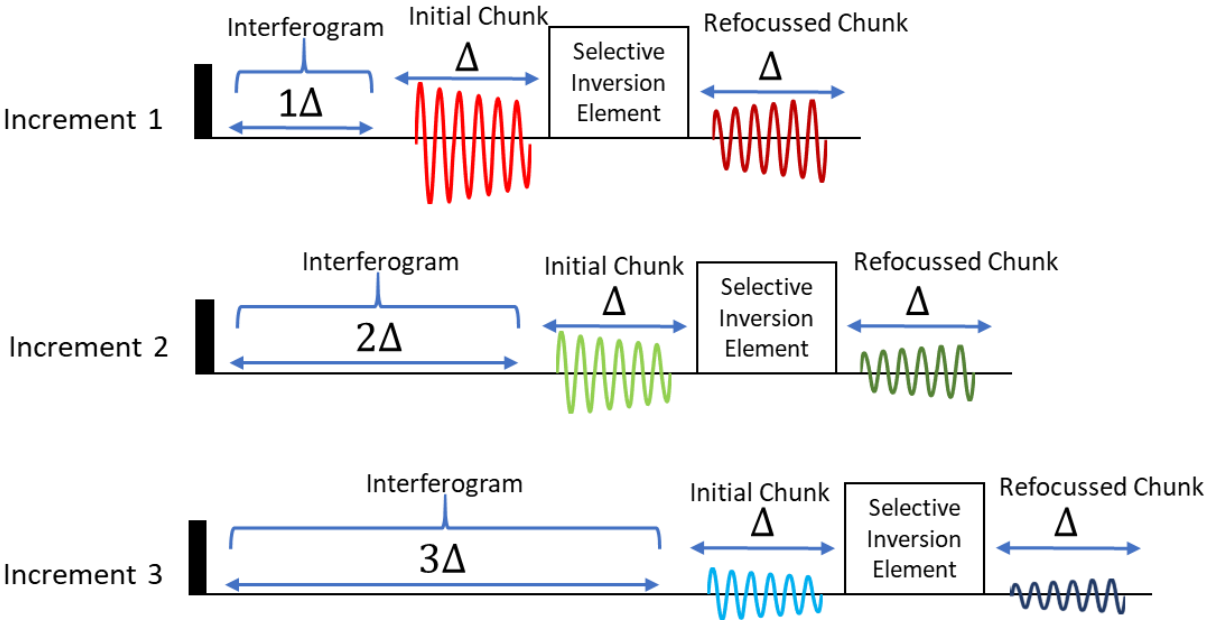

Figure 29: A diagram of a series of increments in an interferogram pure shift experiment that allow a variable amount of chemical shift evolution.

Chemical shift evolution in the first data chunks collected in each increment is continuous – based on Equations 2 and 4 the shift evolution from the first chunk in increment 2 starts where that from increment 1 ended. This means they can simply be concatenated together to provide a single continuous FID, as Figure 30.

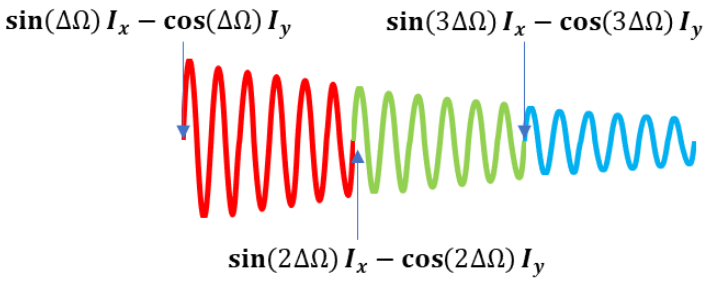

Figure 30: Chemical shift evolution at a number of points in an FID created by concatenating the initial data chunks from each increment.

However, chemical shift evolution in the data chunks collected after refocussing is not continuous in the same manner, as determined with Equations 5 and 7 and displayed in Figure 31. Indeed, chemical shift evolution at the *end* of each refocussed FID is equivalent to that at the *start* of the FID from the *previous* increment.

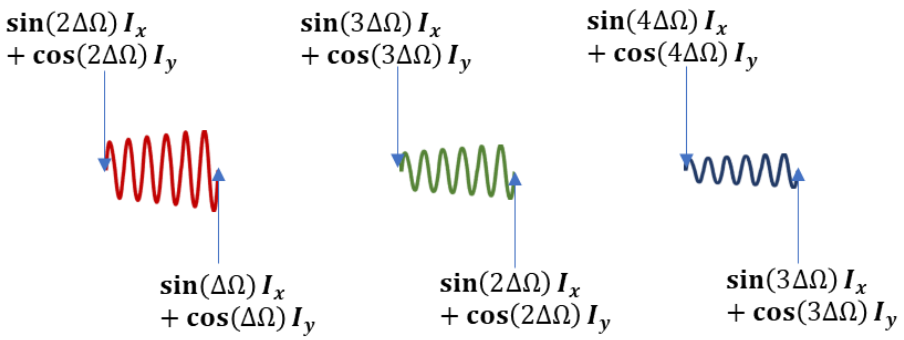

Figure 31: The chemical shift evolution at the beginning and end of the refocussed data chunks for each increment of Figure 29.

By time reversing each refocussed data chunk individually whilst maintaining its order relative to other data chunks, as Figure 32, we can create an FID with a continuous sense of chemical shift evolution.

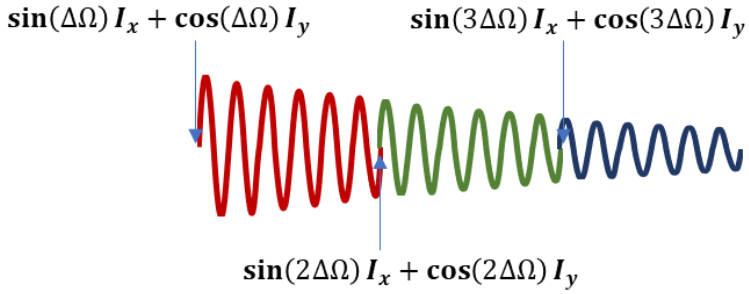

Figure 32: Chemical shift evolution at a number of points in an FID created by time reversal and concatenation of refocussed data chunks from each increment of Figure 29.

However, the chemical shift evolution in Figure 30 and Figure 32 is not equivalent. In the refocussed and time reversed data evolution is described by a term with the opposite sign cos operator. Were they to be Fourier transformed and the results compared frequencies would appear to be mirrored around the offset. This can be simply corrected for by multiplying the cos term by -1, as Figure 33. This can be accomplished in practice by multiplication of the imaginary NMR data by -1.

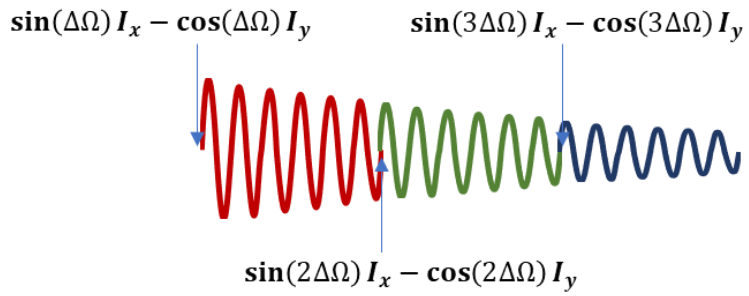

Figure 33: Chemical shift evolution at a number of points in an FID created by time reversal, concatenation and complex conjugation of refocussed data chunks from each increment of Figure 29.

If multiple refocussed data chunks are collected per increment, as in Figure 34, then this additional processing is needed every time an odd number of refocussing pulses have been applied *i.e.* for the data refocussed once and three times. For all other chunks only the standard processing (concatenation of consecutive data chunks) for a pure shift interferogram is required.

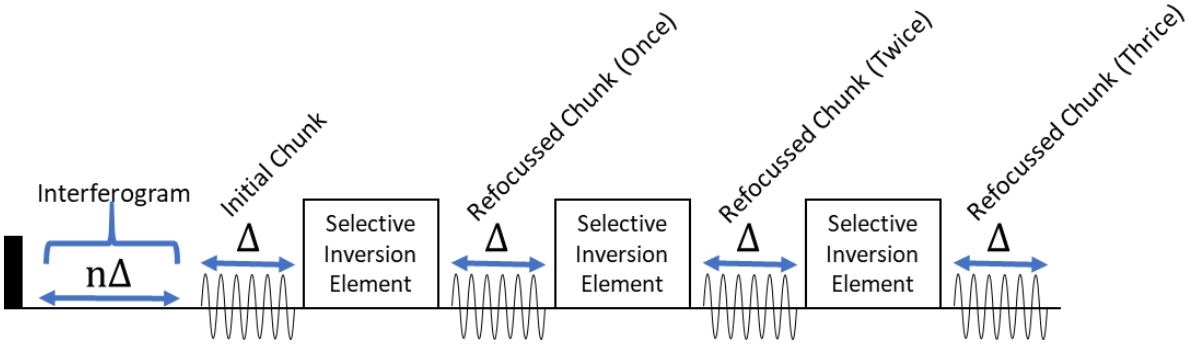

Figure 34: A simplified version of the MSE pure shift sequence with multiple spin echoes.

This was accomplished in practice with the MSE pure shift sequence in Figure 27 by running a series of spectra with incremented values of t1, as a pseudo-2D experiment. Individual FIDs for each t1 value used were extracted as plain text files. A Python 2.7 script (Appendix 8.1.2) was then used to separate the first and refocussed data chunks in each increment. Data chunks were time reversed and complex conjugated as appropriate. Finally, a series of full-length FIDs were produced comprised of the first data chunks or those refocussed a given number of times.

2.6.2 Initial Results

The MSE pure shift sequence shown in Figure 27 was run on a sample of strychnine in $CDCl_3$. 4 scans of 51 increments with a 16 ms chunk time were used. SEDUCE pulses were used for the “Zangger Sterk” elements, as they were found to give the highest signal-to-noise for a standard (non MSE) “Zangger Sterk” pure shift interferogram experiment on this sample. For each increment, five additional spin echoes were acquired. Data chunks acquired after an odd number of additional refocussing pulses were time reversed and complex conjugated before concatenation, as described in the previous Section, with a number of processed FIDs produced, each composed of data chunks that had been refocussed a given number of times. The Fourier transformed spectra arising from these are shown in Figure 35, with noise set to the same level in each spectrum. In all cases we can see that the same signals are present, though the signal-to-noise ratio reduces each time the data is refocussed. The spectra are also shown with the same phase correction applied and some evolution of a 1st order phase error becomes apparent after sequential refocussing cycles. This was corrected in each spectrum prior to summation.

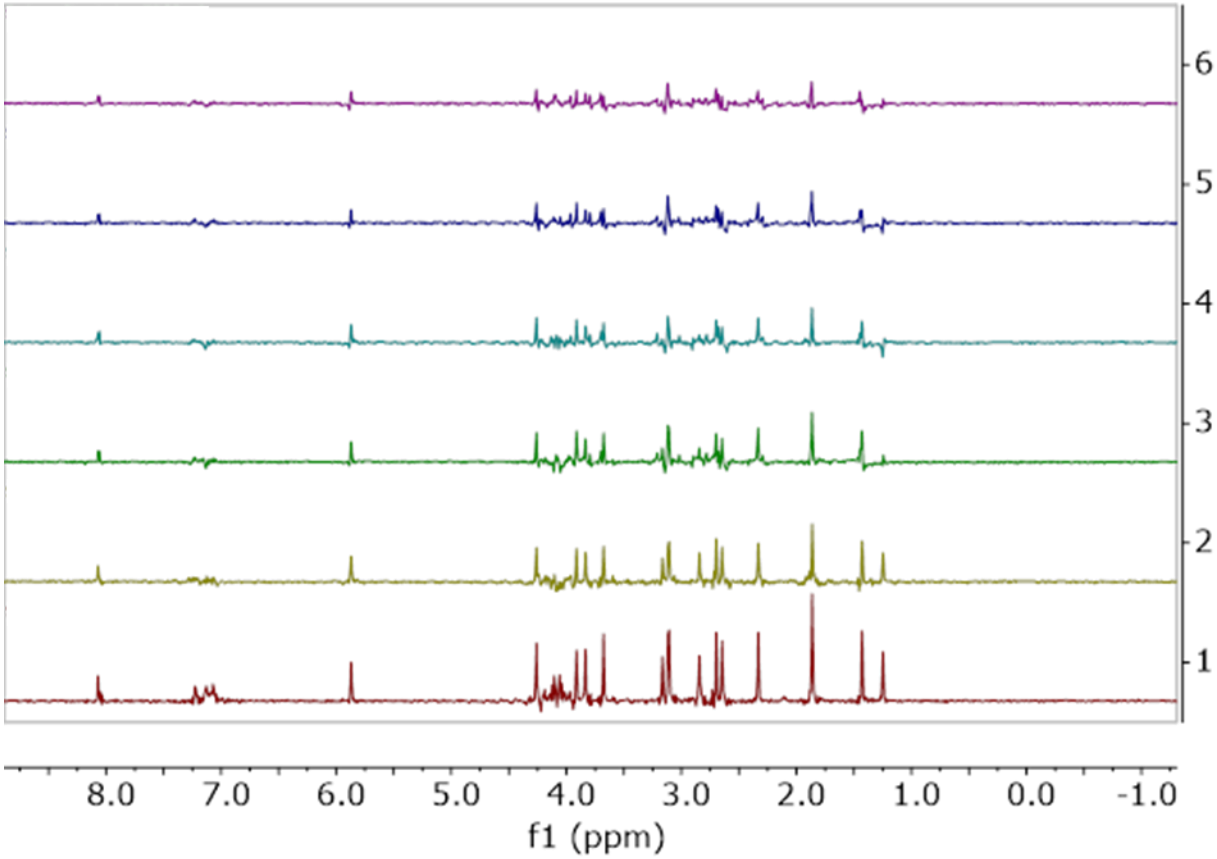

Figure 35: Spectra from MSE pure shift data. The spectrum labelled 1 is essentially a normal “Zangger Sterk” interferogram. The FIDs for 2, 4 and 6 underwent time reversal and complex conjugation.

The spectra comprised of the first two data chunks to be recorded – representing a standard pure shift interferogram's results and a single refocussing cycle (spectra 1 and 2 with reference to Figure 35) were then summed, baseline corrected (1st order polynomial), and the signal-to-noise of each resonance measured. This was compared with the signal-to-noise in the initial non-refocussed spectrum. Resonances show a variety of levels of enhancement, with changes shown in Figure 36. Average enhancement is approximately 8.2%, lower than with previous sequences, but this may be due to the change in selective pulse type. It is worth noting that the minimum enhancement (at ~4%) is higher than any previously trialled phase-sensitive sequence.

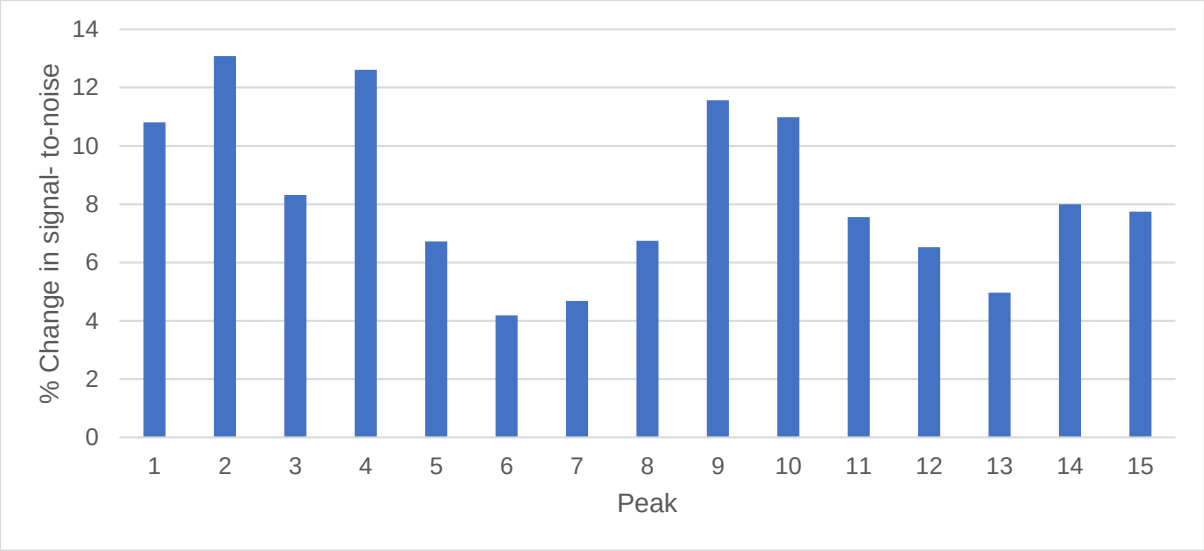

Figure 36: Signal-to-noise ratio of 15 resonances in strychnine from summation of the first two data sets from the MSE pure shift compared to just the non-refocussed. SEDUCE pulses were used.

The spectra comprised of data chunks collected after multiple refocussing cycles (3 – 6 with reference to Figure 35) were manually phase corrected and then incorporated into the summed spectra. Signal-to-noise was averaged across all measured resonances, as shown in Figure 37 with the error bars representing the most and least enhanced resonances. The incorporation of additional refocussing cycles gives the most benefit to average signal-to-noise after two cycles. Some signals continue to improve in signal-to-noise with three or more refocussing cycles, but the incorporation of these extra cycles diminishes signal-to-noise for certain resonances.

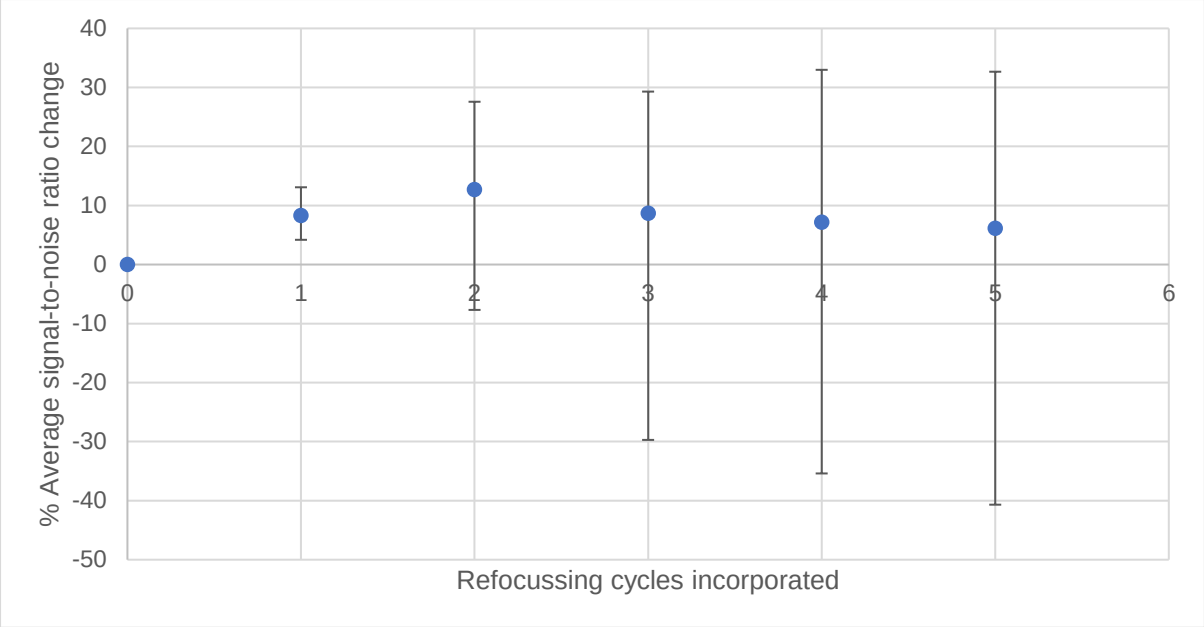

Figure 37: Signal-to-noise improvement from MSE pure shift when additional refocussings are incorporated. Error bars show the most and least enhanced resonances.

The signal-to-noise ratio relative to the initial non-refocussed data was plotted against T_1 and T_2 values for strychnine, shown in Figure 38. Enhancement after summation of all refocussing cycles was considered, but only the first (combining spectra 1 and 2, with reference to Figure 35) and last (combining all 6 spectra in Figure 35) are shown for brevity. No strong correlation with T_1 or T_2 is present, suggesting that another factor is the major driver for the improved (or otherwise) signal-to-noise after refocussing.

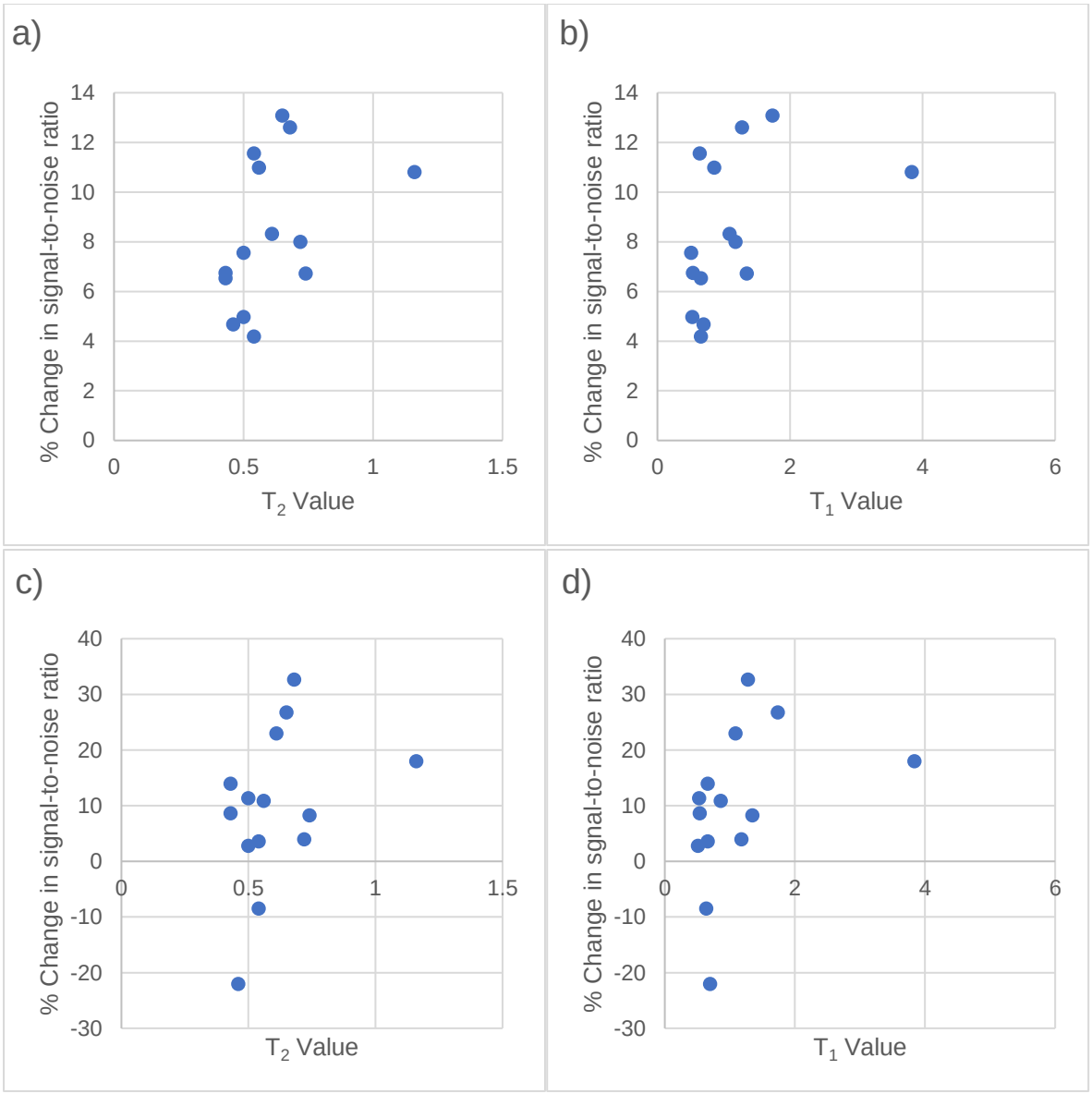

Figure 38: T_1 and T_2 values for strychnine plotted against enhancement observed by the MSE pure shift sequence. (a) and (b) show enhancements from a single refocussing cycle plotted against T_2 and T_1 values respectively (c) and (d) show enhancements from five refocussing cycles plotted against T_2 and T_1 values respectively. (Relaxation values taken from existing work within the group.[64])

An obvious variable which could cause some resonances to refocus more efficiently than others was the choice of selective pulse. The MSE pure shift sequence was rerun using Gaussian 180º and iBURP2 pulses (with otherwise identical parameters). Signal-to-noise ratio was measured in the same way as before and is shown in Figure 39. The Gaussian 180º shows slightly better performance than the SEDUCE pulses, with an average enhancement of 14.2% (compared to 8.2% with SEDUCE pulses). This is approximately the same average enhancement as with the previous Pseudo Real time sequence when Gaussian 180º pulses were used on strychnine. However, the minimum enhancement (at 8.2%) is significantly greater than achieved by previous versions of the sequence (1.9%, Figure 25). This suggests the new sequence behaves more evenly across the different

resonances in the spectrum, which will obviously be a desirable characteristic when looking at novel samples.

The iBURP2 on the other hand showed rather remarkable results, with an average enhancement of 74% and a minimum enhancement of 44% after one refocussing cycle. This exceeds the theoretical maximum of ~41% enhancement from noise-averaging because the signals are substantially more intense in the refocussed second chunk than in the first. A possible explanation is that the second selective pulse used for refocussing is compensating for imperfections in the first selective pulse.

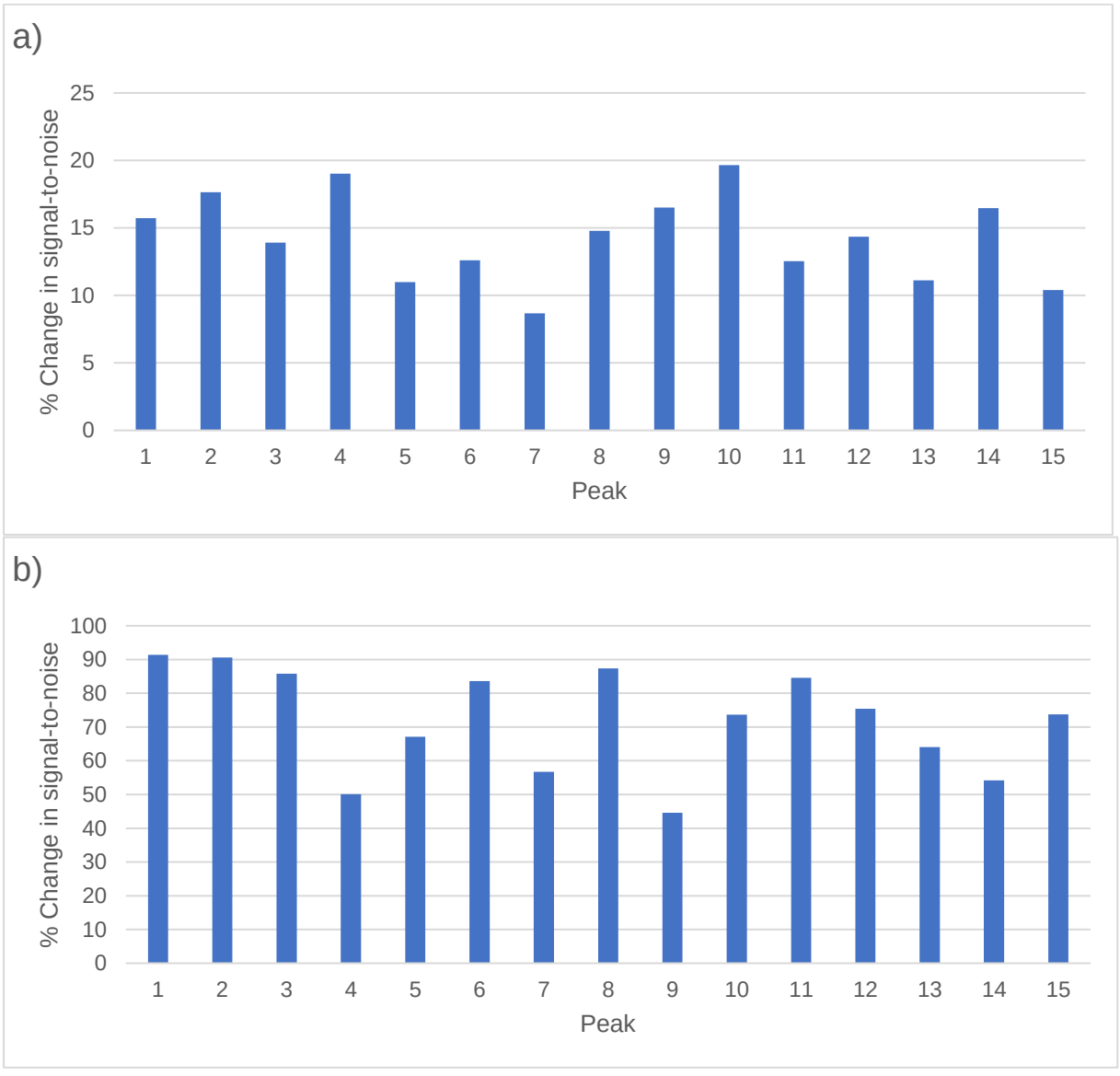

Figure 39: Signal-to-noise ratio of 15 resonances in strychnine from summation of the first two data sets from the MSE pure shift (non-refocused data and a single refocussing cycle) compared to just the non-refocussed data using two different selective pulse types – (a) Gaussian 180º or (b) iBURP2.

2.6.3 Pulse Miscalibration Compensation

Given that in the case of the iBURP2 pulse applied to strychnine signals were actually *increased* in intensity after refocussing it may be that imperfections in the selective pulse are being compensated for by the additional pulses for refocussing in the MSE pure shift sequence. Thus, a systematic examination of the effects of pulse miscalibration was carried out. This was done by repeating the pulse sequence shown in Figure 27, but systematically changing the power of the selective pulse while keeping all other experimental parameters identical. Five refocussing cycles were carried out per scan, though in most cases only the first non-refocussed data chunks and those from the first refocussing cycle were analysed. Instead of summing the Fourier transforms of the FIDs from the first non-refocussed data chunks and the first refocussing cycle these were analysed independently with regard to signal-to-noise for each resonance.

As previous results with the iBURP2 were so remarkable, initial analysis looked at this selective pulse. Results are shown in Figure 40 and at almost every power level tested the refocussed data shows a higher absolute intensity and signal-to-noise ratio than the non-refocussed data. In many cases (4 to 14 dB inclusive) the signal-to-noise in the FID generated from initial, non-refocussed data chunks was less than 41% of the signal-to-noise from the FID generated from one refocussing cycle. In these cases for the purpose of signal-to-noise one would be best to entirely discard the FID generated from the initial non-refocussed data, rather than summing the two FIDs.

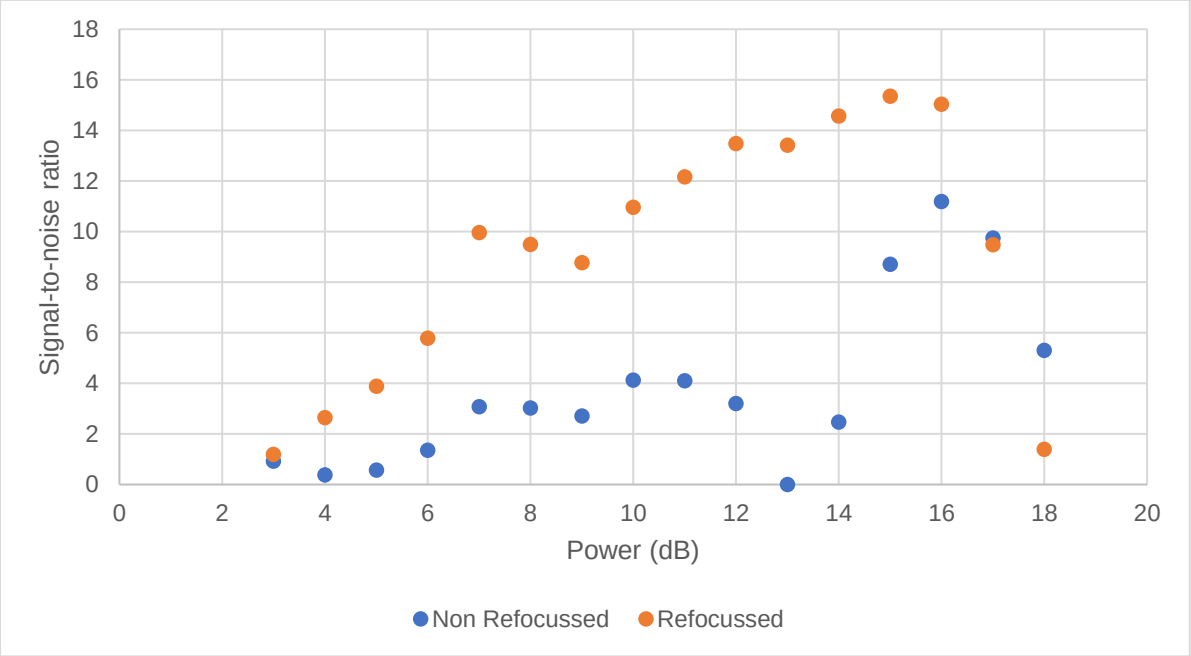

Figure 40: The average signal-to-noise ratio observed in the original and refocused FIDs of strychnine when using iBURP2 pulses of varying power for refocussing.

To check that results were not limited to strychnine in $CDCl_3$, streptomycin in D_2O was also studied in the same fashion. The results, Figure 41, show again that the FIDs generated from the non-refocussed data give consistently lower signal-to-noise than the FIDs generated after one refocussing cycle, and appear to have multiple minima over the range of power values tested.

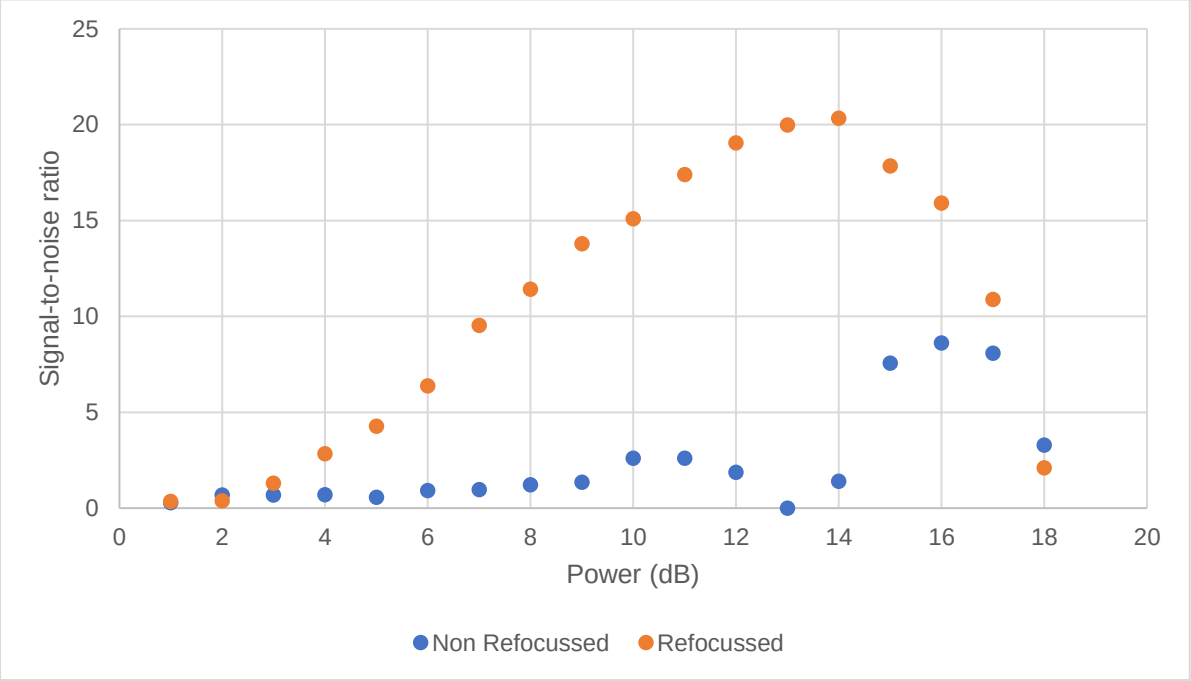

Figure 41: The average signal-to-noise ratio observed in the original and refocused FIDs of streptomycin when using iBURP2 pulses of varying power for refocussing.

The fact that neither of the molecules show a range of power values where the FID generated from the non-refocussed data chunks is more intense than the FID generated after one refocussing cycle is somewhat surprising. This is because it would be expected that when the pulses are perfectly calibrated the major influence on intensity would be expected to be the additional relaxation before the refocussed data is acquired. This may be because the iBURP2 pulse used was miscalibrated with regard to other parameters (such as duration, frequency profile and phase behaviour), and that this miscalibration was severe enough that alteration in power levels could not compensate for it. However, settings for both bandwidth (100 Hz) and duration (46.5 ms) appeared to be reasonable, based on spectrometer calibration (90° pulse width = 7.2 µs). To rule out issues related to the spectrometer and probe a partial sweep of power values was run on a different Varian spectrometer (also 500 MHz but equipped with a broadband observe rather than an indirect detection probe, 90° pulse width = 10.7 µs), shown in Figure 42. These results show broadly similar calibration curves to those observed in Figure 40, where the signals after one refocussing cycle are more intense, sometimes significantly, than the non-refocussed data.

As expected, given the longer pulse widths for the latter probe, there is a significant shift in the X axis – these curves, running from 8 to 13 dB seem to match most closely with the 13 to 18 dB region in the streptomycin data for Figure 41. Note that both spectrometers use the same software for selective pulse generation (VNMRJ 4.2 PBox),[69] so not every potential calibration issue has been ruled out.

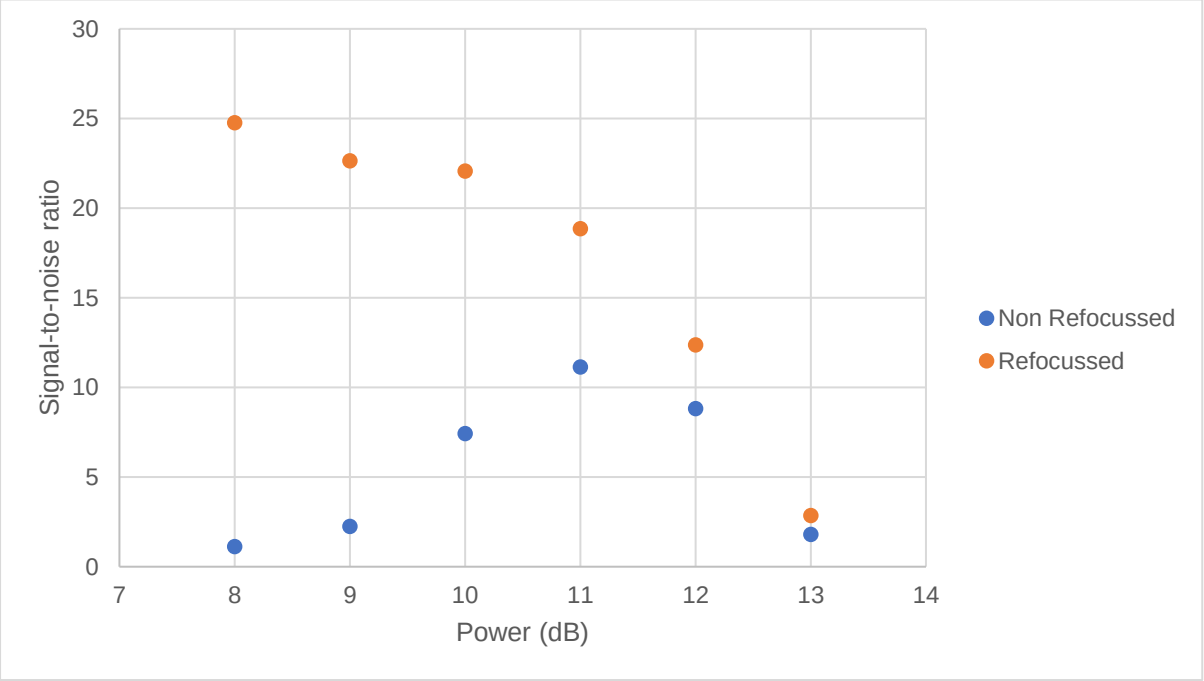

Figure 42: A partial repeat of Figure 40, signal-to-noise ratio values from the MSE pure shift sequence, utilising a different spectrometer and probe but the same sample of strychnine.

So far, only the effects of a single additional refocussing pulse have been examined, and in the most extreme cases this can lead to signals with negligible intensity being refocussed with substantially higher intensities. To demonstrate that this behaviour also extends to additional refocussing cycles, data from an iBURP2 pulse power of 13 dB (which gave a minimal signal-to-noise ratio for non-refocused data and close to maximal signal-to-noise ratio for refocussed data in Figure 41) was considered. Figure 43 shows six Fourier transforms for a region of the spectrum of streptomycin, each relating to FIDs composed of data chunks acquired after an increasing number of refocussing cycles, with spectrum 1 being the initial non-refocussed data. The FIDs relating to 2, 4 and 6 were time reversed and complex conjugated, as described previously in Section 2.6.1. All three show an increased signal-to-noise relative to the preceding refocusing cycle. This suggests that error cancelled by the refocussing pulse is reintroduced and cancelled again by the selective pulses used to refocus the other data chunks.

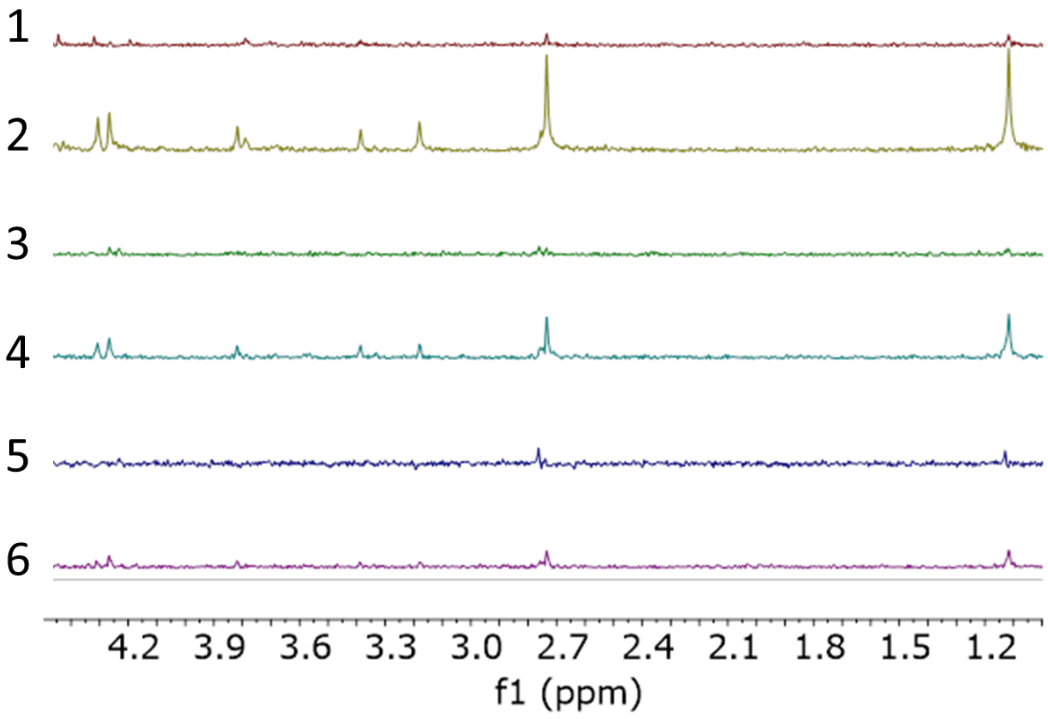

Figure 43: Refocussed pure shift NMR spectra of streptomycin. The first is essentially a normal pure shift 1D result, whilst 2-6 show subsequent refocussing cycles.

All of the iBURP2 pulse miscalibration experiments shown so far have utilised the pulse sequence and phase cycle set out in Figure 27. In this sequence the refocussing pulses have the same phase as the initial selective pulse in the pure shift interferogram (there is 0º shift in phase between them). For further examination of pulse miscalibration the phase cycle of the refocussing pulses was modified to be either 90º or 180º out of phase with the initial pulse. Full phase cycles are shown in Figure 44 along with a copy of the pulse sequence for clarity.

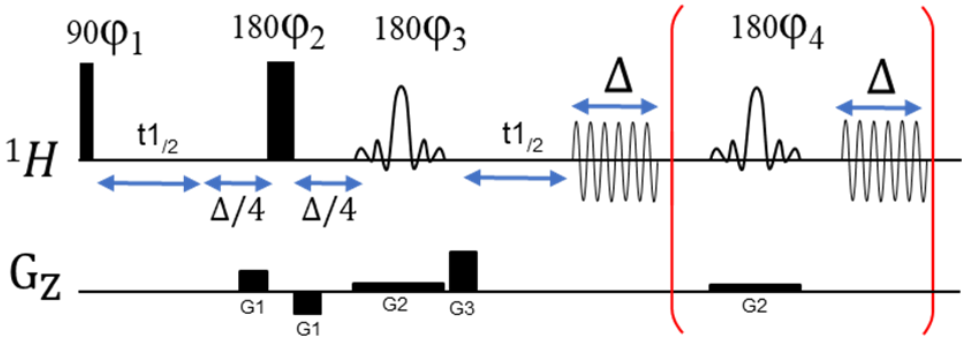

Figure 44: MSE pure shift pulse sequence. Hard pulses are represented by black rectangles, whilst selective pulses are represented by the rounded shapes. Δ indicates the chunk duration. Field gradients are of the indicated sign and strength. Flip angles as indicated, phases as follows, 0º Phase Shift: φ1 = x,y,-x,-y φ2 = x,x,x,x φ3 = x,x,y,y φ4 = x,x,y,y ; 90º Phase Shift: φ1 = x,y,-x,-y φ2 = x,x,x,x φ3 = x,x,y,y φ4 = y,y,-x,-x ; 180º Phase Shift: φ1 = x,y,-x,-y φ2 = x,x,x,x φ3 = x,x,y,y φ4 = -x,-x,-y,-y.

All three phase cycles were tested sequentially by varying the power of the iBURP2 pulse on a sample of streptomycin, as described earlier. All other experimental parameters were unchanged. Figure 45 shows the results of this. As the phase cycles do not differ before the initial non-refocussed data chunks are collected the FID generated should be identical for each of the three experiments, barring any experimental error. It was thus averaged, and standard deviations calculated, with error bars shown. Excellent agreement is shown between the three experiments, suggesting a high degree of reproducibility. The refocussed data examined shows a near identical trend in all three cases, showing that in the case of the iBURP2 the phase characteristics of the selective pulse have no significant effect on compensation for the initial selective pulse. However, it appears clear that the MSE pure shift sequence can yield substantial increases in signal-to-noise over a standard pure shift interferogram approach when using the iBURP2 pulse for the selective inversion elements.

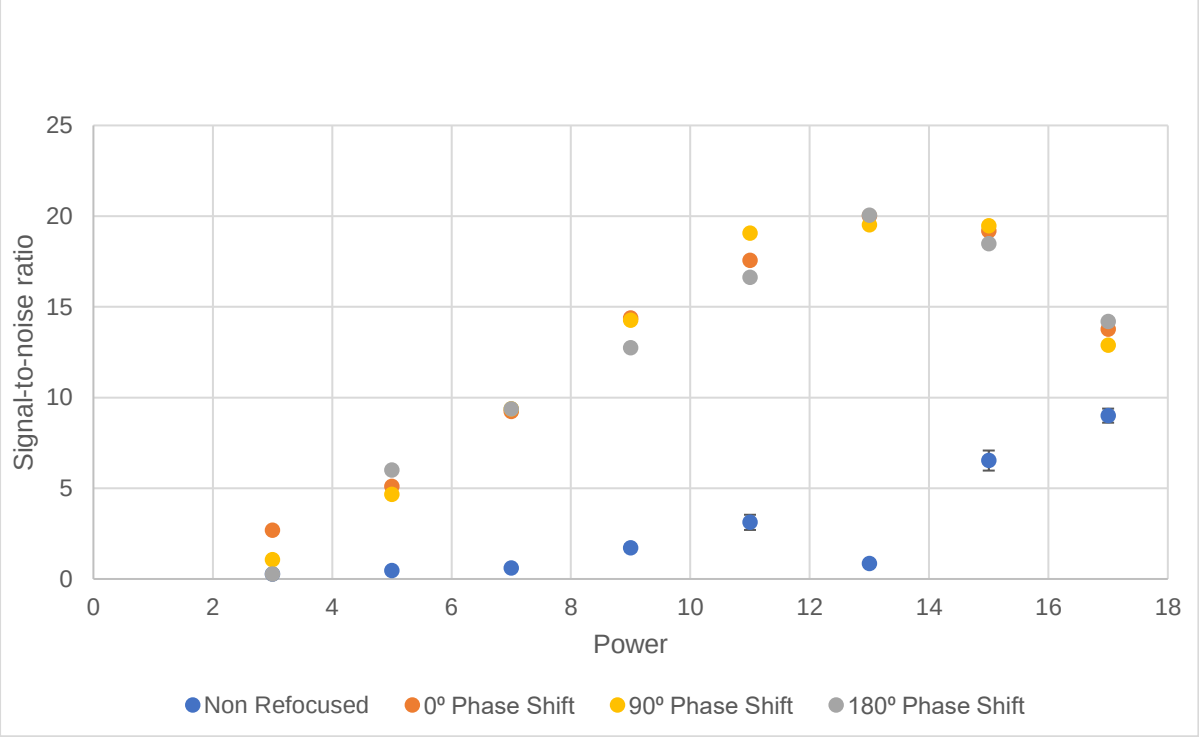

Figure 45: The average signal-to-noise ratio observed in the refocussed FIDs when using iBURP2 pulses of varying power for refocussing, with varying phase relative to that of the first selective pulse in the sequence. Non-refocussed data is averaged, with the error bars showing the standard deviation.

However, so far only the *relative* intensity of signals retained by the refocussing cycles of MSE pure shift has been considered. What has not been considered is the absolute signal-to-noise ratio. If the selective pulse used in the "Zangger Sterk" element is changed this can significantly affect the absolute signal-to-noise ratio. Use of the iBURP2 offers relatively modest absolute intensities, with signal-to-noise in the non-refocussed data peaking at 8.6 when using a power of 16 dB for strychnine (Figure 40). When an identical set of experiments was carried out, but the selective pulse switched to a Gaussian 180º pulse, a

much higher signal-to-noise ratio of 95.1 is achieved when only considering the non-refocussed data (Figure 46). In addition, the signal-to-noise ratio for both the non-refocused data and data collected after one refocussing cycle using a Gaussian 180º pulse show the same maxima (at ~15 dB) and show broadly the same profile, with signal-to-noise falling off consistently away from this optimum. This suggests that whilst pulse miscalibration is a significant issue when using iBURP2 pulses and is partially compensated for by refocusing this is not as true when utilising Gaussian 180º pulses.

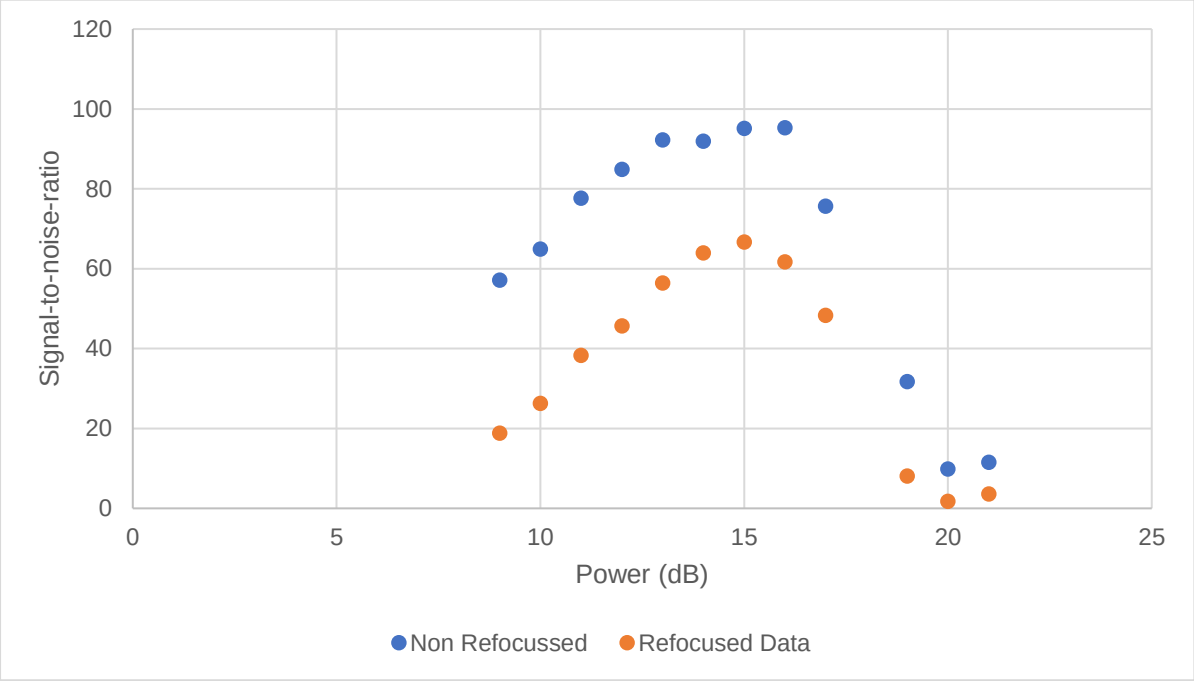

Figure 46: The average signal-to-noise ratio observed in the original and refocused FIDs when using Gaussian 180º pulses of varying power for refocussing.

This is seen more clearly by considering the percentage of the signal-to-noise which is retained after carrying out a refocussing cycle. This shows significant variation, as shown in Figure 47. The 41.4% threshold, above which signals are expected to be enhanced in a summed spectrum is also shown by the dotted blue line. The maximum retention of signal (70.1%) is around a power of 15 dB, where absolute signal-to-noise is also optimised. This suggests that (contrary to the iBURP2) the more poorly calibrated the Gaussian 180º pulse is the less the MSE pure shift sequence can be expected to optimise signal-to-noise.

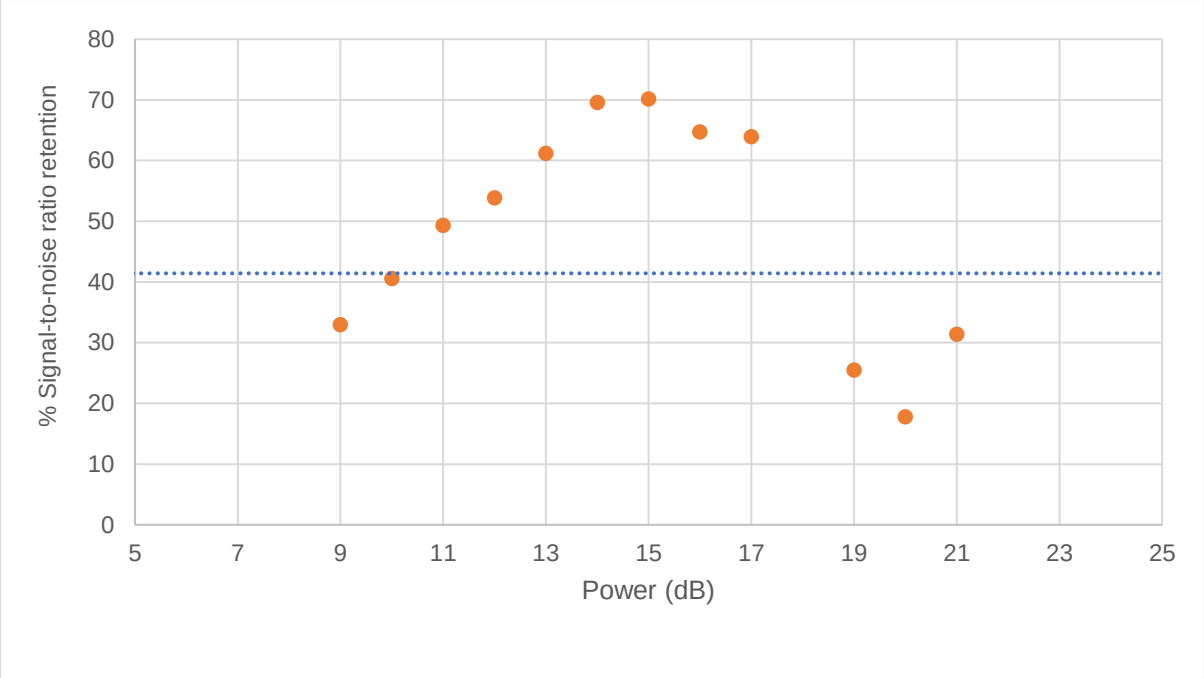

Figure 47: The average signal-to-noise ratio that remains after one refocussing cycle with a Gaussian 180º pulse.

From these results it appears that both the type and calibration of the selective pulses used strongly influences the performance of the MSE pure shift sequence. In the case of the iBURP2 pulse refocussing appears to compensate effectively for imperfections in pulse calibration. Thus excellent enhancement of (relatively poor to start with) signal-to-noise over a standard interferogram experiment can be expected when calibrations are at their worst.

When using the Gaussian 180º selective pulse the enhancements to signal-to-noise that could be expected from MSE pure shift are far lower, because the signal intensity retained after a refocussing cycle is much lower. In addition, the best results appear to be reached when the pulse is well calibrated.

However, the Gaussian 180º pulse offers significantly higher absolute signal-to-noise and thus is preferable overall. With this in mind it is worth comparing the absolute performance of a variety of selective pulse shapes in conjunction with the MSE pure shift experiment.

2.6.4 MSE Pure Shift Results with Differing Selective Pulses

So far, the MSE pure shift sequence has only been trialled on two molecules, with a relatively small number of different selective pulses (SEDUCE, iBURP2 and Gaussian 180º) having been utilised for the “Zangger Sterk” elements. Indeed, only four different combinations of molecule and pulse have been examined (streptomycin has been exclusively examined with an iBURP2 pulse). To better test the general applicability of the method several different molecules were trialled with a wider variety of selective pulse shapes – structures of all four molecules are shown in Figure 48. A variety of solvents were used – quinine and strychnine were in $CDCl_3$, estradiol in CD_3OD and streptomycin in D_2O.

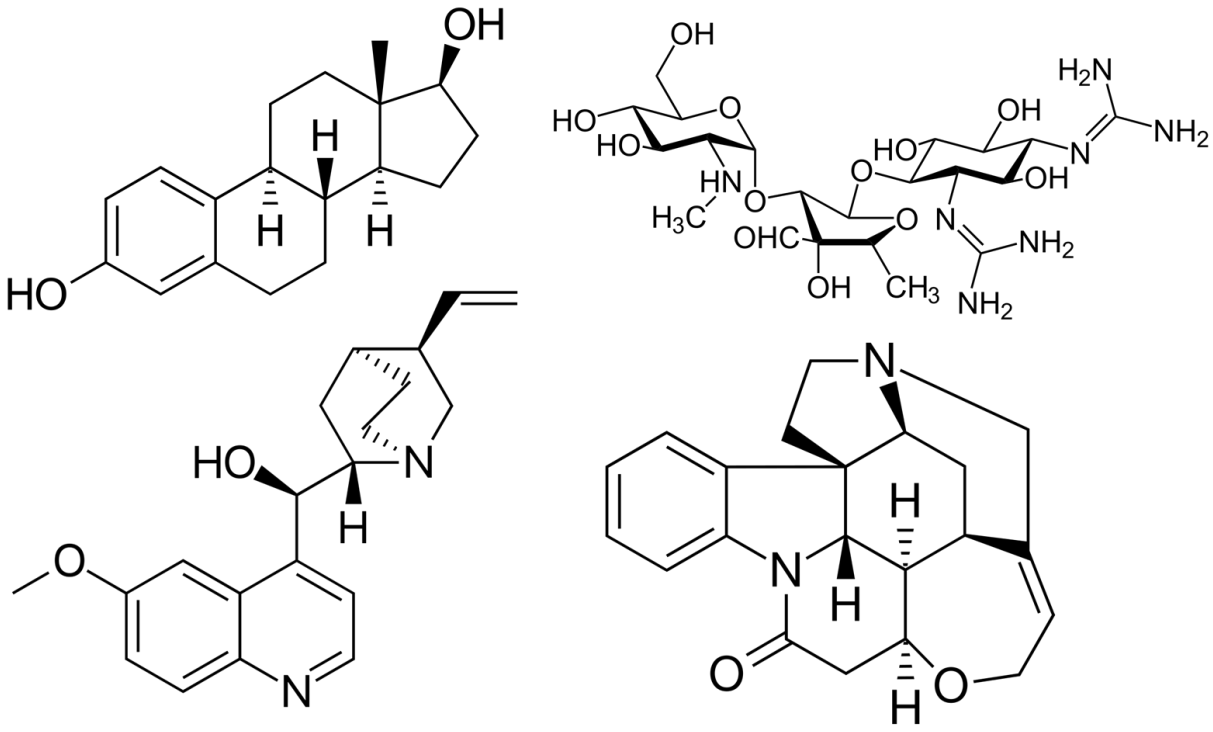

Figure 48: Structures of the molecules examined with the MSE pure shift sequence. Clockwise from top left: estradiol, streptomycin, strychnine, quinine.

Experimental parameters were kept the same in all four cases, with a 16 ms chunk length, 4 scans, 51 t1 increments and the data being refocussed five times. However, only the FIDs generated from the first data chunks recorded per increment and those summed with the FIDs generated from one refocusing cycle were analysed. Spectra were phased manually before addition and baseline correction (1^{st} order polynomial). Signal-to-noise ratios were measured for a number of peaks and averaged. (Intensities prior to averaging are found in Appendix 8.2.)

The different combinations of selective pulse and sample show vastly differing enhancements from the MSE pure shift sequence, as shown in Figure 49. In the majority of cases all signals are enhanced, though the degree of enhancement is minimal in the cases of the SEDUCE and Gaussian 180º pulses. Use of the iBURP2, iSNOB2 and g3 Cascade pulses regularly result in signal-to-noise enhancements of more than the theoretical 41% limit for summing data with the same signal intensity, suggesting that pulse imperfections are being compensated for. However, the combination of g3 Cascade pulses and quinine resulted in a uniform decrease in signal-to-noise for every peak measured. In this case, one would be best to discard the FID resulting from any refocussing cycles. The combination of streptomycin and the iBURP2 pulse results in the opposite. The signal intensity in the FID collected after one refocussing cycle is sufficiently higher than the intensity in the FID generated from the initial non-refocussed data chunks that signal-to-noise drops upon their summation. Thus, the data for streptomycin shows the FID after one refocussing cycle compared to the non-refocussed FID, rather than their summation.

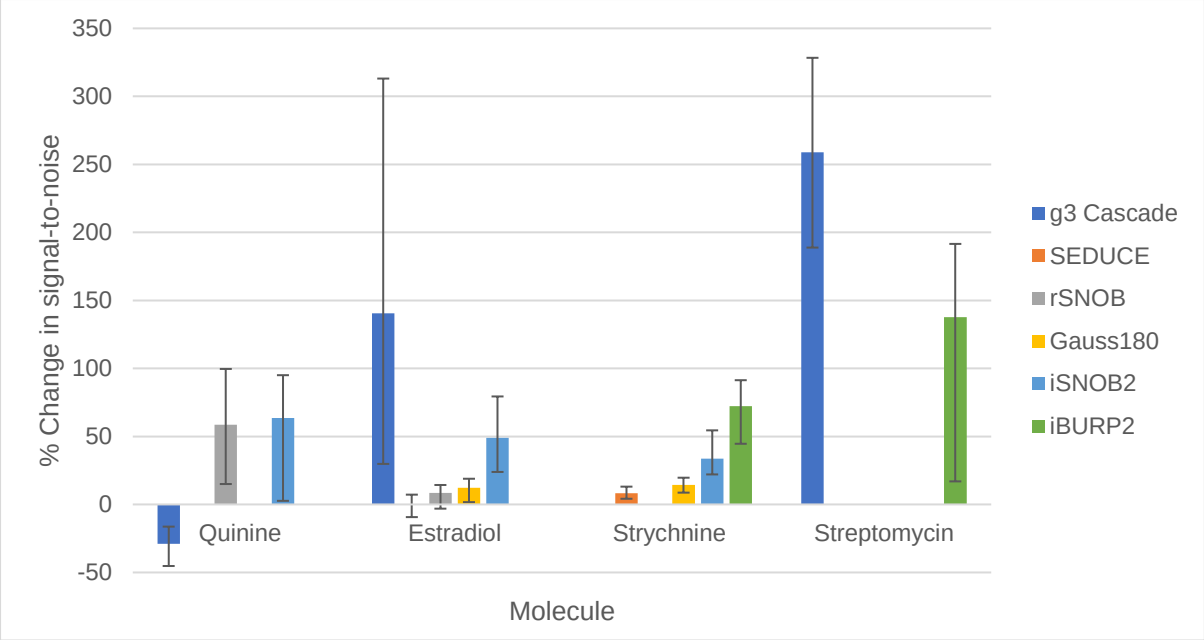

Figure 49: Signal-to-noise change after summation of the Fourier transform spectra of the FID generated from non-refocussed data of the MSE pure shift experiment with the first refocussing cycle. The combination of streptomycin and the iSNOB2 pulse is the exception, as noted in the text.

However, the degree of enhancement compared to the basic pure shift sequence is only half the story. Assuming the same spectral quality is retained, the absolute signal-to-noise will be of more interest to the experimental chemist. This is shown in Figure 50, with signal-to-noise ratio for the MSE pure shift both before and after summation. Notably the SEDUCE and Gaussian 180º pulses show consistently higher signal-to-noise ratios than the other types of selective pulses. Conversely, the pulses which showed substantial enhancement by the MSE pure shift sequence, iBURP2 and iSNOB2, result in relatively low absolute signal-to-

noise. It may be that Gaussian 180º and SEDUCE pulses are not enhanced significantly by MSE pure shift because there is little loss of intensity to compensate for. However, somewhat gratifyingly, the small degree of enhancement provided by the MSE pure shift sequence is enough to change which of the two selective pulses yields the highest signal-to-noise in both estradiol and strychnine – the SEDUCE is favoured before incorporation of data from a refocussing cycle, the Gaussian 180º after.

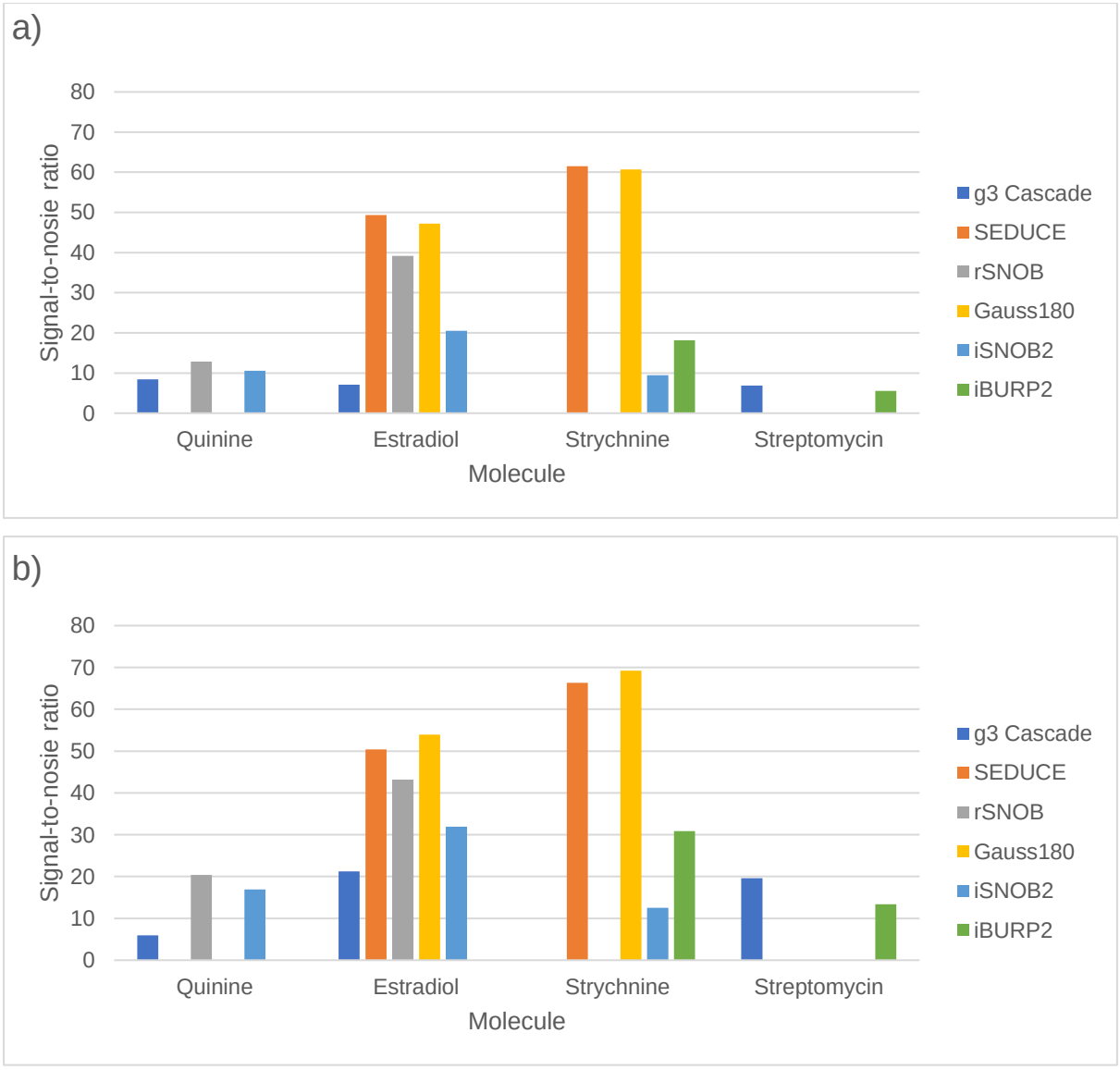

Figure 50: (a) Signal-to-noise ratio for the Fourier transform spectra of the FID generated from non-refocussed data with the MSE pure shift experiment and (b) the signal-to-noise ratio after summation with the first refocussing cycle. The combination of streptomycin and the iSNOB2 pulse is the exception, as noted in the text.

A substantial number of combinations of selective pulse types are missing from the above analysis. This is largely due to cases where significant side band artefact signals were present that hampered analysis of the spectra. These were more of an issue with quinine and streptomycin, where significant solvent peaks (residual $CHCl_3$) and impurities (HDO) were present. An example is shown in Figure 51, which contains several Fourier transforms

from MSE pure shift experiments combining quinine and the Gaussian 180º pulse. A PSYCHE spectrum is also shown, which is largely artefact free. Genuine signals from Fourier transforms of the MSE pure shift FIDs generated from the non-refocussed data chunks and after a single refocussing cycle are difficult to distinguish from artefacts, hence its exclusion from the above analysis. Interestingly, by refocussing cycle number 3, artefacts are significantly attenuated compared to the genuine signals. This may be because signal intensity becomes increasingly relaxation weighted in later refocussing cycles. Whilst this effect was not observed in previous experiments (Figure 38) those only examined different chemical environments within the same molecule. It may be that relaxation properties differ enough between solvent/impurity and solute molecule that this effect is observed, though T_1 and T_2 values were not measured. However, signal-to-noise is poor after multiple refocussing cycles have been applied and artefacts are still not attenuated to the level PSYCHE achieves, so there is likely to be little practical utility for this.

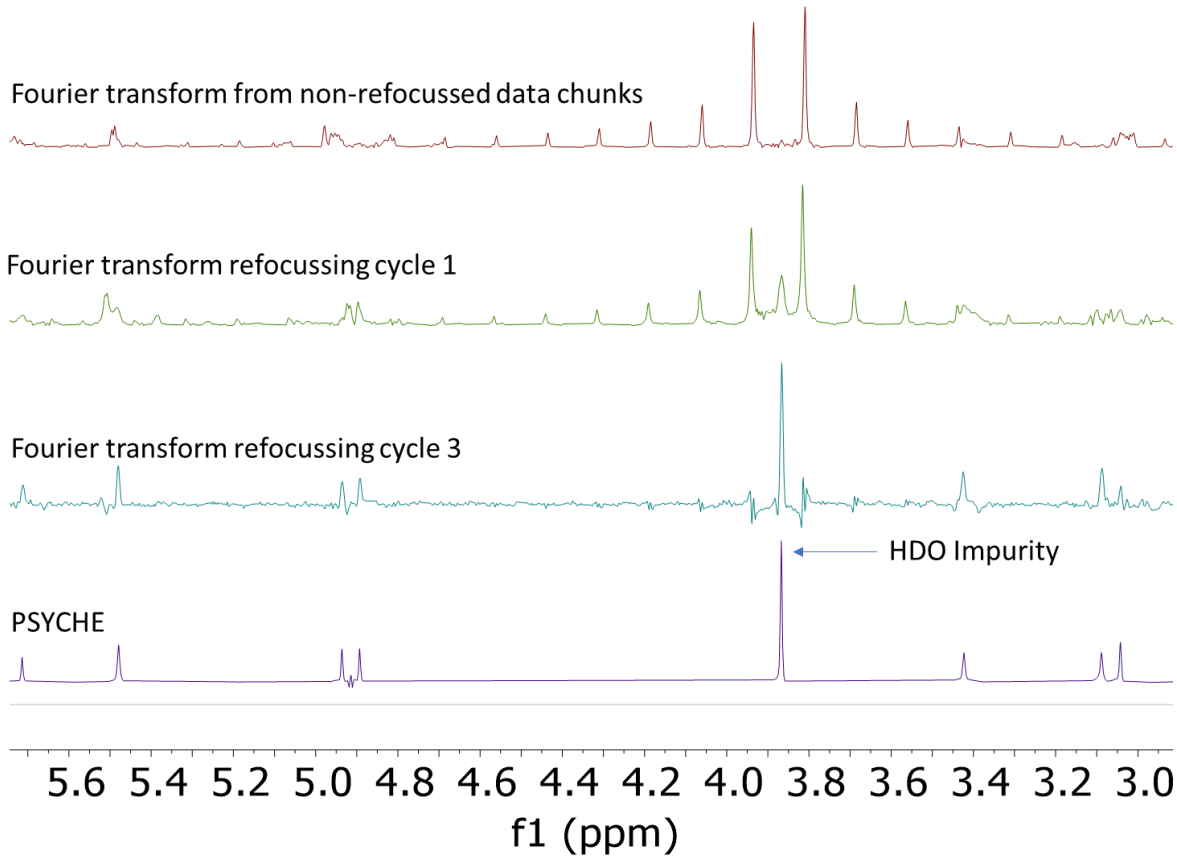

Figure 51: Fourier transforms relating to data chunks after multiple refocussing cycles from the MSE pure shift experiment, applied to a sample of quinine in $CDCl_3$ using Gaussian 180º pulses for refocussing. Significant sideband artefacts can be observed due to the HDO impurity. A PSYCHE spectrum is also shown for reference.

The success (or otherwise) of the different combinations of samples and selective pulses are summarised in Figure 52. Relative performance is shown by the left fill – how much the MSE pure shift sequence improves signal-to-noise for a given combination of selective pulse and sample. Combinations where signal-to-noise has improved by at least 14% (equivalent to a 30% increase in scans) are marked in green, combinations providing enhancements between 0% and 13% in orange and red is used to indicate that the use of MSE pure shift has diminished signal-to-noise.

Absolute performance, relative to the other selective pulses used on that sample is shown by the right fill. A green fill is used when the signal-to-noise ratio of the MSE pure shift spectra after summation was at least 70% of the spectra with the highest signal-to-noise ratio for that sample, an orange fill when it was between 69% and 50%, and a red fill otherwise. A black fill indicates spectra were acquired, but not analysed due to significant sideband artefacts from the solvent. A white fill indicates combinations that were not tested.

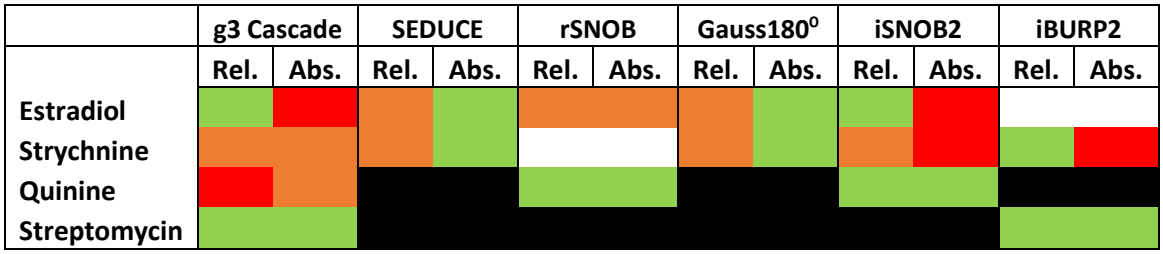

Figure 52: A summary of selective pulse types and whether they offer significant enhancement when used with the MSE pure shift sequence when analysing different molecules. The left fill on each rectangle indicates relative performance, whilst the right fill indicates absolute performance. A green fill indicates good performance, orange moderate, and a red fill poor. Black filled rectangles were not analysed, due to extensive artefacts, and white filled combinations were not tested.

Overall, the only cases where the MSE pure shift performs well in *both* a relative and absolute sense is where the SEDUCE and Gaussian 180º pulses fail due to significant generation of artefacts. It may be that MSE pure shift is a useful tool for taking a set of experimental parameters that will yield a low signal-to-artefact ratio spectrum with poor signal-to-noise and maximising the signal-to-noise ratio. However, the sample size here is too small to come to any firm conclusion, beyond that the choice of selective pulse matters greatly to MSE pure shift.

2.6.5 Comparison with PSYCHE

So far, analysis of the MSE pure shift sequence has considered the enhancement of signal-to-noise ratio from summing multiple data chunks recorded during the same increment. This is useful for comparison to existing pure shift interferogram methods which use the same method of selective inversion (*i.e.* the "Zangger Sterk" approach), where it offers potentially major improvements in sensitivity, depending on choice of molecule and selective pulse.

However, a comparison to PSYCHE, which is often regarded as the modern state of the art interferogram method, is required. To this end a PSYCHE experiment was performed on each of the molecules described in the previous Section. Parameters for the PSYCHE were matched to the MSE pure shift spectra as far as possible, including data chunk duration (16 ms), scans (4) and t1 increments (51). Total experiment time was consistent between the two at 7.5 minutes. A flip angle for the CHIRP pulses of 6.0º was chosen, which represents a very conservative choice with regards to the expected signal-to-noise ratio (though will minimise artefacts).

The resultant spectra were Fourier transformed and processed identically to the MSE pure shift spectra before peak picking. A comparison of the average signal-to-noise across the four molecules tested in the previous Section is shown in Figure 53. In all cases the data for a standard "Zangger Sterk" interferogram approach (data from the FID produced from the initial non-refocussed data chunks in MSE pure shift) and the MSE pure shift data relate to the selective pulses which yielded the highest signal-to-noise ratios for each molecule.

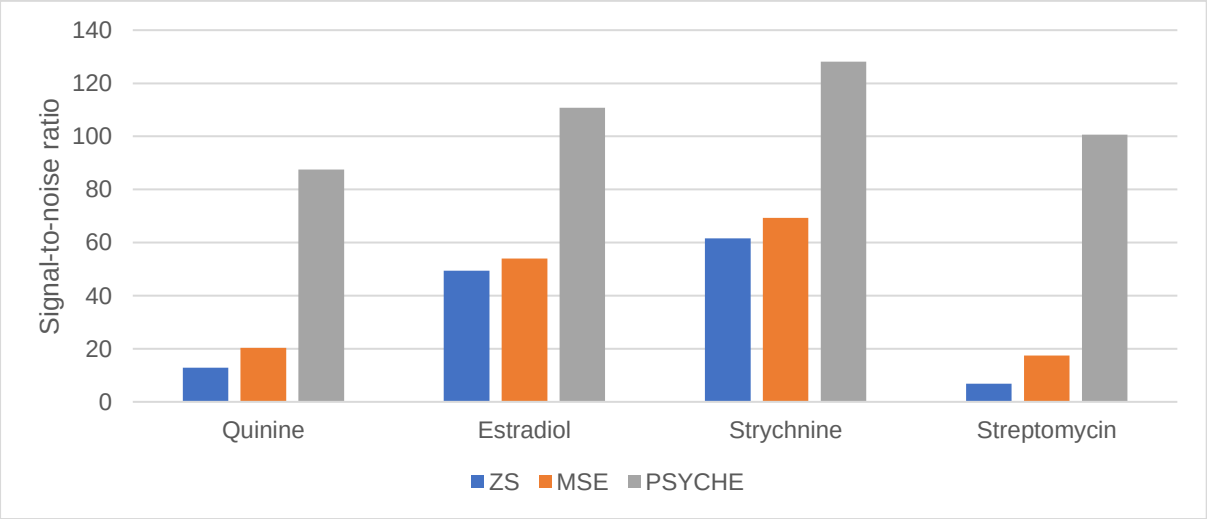

Figure 53: Comparison of absolute signal-to-noise from PSYCHE and "Zangger Sterk" spectra run with the MSE pure shift acquisition scheme. Data labelled "ZS" is the initial non-refocussed data from experiments using the following selective pulses: quinine – rSNOB; estradiol – SEDUCE; strychnine – SEDUCE; streptomycin – g3 Cascade. The MSE data combines the non-refocussed data with that acquired after one refocussing cycle, using the following selective pulses: quinine – rSNOB; estradiol – Gaussian 180º; strychnine – Gaussian 180º; streptomycin – g3 Cascade.

Whilst neither of the experiments have been particularly optimised for signal-to-noise with regard to experimental parameters PSYCHE dramatically outperforms both basic “Zangger Sterk” interferogram approach and the “Zangger Sterk” experiment when enhanced by MSE pure shift acquisition, often achieving more than double the signal-to-noise. For context, however, it is worth bearing in mind that all methods have enormous sensitivity penalties. To demonstrate this an 8 scan 1D ^{1}H spectrum for each molecule was identically processed and peak picked. Signal-to-noise was measured and then extrapolated to what could be expected from a 144 scan spectrum – representing a theoretical 7.5 minutes of acquisition, equivalent to the pure shift spectra. The results, Figure 54, show that sensitivity losses for all pure shift methods are phenomenal.

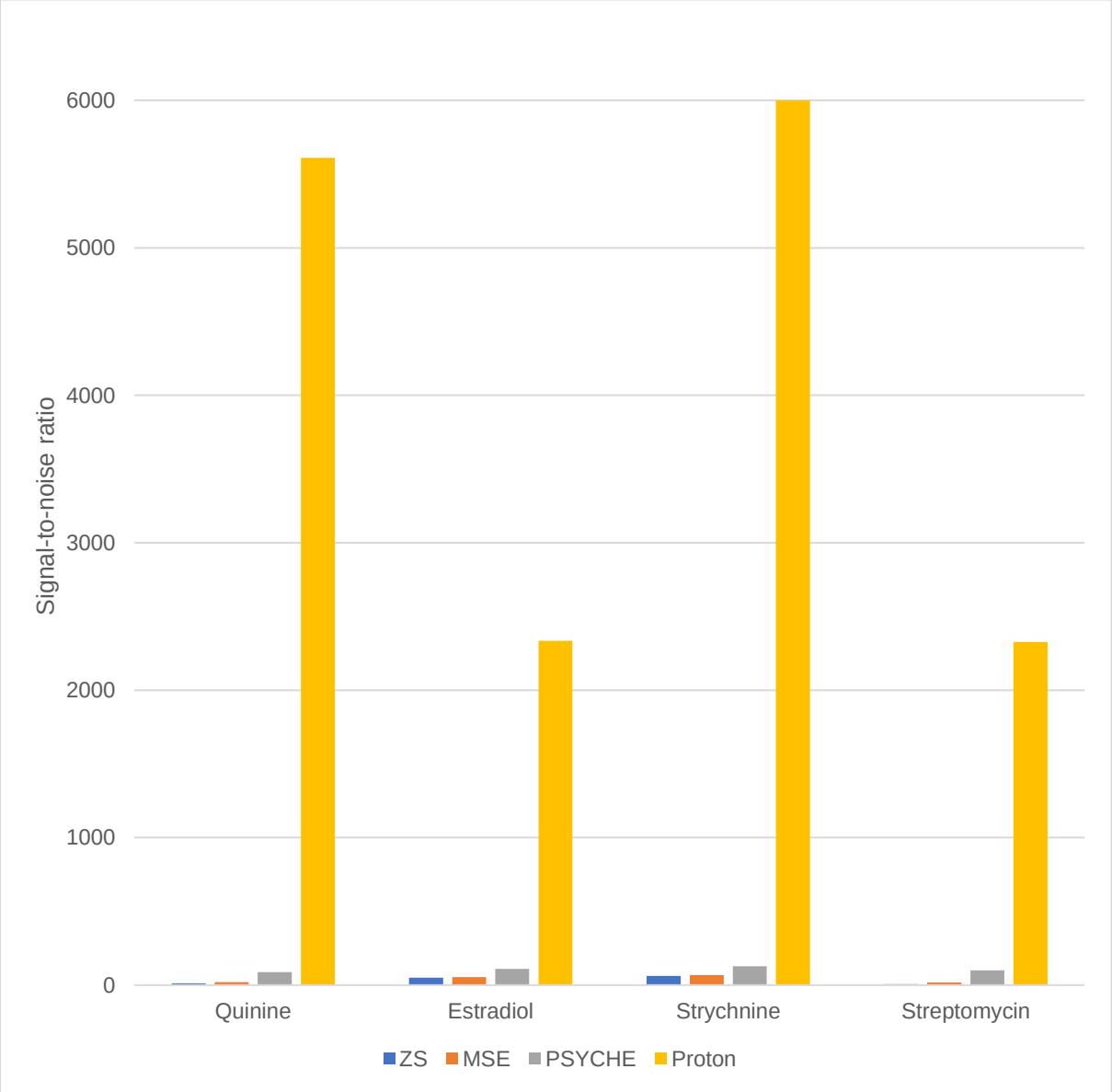

Figure 54: The signal-to-noise from “Zangger Sterk” spectra run with the MSE pure shift acquisition scheme and a PSYCHE spectrum (using the same data as Figure 53) compared to the signal-to-noise ratio that could be expected from running a proton spectrum for the same amount of time.

2.7 Conclusion

The MSE pure shift scheme presented here applied to the “Zangger Sterk” homodecoupling technique offers a more efficient way to collect data in an interferogram, by maximising the signal-to-noise ratio that can be extracted from a single pseudo-2D increment. This is done with no increase to experimental time, and simply requires additional offline processing steps. After summation of the data collected this can offer a potentially significant improvement in signal-to-noise ratio for a given selective pulse or sample. If one were sensitivity limited, rather than limited by a phase cycle this could represent a saving in experimental time, as good signal-to-noise could be achieved with a reduced number of scans. In combination with the EXACT (Extended Acquisition Time) methodology where increments in a psuedo-2D pure shift spectrum can be skipped,[62,63] the reduction in both increments and number of scans could yield substantial reduction in experiment times.

However, the sensitivity increase offered by MSE pure shift over a more regular interferogram using the “Zangger Sterk” approach to homodecoupling is much less than that offered by PSYCHE, the current state of the art broadband pure shift experiment with regard to signal-to-noise.[70] The PSYCHE method itself is unfortunately incompatible with the MSE pure shift acquisition scheme since the selective inversion element is incapable of selecting for the same group of spins repeatedly.[33] Thus the MSE would not actually refocus the same group of spins in each refocussing cycle.

A particular trait of the MSE pure shift sequence which may be useful for reaction monitoring is that it gives a range of enhancements, rather than enhancing all signals uniformly. If how a given sample will behave is known beforehand then the most enhanced signals can be used to report on the concentration change of their containing molecules. Such an approach could be useful for maximising time resolution in an experiment, as it allows for the most sensitivity within a given experimental duration.

Conversely some signals are diminished in the final summed MSE pure shift spectra. However, the results of a standard pure shift interferogram and any number of refocussed sets of data can be processed fully independently of one another. Therefore, there is no reason an experimenter cannot simply examine whichever FID (or combination of FIDs) gives the most intense signals in a region of interest.

Whilst the MSE pure shift acquisition presented here may have some niche uses, such as compensation for pulse miscalibration, it is outclassed for acquisition of 1D pure shift spectra by the PSYCHE experiment. However, as it is simply an acquisition scheme, it should be able to be integrated into other experiments and it is my hope that the methodology may find a more practical application in the future.

2.8 Future Work

As laid out in the conclusion it appears that MSE pure shift methodology (applied to a "Zangger Sterk" approach) cannot compete with PSYCHE. It is worth noting that the BIRD selective inversion element is also capable of repeatedly selecting for the same group of spins. Thus, it could be used in conjunction with an MSE pure shift approach. It has not been explored in this thesis, partly because BIRD spectra typically offer extremely low sensitivity.[33] However, BIRD can offer extremely high levels of sensitivity when applied to experiments where the sensitivity penalty for isotopic selection has already been paid.[34] Whilst the MSE pure shift scheme is not applicable to the higher sensitivity real time pure shift HSQC it could be used in conjunction with pseudo-3D experiments.[71]

Indeed, the MSE pure shift scheme may find application to pseudo-3D experiments, which typically offer reduced artefacts, superior resolution and improved line shape over their 2D and pseudo-2D cousins.[38,72,73] For example the 2D*J*-ZQS-PSYCHE experiment requires a triple axis field gradient probe – nonstandard equipment, whilst the "Zangger Sterk" version of the experiment does not.[74] As these experiments often have extremely long acquisition times (multiple hours) even a modest improvement in sensitivity could lead to a significant saving in experimental time.

Another potential application of the MSE pure shift sequence could be to produce *J* scaled spectra. Such schemes allow differential evolution between coupling and chemical shift, rather than simply allowing negligible coupling evolution. This can allow easier measurement of small couplings[75] or offer some of the resolution advantages of pure shift whilst retaining coupling information.[76] As the refocussing elements used in the predecessor to the MSE pure shift sequence already differentially manipulate coupling and chemical shift evolution it may be possible to design a variant experiment that can produce both a "normal" pure shift interferogram and a *J* scaled spectrum from the same experiment.

3 Off-Resonance SHARPER

3.1 Introduction

This Chapter deals with the basis behind improvements to the SHARPER (Sensitive Homogenous and Resolved Peaks in Real time) NMR experiment, a technique introduced to improve both signal-to-noise and bypass complications from poor or changing field homogeneity when using NMR spectroscopy for reaction monitoring.[36]

3.1.1 Reaction Monitoring by NMR Spectroscopy

Monitoring chemical reactions by following changes in reactant, intermediate and product concentrations can allow chemists to determine reaction kinetics and mechanisms.[77] For solution state reactions NMR spectroscopy is inherently well suited to this kind of monitoring for several reasons:

- NMR spectroscopy is an inherently quantitative technique, as the strength of a signal (in a properly parameterised experiment) will be directly proportional to the quantity of any given reactant or product.
- A wide choice of different nuclei with NMR active isotopes are readily experimentally accessible.[78] This allows a broad range of chemical reactions to be investigated.
- Most nuclei have relaxation times on the order of seconds,[78] allowing similar time resolutions, sufficient for a great deal of reactions. This can be extended further by more sophisticated experimental techniques (giving time resolutions on the order of milliseconds) at the cost of sensitivity.[79]
- Sensitivity is relatively low compared to many other types of spectroscopy,[80] but is still sufficient to allow use of relatively small (~700 µL) sample volumes.
- NMR spectroscopy can provide a significant amount of structural information, which may be useful in determining reaction mechanisms.[80]

In recent years ^{19}F has become a popular choice for reaction monitoring by NMR spectroscopy, owing to its near 100% natural abundance and high gyromagnetic ratio combined with its presence in a great deal of chemistry of interest. Indeed, some 25% of pharmaceuticals and almost 50% of agrochemicals contain at least one ^{19}F nucleus.[81] It has a wide chemical shift range and minimal homonuclear coupling in most cases, so spectral overlap is rarely a problem.

Consequently a great deal of hardware development has been invested into its measurement. ^{19}F can be monitored by an increasing number of low field “benchtop” NMR spectrometers,[82] which are substantially lower cost and can be more versatile than traditional NMR spectrometers due to their small size[83] – for example, they could be conceivably placed inside a fume hood if required. The relatively weak magnetic fields used do lead to reduced signal-to-noise, but this can be sidestepped either by hyperpolarisation techniques[84,85] or post processing.[86] Hardware developments relevant to ^{19}F have not been limited to low field – some modern probes are capable of rapidly switching between ^{1}H and ^{19}F channels.[87] Such hardware enables NMR experiments where multiple nuclei are simultaneously detected,[88] yielding additional information that may allow better understanding of a reaction system.

Unfortunately, there are limitations with monitoring reactions using standard 1D and 2D NMR spectroscopic methods. In particular, most standard NMR spectroscopic techniques rely on maintaining a highly stable magnetic field to provide sensitive high-resolution spectra – typically uniform to around 1 part in 10^9 over the active volume (typically around 500 µL)[89] in order to avoid deterioration in linewidth and signal-to-noise. This is normally achieved by use of shim coils, which are ordinarily optimised based on maximising the intensity of the solvent signal, usually using either ^{2}H or ^{1}H.[90] However, a reaction which causes a gas to be evolved will temporarily disrupt the homogeneity of the magnetic field during the reaction. As this disruption is transient it will be impossible to compensate for this using the shim coils, potentially making measurement difficult or impossible with conventional NMR techniques.[36]

Photochemistry is another example of where reaction monitoring by NMR spectroscopy is challenging, relying on illuminating a small sample volume deep inside a narrow probe inserted into a superconducting magnetic field. A successful approach to this problem has been to generate the light outside of the NMR spectrometer with an LED and then use a fibre optic cable to direct the light onto the sample.[91,92] However, such setups are very sensitive to experimental errors. The end of the fibre optic cable needs to be placed outside, but as close as possible, to the detection region. Misplacement inside will significantly disturb magnetic field homogeneity. Conversely, if the fibre optic cable is placed too far from the detection region the rate of product formation can be expected to be highest close to the fibre as intensity will rapidly fall off due to the inverse square law. This means rates of reaction may be convoluted with the time taken for products formed near the fibre optic cable to diffuse into the detection region.[93]

Experimental fixes have been proposed to the problem of magnetic field inhomogeneity, which can acquire high resolution spectra with good line shapes relatively independently of the shimming conditions – though typically not without significant trade-offs. For example, the UPSIF (Ultrahigh Resolution Pure Shifts in Inhomogeneous Fields) technique can yield high quality broadband NMR spectra regardless of magnetic field conditions. This intermolecular quantum coherence evolves at a rate based on the frequency difference between the solvent and solute, which can overcome influences of magnetic field inhomogeneity on absolute frequencies.[94] However the inclusion of a constant time period will make signal intensities dependent upon relaxation and coupling properties, rather than just concentration, complicating data analysis. As a pseudo-2D experiment it also requires lengthy minimum data collection times, and so could not be employed in examining fast chemical reactions.

An alternative, which may offer something closer to standard acquisition is the utilisation of so called “shim pulses” which cause resonances to behave as if they are in a different magnetic field to the one provided by the hardware.[95] These could conceivably be used to eliminate static magnetic field inhomogeneity created by modification to NMR probes used in reaction monitoring *e.g.* when incorporating fibre optics for photochemistry. By observing what disruption was caused to magnetic field homogeneity before starting the reaction shim pulses could be calibrated to cancel it out. However, such an approach could not be expected to be able to effectively compensate for field inhomogeneity that changed during the reaction *e.g*. arising from bubbling.

There is, however, an experimental method which is capable of producing intense high quality NMR spectra from a sample in a constantly changing inhomogeneous field in real time. This is the SHARPER experiment proposed by the University of Edinburgh, which integrates refocussing pulses applied every few milliseconds between data chunks of acquired chemical shift evolution in order to refocus heteronuclear coupling and the effects of magnetic field inhomogenity.[36] The work described in this thesis attempts to reduce or eliminate some of the drawbacks of SHARPER (described in the next Section) whilst retaining the benefits of insensitivity to both static and dynamic magnetic field inhomogeneity in the sample.

3.1.2 SHARPER

SHARPER is an NMR experiment well suited to difficult reaction monitoring problems. It can produce high signal-to-noise spectra with narrow linewidths under conditions where more standard NMR spectroscopic approaches fail. An example of a SHARPER ^{19}F spectrum and a standard 1D ^{19}F, both recorded in an inhomogeneous field is shown in Figure 55 (note that the spectra have been scaled so maximum peak intensity is approximately the same, thus noise is not). Unlike other methods which are tolerant of field inhomogeneity, such as UPSIF[94] SHARPER works in real time (*i.e.* within the time period of a single FID) and so can be utilised for monitoring fast chemical reactions.[36]

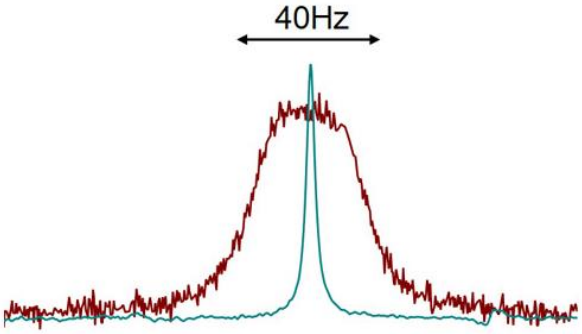

Figure 55: A ^{19}F spectrum (red) and equivalent SHARPER spectrum (blue) in an inhomogeneous field. (Adapted from A.B. Jones et al 2017.[96])

SHARPER achieves this field inhomogeneity compensation by repeatedly refocussing the NMR signal using 180º refocusing pulses between acquired chunks of data, with the pulse sequence shown in Figure 56. Note that while only hard pulses are used here a selective version of the experiment, sel-SHARPER uses a selective DPFGSE (Double Pulsed Field Gradient Spin Echo) for selection and selective 180º refocussing pulses throughout the FID.[36]

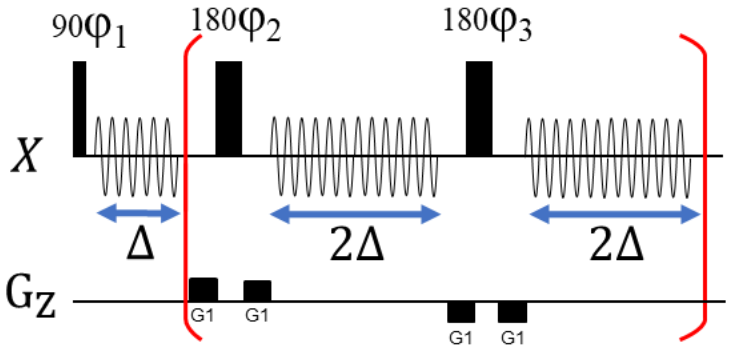

Figure 56: The SHARPER pulse sequence. Flip angles and signs of field gradients are as indicated. "X" can be any nucleus of interest. Phase cycle as follows φ1 = x, x, -x, -x, y, y, -y, -y; φ2 = y, -y, y, -y, x, -x, x, -x; φ3 = -y, y, -y, y -x, x, -x, x; and receiver phases are x, x, -x, -x, y, y, -y, -y.

Figure 57 demonstrates the refocussing effect of the sequence above, with the initial magnetisation placed along the Y axis by a 90_X^o pulse. Evolution of the magnetisation under an inhomogeneous magnetic field dephases coherent magnetisation over a given period, Δ. A 180_Y^o pulse, then inverts the X components of the spins, which are then completely refocussed after another period Δ *i.e.* creating a spin echo within the FID for all excited spins.[89]

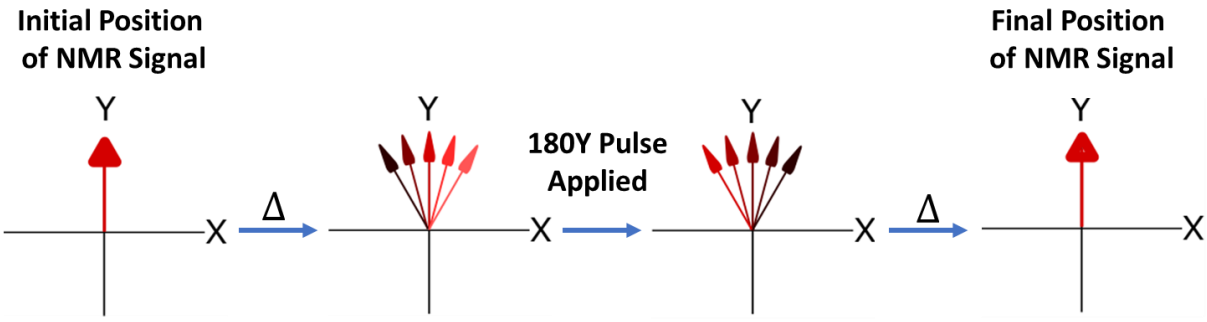

Figure 57: Dephasing and rephasing during a spin echo in an inhomogeneous field. Spins experiencing higher or lower fields (and thus having higher or lower Larmor frequencies) are shown in lighter or darker shades of red.

Indeed, trains of spin echoes are a well-documented NMR technique – essentially being a CPMG experiment. Where SHARPER is novel is that data is acquired in between these refocussing pulses. When the pulses are applied rapidly enough, at the cost of constraining the length of the data acquisitions, a significant amount of magnetic field inhomogeneity can be effectively cancelled out during the FID – shown in Figure 58a. However, if the acquisition periods become too long relative to the field inhomogeneity (such that refocussing pulses are not frequently applied) significant sideband artefacts become apparent in the spectrum, though without broadening of the central peak, as can be seen in Figure 58b.

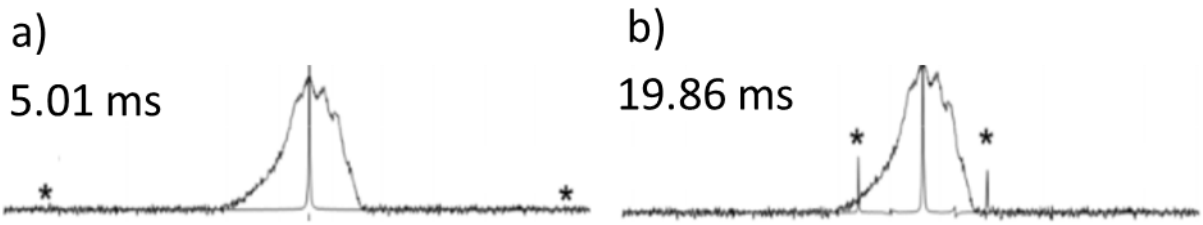

Figure 58: SHARPER spectra with shims mis-set, overlaid with 1D spectra recorded under the same conditions. The SHARPER overlays use either 5.01 ms or 19.86 ms data acquisitions, which result in significant differences in sideband intensities, marked with an asterisk. (Adapted from A.B. Jones et al, 2017, SI.[96])

SHARPER is even effective when applied to a sample in a well shimmed magnetic field, removing the effect of additional dephasing caused by any residual inhomogeneity of the field, $T_{2(\Delta B0)}$, which is often the major contribution to transverse relaxation for small molecules[70] (Equation 8). Hence by removing, or at least diminishing this effect, SHARPER allows measurement where linewidth is limited by T_2, not T_{2*}, thus maximising the signal-to-noise ratio of the signal of interest.

$$\frac{1}{T_2*} = \frac{1}{T_2} + \frac{1}{T_{2(\Delta B0)}}$$

Equation 8: Calculation of T_2, the rate of dephasing in the XY plane for NMR experiments.*

This improvement in signal-to-noise per scan is potentially very useful in reaction monitoring where products, intermediates and reactants will all be present only in low concentrations at some point in the reaction.

SHARPER also refocuses evolution due to scalar coupling during the FID, producing a decoupled spectrum, which further contributes to signal-to-noise improvement. The spin echo refocuses all heteronuclear coupling and refocussing of homocoupling can also be achieved by using the sel-SHARPER variant. The only proviso here is that the magnitude of the coupling will dictate how regularly the refocussing pulses must be applied. If data acquisitions are significantly longer than 1/3*J*, then significant sideband artefacts may arise, similar to those observed in Figure 58. Collapsing multiplicity yields significant sensitivity gains – in simple systems, such as doublets or triplets this will result in doubled signal-to-noise, whilst signal improvements will be greater in more complex multiplets. It is notable that this decoupling is achieved without ever having to pulse on any coupled partner nucleus. For example, a $^{19}F\{^{1}H\}\{^{13}C\}$ spectrum can be acquired by solely pulsing on ^{19}F. This contrasts with conventional decoupling which entails irradiation on the channels of all relevant heteronuclei. This makes SHARPER an attractive option for spectrometers with fewer channels, or where a lower duty cycle is required.

Whilst SHARPER possesses the significant benefits outlined above, the 180º pulses will perturb chemical shift evolution during acquisition. This means that the experiment only gives simple sharp singlets when used on-resonance – where there is no chemical shift evolution to perturb. As the transmitter offset is moved further away from resonance the chemical shift evolution gives rise to increasingly intense sideband artefacts in the SHARPER spectra relative to the central peak (marked as 0 Hz in Figure 59).

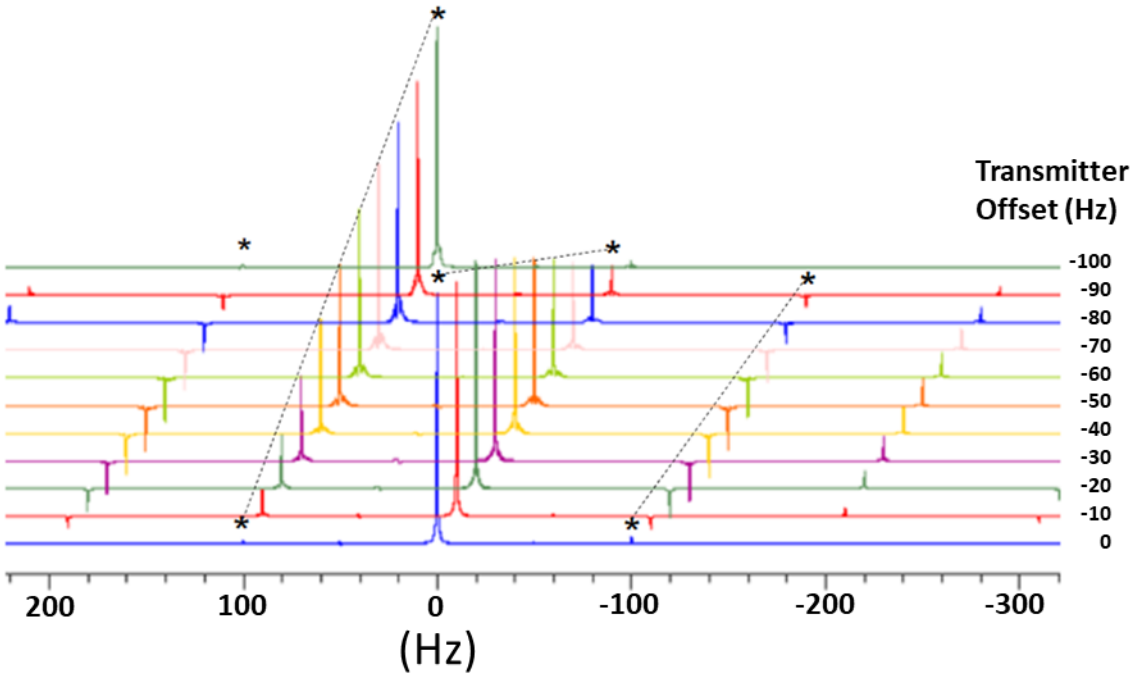

Figure 59: Effects of altering transmitter offset in SHARPER. (Adapted from A.B. Jones et al, 2017, SI.[96])

This means that SHARPER only works for a single on-resonance signal at a time and requires precise prior knowledge of its chemical shift. This is often not crippling for a reaction monitoring experiment as a single signal can often be used to track the concentration of a molecule of interest.[36] However, it is still an undesirable property if there are multiple molecules of interest in a chemical reaction – *e.g.* both the product and the reactant.

There are several obvious solutions to recording SHARPER spectra for multiple signals in a chemical reaction. Perhaps the simplest is simply to repeat the reaction using SHARPER to examine a different signal each time. This of course introduces an additional point of experimental error and may be impractical in some applications *e.g.* large scale reactions, or where expensive reactants are being used. Another approach would be to run two or more SHARPER experiments in an interleaved fashion, examining a different signal in each interleaved increment. This, however, limits temporal resolution. It also results in datapoints which are slightly shifted in time relative to each other, which may complicate further analysis. Another problem caused by this requirement for the signal to be *exactly* on-resonance is that chemical shift values may change as a reaction progresses, such that the signal is no longer on-resonance by the end of the reaction. This will cause a shift in intensity from the main peak to the sidebands, as shown in Figure 59.

More elegant solutions to these problems would be to run SHARPER spectra for multiple resonances simultaneously, and to track the frequency of a resonance in real time, so as to update the transmitter offset used in SHARPER experiments. Methods to achieve both of these things are presented in Chapters 4 and 5 respectively but require an understanding of how SHARPER behaves off-resonance. This Chapter therefore details the conditions under which SHARPER can be used effectively off-resonance and details the artefacts generated from running experiments where these conditions are not met, which provides the theoretical underpinning for both of these methods.

3.2 Experimental Off-Resonance SHARPER

In this Section it is shown that it is possible to run SHARPER off-resonance under certain conditions. A detailed analysis of the artefacts produced when doing so is presented, which is used in later Chapters to mitigate the issues faced by the SHARPER experiment.

3.2.1 Theory for Off-Resonance SHARPER

The original SHARPER experiment placed the signal of interest precisely on-resonance. This means that a 90_X^o pulse places the bulk magnetisation along the Y axis, with no X component at that point (Figure 60). As the signal is on-resonance there is no chemical shift evolution for this signal and thus an X component of the bulk magnetisation can only develop from coupling, T_2 relaxation or magnetic field inhomogeneity. A subsequent 180_Y^o pulse will invert any X component of magnetisation whilst leaving the Y component untouched, providing refocussing of coupling and field inhomogeneity without perturbing chemical shift evolution and thus yielding a single sharp peak as a Fourier transform. The Y component of magnetisation in this case will be a simple exponential decay with no frequency.

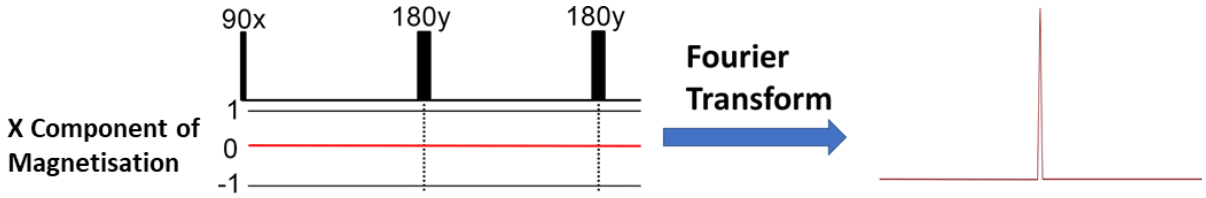

Figure 60: A cartoon showing the X component (on a scale of +1 to -1) of magnetisation during a SHARPER experiment on a perfectly on-resonance signal and its Fourier transform.

If a signal is not precisely on-resonance – then an X component of magnetisation will develop due to chemical shift evolution, as shown in Figure 61. The 180_Y^o pulses invert this X component of magnetisation, causing apparent jumps in the phase of the chemical shift evolution of the FID. This leads to artefactual spectra after Fourier transformation with characteristic sidebands.

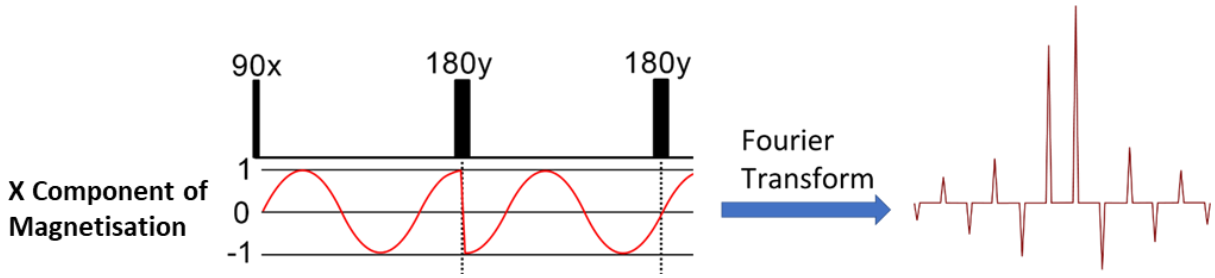

Figure 61: A cartoon showing the X component (on a scale of +1 to -1) of magnetisation during a SHARPER experiment on an off-resonance signal and its Fourier transform.

However, a special case exists where off-resonance SHARPER is possible. If one considers an NMR signal with a frequency such that its wave period is *exactly* equal to the timing between 180_Y^o pulses then the bulk magnetisation will lie along the Y axis at the moment of application of the pulses. This is illustrated diagrammatically in Figure 62. Such a scheme should not lead to jumps in phase for this signal but essentially normal chemical shift evolution, giving the same single sharp peak as on-resonance SHARPER.

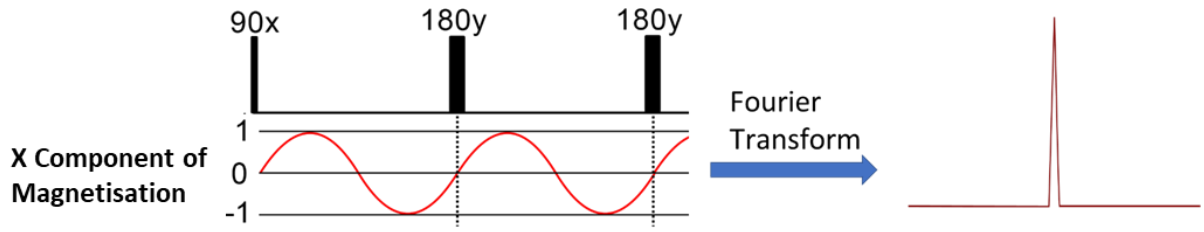

Figure 62: A cartoon showing the X component (on a scale of +1 to -1) of magnetisation during a SHARPER experiment on an off-resonance signal and its Fourier transform, but where signal frequency and 180º pulse separation have been matched.

Whilst the example shown demonstrates *exactly* a single revolution the criterion is that the signal has no X component of magnetisation at the time of application of the 180_Y^o pulses. Thus, the magnetisation needs to be either aligned along its original axis (after the 90_X^o pulse) or at 180º to it, *i.e.* in the Y or -Y direction with reference to Figure 62. Therefore, any frequency where the period of the NMR signal is either an integer or half integer multiple of the timing between the 180_Y^o pulses should give rise to non-artefactual SHARPER spectra. For any given off-resonance frequency there should thus be a range of suitable timings between 180_Y^o pulses that will give non-artefactual SHARPER spectra.

3.2.2 Experimental Off-Resonance SHARPER

Initial testing of off-resonance SHARPER was conducted on a sample of neat 99% D_2O. As only a single signal is present in a 1D ^1H spectrum, from the residual HDO, the frequency can be set entirely arbitrarily by altering the transmitter offset. The pulse sequence used is shown in Figure 63. Unlike the original SHARPER sequence[36] it does not start with an initial half-length chunk, as it was intended to mimic the theoretical setup described in Figure 62 as closely as possible at this stage.

Delays are required between the 180º pulses and acquisition in order to prevent ringdown. These are of minimal length (100 μs) and placed evenly on either side of the pulse, so that any chemical shift evolution that occurs in them should cancel. Consequently only the length of the data chunks, Δ, matters for chemical shift evolution.

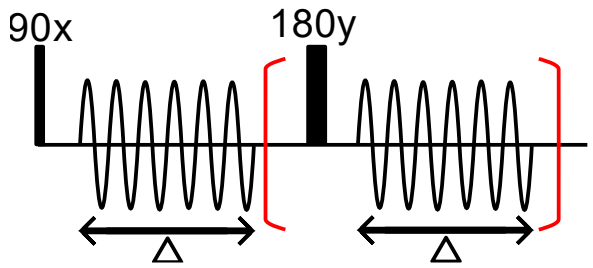

Figure 63: Pulse sequence diagram for a simplified SHARPER pulse sequence. The timing Δ was set to 10 ms.

The sample was shimmed as well as possible and the 90º pulse length calibrated. The value of Δ was set to 10 ms, with 1000 data chunks recorded, resulting in a 10 second long FID. The transmitter offset was adjusted such that the NMR signal was placed precisely on-resonance. Fourier transformation gave the expected single intense sharp peak, shown in Figure 64b. The FID is a simple exponential decay and significantly extended due to removal of $T_{2(\Delta B0)}$ contributions to T_2* (Figure 64a), with the time that signal is detectable for extended dramatically (the NMR signal lasts ~1 second in a normal 1D ^1H experiment). The simplified sequence in Figure 63 therefore behaves in the same way as the original SHARPER sequence[36] when on-resonance. Sideband artefacts are present in Figure 64b though with very low intensities compared to the central peak. After apodisation with a 0.1 Hz Gaussian to remove additional truncation artefacts the linewidth of the peak at the centre of the spectrum was 0.14 Hz (approximately 0.09 Hz before apodisation).

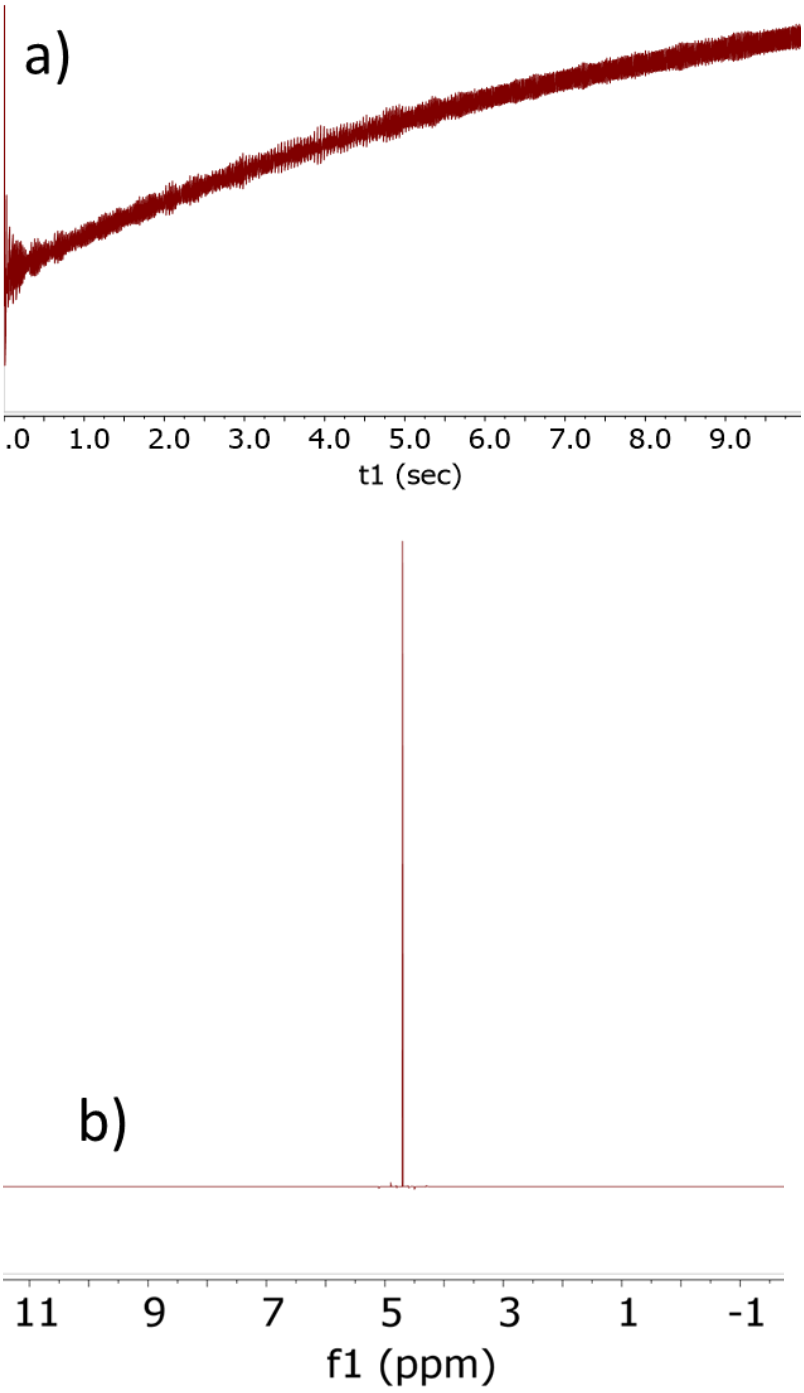

Figure 64: An on-resonance SHARPER experiment showing (a) the FID and (b) the Fourier transformed spectrum with a 0.1 Hz Gaussian window function applied.

The transmitter offset was then shifted off-resonance by either 25 Hz or 100 Hz. In both cases, this results in a slow relaxing FID, Figure 65a and Figure 65b respectively, with signal present for the full 10 seconds. This demonstrates that the characteristics of SHARPER regarding cancelling $T_{2(\Delta B0)}$ contributions to T_2* are retained off-resonance.

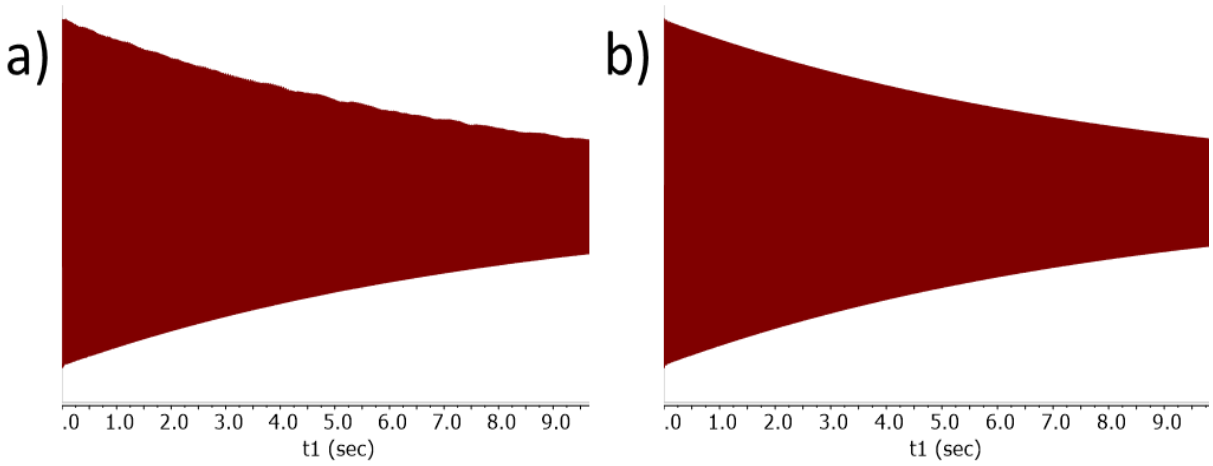

Figure 65: FIDs from off-resonance SHARPER using either (a) 25 Hz frequency or (b) 100 Hz frequency.

However, a 25 Hz frequency only evolves by 90º in the 10 ms data chunk, meaning that the bulk magnetisation is along the X axis when the 180_Yº refocussing pulses are applied – the worst possible case. Figure 66a shows a zoomed region of Figure 65a, with significant jumps in the phase of the signal being evident. Conversely, the 100 Hz frequency has a wave period of exactly 10 ms. Thus, during a 10 ms data chunk the bulk magnetisation rotates 360º and lies along the Y axis at the time of application of the 180_Yº refocussing pulses. Figure 66b, which zooms in on Figure 65b, confirms that there are no significant jumps in phase in this case.

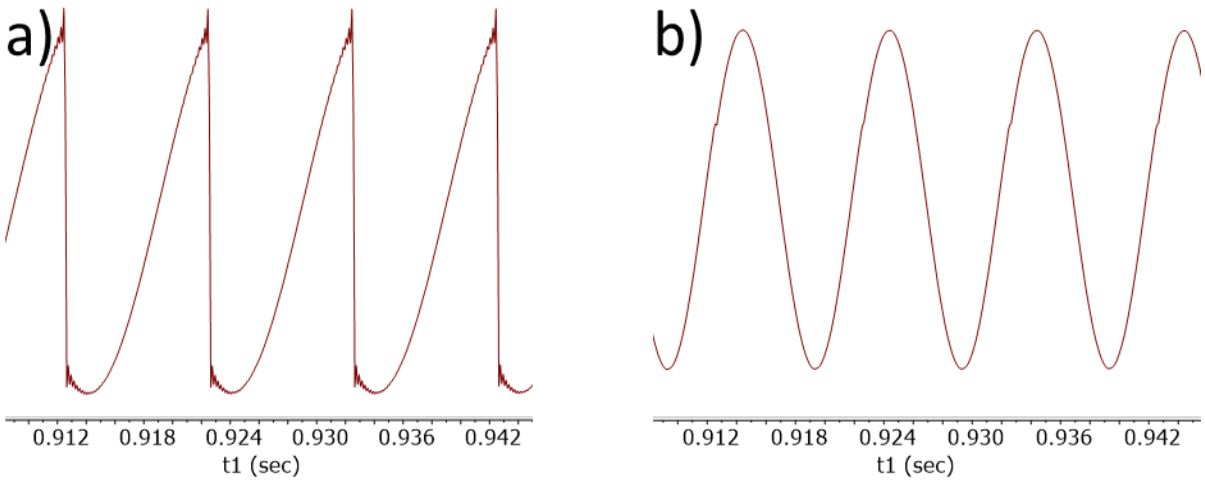

Figure 66: Zoomed in views of FIDs from off-resonance SHARPER using either (a) 25 Hz frequency or (b) 100 Hz frequency.

The FIDs for the 25 Hz and 100 Hz frequencies were then Fourier transformed, Figure 67a and Figure 67b respectively. The jumps in the phase of the FID when a 25 Hz frequency was used can be seen to yield a Fourier transform spectrum with intense regular sideband artefacts. Conversely when the 100 Hz frequency was used Fourier transformation produces the same spectrum as the on-resonance SHARPER case – a single intense sharp peak (0.09 Hz linewidth before application of apodisation) with much lower intensity sideband artefacts. Indeed, the only apparent difference between the two is that the peak is no longer located at the offset, but 100 Hz away from the centre of the spectrum.

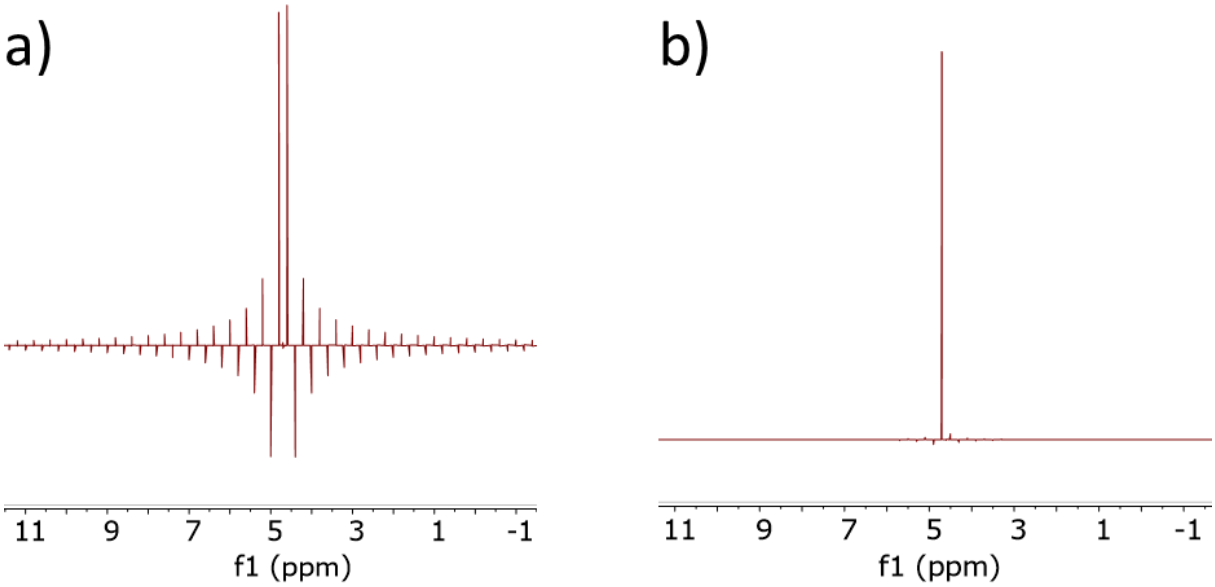

Figure 67: Fourier transform spectra of off-resonance SHARPER FIDs using either (a) 25 Hz frequency or (b) 100 Hz frequency. A 0.1 Hz Gaussian window function has been applied.

This illustrates that off-resonance SHARPER is a practical experiment given hardware limitations and realistic experimental parameters, at least under perfectly calibrated conditions. To better understand what factors might perturb off-resonance SHARPER experiments the artefacts caused by mismatching of parameters are further explored in the rest of this Chapter.

3.2.3 Incomplete Rotations

As previously shown, off-resonance SHARPER can provide both extraordinarily good and poor-quality spectra for an off-resonance signal depending on the match between the frequency of the NMR signal being examined and the durations within the pulse sequence. However, so far only the best and worst cases have been examined with regard to the position of the bulk magnetisation at the time of application of the 180º refocussing pulses. The offset frequencies used were also close to being on-resonance (≤100 Hz). This Section examines the effects of a larger range of mismatches, over a much wider range of offsets.

The experiments here utilise the sequence in Figure 68, which has an initial half-length data acquisition. This will cause any evolution due to heterocoupling or field inhomogeneity to refocus in the centre of a full-length data chunk (2Δ) minimising its development within any one data chunk. This should allow longer gaps between pulses and thus a reduced duty cycle. Whilst unneeded for this particular set of experiments, as the same D_2O sample was used to provide a single signal with an arbitrary frequency (and is devoid of scalar coupling), this feature is desirable for practical application of this sequence. In addition the field gradient pulses, before and after the refocussing pulses, used in the originally reported SHARPER experiment[36] were omitted as it was found they made no significant difference when hard pulses are utilised for refocussing. 100 µs delays, either side of the 180º pulses were used to prevent ringdown or similar experimental issues. The bracketed section is repeated as many times as needed to produce an FID of the desired length.

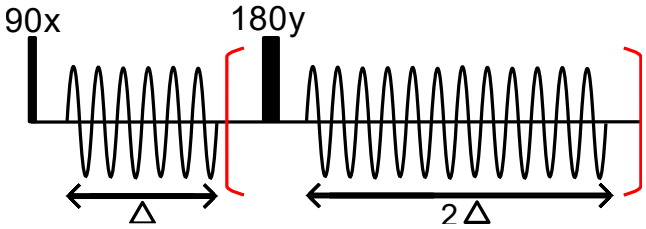

Figure 68: Pulse sequence diagram for the off-resonance SHARPER experiments.

Initial experiments used a 5 ms value of Δ with enough data chunks collected to generate 10 s long FIDs. The offset was systematically altered in order to provide a range of frequencies for the single HDO signal. In total 79 different offsets were used over a range of ~2700 Hz with increments focussed around regions that are 0-200 Hz, 1000-1100 Hz and 2500-2700 Hz off-resonance (full list in Appendix 8.5.2). As a 500 MHz spectrometer was used this represents chemical shift ranges over 5.4 ppm from on-resonance – a practical range for reaction monitoring problems where ^1H detection is used. Four off-resonance SHARPER spectra are shown in Figure 69, and are broadly representative of the variety of spectra acquired. Depending on the severity of the mismatch between the 5 ms value of Δ

and the frequency of the NMR signal the intensity of the sideband artefacts relative to the most intense peak in the spectrum shows tremendous variation, where in the worst cases the most intense sidebands are of nearly equal intensity to the most intense peak such as the top right spectrum in Figure 69.

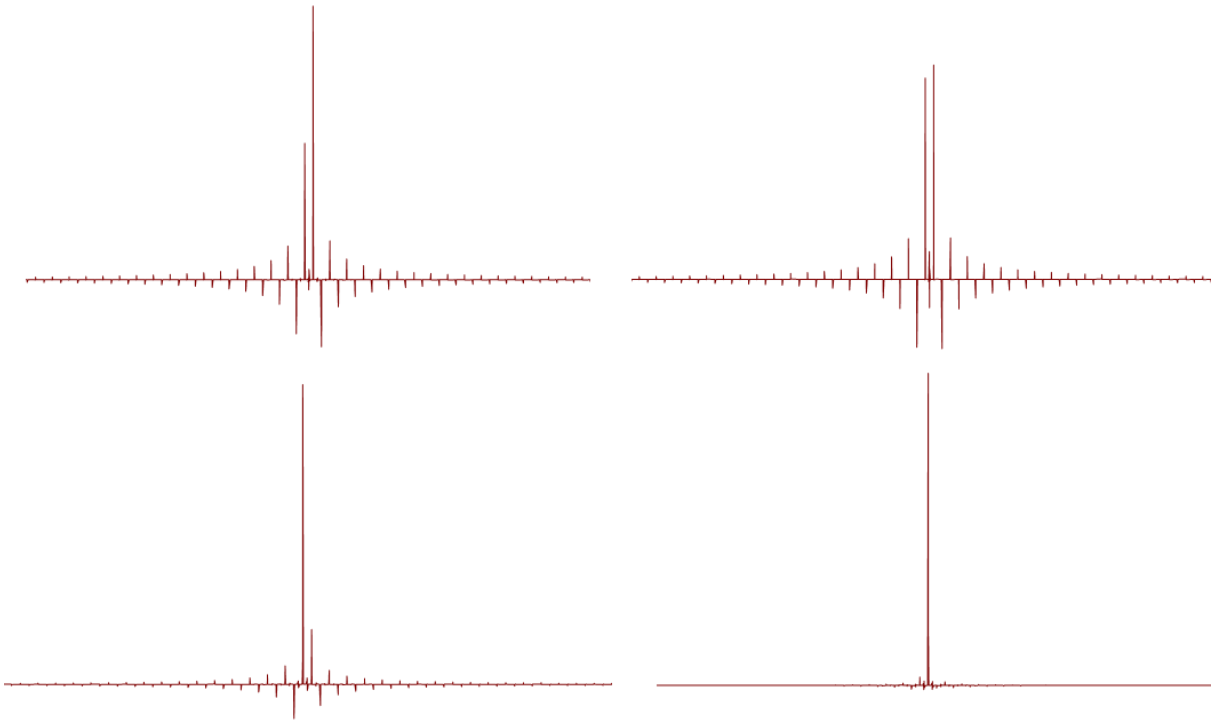

Figure 69: A selection of four off-resonance SHARPER spectra. Δ remained constant, the variation in the spectra is due to altered transmitter offset.

A simple measure of spectral quality is to calculate a signal-to-artefact ratio, based on the intensity of the most intense peak in the spectrum compared to the intensity of the most intense sideband artefact. In all cases the most intense peak is also the closest signal to the frequency of the HDO signal (as determined from the peak maximum in a 1D ^{1}H spectrum). In the best SHARPER spectra recorded signal-to-artefact ratio exceeds several hundred to one, yielding spectra with clean baselines where almost all intensity is concentrated in one sharp intense peak. In the worst cases the intensity of the most intense sideband almost equals the intensity of the most intense peak in the spectrum, so the signal-to-artefact ratio approaches one.

When the signal-to-artefact ratio is plotted against the offset relative to the apparent position of HDO in a 1D ^{1}H spectrum, Figure 70, the signal-to-artefact ratio increases and decreases several times over the range of frequencies tested, with the highest ratios being observed at multiples of 100 Hz (100 Hz, 1000 Hz, 1100 Hz and 2500 Hz).

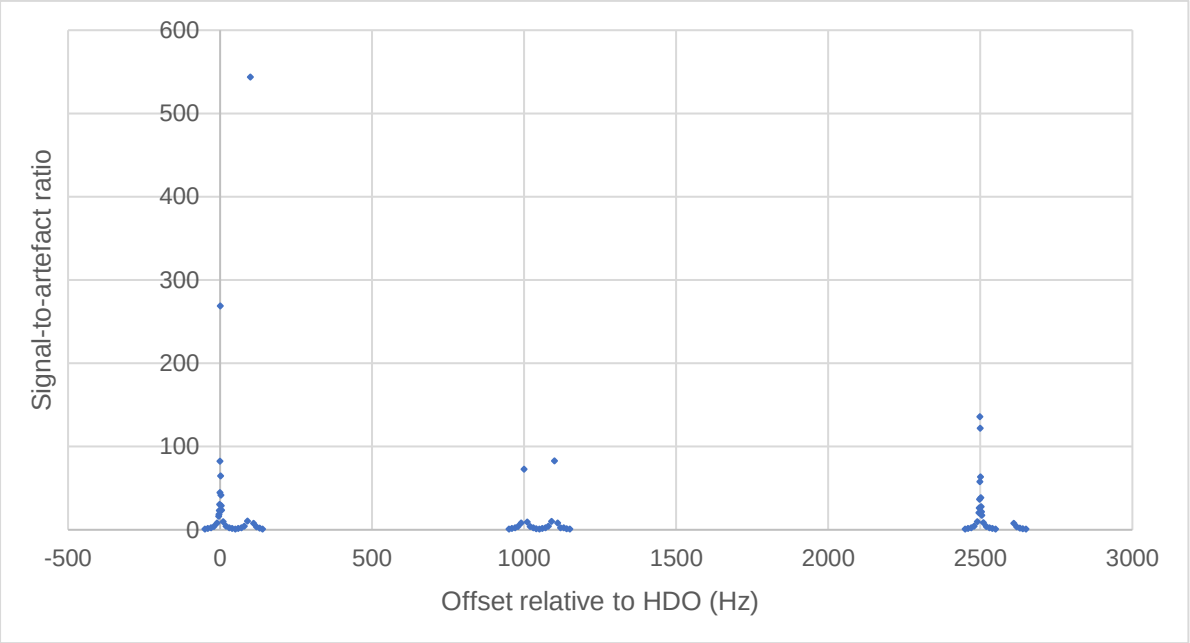

Figure 70: Signal-to-artefact ratio yielded by off-resonance SHARPER plotted against the frequency of the HDO signal.

In order to better understand this behaviour across the range of offset frequencies tested we can calculate the final position of the magnetisation vector after evolution for period Δ, immediately before application of the first 180º refocussing pulse. This is given by the modulo function defined in Equation 9, where the initial position of the magnetisation vector after the 90º excitation pulse is defined as 0º.

$$\text{Final position of magnetisation vector} = \frac{360(\Delta \; modulo \; \rho)}{\rho}$$

Equation 9: Δ is the timing between 180º pulses, ρ is the period of the off-resonance signal.

As expected, when this is plotted against signal-to-artefact ratio, Figure 71, the optimum is achieved when the signal has completed an integer or half integer number of rotations, *i.e.* 0º/180º/360º and thus is at 90º to the axis refocussing pulses are applied along. The results from the distinctly different offsets (a 2700 Hz range) show good agreement with each other, indicating that the behaviour of off-resonance SHARPER with regard to signal-to-artefact ratio is consistent across a wide range of offsets.

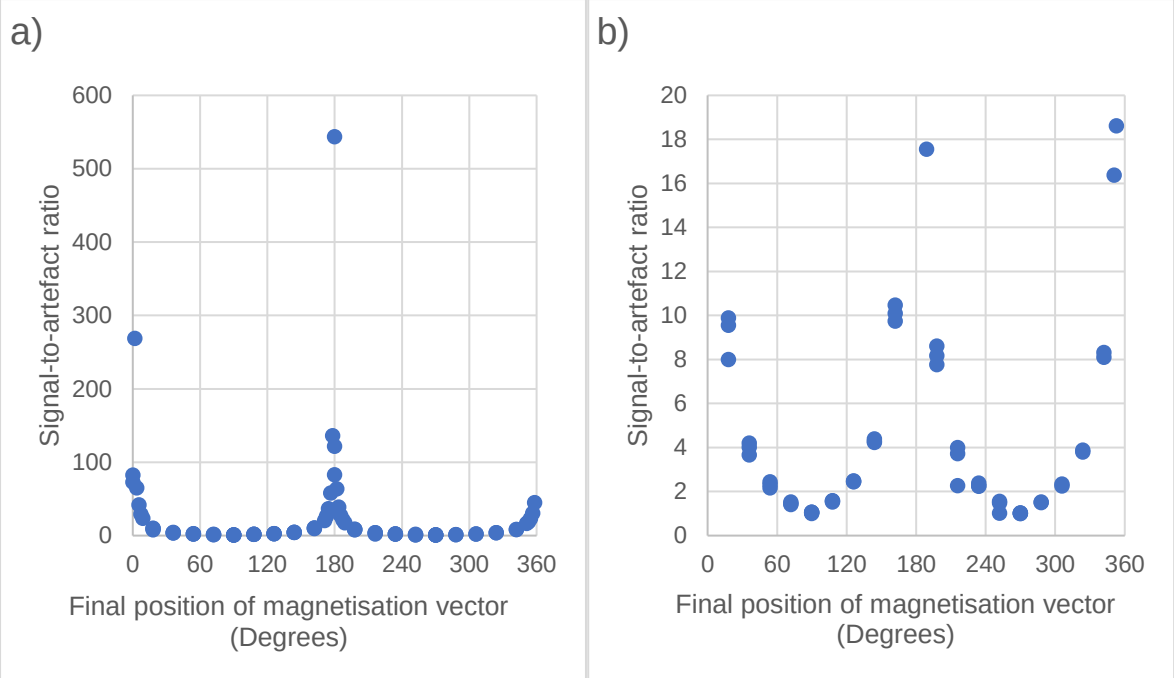

Figure 71: Signal-to-artefact ratio plotted against a measure of evolution in period Δ. The two graphs display (a) an overview of all signal-to-artefact ratios and (b) a zoomed in view of the low signal-to-artefact ratio region.

The final position of the magnetisation vector can also be plotted against the location of peaks in the off-resonance SHARPER spectra, both sideband artefacts and the most intense peak. This allows examination of the relationship between the frequency of the signal (as determined from the peak maximum in a 1D ^{1}H spectrum) and frequencies observed in the SHARPER spectra. This analysis, Figure 72, confirms that the most intense peak in the SHARPER spectrum comes closest to the real frequency of the signal when the final position of the magnetisation vector is close to 0º/180º/360º. Conversely, the position of the sideband artefact moves further from the real signal frequency as the magnetisation vector approaches 0º/180º/360º. Note that whilst the position of the sideband artefacts changes, a 100 Hz separation is always maintained, as this is a function of the delay between refocussing pulses in the sequence (10 ms in this case).

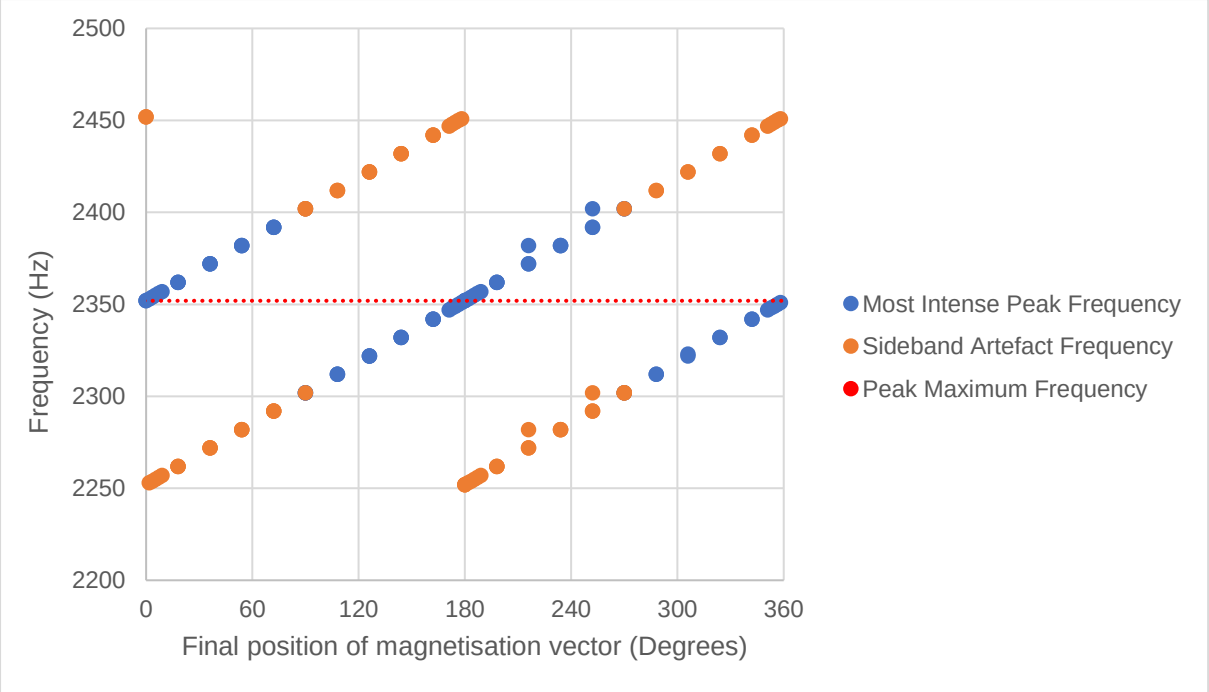

Figure 72: Frequencies observed in off-resonance SHARPER spectra for the two most intense peaks in the spectra. The frequency of the peak maximum in a 1D ^{1}H spectrum is indicated by the dotted red line.

The intensity of the sideband artefacts relative to the most intense peak has been shown to behave systematically when the transmitter offset is altered. Signal-to-artefact ratios improve as we approach offset frequencies where the bulk magnetisation will evolve during Δ to either lie along its original axis *i.e.* 0º/360º after the 90_Xº pulse, or exactly opposite to it *i.e.* 180º. Conversely, signal-to-artefact ratio declines as we approach frequencies where the bulk magnetisation evolves to be at 90º (or 270º) to its original position after the 90_Xº pulse. Multiple offset frequencies across the range tested yield good quality spectra for the timing of Δ tested, though only a single value (10 ms) was tested.

3.2.4 Effects of Variation of Chunk Duration

The artefacts in a SHARPER spectrum (Figure 73) fall into two categories:

- Sharp sidebands with similar line shape to the central peak, though reduced intensity
- Broader artefacts with distorted line shapes

Because the broad artefacts have low intensities and are antiphase their integrations are normally negligible in phase-sensitive spectra so they have not been extensively studied here. In on-resonance SHARPER both of these groups of artefacts are regularly spaced by the inverse of the length of a full data chunk[36] (2Δ in the context of this thesis).

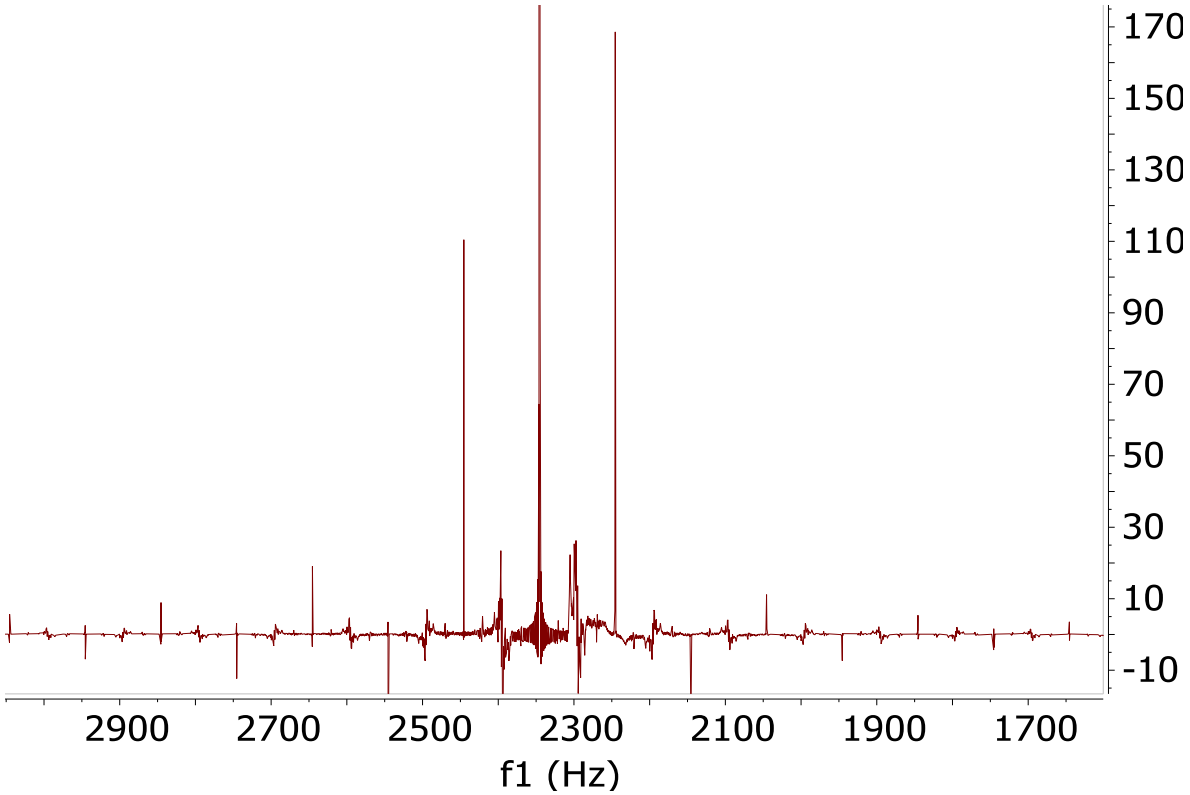

Figure 73: A view of the baseline of an off-resonance SHARPER spectrum, showing the regularity of the artefacts. The most intense peak has an intensity of 8144, making it over 47 times more intense than the second most intense peak in the spectrum.

This observation was tested for off-resonance SHARPER and for non 0º/180º/360º rotations. Off-resonance SHARPER experiments were carried out on HDO using the pulse sequence in Figure 68, with the value of Δ systematically altered (using values of 2.5, 5.0, 6.25, 7.5, 10.0, 12.5, 16.5 and 20.0 ms). The number of refocussing cycles was varied to maintain a constant acquisition time of ~10 s. Five spectra were run with each value of Δ, with varying transmitter offsets. Transmitter offset was selected in order to provide a wide range of both offset frequencies and matches between the frequency of the NMR signal and value of Δ. This provides good coverage of the possible values, as can be seen graphically in Figure 74 (full list available in Appendix 8.5.2).

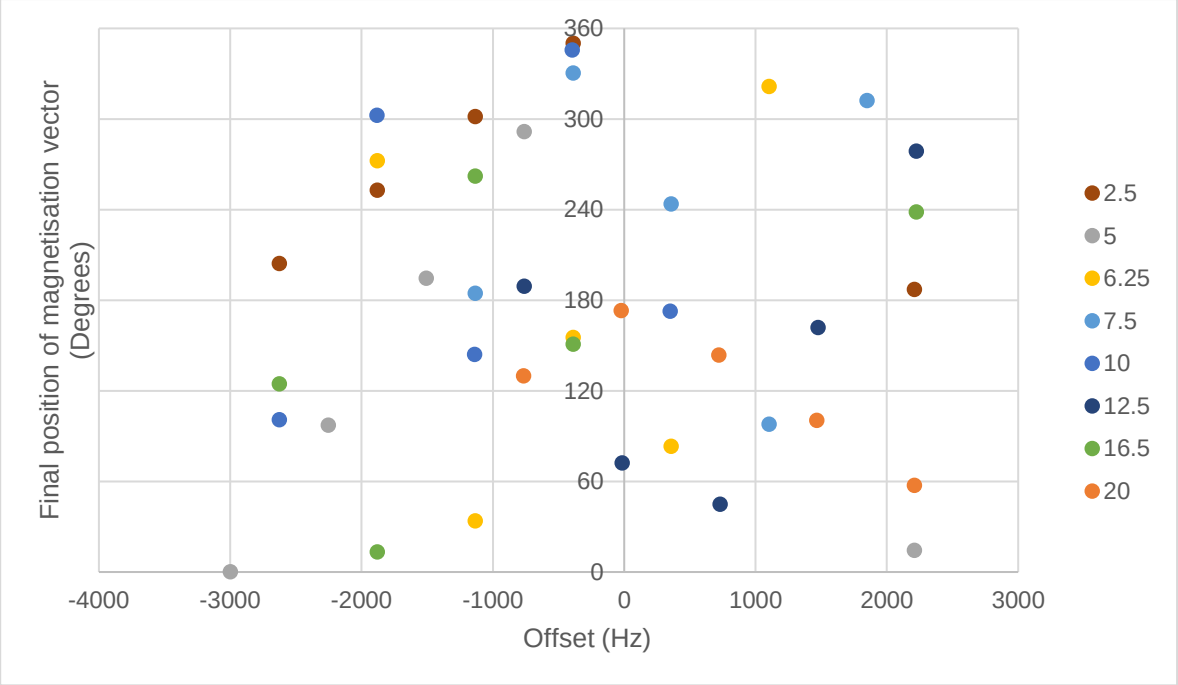

Figure 74: The range of offsets and final position of magnetisation vectors tested. Data chunk durations in ms are indicated by the colour of the dots.

FIDs were zero-filled to 2048 K datapoints and the resulting spectra were baseline corrected before measuring peak positions, and the separation of sideband artefacts examined. Sideband artefact separation was found to be independent of the final position of the magnetisation vector, so the sideband artefact separation was averaged for all spectra recorded with a given value of Δ (standard deviations shown in the table in Figure 75). Sideband artefact separation does vary with the value of Δ, and correlates impeccably with the inverse of 2Δ, as can be seen in Figure 75.

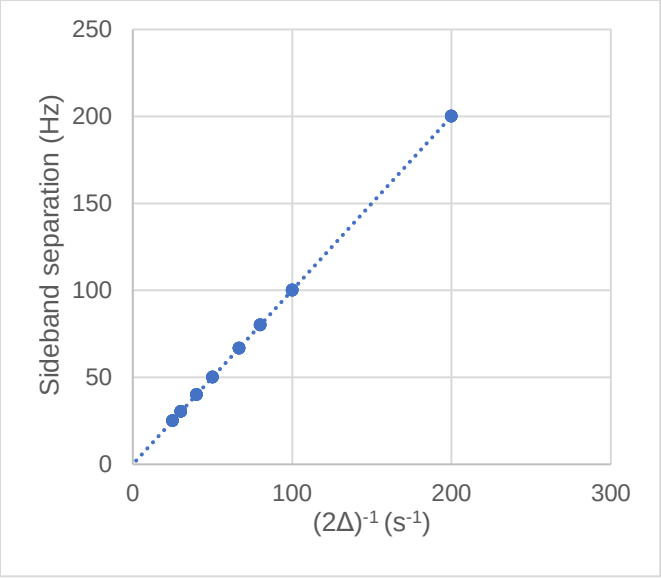

Δ	Separation (Hz)	St. Dev (Hz)
2.5	200.07	0.12
5.0	100.04	0.12
6.25	80.06	0.08
7.5	66.67	0.04
10.0	50.06	0.08
12.5	40.01	0.03
16.5	30.32	0.03
20.0	25.01	0.04

Figure 75: Correlation between the duration of the Δ periods in off-resonance SHARPER spectra and artefact positions, and a table indicating the standard deviations.

This confirms that the position of artefacts in off-resonance SHARPER is still solely determined by the choice of transmitter offset and the duration of Δ (Equation 10) and is not influenced by the frequency of the NMR signal.

$$Artefact\ Position = Offset + n\frac{1}{2\Delta}$$

Equation 10: Frequency of the sideband artefacts in SHARPER spectra, where n is any integer, positive or negative.

Another observation that was made in the original SHARPER paper regarding variation in the duration of data chunks is that the signal-to-artefact ratio increases at shorter data chunk length (*i.e.* decreased values of 2Δ).[36] In order to demonstrate that this property is retained for off-resonance SHARPER a sample of HDO was used again, with the signal at a fixed position, 100 Hz off-resonance. This yields a 1 ms wave period. By variation of Δ in 1 ms increments from 1 to 13 ms a number of off-resonance SHARPER spectra were collected with the same final position of the magnetisation vector *i.e.* 0º.

Spectra were zero-filled to 2048 K datapoints, baseline corrected (1st order polynomial fit) and the intensities of the central peak and most intense sideband used to calculate a signal-to-artefact ratio for these spectra. When plotted against the data chunk duration, Figure 76a, a clear relationship can be seen, where signal-to-artefact ratio improves at shorter values of Δ, however, it does not scale linearly with the inverse of 2Δ (Figure 76b).

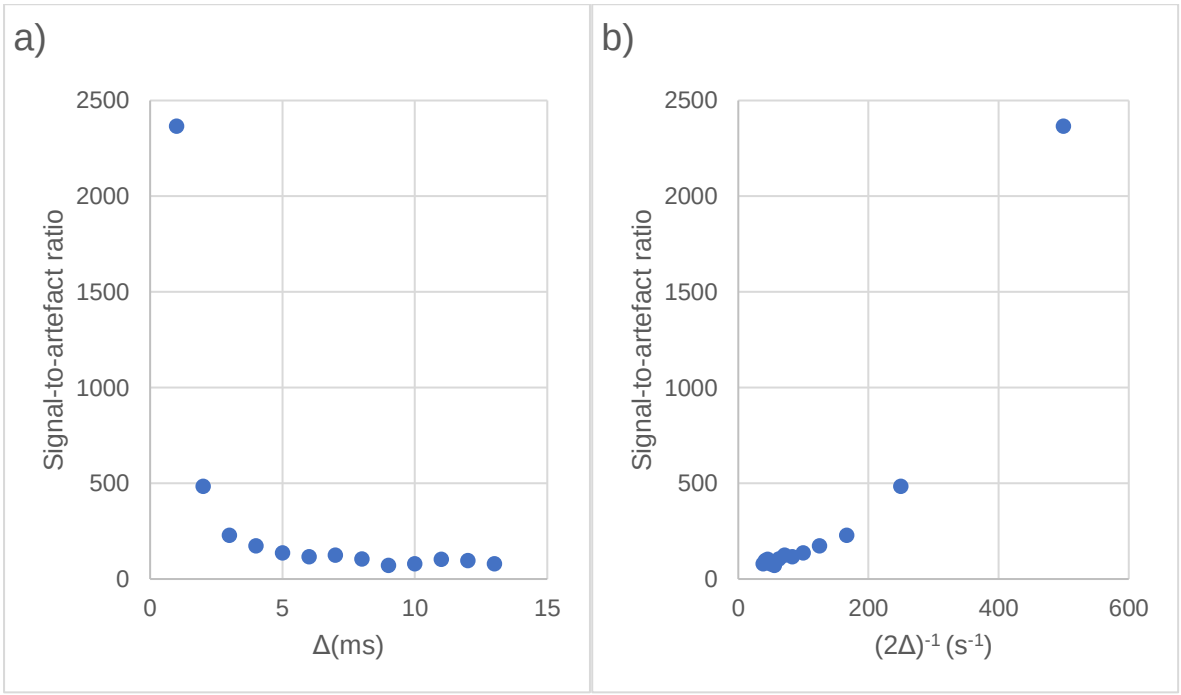

Figure 76: The signal-to-artefact ratio in off-resonance SHARPER plotted against (a) Δ and (b) the inverse of 2Δ.

The results in this Section indicate that off-resonance SHARPER spectra behave in a very similar fashion to on-resonance SHARPER spectra. The position of the sideband artefacts can be predicted, as it scales with the inverse of data chunk duration, $(2\Delta)^{-1}$. Data chunk duration affects sideband intensity (relative to that of the central peak) in the same way for both on and off-resonance SHARPER, with shorter values of Δ yielding higher signal-to-artefact ratios. Thus, running off-resonance SHARPER with shorter values of Δ is always preferable, assuming a suitable match between the Δ value chosen and the frequency can still be found. Practical concerns such as duty cycle also limit the minimum value of Δ that can be used.

These results demonstrate that off-resonance SHARPER spectra are viable given practical experimental concerns with careful selection of the off-resonance position of the resonance of interest and the timings within the pulse sequence.

4 Multiple Resonance SHARPER

The off-resonance SHARPER experiments demonstrated in the previous Chapter exclusively used only a single NMR signal. By matching the frequency of this signal with the application of the 180º refocussing pulses artefact free SHARPER spectra were run off-resonance. This Chapter applies this to multiple resonances within the same scan, to give an experiment termed “MR-SHARPER” (Multiple Resonance SHARPER).

4.1 Theory for MR-SHARPER

When only a single resonance is present, its frequency can be arbitrarily set by altering the transmitter offset. This allows a great deal of flexibility when matching the frequency to the timings between the 180º refocussing pulses. However, when multiple signals are present the frequency differences between them in Hz will be fixed (for a given sample and spectrometer), thus requiring adjustment of the timings within the SHARPER sequence as well as the transmitter offset to obtain a good match. In a spectrum with only two resonances there are two ways to select an optimal transmitter offset: (i) One resonance can be placed on-resonance with the other resonance then a specific frequency off-resonance (as Figure 77a); (ii) The transmitter offset can be placed precisely between the two resonances (as Figure 77b). In both cases this means the pulse sequence timings only need to account for a single off-resonance frequency (2*x* or *x*) of chemical shift evolution between the refocussing pulses during the FID.

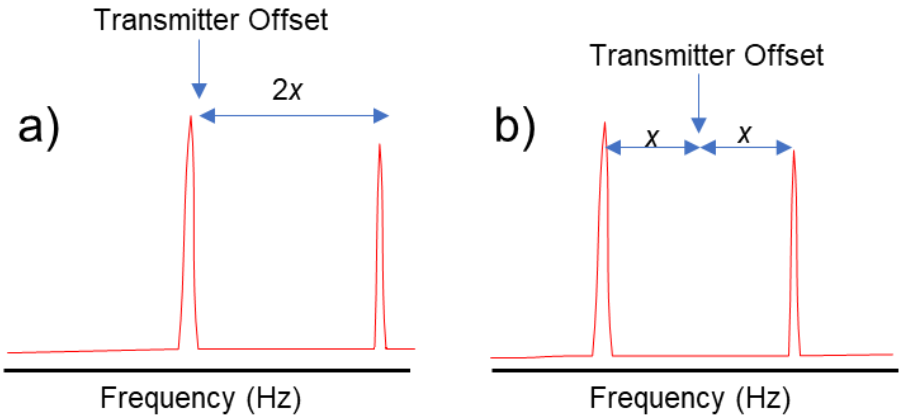

Figure 77: Ideal offset placement MR-SHARPER with two signals.

The MR-SHARPER experiment uses the same pulse sequence as off-resonance SHARPER (shown again here for clarity in Figure 78).

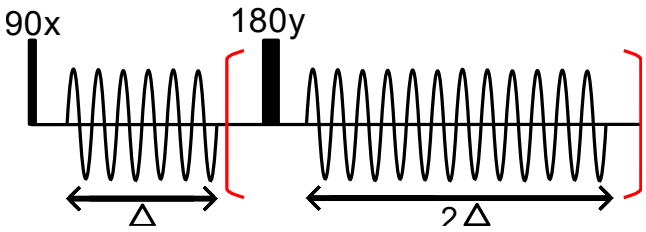

Figure 78: The pulse sequence used for MR-SHARPER.

The timing Δ is set with regard to the single frequency present, (2*x* or *x*) in order to allow an integer or half integer number of rotations during period Δ, such that all resonances lie either along the Y or -Y axes when the $180_Y{}^0$ refocussing pulses are applied. The values of Δ that fulfil this requirement are given by any integer or half-integer multiples (***n***) of the wave period of the off-resonance frequency, ωoff , as described in Equation 11.

$$\Delta = \boldsymbol{n}\ \frac{1}{\omega off}$$

Equation 11: The timing required for MR-SHARPER experiments.

Depending on the location of the transmitter offset we are acquiring either: (i) simultaneous on and off-resonance SHARPER spectra (as Figure 77a) or (ii) two off-resonance SHARPER spectra (as Figure 77b). The former has the advantage that ωoff is twice as large, resulting in a shorter wave period and thus more potential values of Δ. The latter has the advantage that experimental error in the setting of the duration of Δ will affect both resonances in the same fashion, making comparative integration more straightforward.

This approach can be extended to spectra containing an arbitrary number of resonances, but with the limitation that the timing Δ now must match more than one off-resonance frequency. This is described in Equation 12 for a three-resonance experiment, with two differing offset frequencies, ωoff_1 and ωoff_2.

$$\Delta = \boldsymbol{n_1}\ \frac{1}{(\omega off_1)} = \boldsymbol{n_2}\ \frac{1}{(\omega off_2)}$$

Equation 12: The timing required for MR-SHARPER experiments with three resonances. Subscripts refer to different frequencies.

However, in cases with more than two resonances of interest, there is more freedom in selecting the transmitter offset. The transmitter offset can be centred on *any* resonance or placed precisely between *any two* resonances (Figure 79). Each of these transmitter offsets results in a different value of ωoff_1 and ωoff_2 and thus different values of Δ that will satisfy Equation 12.

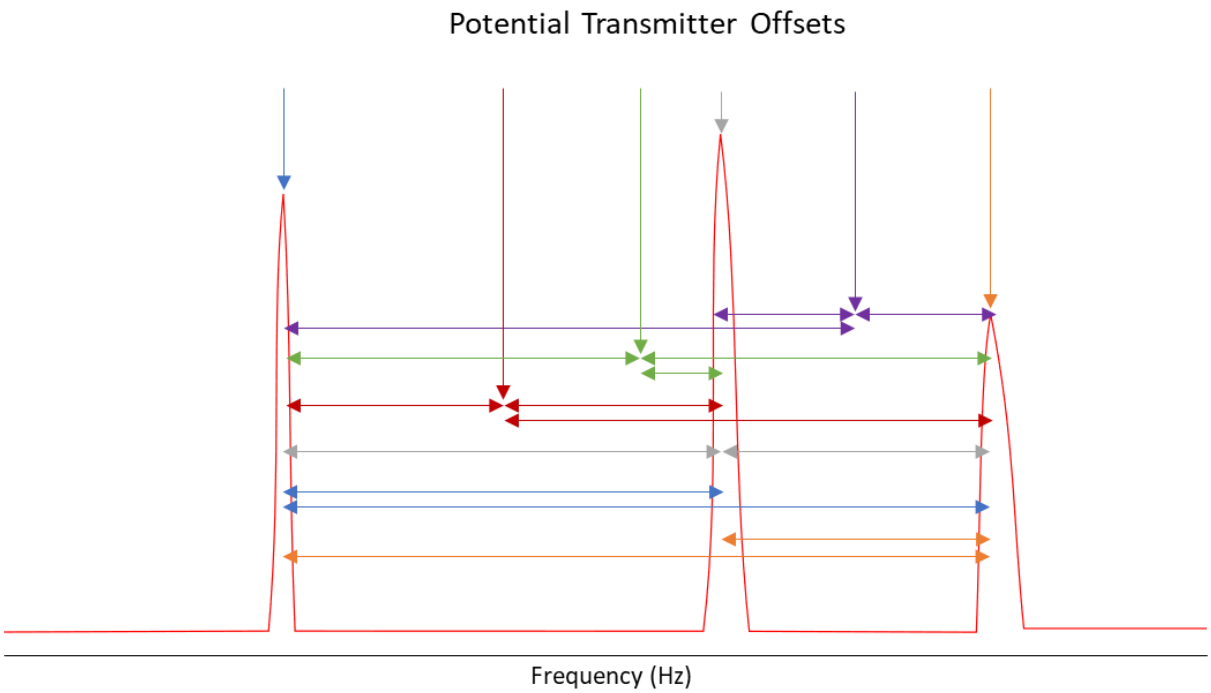

Figure 79: Potential transmitter offset placements in a three resonance MR-SHARPER experiment that result in only two distinct frequencies, each shown in a different colour.

4.2 Practical Determination of Timings

The MR-SHARPER methodology described in the previous Section relies on use of precise values of Δ, and thus precise setting of the dwell times and number of data points within the data chunks. Whilst delay values in an NMR spectrum can be trivially set with a high degree of precision (to 12.5 ns for Bruker[97] and Varian[98]) setting precise acquisition durations is more challenging.

The number of data points acquired per chunk must be an integer value and the dwell time can only take a discrete series of values (with less than 12.5 ns precision). Hence, some values of Δ which satisfy Equation 11 may be experimentally inaccessible because the dwell time cannot be set with sufficient precision. Thus, the choice of Δ value for a MR-SHARPER experiment requires finding a theoretically valid value of Δ which is also experimentally accessible given the limitations of the spectrometer.

There are further experimental constraints placed on the choice of dwell time and the total length of the acquisitions. Dwell time is inversely proportional to spectral width, and thus a value should be chosen that gives a suitable spectral width for the resonances being examined. The value of Δ chosen also needs to provide sufficient refocussing during the SHARPER sequence, setting an upper bound on Δ, without an excessively high duty cycle from the refocussing pulses, setting a lower bound on Δ.

A practical solution to this problem was to generate a matrix of all experimentally accessible values of Δ and then search for a match between these and the theoretically valid timings, as per Equation 11 and Equation 12. This was achieved with a Python 2.7 script (Appendix 8.5.3), the operation of which is summarised by the flow chart in Figure 80.

Three arrays of equal size are used, consisting of (i) every possible value of Δ; (ii) every possible dwell time and (iii) the number of data points. Array (i) is the product of arrays (ii) and (iii), so once a suitable value of Δ is identified in array (i) the dwell time and number of datapoints per chunk required to generate it experimentally can be found at the same index in arrays (ii) and (iii).

Values in array (ii) were experimentally determined using either OpenVNMRJ 4.2 or Topspin 3.6.1. Array (iii) is a simple list of integers.

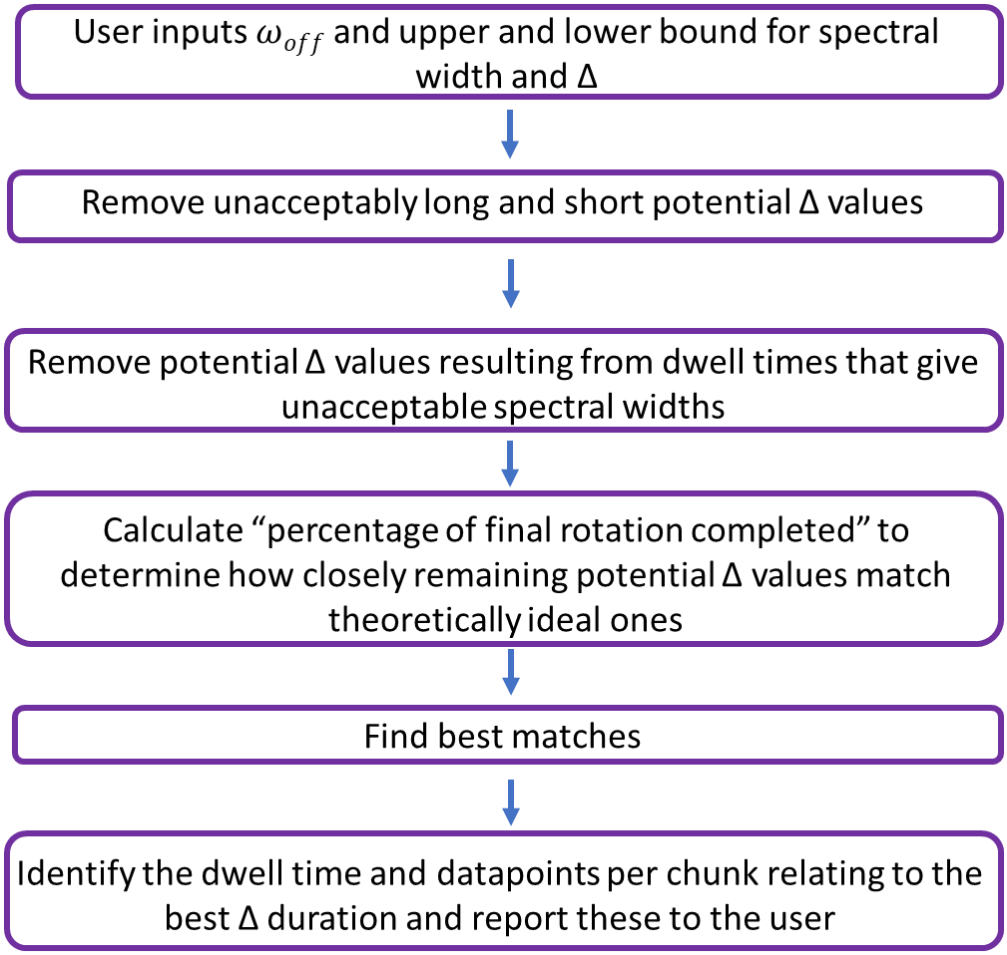

Figure 80: A flowchart summarising the operation of the MR-SHARPER scripts.

Initially, the user defines the value of ωoff and acceptable ranges for spectral width and Δ. These acceptable ranges are used to remove any values of Δ which are either too long, too short or result from a dwell time which gives an unacceptably small or large spectral width (considering spectrometer frequency for the nucleus of interest).

Based on the value of ωoff the remaining potential values of Δ are then converted into degrees of rotation and then into a percentage of a complete (360°) rotation, between 0.0 and 100.0. The values 0.0, 50.0 and 100.0 correspond to the theoretically ideal timings of Δ which give a final position of the magnetisation vector of 0°/180°/360° respectively. The value closest to 0.0, 50.0 or 100.0 is identified and the number of datapoints per chunk and dwell time required to produce that value of Δ is presented to the user. If multiple timings match equally well to the value of ωoff then these are all presented to the user for selection.

This relies greatly on what range of dwell times are experimentally accessible on a given spectrometer. The two instruments on which this methodology was tested were a 500 MHz Varian VNMRS spectrometer running VNMRJ 4.2 and a 500 MHz Bruker AVIII HD spectrometer running Topspin 3.6.1.

There is a notable difference between the dwell times available on the two different systems. The Varian system offers dwell times which vary systematically in 800 ns increments. The Bruker system however has variable increments between each dwell time, ranging from between 33 ns to 300 ns. This behaviour was not obviously systematic and available dwell times were determined empirically (Appendix 8.5.10). Due to the smaller increment size Bruker offers significantly more dwell times within a given range. For example it offers 574 unique dwell times within a 17.6 μs to 80.0 μs range, whilst the Varian instrument only offers 79.

More available dwell times on the Bruker instrument means that there is a greater chance of finding a close match between experimentally accessible and theoretically valid values of Δ. In addition, the variable increments of dwell times on the Bruker instrument (as opposed to the regular 800 ns increments on the Varian instrument) introduces a greater likelihood of a close match because regular increments are more likely to result in identical Δ durations being generated with different dwell time and chunk point combinations, rather than precise and discrete acquisition durations.

To examine how this affects the expected quality of the MR-SHARPER spectra, 5000 ωoff frequencies were randomly generated to 2 decimal places between 0 and 5001 Hz. The MR-SHARPER scripts were modified to loop through the list of frequencies and calculate Δ values using either dwell times available on our Bruker or Varian instruments. Potential Δ values were constrained to 10 ms < Δ < 25 ms and with dwell times that would result in a spectrum width between 5000-12500 Hz, 10-25 ppm at 500 MHz. (The modified script and the list of frequencies are provided in Appendix 8.5.5 and 8.5.6.)

The “percentage of final rotation completed” was then calculated for each Δ value produced by the script for a given value of ωoff. This is a measure in percentage terms of how close an experimentally accessible value of Δ matches to a theoretically valid one, *i.e.* how close it is to allowing either an integer *or* half integer number of rotations for a given ωoff frequency. A value of 0% indicates a perfect match, where the final position of the magnetisation vector is at 0°/180°/360°. The worst possible case would be 25%, corresponding to a final position of the magnetisation vector of 90°/270°. The percentage of final rotation completed for the optimal value of Δ for each ωoff tested is shown in Figure 81. Both systems perform poorly at very low frequencies (below 50 Hz, thus with very long wave periods), where very few timings are experimentally available shorter than the 25 ms upper bound – so this data is excluded from the figures and further analysis.

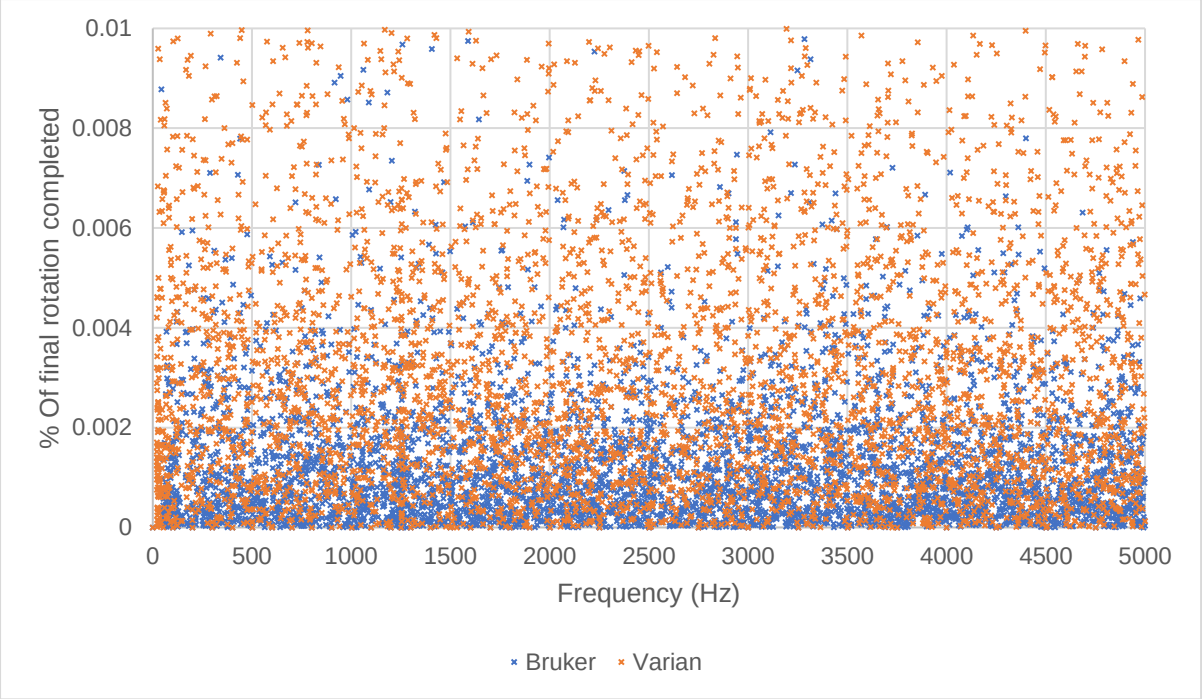

Figure 81: The percentage of final rotation completed (a measure of expected spectrum quality) for randomly generated frequencies using timings that can be generated on Bruker (shown in blue) or Varian (shown in orange) NMR spectrometers. Frequencies below 50 Hz have been excluded.

At frequencies above 50 Hz Bruker gives a lower (thus better) percentage of final rotation completed for 82% of frequencies tested and a lower mean percentage of final rotation completed (0.0013%). Varian performs better for only 15.5% of frequencies and has a higher mean percentage of final rotation completed overall (0.0048%). Figure 82 shows this difference between the two spectrometers more clearly with a 9-point moving average of this same data.

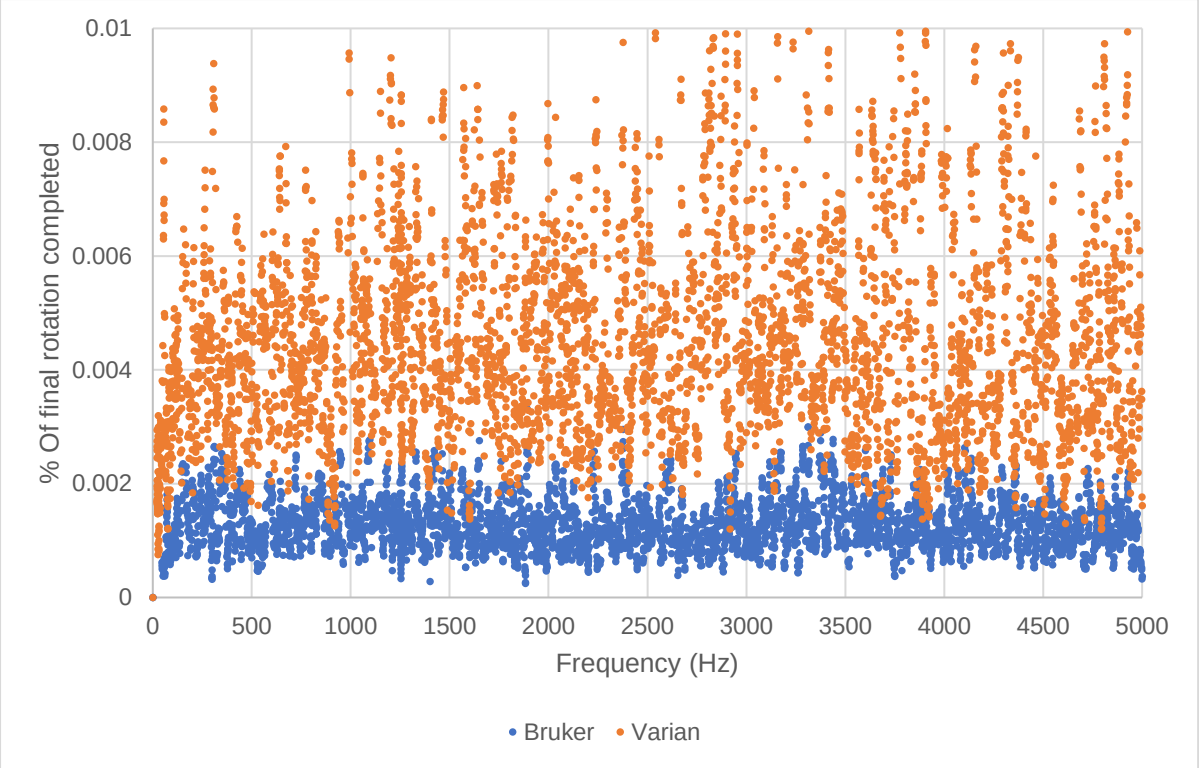

Figure 82: A 9-point moving average of the percentage of final rotation completed (a measure of expected spectrum quality) for randomly generated frequencies using timings that can be generated on Bruker (shown in blue) or Varian (shown in orange) NMR spectrometers. Frequencies below 50 Hz have been excluded.

Interestingly, a (newer) Bruker NEO spectrometer running Topspin 4 is expected to be significantly worse for MR-SHARPER than both the Bruker AVIII HD and Varian VNMRS systems detailed here, as it is limited to 1000 ns to 5000 ns increments between available dwell times.[99]

4.3 Retention of SHARPER Properties

The SHARPER experiment displays several desirable properties such as the ability to produce heterodecoupled spectra without pulsing on any nucleus other than the actively measured one and provide compensation for magnetic field inhomogeneity. Whilst in principle the MR-SHARPER methodology should retain these properties this needed to be confirmed experimentally.

To test the performance with respect to heterodecoupling, ^{13}C based SHARPER experiments were acquired on a sample of 50:50 $CHCl_3$:CD_3OD. This provides a system with only two resonances, but two types of heterocoupling – $^1J_{CH}$ and $^1J_{CD.}$ A single scan $^{13}C\{^1H\}$ NMR experiment was run for reference. The MR-SHARPER experiment placed the transmitter offset on the $CHCl_3$ resonance, with an off-resonance frequency for CD_3OD of 9931.93 Hz. A relatively short upper limit was placed on the value of Δ due to the large $^1J_{CH}$ coupling in the chloroform, so values of 1 ms < Δ < 4 ms were considered. The Python script gave an optimum Δ value of 2.175 ms, and the number of data chunks collected was set to 3216, to yield a 14 second FID.

Figure 83 shows the MR-SHARPER spectrum (red) overlaid with the $^{13}C\{^1H\}$ (blue). The $CHCl_3$ and CD_3OD resonances are shown separately because the level of apodisation required to remove truncation artefacts differed significantly. As expected, the MR-SHARPER experiment removed both $^1J_{CH}$ and $^1J_{CD}$ heterocouplings. This led to an increase in signal-to-noise of more than an order of magnitude for the CD_3OD signal. This was primarily due to an order of magnitude reduction in linewidth, combined with the reduction in multiplicity. Remarkably the spectrometer software was found to be the limiting factor in the ultimate linewidth achieved for this resonance, as the 14 s FID contained the maximum number of datapoints that could be collected in a single scan. The signal-to-noise increase is more modest for the $CHCl_3$ as it comes solely from linewidth reduction (which in turn was much more modest), as the comparison is to a $^{13}C\{^1H\}$ spectrum. The difference in how far the MR-SHARPER experiment reduced the linewidth is likely due to a difference in the T_2 value of the two resonances, as like the parent experiment MR-SHARPER can be expected to give linewidths that more closely reflect T_2, rather than T_2* by removing contributions from the residual magnetic field inhomogeneity.[36]

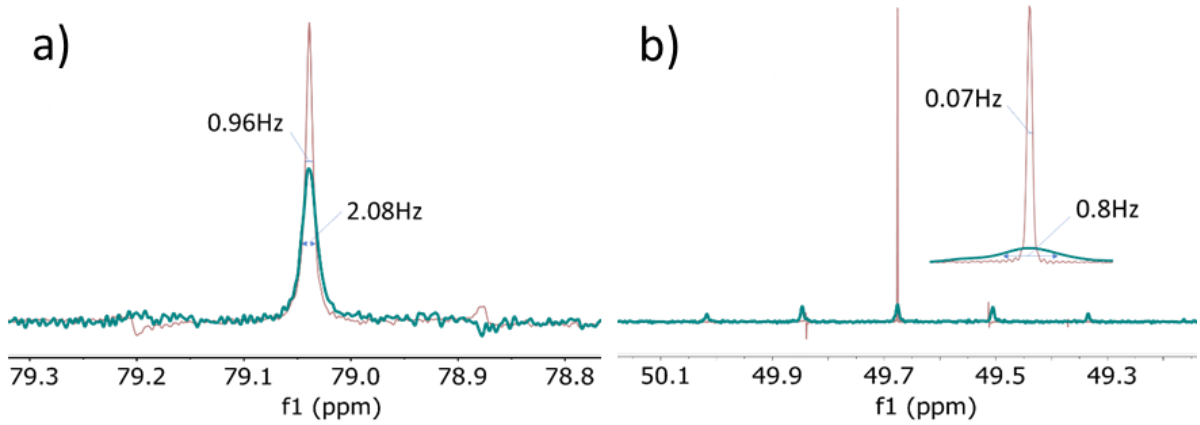

Figure 83: A ^{13}C detected MR-SHARPER experiment on (a) $CHCl_3$ (red) and (b) CD_3OD (red) with a $^{13}C\{^1H\}$ overlaid in blue. Noise levels have been matched between the two spectra and the two displays differ by the apodisation applied to the MR-SHARPER spectra – (a) 0.4 Hz Gaussian and (b) 0.06 Hz Gaussian.

Another property of the originally reported SHARPER experiment is its compensation for magnetic field inhomogeneity. This was tested for in MR-SHARPER in a series of experiments where the Z1 shim was incrementally perturbed from its optimal value. The off-resonance CD_3OD signal is shown at each level of shimming fault for both the $^{13}C\{^1H\}$ and MR-SHARPER spectra in Figure 84. No reduction in linewidth or signal-to-noise is apparent in the MR-SHARPER spectra even at shimming faults that leave the CD_3OD signal little above the noise in the $^{13}C\{^1H\}$ spectra.

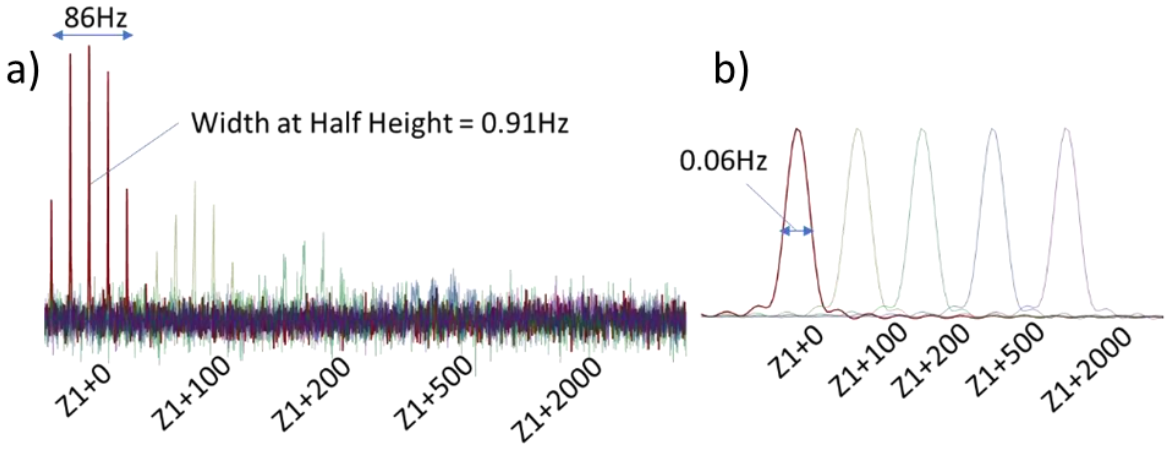

Figure 84: A set of overlaid spectra with altered Z1 shim values showing the off-resonance CD_3OD signal using (a) $^{13}C\{^1H\}$ and (b) MR-SHARPER. Frequencies have been shifted to show all spectra on the same axis.

Spectra were then baseline corrected (1st order polynomial fit) and the CD_3OD signal integrated, with integrals shown in Figure 85. Not only were the absolute integrals higher for the MR-SHARPER spectra (likely due to the slower relaxation), but the absolute integral from the $^{13}C\{^1H\}$ spectra decreases as the shimming fault increases. This is likely due to increased contribution of noise to the integral as the signal-to-noise ratio decreases and linewidth increases. In contrast, the MR-SHARPER spectra yield consistent integrals regardless of shimming conditions. These results indicate that the properties that make SHARPER a desirable experiment for reaction monitoring, where magnetic field homogeneity is often compromised by the reaction conditions, are retained in the MR-SHARPER variant.

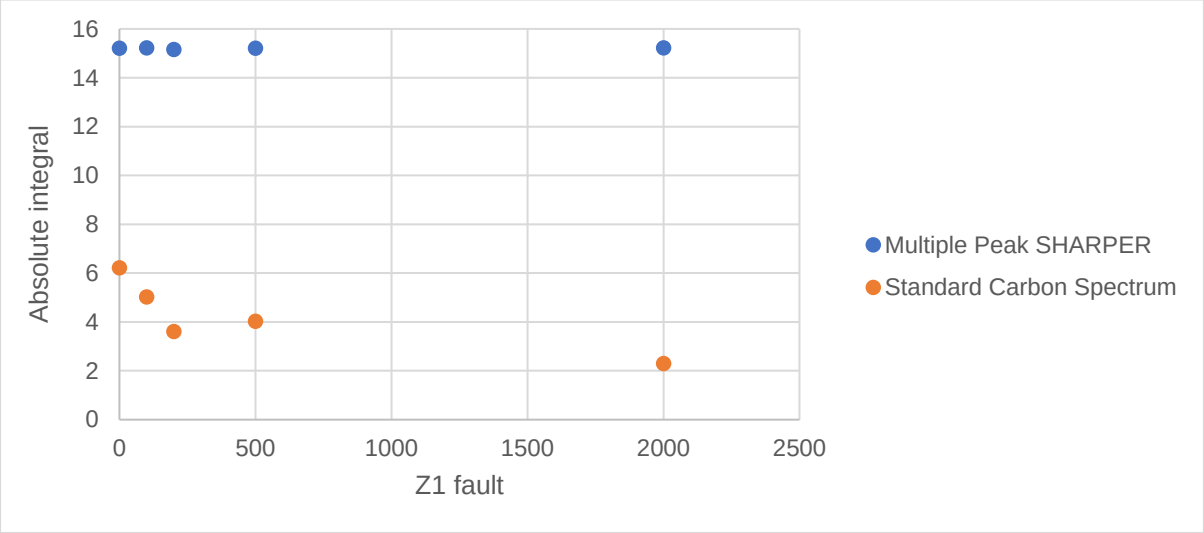

Figure 85: Absolute integrals of the CD_3OD region of the spectra shown in Figure 84, showing both integration of $^{13}C\{^1H\}$ spectra and MR-SHARPER spectra as the value of the Z1 shim is perturbed from its optimum.

4.4 Quantitative Integration for MR-SHARPER

One critical question regarding MR-SHARPER is whether it remains quantitative. In order to test this continual addition of $CHCl_3$ into CD_3OD was monitored by NMR using both MR-SHARPER and a 1D ^1H spectrum which serves as a control. Both solvents had a significant water impurity, giving a three-resonance spectrum (7.92 ppm ($CHCl_3$), 4.87 ppm (HDO) and 3.32 ppm (CD_3OD)).

The experiment was carried out by adding a small volume (2 to 10 µL) of $CHCl_3$ to 5 mL of CD_3OD before pipetting to mix and transferring 700 µL to an NMR tube. This was allowed to equilibrate in a 500 MHz NMR spectrometer for four minutes before gradient auto shimming. A long (10 second) relaxation delay was used for the 1D ^1H spectrum. Two MR-SHARPER spectra were acquired for each concentration, each examining two resonances with the transmitter offset placed between them. The first of the SHARPER spectra had an offset between the $CHCl_3$ and HDO resonances, using a 41.5 µs dwell time with 174 points per chunk, giving a Δ value of 7.221 ms. The second SHARPER spectrum had an offset between the $CHCl_3$ and CD_3OD, using a 62.8 µs dwell time with 104 points per chunk, giving a Δ value of 6.5312 ms. The constraints placed on the Python scrips to calculate Δ allowed values of 4 ms < Δ < 8 ms with dwell times that would correspond to 7500-12500 Hz spectral width
(15-25 ppm at 500 MHz). The number of data chunks collected was set such that both MR-SHARPER FIDs were approximately 10 s long and a 10 s relaxation delay was used.

During processing the MR-SHARPER spectra were zero-filled to 2048 K datapoints and had a 0.3 Hz Gaussian applied to remove truncation artefacts. Zero-filling and apodisation was not used for the 1D ^1H spectrum. All spectra were then baseline corrected (1st order polynomial fit) before integration. Integrals were then normalised relative to the most intense signal recorded for that set of spectra *i.e.* all of the MR-SHARPER spectra examining $CHCl_3$ and HDO were normalised against the most intense peak recorded in the MR-SHARPER spectra examining both $CHCl_3$ and HDO, and likewise for the other MR-SHARPER spectra and the 1D ^1H.

The normalised MR-SHARPER integrals, Figure 86, showed good agreement with the integrals from the 1D ^1H spectrum. The integrals of both the $CHCl_3$ and HDO signals consistently rose as increasing amounts were added. The solvent, CD_3OD, only fell from a concentration of 100% to 98.8%, so little change in the integral of the associated CH_3OD resonance was expected, and this is reflected in both sets of spectra.

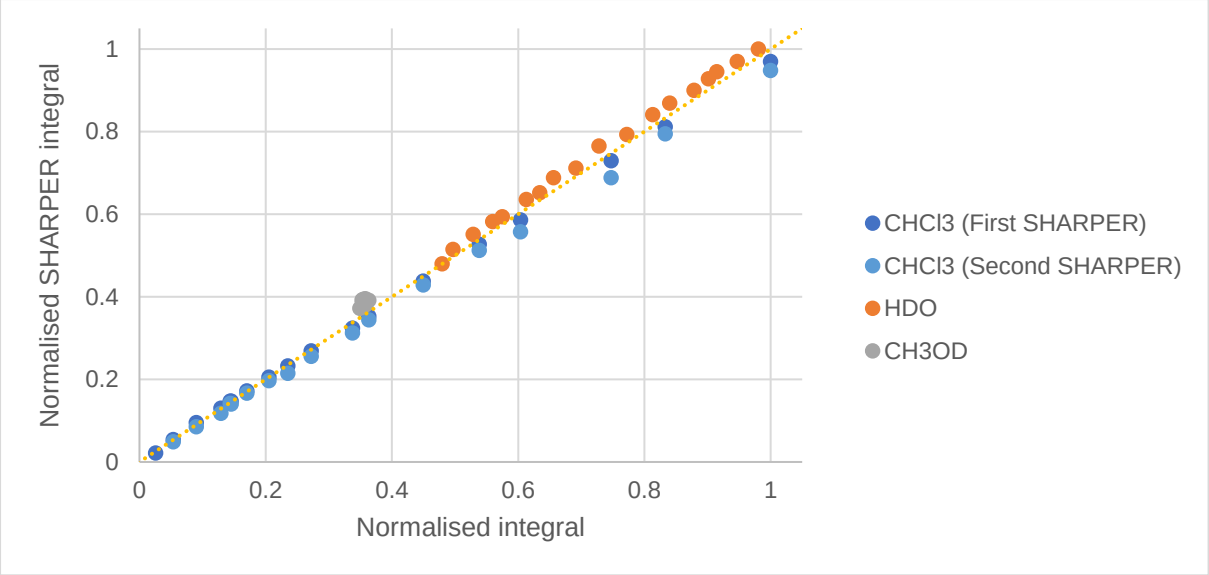

Figure 86: Comparison of the integrals obtained from MR-SHARPER experiments and a 1D ^{1}H experiment.

Comparison of the integrals of HDO and $CHCl_3$ signals within the same MR-SHARPER spectrum yields almost identical results to those derived from the 1D ^{1}H spectrum, Figure 87. This comparison shows a jump in HDO concentration between datapoints five and six. The reason for this was not identified, and is likely due to a handling error, though reassuringly it is observed in both the 1D ^{1}H spectrum and the MR-SHARPER spectrum.

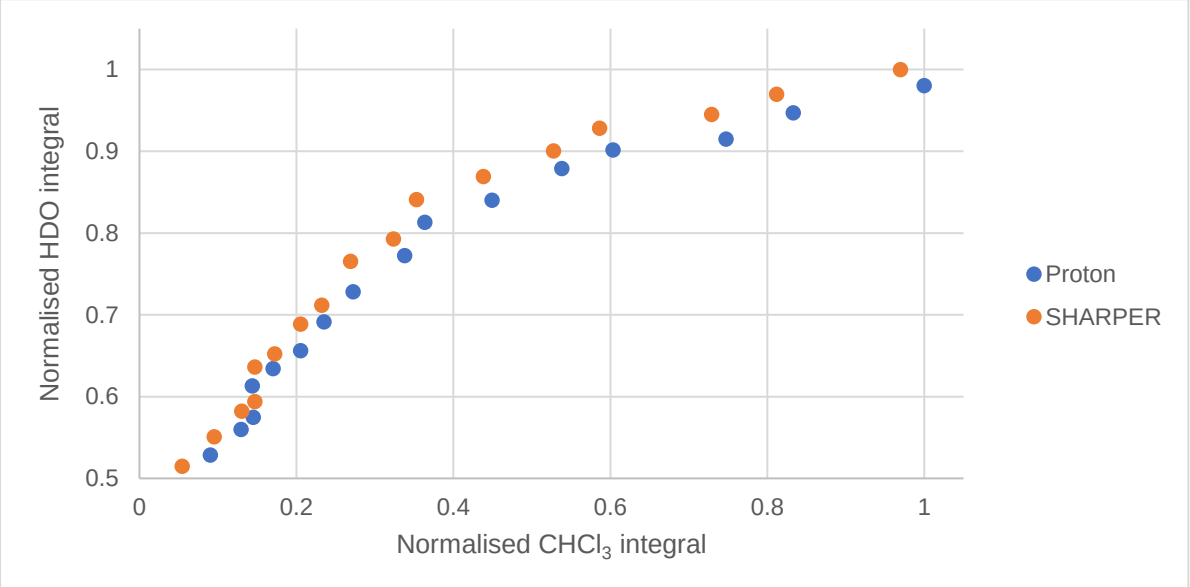

Figure 87: Comparison of the $CHCl_3$ integral and HDO integral, as monitored by MR-SHARPER and 1D ^{1}H spectra.

The agreement between the two MR-SHARPER spectra, with regard to $CHCl_3$, is near perfect when normalised integral is considered (Figure 88a). However, as expected the absolute intensities vary substantially between the two due to different pulse sequence parameterisations (Figure 88b).

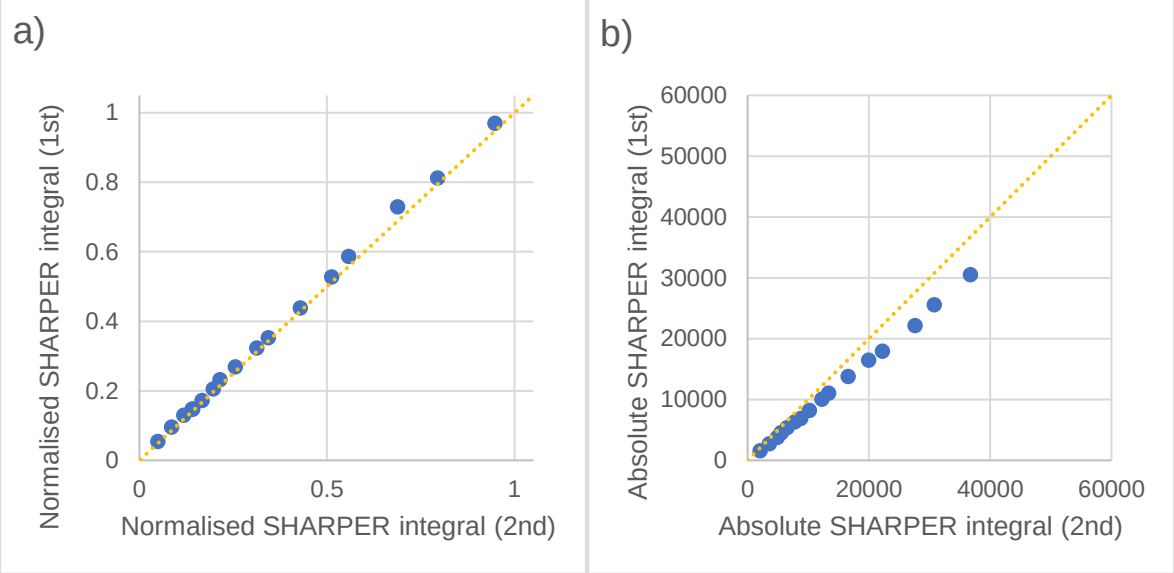

Figure 88: A comparison of the integrals, both (a) normalised and (b) absolute, from the two different sets of MR-SHARPER experiments, both examining the $CHCl_3$ signal. A dotted yellow X=Y line is plotted in both cases.

As can be seen in Figure 89 this variation in absolute integrals is not accounted for by intensity having been shifted into the sideband artefacts since the sideband artefacts are actually less intense in the final SHARPER spectrum run considering $CHCl_3$ and CH_3OD (blue) than in the one considering $CHCl_3$ and HDO (red).

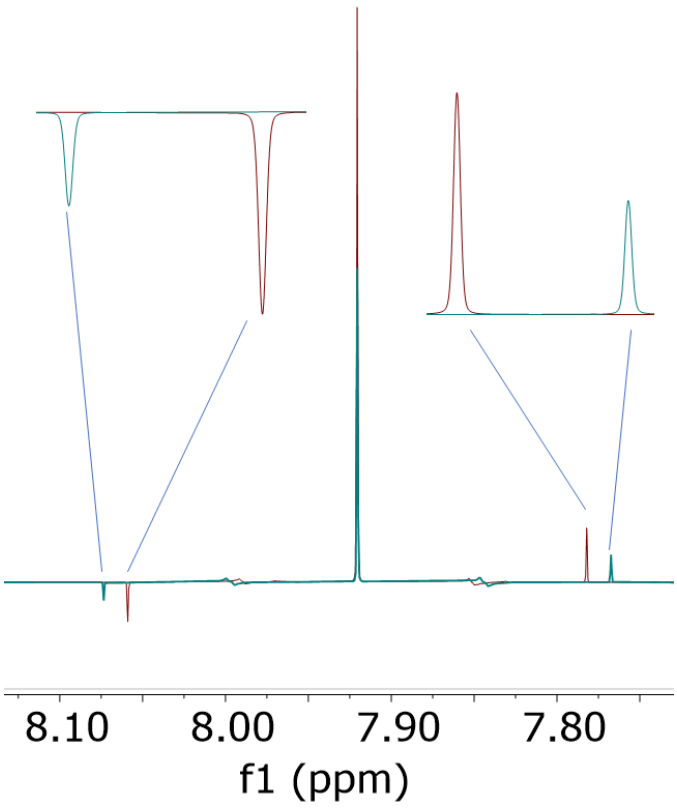

Figure 89: Overlay of the $CHCl_3$ peaks and the first two sideband artefacts in MR-SHARPER spectra, with either 7.221 ms Δ (red) or 6.5312 ms Δ (blue). All peaks in the red spectrum have larger absolute integrals (be they positive or negative). Both spectra are displayed on the same scale with regard to intensity.

Two other possible explanations are the processing differences. As the two MR-SHARPER spectra have different spectral widths but are zero-filled to the same level they have different numbers of datapoints per ppm, which could conceivably affect the integration if it led to the resonances in one spectrum being better defined than the other. However, the level of zero-filling used appeared to be sufficient in both MR-SHARPER spectra to give well defined line shapes.

The other processing related explanation is related to how the spectrometer collects datapoints. In the Bruker spectrometer used, alteration in the dwell time parameter changes the DECIM parameter (decimation rate), which alters how the spectrometer processes oversampled data.

In order to test these ideas two identical SHARPER experiments, both on-resonance, were run on the residual HDO in a sample of neat D_2O. Both used a 10 ms value of Δ, but in one this duration was made up with 200 data points per chunk and a 50 µs dwell time, whilst the other used 100 data points per chunk and a 100 µs dwell time. Both FIDs were 10 s long, and three repeats were carried out. As the spectral width differs, zero-filling was to either 2048 K or 1024 K datapoints to either maintain a constant level of zero-filling or a constant number of points per ppm in the Fourier transformed spectra. After baseline correction and apodisation (1st order polynomial fit, 0.1 Hz Gaussian) signals were integrated, with results shown in Figure 90. The doubling of dwell time causes a doubling of the absolute integral, with zero filling having made no difference.

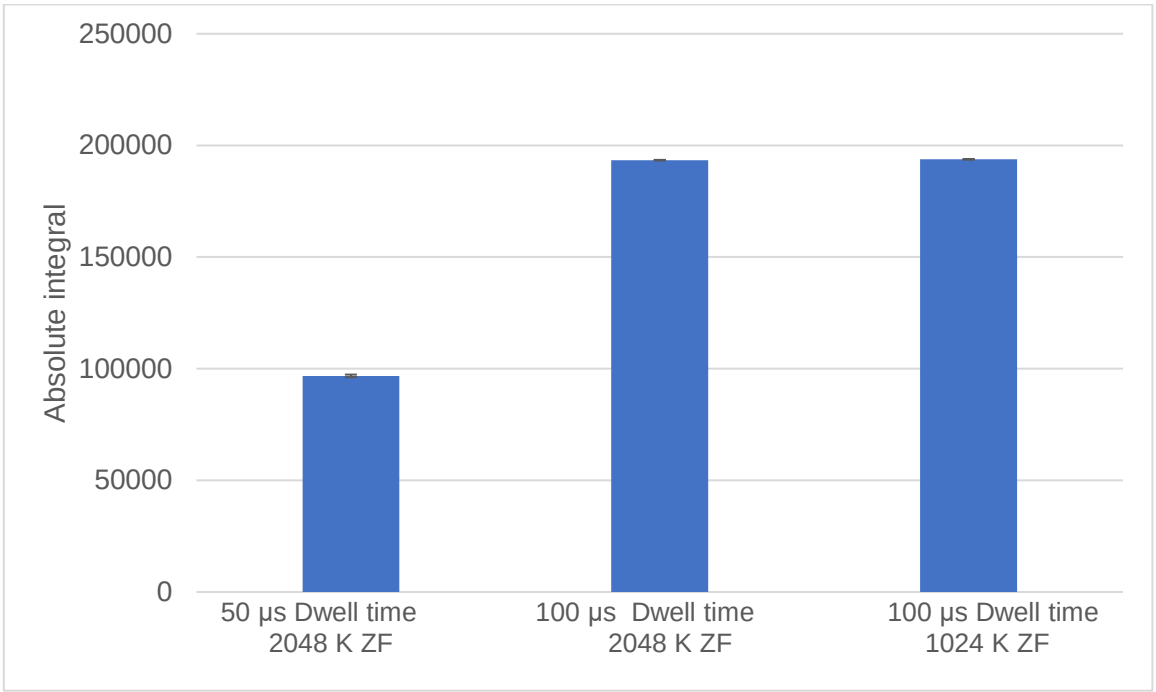

Figure 90: Average absolute integrals of HDO, as measured with SHARPER spectra with the indicated dwell time and level of zero filling. Error bars show standard deviations.

Based on this a correction factor was derived from the ratio of the dwell times for the MR-SHARPER spectra. When this correction factor (1.513) is applied to Figure 88b this causes the error to reverse, Figure 91, in terms of which set of MR-SHARPER spectra register a higher absolute integral. This suggests that the dwell time is not the only source of difference in absolute integral between MR-SHARPER spectra with differing parameters.

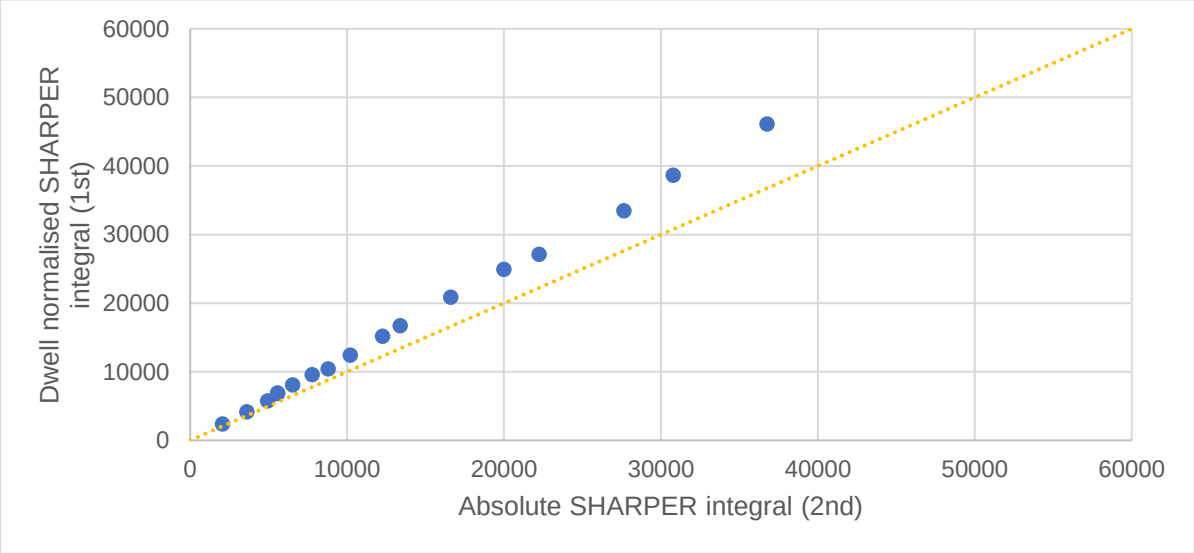

Figure 91: A comparison of the absolute integrals from the two different sets of MR-SHARPER experiments, both examining the $CHCl_3$ resonance, with one having been normalised based on the difference between dwell times. A yellow X=Y line is plotted.

Another possible explanation for the shorter Δ value SHARPER spectrum yielding a lower integral is that it utilises substantially more refocussing pulses to achieve a 10 s FID. As every pulse is around 10 μs and has a 100 μs delay either side each accounts for 210 μs of additional time for relaxation to occur. As one SHARPER experiment used 692 cycles and the other 765, this represents a full 15.33 ms difference in terms of relaxation between them. The increased number of pulses could also affect the level of relaxation that occurred in the FID *i.e.* more frequently applied refocussing pulses give narrower linewidths. However, both MR-SHARPER spectra gave the same linewidth for $CHCl_3$ without apodisation (0.16 Hz). This suggests that in both cases refocussing pulses are applied frequently enough that T_2 becomes the limiting factor for linewidth, rather than residual contributions from T_2*.

Regardless, MR-SHARPER is capable of producing quantitative spectra for a given set of parameters after normalisation. This should be perfectly sufficient for most practical applications.

4.5 Three Resonance MR-SHARPER

So far in this Chapter the MR-SHARPER methodology has been limited to examining just two resonances. Here, we demonstrate the methodology applied simultaneously to three resonances. A solution of 50:50 $CDCl_3$ and MeOD provides a system with three resonances in a ^1H spectrum – two from the residual ^1H signals from the solvents, and a third relating to an HDO impurity.

When the $CDCl_3$ at ~7.6 ppm is placed on-resonance this yields two distinct offset frequencies, ωoff_1 (1473.06 Hz) and ωoff_2 (657.37 Hz) relating to the residual CH_3OD (~3.3 ppm) and HDO impurity (~4.6 ppm). The MR-SHARPER script was modified (Appendix 8.5.4) to carry out all operations up to and including the production of an array of the "final percentage of rotation completed" for both ωoff_1 and ωoff_2 in parallel. This provides a pair of arrays which describe how closely each experimentally available value of Δ matches to ωoff_1 or ωoff_2. The product of these two arrays was then taken, and the lowest value found, which should give an experimentally accessible value of Δ which is suited to both ωoff_1 and ωoff_2.

The allowed ranges for the value of Δ were 5 ms < Δ < 8 ms using dwell times that would correspond to 7500-20000 Hz (15-40 ppm at 500 MHz) spectral width. The spectral width parameter was deliberately allowed to vary significantly to give the best chance of locating an experimentally available timing suited to the frequencies present. The optimal value of Δ determined by the script was 6.11 ms, with 532 data chunks collected producing an FID of approximately 6.5 seconds duration. After processing (zero-filling to 2048 K datapoints, 1st order polynomial baseline correction, 0.2 Hz Gaussian apodisation) integrals were taken. The proton spectrum (Figure 92b) was baseline corrected in the same fashion and gave normalised integrals of 1.00:10.90:4.38 for the three peaks (in order of reducing chemical shift), whilst the MR-SHARPER spectrum (Figure 92a) gives 1.00:10.86:4.39. This demonstrates that the MR-SHARPER experiment still produces quantitative results when extended to more than two resonances.

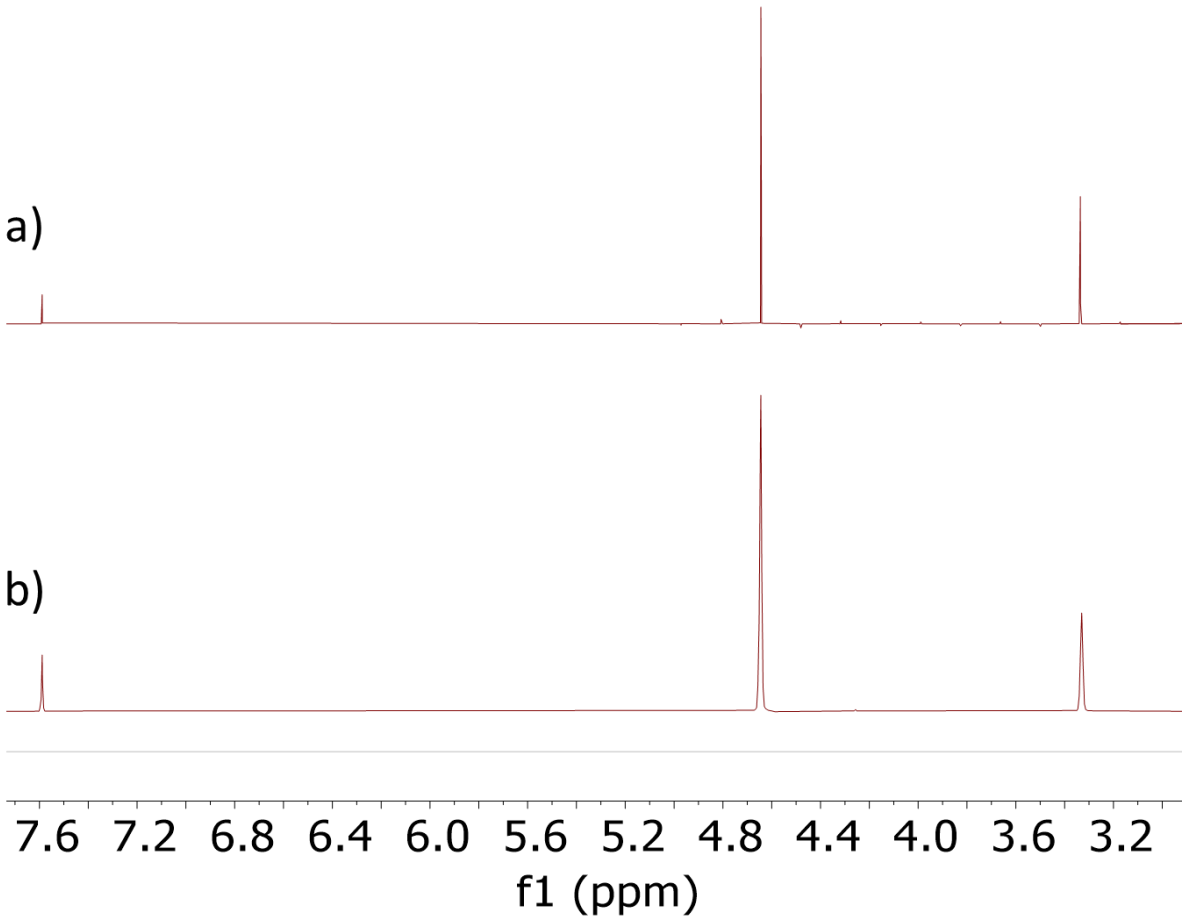

Figure 92: (a) Three resonance MR-SHARPER spectrum and (b) 1D ^{1}H spectrum.

The signal-to-artefact ratio in this SHARPER spectrum is good, with the most intense peaks relating to each resonance being at least 50 times more intense than the adjacent sideband artefacts.

However, as detailed earlier in this Chapter (Figure 79) there are several locations the transmitter offset can be placed when considering three resonances. When the transmitter offset was placed between the $CHCl_3$ and HDO resonances, yielding a ωoff_1 of 736.53 Hz (relating to the $CHCl_3$ and HDO) and a ωoff_2 of 1393.9 Hz (relating to the CD_3OD) the scripts were unable to locate an ideal experimentally available value of Δ, given the constraints. The “best” value was identified to be 5.74 ms, but led to an artefact heavy spectrum, Figure 93a. If restraints on Δ are relaxed to 5 ms < Δ < 30 ms an ideal value of 12.22 ms is given, which does yield a high-quality SHARPER spectrum, Figure 93b.

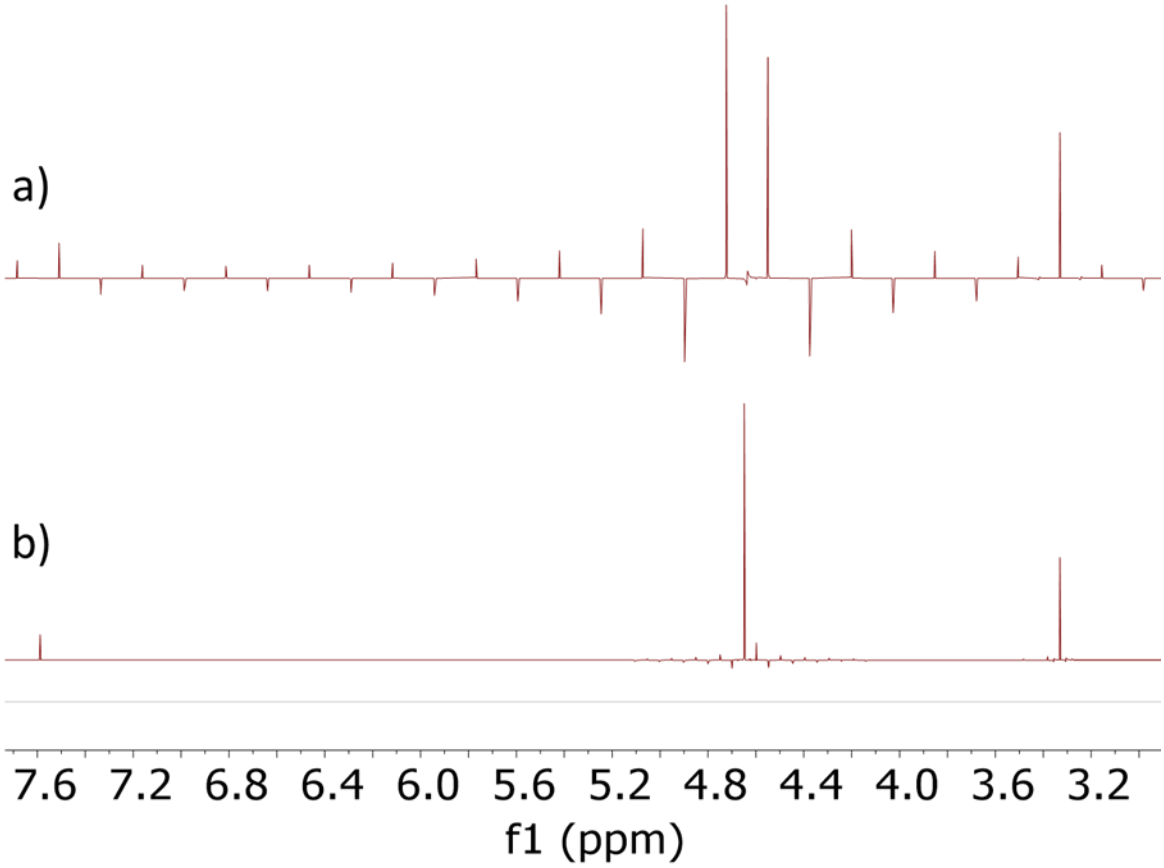

Figure 93: Three resonance MR-SHARPER spectra with Δ values of (a) 5.74 ms and (b) 12.22 ms. Both use a transmitter offset of ~5.5 ppm, exactly halfway between the highest and lowest chemical shift peaks.

With these relaxed restraints on the value of Δ all possible transmitter offsets produced high quality SHARPER spectra. However, Δ values of up to 30 ms may be too long when working with samples where large homocouplings are present or there is significant magnetic field inhomogeneity. Thus, transmitter offset placement appears critical for determining short experimentally accessible values of Δ that also match well to theoretically required values, as given by Equation 12. This suggests that for the frequency ranges of 500 MHz ^{1}H spectra, three resonance MR-SHARPER is operating near the limit of the precision of the timings that can be achieved with the hardware used here (a Bruker 500 MHz AVIII HD) in conjunction with this method of generating the timing Δ.

5 Mobile-SHARPER

Another issue faced by the SHARPER experiment is that if the frequency of the resonance being studied changes over time the quality of the spectra collected will deteriorate if the transmitter offset of the SHARPER experiment is not altered accordingly.

This Chapter demonstrates a method to track the frequency of a resonance as it changes and update the parameters of SHARPER and MR-SHARPER spectra accordingly.

5.1 Estimation of Resonance Frequency

As shown in Chapter 3, the most intense peak in a SHARPER spectrum and the most intense sideband artefact are always located either side of the actual frequency of the NMR signal. This applies regardless of whether the spectrum is recorded on or off-resonance.

Here we attempt to accurately calculate the actual frequency of the resonance under study from SHARPER spectra recorded with different transmitter offsets. To do this we reconsider the dataset described previously in Figure 70. This consisted of a series of off-resonance SHARPER spectra of HDO recorded over a wide range of offsets (~2700 Hz) with increments between them varying from 1300 Hz to 1 Hz.

An intensity-weighted average of the frequencies of the most intense peak and the most intense sideband artefact in these spectra, as per Equation 13, was taken:

$$Intensity\ Weighted\ Average\ Frequency = (I_{IP} * \omega_{IP} + I_{SA} * \omega_{SA})/(I_{IP} + I_{SA})$$

Equation 13: I refers to Intensity, ω to frequency and the subscripts IP and SA to most intense peak and most intense sideband artefact respectively.

This results in a range of values for the intensity-weighted average frequency of 2351.83 Hz ±1.5 Hz. This value is close to the real frequency of the NMR signal, 2351.95 Hz, which was determined from the peak maximum in a 1D ^{1}H spectrum acquired on the sample at the same time.

These experiments were repeated with identical parameters (5 ms value of Δ, 10 s total acquisition) but with a much narrower range of transmitter offsets explored. In total 43 values were used, all within a 5 Hz range of being on-resonance. Curiously, signal-to-artefact ratio was not maximised when the transmitter offset was set to precisely the apparent on-resonance position suggested by the 1D ^{1}H spectrum, but rather ~0.85 Hz off-resonance from it, as shown in Figure 94.

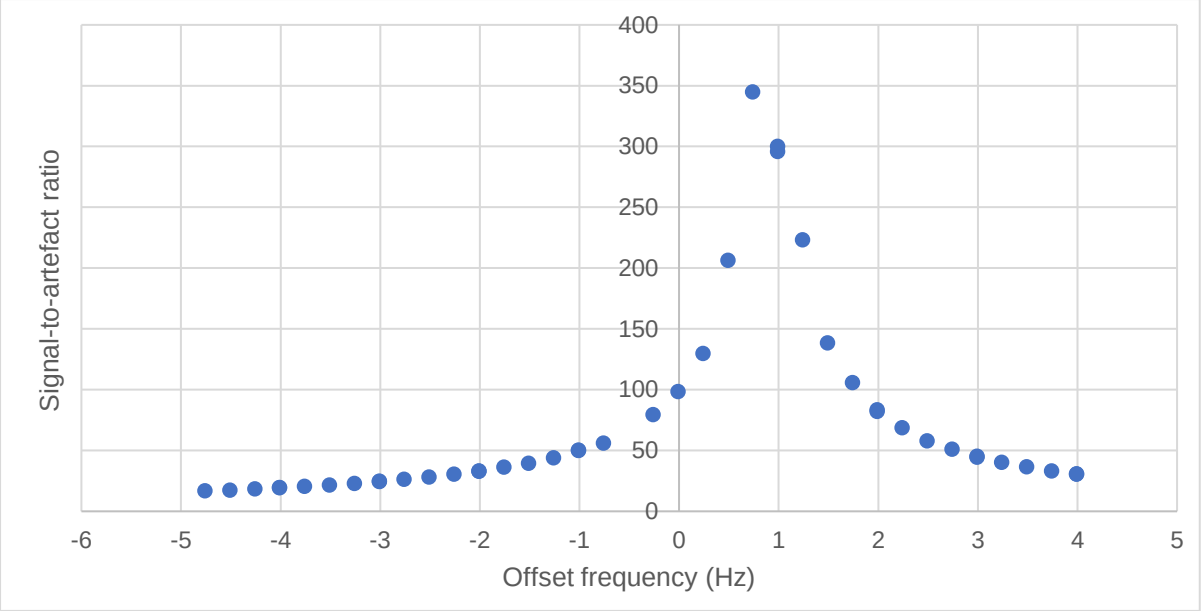

Figure 94: Signal-to-artefact ratio produced by running SHARPER just off-resonance. The offset frequency is relative to the peak maximum in a 1D 1H spectrum.

When an intensity-weighted frequency average is taken for this narrower offset sweep, as Equation 13, a narrower range of values (±0.4 Hz) is yielded. These values, shown in Figure 95 match more closely to the transmitter offset for optimal signal to artefact ratio, identified from Figure 94, than to the peak maximum of the HDO in the 1D ^{1}H spectrum. This suggests that the optimal offset for SHARPER spectra is not the peak maximum in a 1D ^{1}H spectrum but just off-resonance and can be better estimated using Equation 13. An explanation for this behaviour is presented later in this Chapter, in Section 5.5.

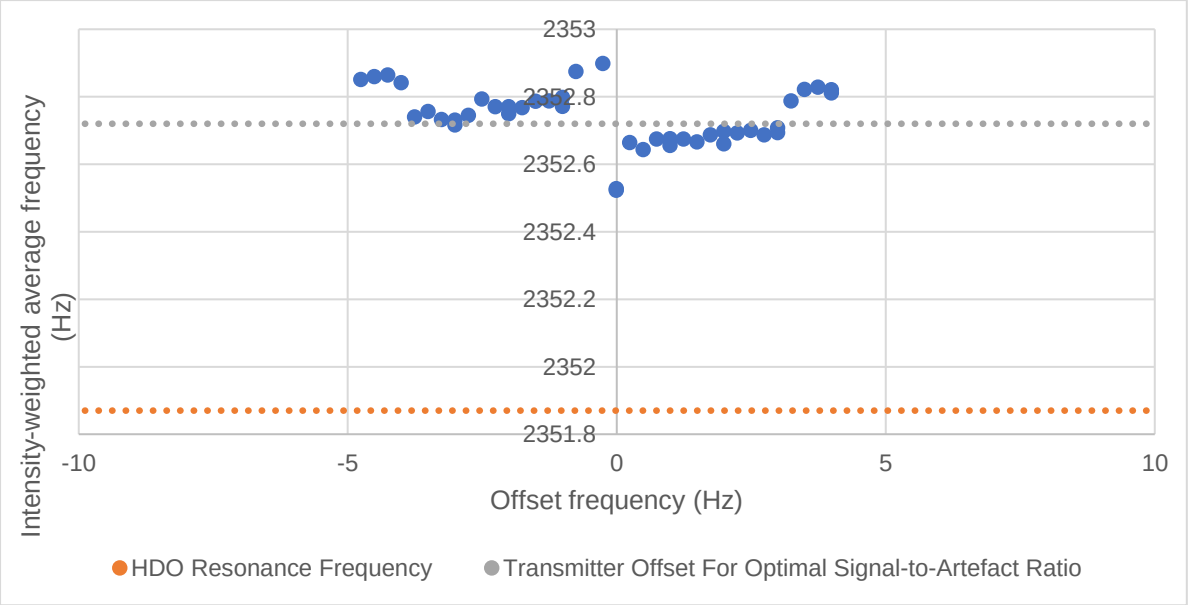

Figure 95: Intensity-weighted frequency averages from a set of off-resonance SHARPER spectra run close to resonance, with the optimum transmitter offset for signal to artefact ratio shown as a dotted grey line, and the frequency of the HDO resonance shown as a dotted orange line. The offset frequency is relative to the peak maximum in a 1D 1H spectrum.

5.2 Mobile-SHARPER Macro

In order to be of experimental utility for setting the optimal transmitter offset for SHARPER spectra, any analysis needs to be able to be carried out rapidly and continuously throughout the reaction monitoring procedure. This is achieved by combining a set of Python 2.7 scripts which calculate a new offset based on a peak list generated by a Topspin 3 macro which is responsible for processing spectra and acquiring subsequent spectra with the updated transmitter offset. The workflow is outlined in Figure 96.

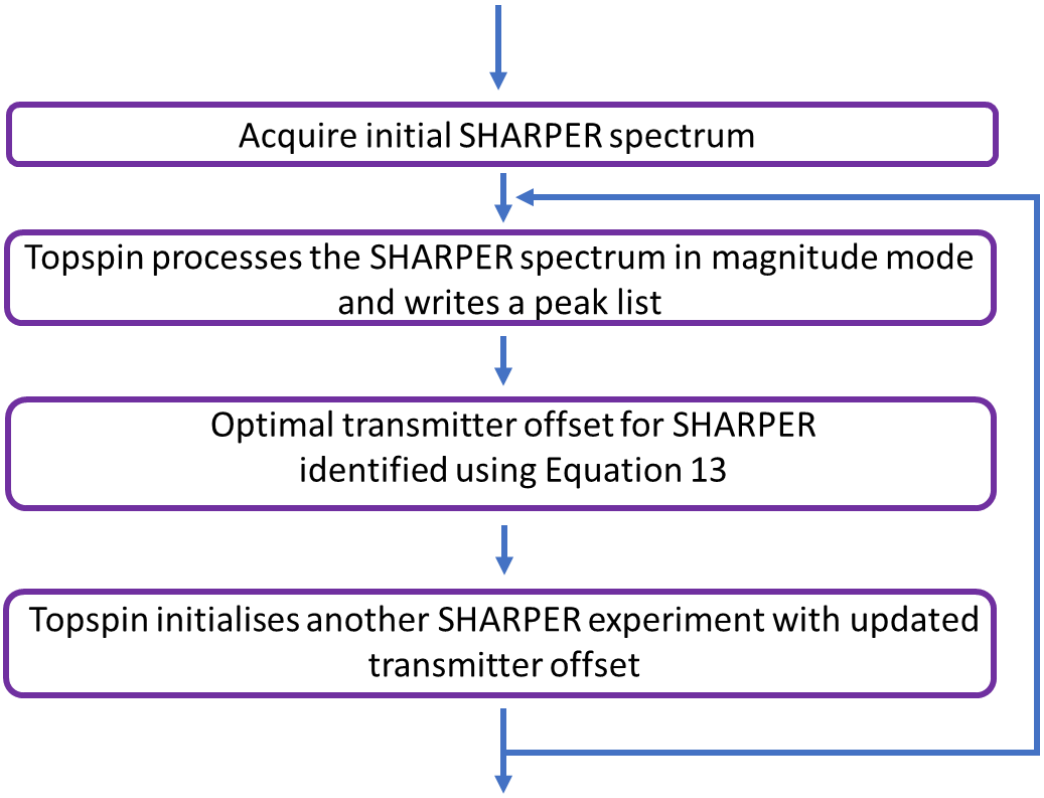

Figure 96: Workflow for the mobile-SHARPER macro.

The user is required to run an initial SHARPER spectrum, which defines all experimental parameters save for the transmitter offset, which will be adjusted based on the macro's calculations.

The Topspin 3 macro initially applies magnitude mode processing to the spectrum. This is preferred over phase-sensitive analysis because Topspin 3.6.1's automated phasing was found to deal poorly with low signal-to-artefact ratio spectra which can arise when the frequency of the resonance changes such that the SHARPER spectrum has not been run on resonance. The macro then produces a peak list and passes it to the Python 2.7 script, along with the duration of Δ in the acquired SHARPER spectrum.

The Python script then identifies the most intense peak in the spectrum. As the separation of the sideband artefacts is inversely proportional to the value of Δ, this can then be used to identify the locations of the two adjacent sideband artefacts (at $(2\Delta)^{-1}$ Hz away from the most intense peak). If neither artefact peak is found near the expected location (by default 2 Hz, though this is entirely arbitrary) then the transmitter offset is not updated. This can occur because Topspin 3.6.1 will only pick peaks of a certain intensity relative to the most intense peak in the spectrum, in order to avoid peak picking noise. Thus in this scenario it can be assumed that the current transmitter offset is already giving an essentially artefact free spectrum.

If the sideband artefact peaks are located then an intensity-weighted average frequency is calculated, as per Equation 13, in order to establish an updated value for the transmitter offset.

The Topspin 3 macro then creates and runs a new SHARPER experiment with an updated transmitter offset based on the intensity-weighted average frequency. All other parameters are identical to the initial SHARPER spectrum. The macro can run any number of SHARPER experiments, as defined by the user.

5.3 Initial Experiments on a Stationary Resonance

The mobile-SHARPER macro was initially tested on a sample of neat D_2O, with a 5 ms value of Δ and 1000 cycles, yielding a 10 s FID. The initial offset was arbitrarily set to 50 Hz away from the 1D ^1H spectrum peak maximum. This gives a spectrum with close to the worst possible signal-to-artefact ratio (Figure 97a). The mobile-SHARPER macro was then run for seventeen iterations, the first two of which are shown below (Figure 97b and c). Signal-to-artefact ratio is notably higher in Figure 97b, and improves again in Figure 97c.

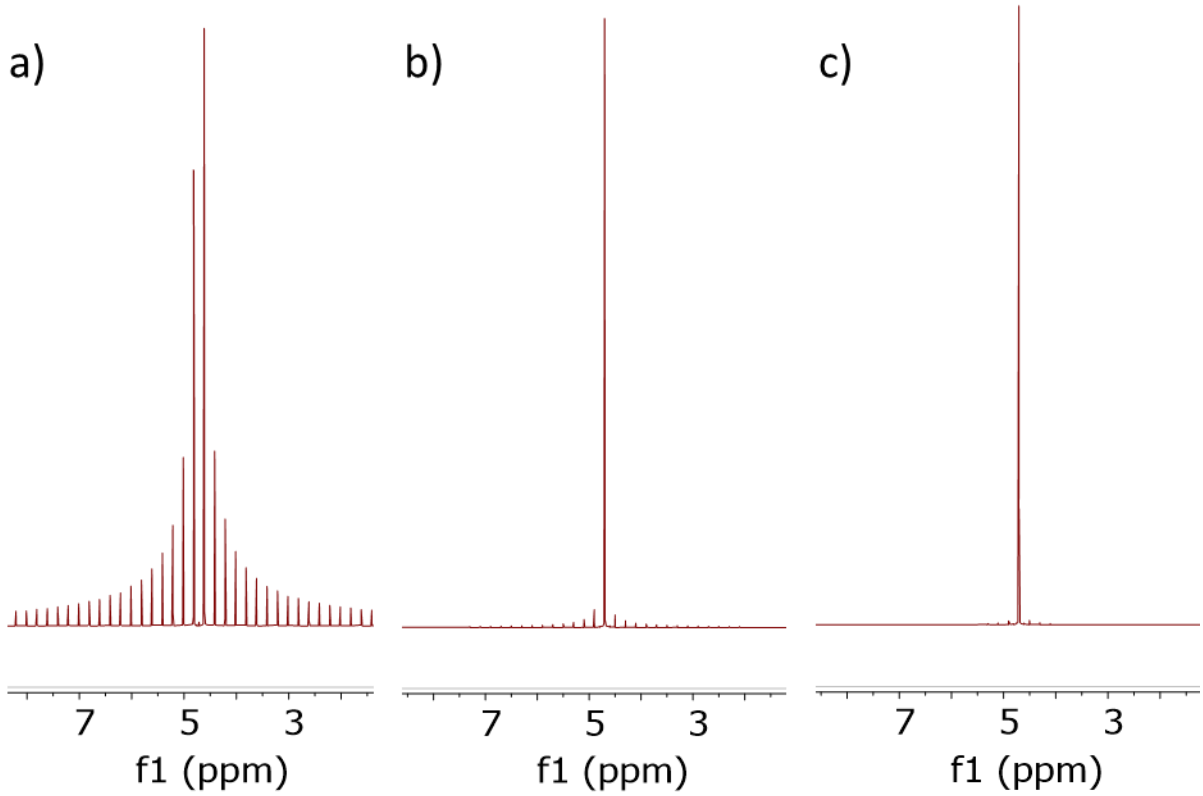

Figure 97: SHARPER from experiments run (a) with a poorly set offset (b) after the first iteration of the mobile-SHARPER macro and (c) after the second iteration of the mobile-SHARPER macro. Spectra shown in magnitude mode.

The signal-to-artefact ratios of the magnitude mode mobile-SHARPER spectra are plotted in Figure 98. This shows that after the second mobile-SHARPER spectrum acquired with an updated offset (Figure 97c) a maximum signal-to-artefact ratio is reached and then begins to oscillate, though values are consistently high, at around 300:1.

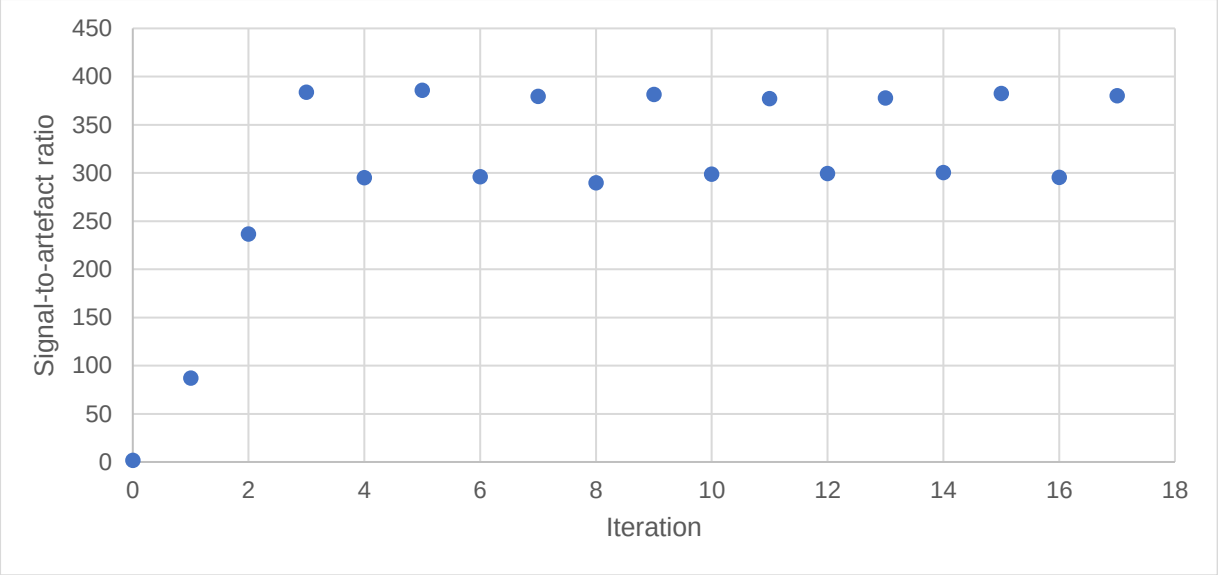

Figure 98: A set of experiments with the mobile-SHARPER macro, showing increasing signal-to-artefact ratio before it oscillates between two high signal-to-artefact ratios.

The offsets of the mobile-SHARPER spectra are shown graphically in Figure 99b and the Fourier transforms of the last 10 iterations shown overlaid with a standard 1D ^{1}H spectrum in Figure 99a. From this it can clearly be seen that the choice of transmitter offset by the mobile-SHARPER macro oscillates between two positions, neither of which is centred around the peak maximum in the 1D ^{1}H spectrum. The reasons for this latter effect are discussed in Section 5.5.

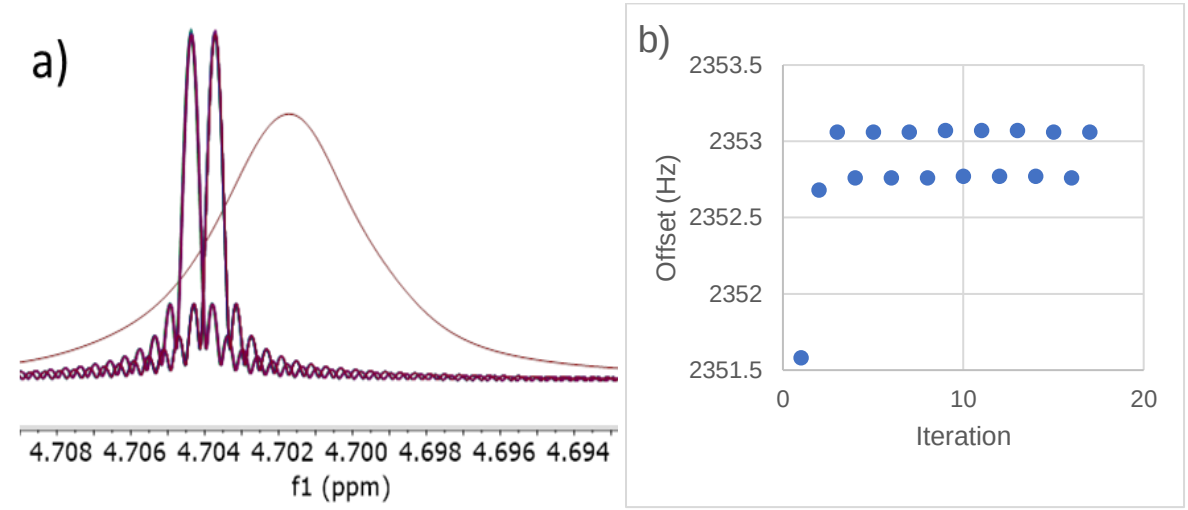

Figure 99: (a) Overlay of the most intense peak from a series of Fourier transforms of mobile-SHARPER experiments after reaching equilibrium regarding signal-to-artefact ratio. A 1D ^{1}H spectrum is shown for reference. (b) Graphical representation of the offsets of a series of mobile-SHARPER spectra.

To see how the two frequencies mobile-SHARPER oscillates between relate to the optimum transmitter offset for signal-to-artefact ratio the optimal transmitter offset was determined by acquiring SHARPER spectra with varying transmitter offsets (but otherwise identical parameters). Figure 100 shows the results of this offset sweep, with the signal-to-artefact

ratio being maximised at 2353.1 Hz. The frequencies mobile SHARPER oscillates between are either side of this (marked with yellow and blue lines) and a simple average of these gives an answer within 0.02 Hz of the optimum transmitter offset for signal-to-artefact ratio. The offset determined from the peak maximum in a 1D ^{1}H spectrum is shown in grey.

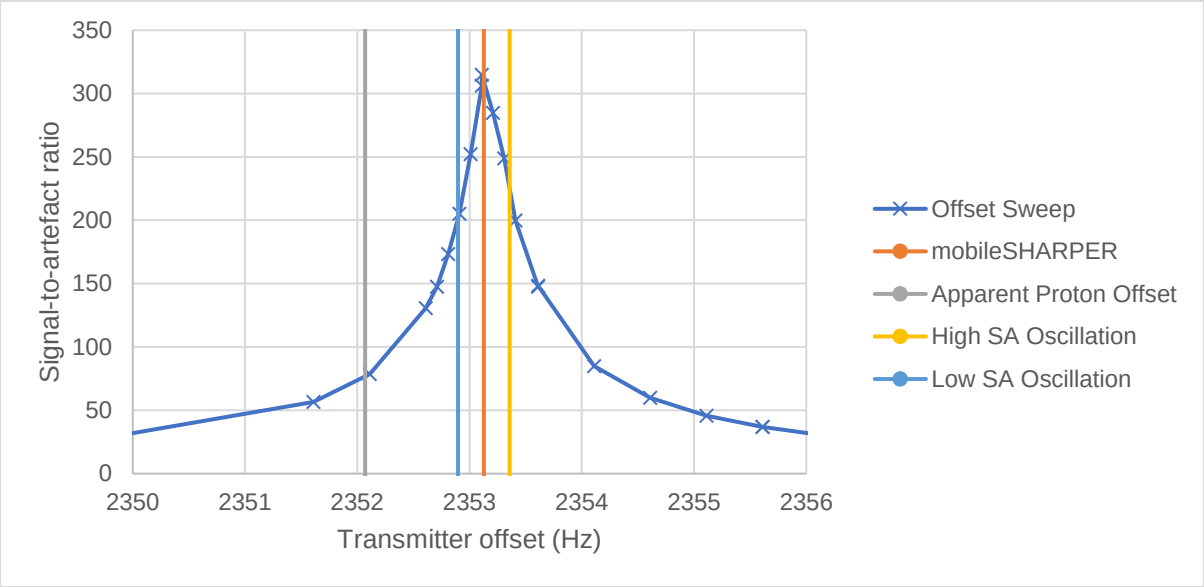

Figure 100: A transmitter offset sweep with SHARPER to determine the optimum transmitter offset for signal-to-artefact ratio. Also shown are vertical lines which indicate the peak maximum in a 1D ^{1}H spectrum, the two frequencies mobile-SHARPER oscillates between and the average of these frequencies.

In order to determine the source of these oscillations alternate methods of processing spectra run by mobile-SHARPER were tried. Peak integral (rather than intensity) was examined for each of the spectra produced by the mobile-SHARPER macro. This was used to calculate an integral-weighted frequency average, Equation 14, comparable to the intensity-weighted frequency average in Equation 13.

$$Integral\ Weighted\ Average\ Frequency = (i_{IP} * \omega_{IP} + i_{SA} * \omega_{SA})/(i_{IP} + i_{SA})$$

Equation 14: i refers to Integral, ω to frequency and the subscripts *IP* and *SA* to most intense peak and the highest intensity sideband artefact respectively.

Integrals were measured from magnitude mode spectra after baseline correction (1st order polynomial fit). Figure 101 shows the transmitter offset oscillation using either intensity or integral weighting. It is notable that integral analysis appears less reliable, with a greater range of offsets and less regular behaviour between iterations. This may be because at very high signal-to-artefact ratios the integral of sideband artefacts is significantly influenced by broad baseline features of the most intense peak in the spectrum.

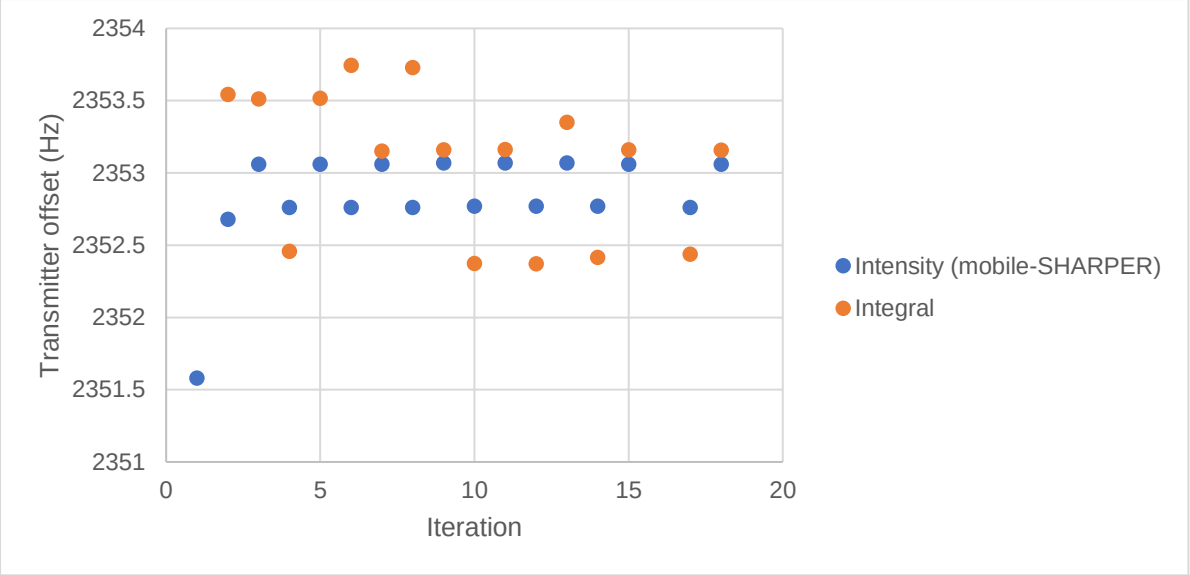

Figure 101: Transmitter offsets from the mobile-SHARPER experiments, overlaid with predictions of the updated transmitter offsets the mobile-SHARPER macro would have calculated given use of integral rather than intensity.

In order to remove these broad features from the spectrum the FID was left-shifted by 200 datapoints *i.e.* the first 200 datapoints were deleted, and datapoint 201 defined as being at time 0. Both integral and intensity-weighted average frequencies were calculated after this processing step, Figure 102. This substantially reduces the oscillations that could be expected when considering integral-weighted analysis but has little effect on intensity-weighted analysis. This suggests that integral-weighted analysis (with a left-shift) could be superior for identifying optimal transmitter offset positions for mobile-SHARPER. However, achieving precise enough integrals in the short time between scans proved challenging, and so intensity-weighted analysis appears to be the more practical option.

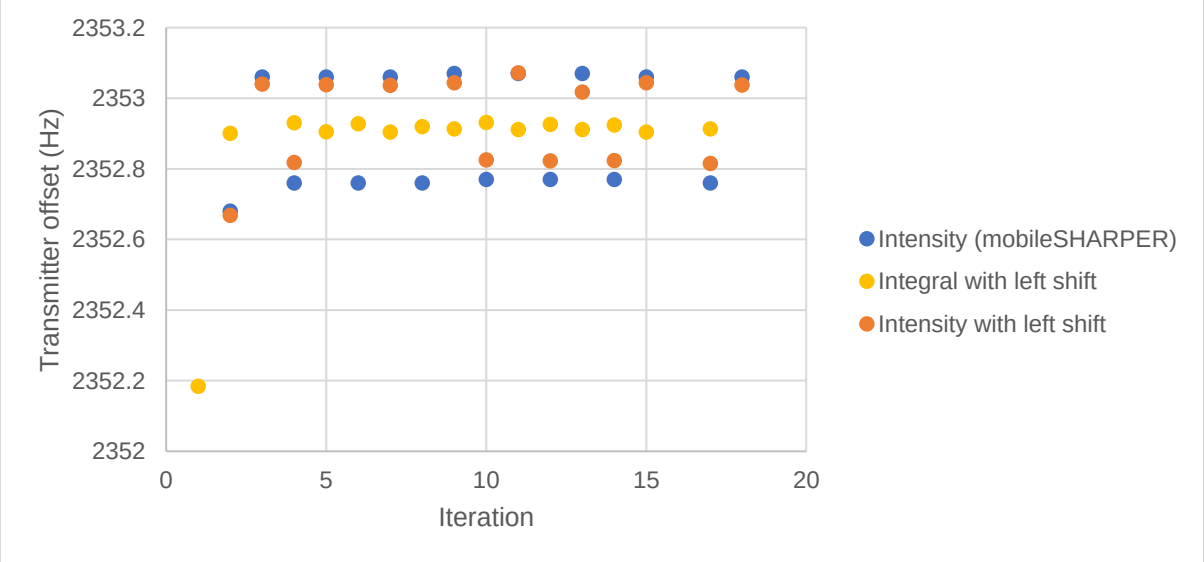

Figure 102: Transmitter offsets from the mobile-SHARPER experiments, overlaid with predictions of the updated transmitter offsets the mobile-SHARPER macro would have calculated given use of integral or intensity with the first 200 datapoints removed.

In order to gauge the effect of the oscillatory behaviour of mobile-SHARPER in practical applications, a series of SHARPER spectra were run on the neat D_2O sample with a range of transmitter offsets. Δ was set to 10 ms, and 500 cycles were used. Spectra were zero filled to 2048 K, baseline corrected (1st order polynomial fit) before measurement of signal-to-artefact ratio and the absolute integral of the most intense peak.

These results, Figure 103, show that at low signal-to-artefact ratios (<5:1) the absolute integral of the most intense peak is very low. In the worst case integral drops to 67.3% of the largest integral measured. This is because a significant amount of the intensity is present in the sidebands of a low signal-to-artefact SHARPER spectrum, rather than being concentrated in a single intense peak. However, when considering the high signal-to-artefact ratio spectra (>20) there is negligible difference in integral between them. As the spectra produced by the mobile-SHARPER macro are *all* very high signal-to-artefact ratio (often >200:1), the oscillations in integral are unlikely to cause any significant problems in practice with analysis.

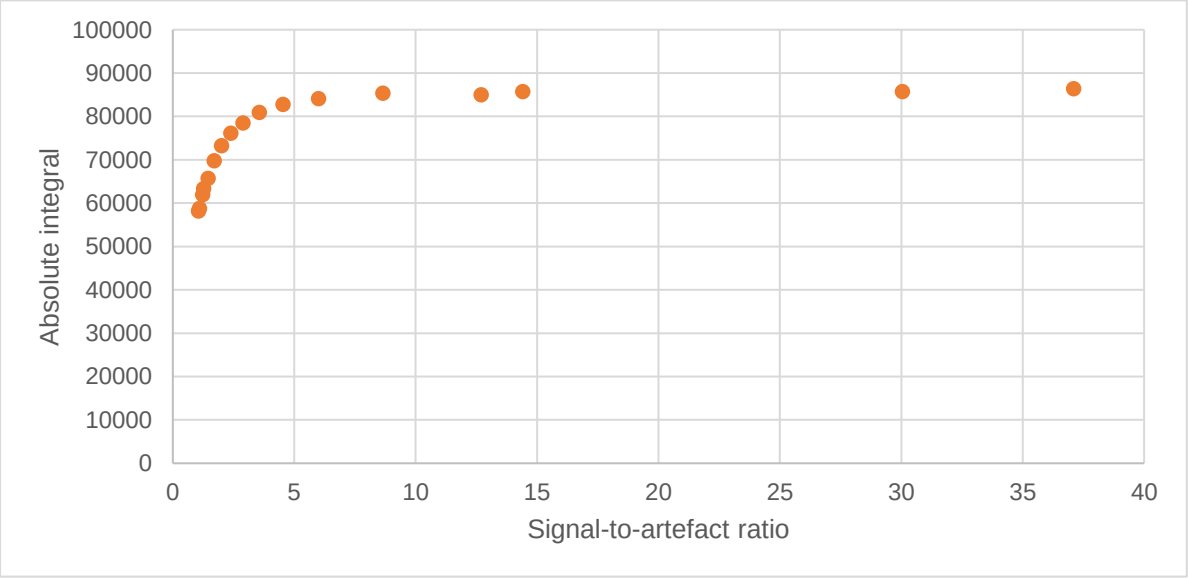

Figure 103: Signal-to-artefact ratio plotted against absolute integral of the most intense peak for a series of SHARPER spectra with varied transmitter offsets.

5.4 Mobile-SHARPER on a Resonance with a Changing Frequency

To provide a system with a single resonance with a frequency that changed over time variable temperature studies were carried out on a sample of neat D_2O. A temperature change from 70 ºC to 15 ºC caused a 7 Hz change in the frequency of the residual HDO signal. This took 150 seconds, according to the spectrometer thermostat (although the sample will equilibrate more slowly).

SHARPER experiments used a 5 ms value of Δ, and 500 cycles yielding a 5 s FID long with a 5 s relaxation delay allowing recording of a spectrum every 10 s during the temperature change. The sample was equilibrated for 15 minutes at 70 ºC before simultaneously commencing the mobile-SHARPER macro for 26 iterations and beginning the temperature decrease. The initial transmitter offset was based on the peak maximum in a 1D ^{1}H spectrum. A set of control SHARPER experiments with a fixed transmitter offset were also acquired. These made use of a modified version of the mobile-SHARPER macro that did not update the offset, but still carried out all calculations. This means any additional delays added between scans by the use of the macro should be identical in both sets of experiment.

SHARPER spectra were zero-filled (2048 K), baseline corrected (1st order polynomial fit) and apodised (0.1 Hz Gaussian). A selection of both sets of spectra are shown in Figure 104. The sideband artefacts become progressively worse when the offset is fixed, whereas sideband artefacts remain at a constant low level when the mobile-SHARPER macro is used to dynamically update the offset.

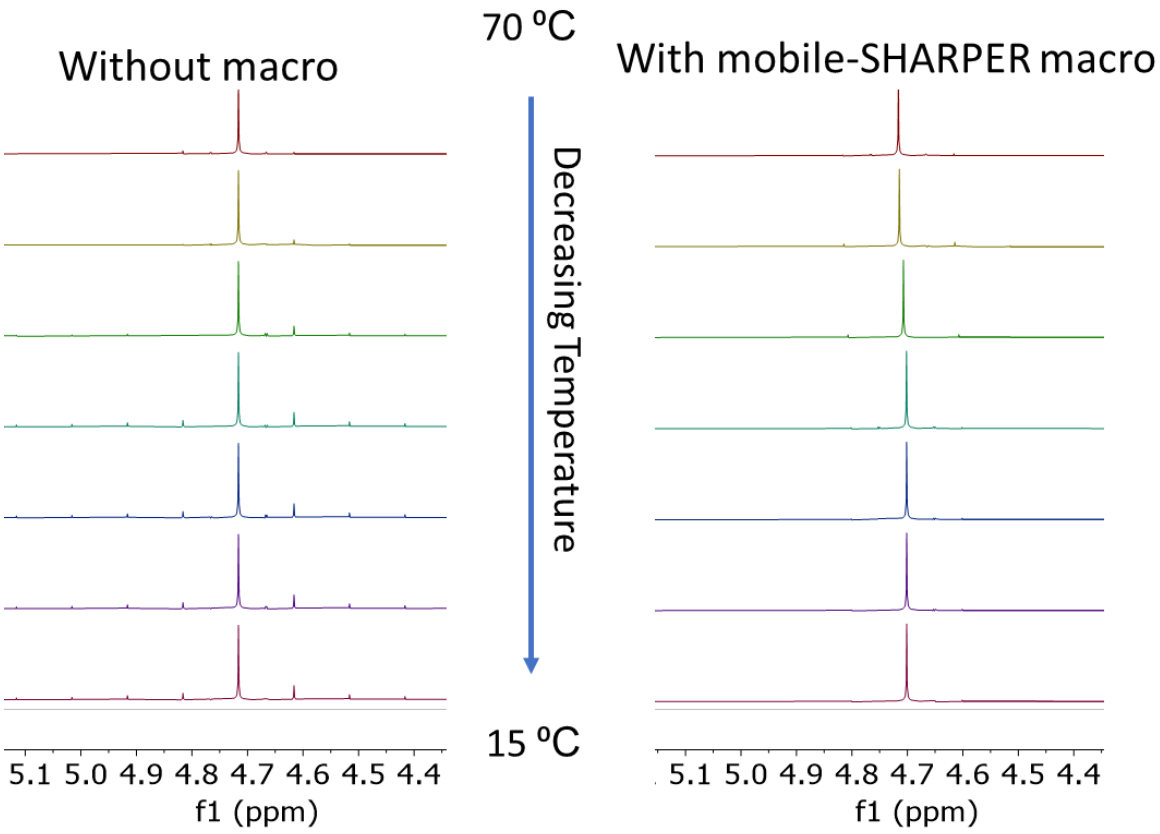

Figure 104: A selection of SHARPER spectra run during a temperature decrease with and without dynamic updates of the transmitter offset.

When the signal-to-artefact ratio is analysed and shown graphically, Figure 105, the mobile-SHARPER spectra show an initial lag period where signal-to-artefact ratio drops at a similar rate to the standard SHARPER spectra recorded without the macro. However, before 15 ºC is reached the signal-to-artefact ratio begins to increase substantially – to an even higher level than in the initial spectra. As expected the signal-to-artefact ratio when the transmitter offset is fixed declines during the temperature reduction and never recovers.

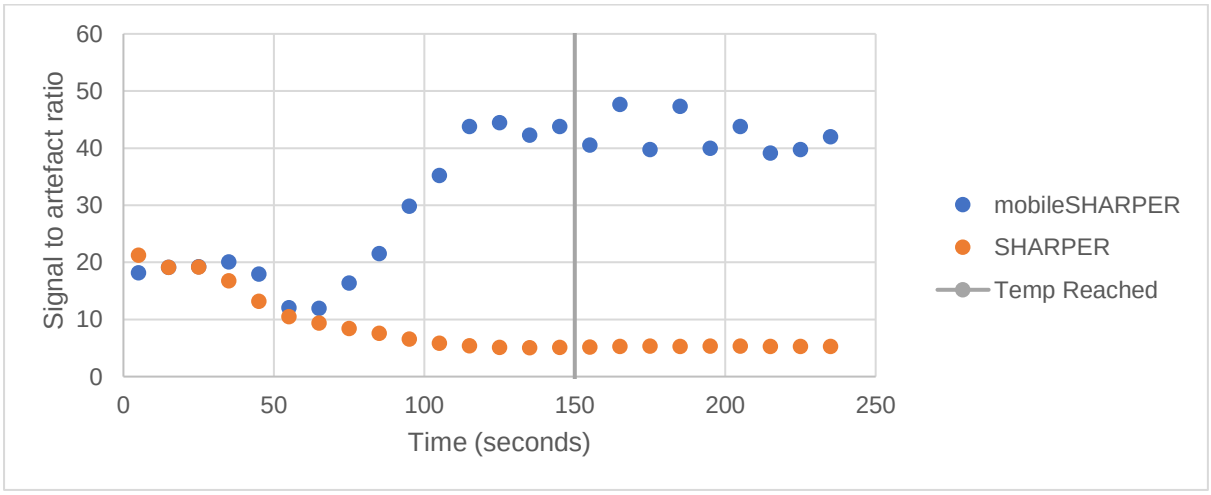

Figure 105: Signal-to-artefact ratio for SHARPER experiments both with and without use of the mobile-SHARPER macro to dynamically update the transmitter offset during a temperature sweep from 70 ºC to 15 ºC.

5.5 Experimental Factors Affecting Optimum Transmitter Offset

As shown earlier in this Chapter, the optimum transmitter offset for signal-to-artefact ratio for SHARPER is not the same as the frequency of the peak maximum in a 1D ^{1}H spectrum. In this Section the factors that affect this are examined experimentally and used to develop a model to explain some of these effects.

In order to determine the position of the optimum transmitter offset for signal-to-artefact ratio a series of otherwise identical SHARPER experiments were carried out with the transmitter offset changed in regular increments (2 Hz apart) but with otherwise identical parameters. The frequencies near the signal-to-artefact maximum of these initial spectra were then examined again with finer frequency steps down to 0.1 Hz in most cases.

5.5.1 Initial Pulse Flip Angle

Variation of the initial excitation pulse used a modified version of the pulse sequence in Figure 68 where the initial excitation pulse could be calibrated independently of the 180º refocussing pulses. The value of Δ was set to 10 ms, with a 10 s total FID recorded.
A sample of neat D_2O was again used, examining the HDO signal.

Initial pulse flip angles of 90º and 30º were used, with either a power of 14 W or 1.4 W, with pulse duration adjusted to compensate (90º flip angle, 14 W power = 10.0 μs). In all cases the 180º pulses used 14 W power.

Three of the four combinations had optimum transmitter offsets for signal-to-artefact ratio determined to 0.1 Hz resolution. However, due to time constraints this was only determined to 2 Hz resolution for the combination of a 1.4 W and 30º flip angle pulse. The results are shown in Figure 106, with a difference of several Hertz between maxima where the flip angle has changed, and the maxima where 90º flip angle pulses were used being closer to the frequency of the peak maximum in a 1D ^{1}H spectrum. The effects on maximum achievable signal-to-artefact ratio are substantial, with the change from a 90º pulse to a 30º pulse appearing to reduce this by around 65%.

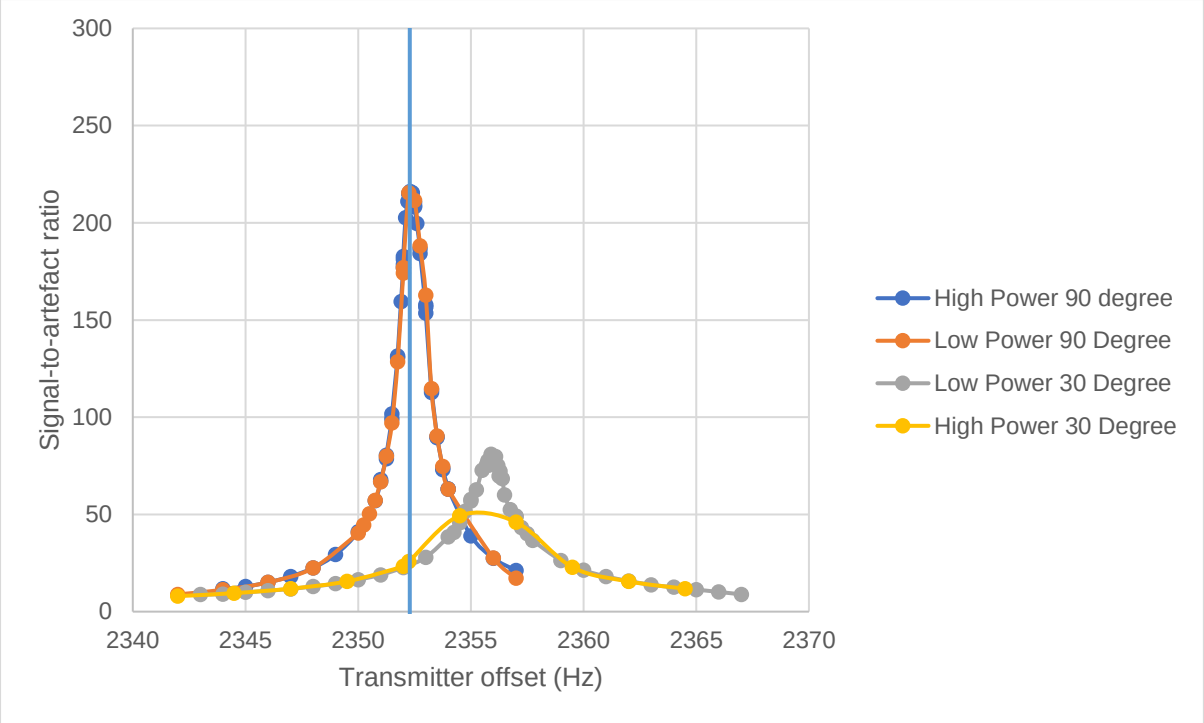

Figure 106: Effects of varying transmitter offset on the signal-to-artefact ratio of SHARPER spectra where the initial excitation pulse has been changed. The blue line indicates the real frequency of the NMR signal, as determined from the peak maximum of a 1D ^{1}H spectrum.

5.5.2 Delta Duration

Variation of the Δ parameter was then investigated, using settings of 5, 10 or 20 ms. The number of refocussing pulses and data chunks collected was changed to give a 10 s FID in all cases. The resulting curves are shown in Figure 107, and increasing the value of Δ has a dramatic effect on the maximum achievable signal-to-artefact ratio. It also affects the optimum offset for signal-to-artefact ratio, with it deviating from the peak maximum of a 1D ^{1}H spectrum acquired at the same time by 4.95 Hz when Δ = 5 ms; 5.90 Hz when Δ = 10 ms; and 7.3 Hz when Δ = 20 ms.

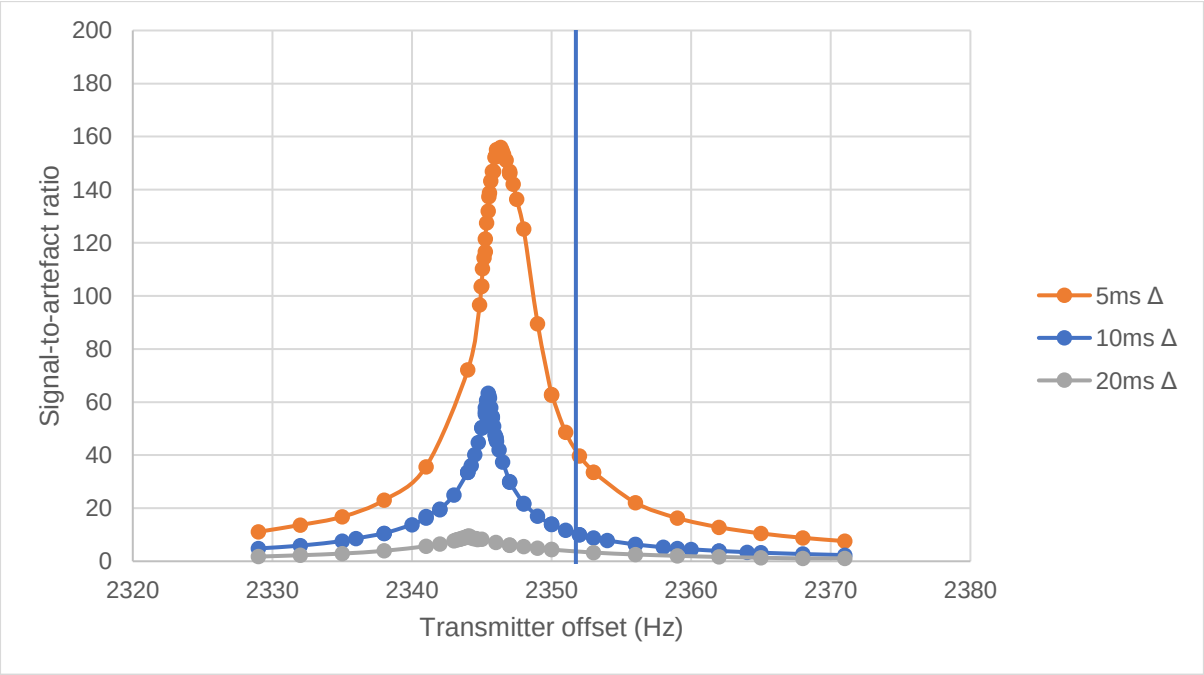

Figure 107: Effects of varying transmitter offset on the signal-to-artefact ratio of SHARPER spectra where the duration Δ within the pulse sequence has been altered. The vertical blue line indicates the real frequency of the NMR signal, as determined from the peak maximum of a 1D ^{1}H spectrum.

5.5.3 Shimming

To initially explore the effects of magnetic field inhomogeneity SHARPER spectra with varied offsets were run (10 ms Δ, 10 s total FID) both with and without introduction of a deliberate shimming fault – a mixture of Z1, Z2 and Z3 faults. The results, Figure 108, show that shimming has a substantial effect on both maximum achievable signal-to-artefact ratio and the transmitter offset required to achieve it.

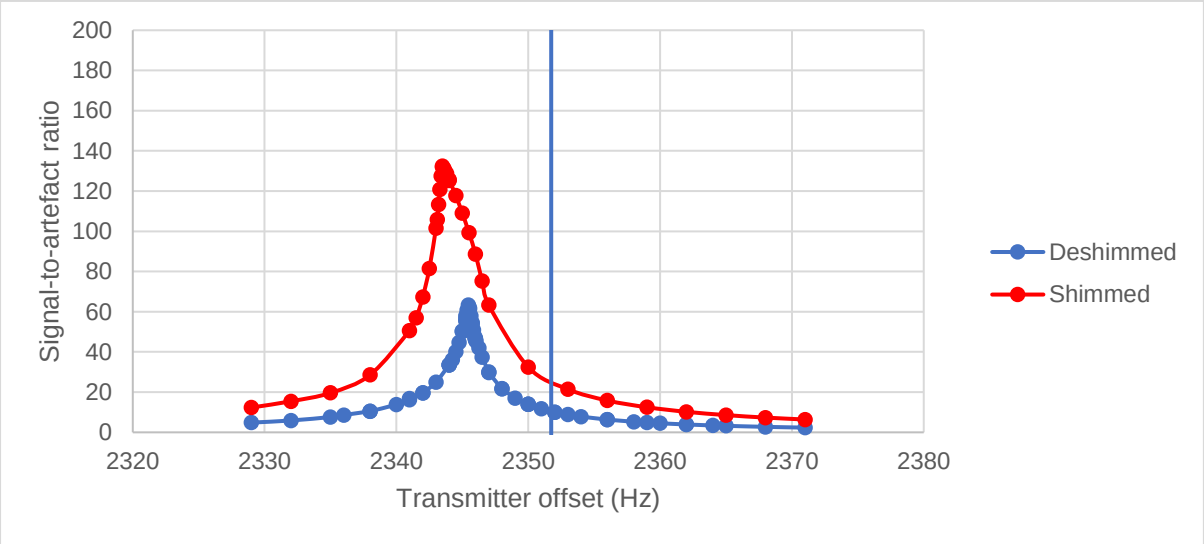

Figure 108: Effects of varying transmitter offset on the signal-to-artefact ratio of SHARPER spectra both with and without a deliberately introduced shim fault. The vertical blue line indicates the real frequency of the NMR signal, as determined from the peak maximum of a 1D ^{1}H spectrum.

To examine the effects of each individual shim SHARPER spectra were acquired with systematic alteration of shim coils Z1 through Z4. Experimental parameters for these SHARPER spectra were the same as previous experiments, using a 10 ms value of Δ and 10 s FID. Mobile-SHARPER was used to optimise the transmitter offset after each shim alteration. In each case 15 mobile-SHARPER iterations were used, with both the maximum achievable signal-to-artefact ratio and the optimum transmitter offset for signal-to-artefact ratio calculated from an average of the last 10 iterations.

As these experiments were conducted over the course of six hours the first SHARPER spectrum (with optimal shimming) was repeated at the end of the experiments. This resulted in a shift of the optimum transmitter offset of 0.02 Hz and a change in the maximum achievable signal-to-artefact ratio of around 0.2% (from 163.7:1 to 164.0:1). As a comparable amount of variation was present between each of the mobile-SHARPER spectra used prior to averaging (after accounting for the oscillatory behaviour) this was assumed to be a random statistical difference. Thus it was assumed that, aside from the deliberately introduced shimming faults, the homogeneity of the magnetic field remained constant throughout the experiment and no corrections to the data collected were needed.

The deviation between the optimum transmitter offset at each set of shim values from the optimally shimmed SHARPER spectra was calculated (Figure 109). It is immediately apparent that the Z2 shim has a more significant effect than the other three shims over the range of values tested. The broadly linear effects of Z2 are interesting because it is an asymmetric shim and can be expected to introduce a fault upfield of the most intense peak when the value of the fault is positive and vice versa for negative values. This means that the optimum transmitter offset for signal-to-artefact ratio moves in the same direction as the introduced shimming fault. Thus it may be that the change in offset frequency causes cancellation of the faults introduced by Z2.

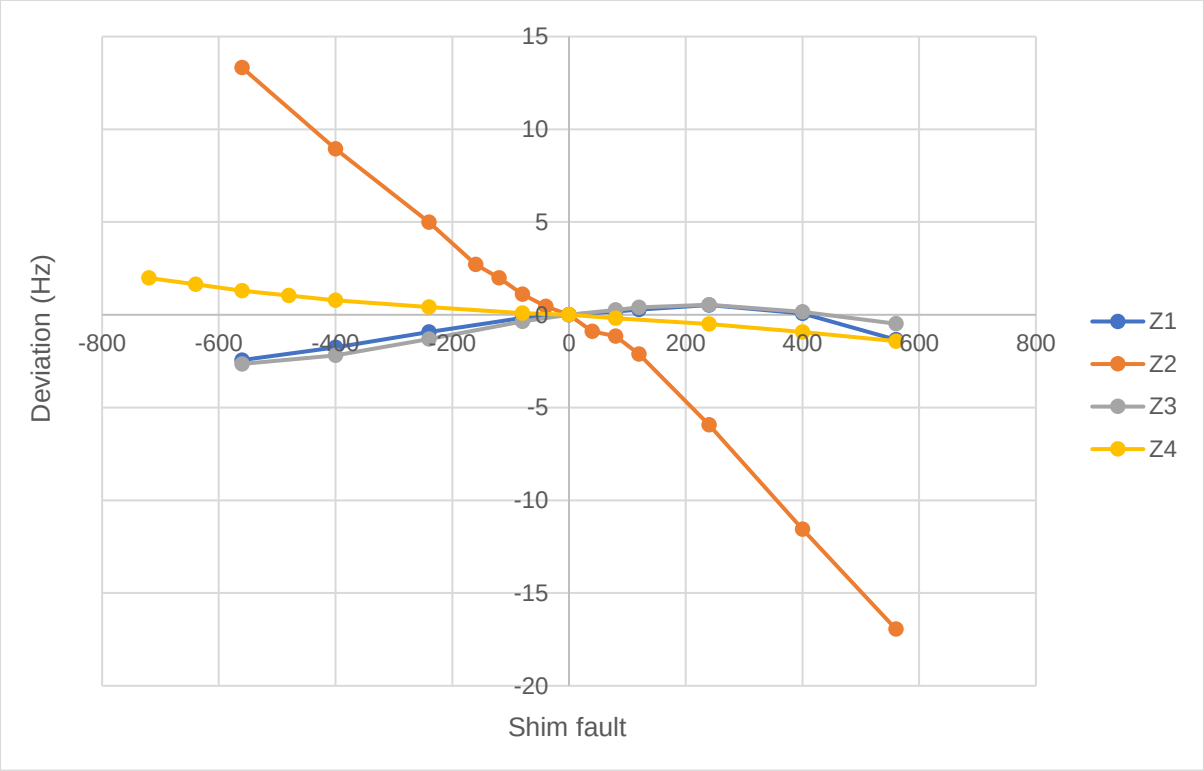

Figure 109: The change in optimum transmitter offset for signal-to-artefact ratio with shimming faults of differing magnitudes.

The other asymmetric shim, Z4, behaves in the same broadly linear fashion as Z2, though the magnitude of the changes is much smaller. The symmetric shims, (Z1 and Z3) show a pair of curves (zooms shown in Figure 110).

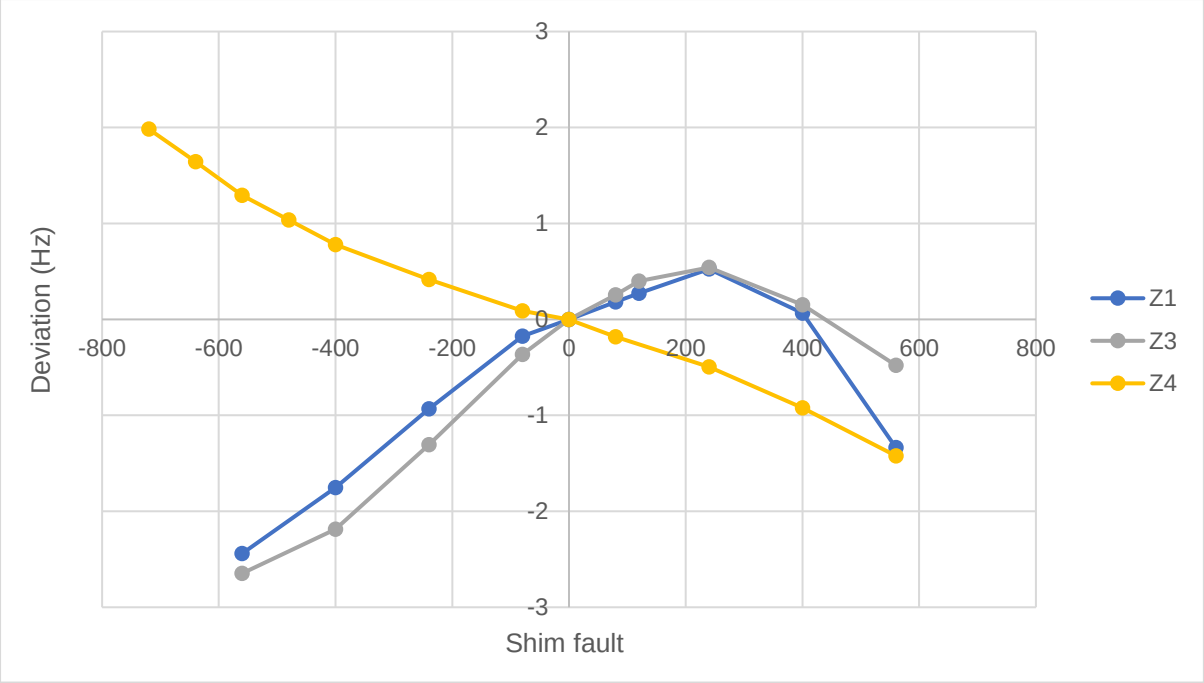

Figure 110: The change in optimum transmitter offset for signal-to-artefact ratio with shimming faults of differing magnitudes. Only the range the Z1, Z3 and Z4 shims cause change over is displayed, and Z2 is omitted for clarity.

The maximum achievable signal-to-artefact ratio as a function of shim fault is shown in Figure 111. The changes in the asymmetric shims (Z2 and Z4) have more of an effect than the symmetric shims (Z1 and Z3), though the effect of altering these is still substantial.

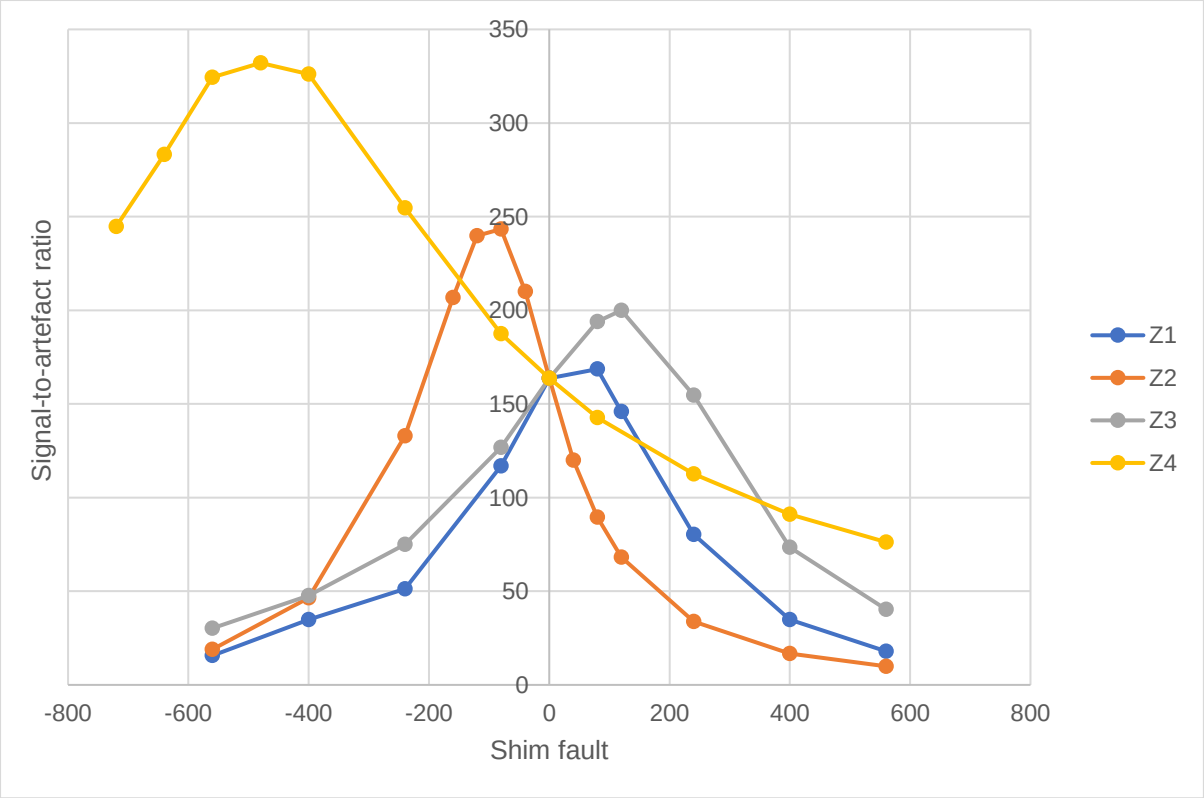

Figure 111: Maximum signal-to-artefact ratio obtainable with SHARPER under various shim conditions.

It is interesting to note that the optimal signal-to-artefact ratio is achieved for SHARPER spectra at relatively poor shim settings. Figure 112 shows 1D ^{1}H spectra produced with the shim faults that led to the optimal signal-to-artefact ratios for SHARPER spectra. The spectrum acquired with the initial shims shows the expected Lorentzian line shape of a well shimmed peak. Line shape in the 1D ^{1}H spectrum run under the Z3 shim settings that produced the optimal SHARPER signal-to-artefact ratio is still reasonably good, albeit the line width is poor, at around 4 Hz. However, the 1D ^{1}H spectra that relate to the optimal Z1, Z2 and Z4 shims for SHARPER are not just significantly broadened, they give poor line shapes. This suggests that the intensity of sideband artefacts relative to the most intense peak in SHARPER spectra is controlled by favourable interaction of shimming faults, rather than by minimisation of those faults.

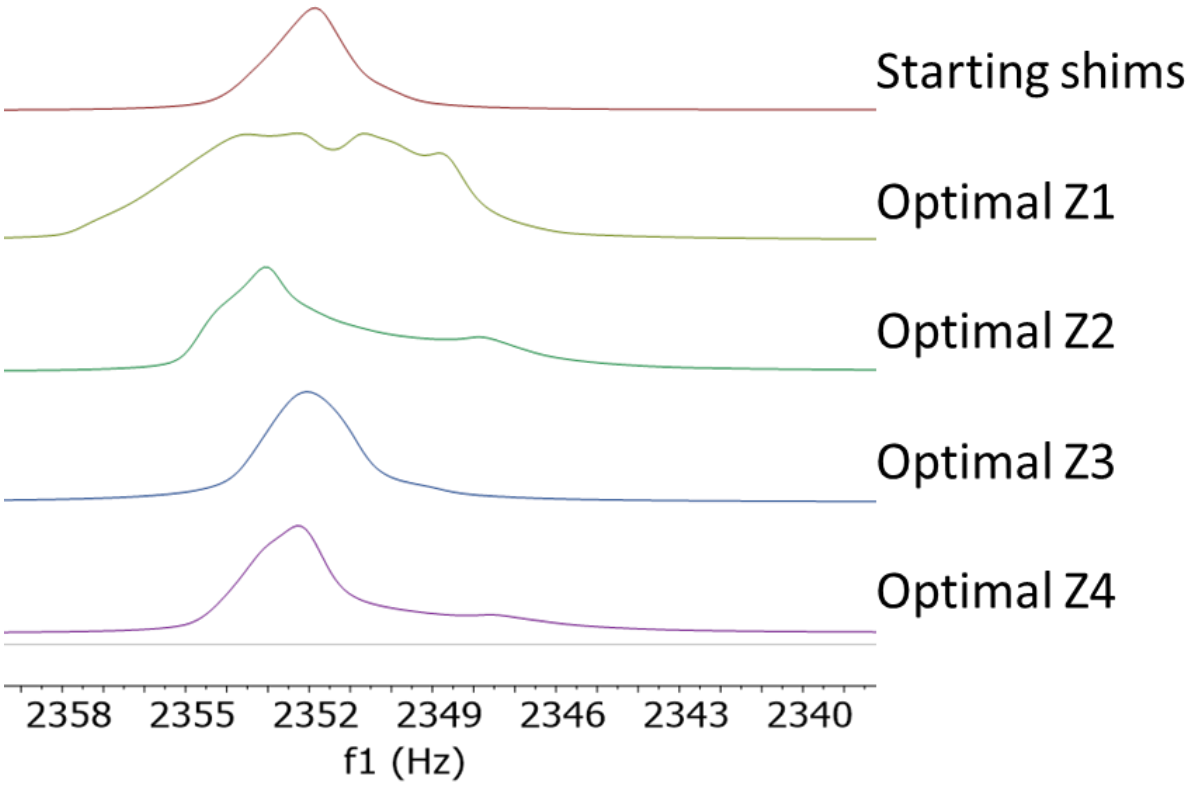

Figure 112: The 1D ^{1}H spectra obtained under shimming conditions that yielded the optimal signal-to-artefact ratio for SHARPER spectra.

5.5.4 Theoretical Model for Effects on Optimum Transmitter Offset

In this Section, the theoretical basis for the shim-dependence of the experimental results described previously is explored. The proposed mechanism is that at certain transmitter offsets partial phase cancellation occurs between an NMR signal and its shimming faults, yielding an FID closer to the optimum case – a single frequency perfectly on-resonance.

In order to test and demonstrate this a series of model SHARPER FIDs with shimming faults were produced. Shimming faults can be modelled by summing multiple NMR signals with similar frequencies.[100] To effectively model SHARPER FIDs we need to be able to account for the effects of 180º refocussing pulses on the chemical shift evolution of off-resonance signals. Using the product operator formalism chemical shift evolution during the sequence can be analysed in an offset independent fashion. A diagram with multiple points labelled for reference in this analysis is shown in Figure 113.

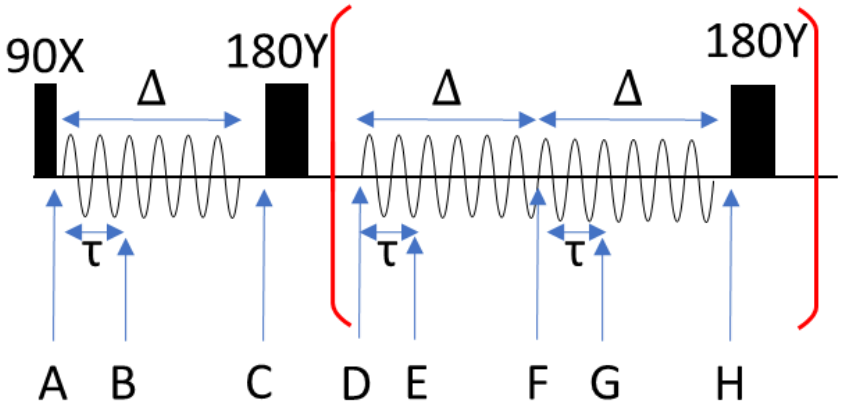

Figure 113: A diagram of the SHARPER pulse sequence and labels for clarity in the product operator analysis. The section in red brackets can be repeated.

As the sequence starts with a 90_Xº pulse the chemical shift evolution for frequency Ω at position (A) is simply:

$$-I_y \qquad \textit{Equation 15}$$

After free evolution for an arbitrary time τ, where $\tau \leq \Delta$, chemical shift evolution at (B) can be described as:

$$sin(\tau\Omega)\, I_x - cos(\tau\Omega)\, I_y \qquad \textit{Equation 16}$$

At position (C), immediately before the first 180_Yº pulse, $\tau = \Delta$, so this becomes:

$$sin(\Delta\Omega)\, I_x - cos(\Delta\Omega)\, I_y \qquad \textit{Equation 17}$$

The effect of the 180_Yº pulse is to change the sign of the X component of magnetisation, so chemical shift evolution at position (D), immediately after the 180_Yº is:

$$-sin(\Delta\Omega)\, I_x - cos(\Delta\Omega)\, I_y \qquad \textit{Equation 18}$$

At point (E) chemical shift evolution has been allowed to freely evolve for period τ, so net chemical shift evolution can be described as:

$$sin(\tau\Omega)cos(\Delta\Omega)I_x - cos(\tau\Omega)\sin(\Delta\Omega)\,I_x - \cos(\tau\Omega)\cos(\Delta\Omega)I_y - \sin(\tau\Omega)\sin(\Delta\Omega)I_y$$

This simplifies to:

$$sin(\tau\Omega - \Delta\Omega)\,I_x - cos(\tau\Omega - \Delta\Omega)\,I_y \qquad \textit{Equation 19}$$

At point (F) τ = Δ, causing the sin term to equal 0 and the cos term to equal 1, so chemical shift evolution is simply:

$$-I_y \qquad \textit{Equation 20}$$

Under free evolution the chemical shift evolution at point (G) is:

$$sin(\tau\Omega)\,I_x - cos(\tau\Omega)\,I_y \qquad \textit{Equation 21}$$

At point (H) τ = Δ, so chemical shift evolution immediately before the second $180_Y{}^o$ pulse is:

$$sin(\Delta\Omega)\,I_x - cos(\Delta\Omega)\,I_y \qquad \textit{Equation 22}$$

Notably chemical shift evolution at (H) is identical to that immediately before the *first* $180_Y{}^o$ pulse at (C) (Equations 17 and 22), so from this point onwards chemical shift evolution in the SHARPER sequence will cycle between points (C) and (H). All above equations (15 to 22 inclusive) and any repeats of the section in red brackets can thus be described by the general formula below, where *n* is the number of $180_Y{}^o$ pulses that have been applied and κ is the number of preceding complete Δ periods:

$$sin(\tau\Omega + \kappa\Delta\Omega - 2n\Delta\Omega)\,I_x - cos(\tau\Omega + \kappa\Delta\Omega - 2n\Delta\Omega)\,I_y \qquad \textit{Equation 23}$$

Any multiple, κ, of duration Δ added to the duration τ can be used to describe any point in time, ***t***, in the sequence:

$$\boldsymbol{t} = \kappa\Delta + \tau \qquad \textit{Equation 24}$$

Thus, chemical shift evolution at any datapoint, ***t***, can be described by:

$$sin(\boldsymbol{t}\Omega - 2n\Delta\Omega)\,I_x - cos(\boldsymbol{t}\Omega - 2n\Delta\Omega)\,I_y \qquad \textit{Equation 25}$$

This allows us to determine the expected SHARPER FID for all values of ***t***, a given frequency, Ω, and value of Δ. Thus, a SHARPER FID containing an arbitrary number of frequencies can be described by its sin and cos components as shown in Equation 26 and Equation 27, where *A* allows variations in amplitude between the different frequencies. Subscripts refer to differing discrete frequencies.

$$Signal_Y = A_1\cos(\Omega_1 t - 2n\Delta\Omega_1) + A_2\cos(\Omega_2 t - 2n\Delta\Omega_2) + \cdots + A_n\cos(\Omega_n t - 2n\Delta\Omega_n)$$

Equation 26: The cos (Y) component of modelled SHARPER FIDs.

$$Signal_X = A_1\sin(\Omega_1 t - 2n\Delta\Omega_1) + A_2\sin(\Omega_2 t - 2n\Delta\Omega_2) + \cdots + A_n\sin(\Omega_n t - 2n\Delta\Omega_n)$$

Equation 27: The sin (X) component of modelled SHARPER FIDs.

Using Equations 26 and 27, a series of SHARPER FIDs containing an arbitrary number of frequencies were modelled. In each of these the highest amplitude frequency is referred to as the "shimmed" component, whilst all other frequencies are referred to as "shim faults." 1000 datapoints were calculated in each case, and the time between them was set to 1 ms.

An initial model FID of a perfectly shimmed on-resonance SHARPER spectrum was created – a single signal with a frequency of 0 Hz, an amplitude of 1.0 and a Δ value equal to 50 ms. As no exponential decay component is present and the signal is on-resonance the model FID consists of straight lines at 1 and 0 respectively for both the cos and sin components, as shown in Figure 114. Any deviation from this, which can be easily measured as a range, will lead to artefacts in a Fourier transform.

Figure 114: Model FIDs for a perfectly on-resonance SHARPER experiment with no shimming fault.

To model an *asymmetric shimming fault* a second signal was introduced with a frequency of 10 Hz and 0.2 amplitude, whilst the normalised amplitude of the existing 0 Hz signal was reduced to 0.8. The expected signals from two frequencies as well as the summed sin and cos waves are shown in Figure 115. The summed cos signal shows a small range of 0.026, whilst the range in the sin component is more substantial at 0.197.

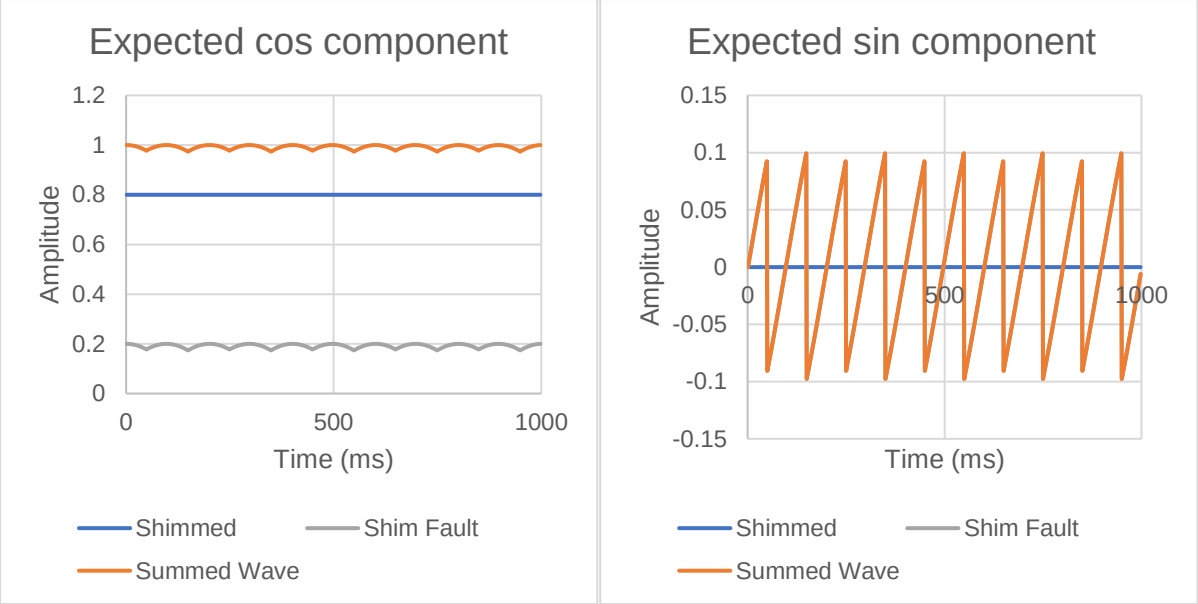

Figure 115: Model FIDs for an on-resonance SHARPER experiment with a single shimming fault. The orange line showing the sum obscures the grey line showing the shim fault in the expected sin component.

The effective transmitter offset can be changed by adding or subtracting a common factor from all frequencies. The range of the summed sin and cos waves was minimised by subtracting 1.968 Hz from both frequencies, to give an FID composed of -1.968 Hz (0.8 amplitude) and 8.032 Hz (0.2 amplitude) signals. This causes a modest change in the range of the cos component, changing to 0.014, a reduction of -0.012. However, the change in the sin component is more significant, reducing to 0.005 – a reduction of -0.192. Examination of the plot of this data, Figure 116, shows that this is caused by phase cancellation between the two different frequencies. As this cancellation brings the FID closer to the ideal case for a single on-resonance frequency it should result in an improved signal-to-artefact ratio in a Fourier transformed spectrum. Thus, for a sample with asymmetric shimming faults, this explains why (slightly) off-resonance SHARPER spectra can produce higher signal-to-artefact ratios than a perfectly on-resonance experiment (based on the peak maximum of a 1D ^{1}H spectrum).

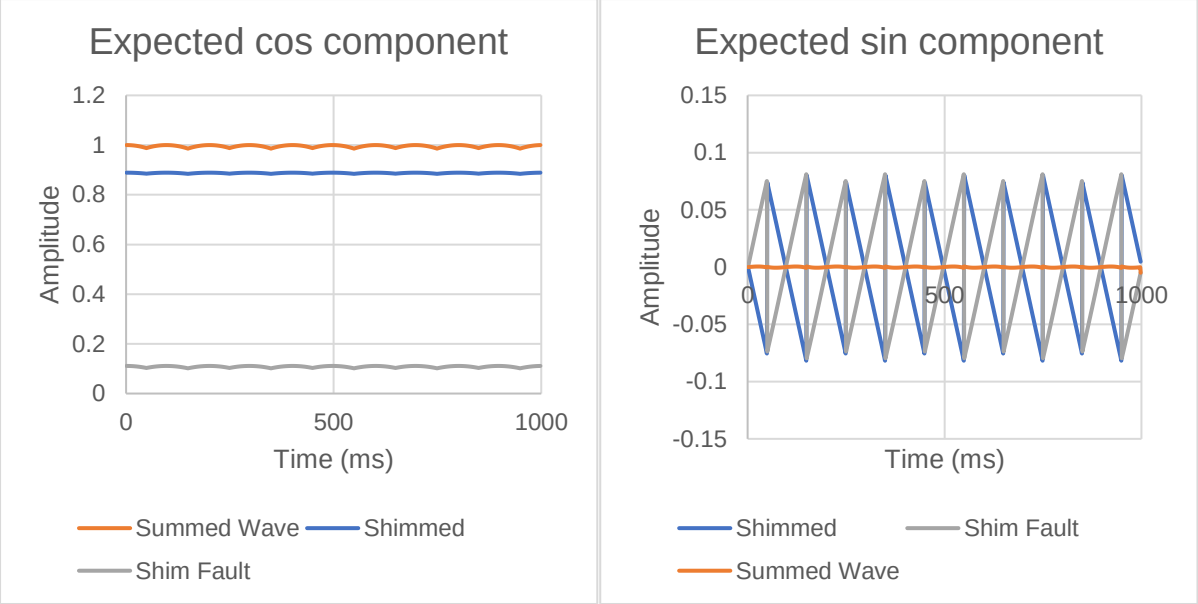

Figure 116: Model FIDs where a common factor has been subtracted from both frequencies to minimise the range of the summed sin and cos waves.

However, this cancellation is between two *different* frequencies and thus can be expected to be less perfect if frequencies are allowed to freely evolve for longer (*i.e.* for longer Δ periods), such that the difference between them becomes more apparent. To test this the value of Δ was then doubled to 100 ms. When modelling 0 Hz (0.8 amplitude) and 10 Hz (0.2 amplitude) signals, Figure 117, the range in both the summed cos and sin components is increased compared to Figure 115, to 0.095 and 0.340 respectively.

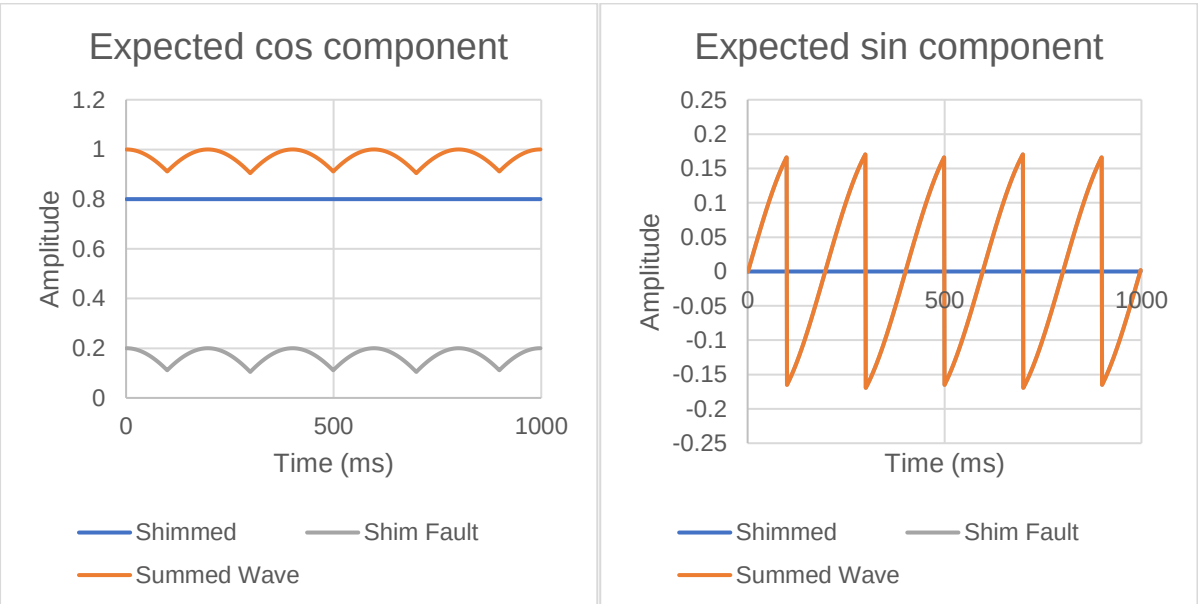

Figure 117: Model FIDs for an on-resonance SHARPER experiment with a single shimming fault (10 Hz) where Δ has been doubled to 100 ms. The orange line showing the sum obscures the grey line showing the shim fault in the expected sin component.

The range of the summed sin and cos waves was then minimised as before by subtracting a common factor from both frequencies (*i.e.* changing the effective transmitter offset), with results displayed in Figure 118. Whilst this does result in a reduction of the range of both summed cos and sin waves (to 0.080 and 0.009 respectively) both ranges are greater than when this procedure was carried out on data with the same shimming fault but a shorter value of Δ (Figure 116). The factor subtracted from both frequencies, -1.870 Hz, is also smaller (as opposed to the previous case, Figure 116, where the change was -1.968 Hz). This demonstrates how the duration of Δ can impact both the transmitter offset for optimum signal-to-artefact ratio of SHARPER spectra and the maximum achievable signal-to-artefact ratio, in the presence of an existing shimming fault.

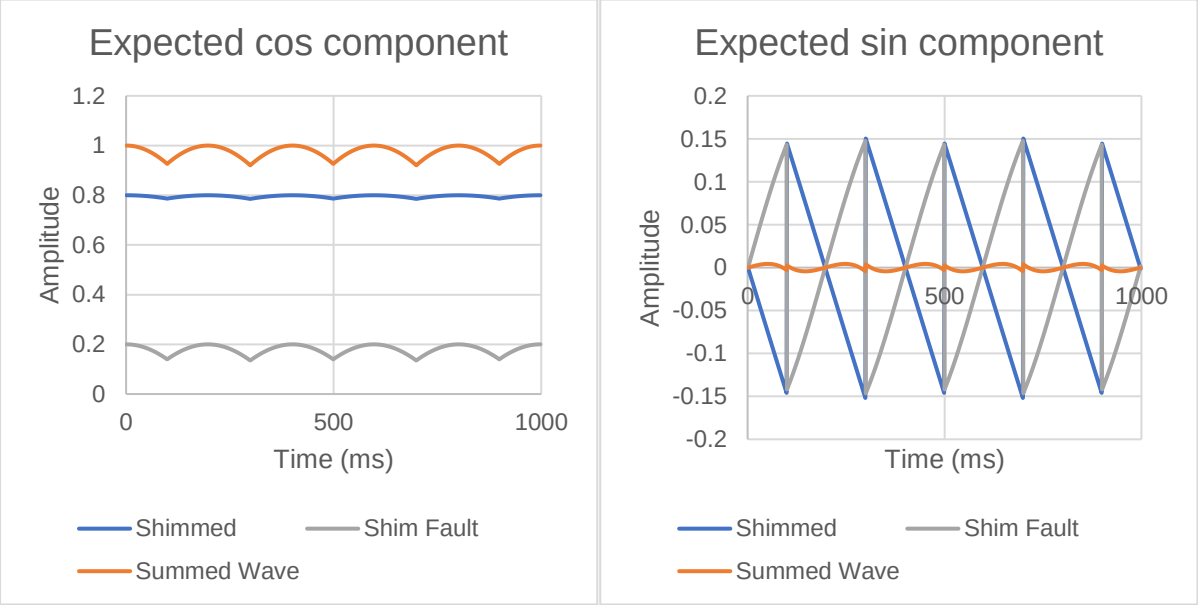

Figure 118: Model FIDs with a doubled value of Δ where a common factor has been subtracted from both frequencies to minimise the range of the summed sin and cos waves.

However, this raises the question of what happens with *symmetrical shimming faults*, which can be expected to already give optimum phase cancellation because they introduce faults on either side of an NMR signal. To model this a signal at 0 Hz with 0.8 amplitude was used, along with two symmetrical faults, at ±10 Hz each with an amplitude of 0.1. The value of Δ was set to 50 ms. As seen in Figure 119 phase cancellation in the expected sin component is perfect. However, this does not occur in the cos component, which has a range of 0.026, and this range is increased if the amplitude of the shimming faults is increased. This demonstrates why alteration of the symmetric shims (Z1, Z3) affects the maximum achievable signal-to-artefact ratio in SHARPER spectra. However this model predicts that the optimum transmitter offset should not change based on the magnitude of the shimming fault, because the sum of the range of the two components cannot be improved by adding or subtracting a common factor to all frequencies. As observed in Figure 109 this is not the

case experimentally, though the magnitude of the change is smaller than for the asymmetric shims.

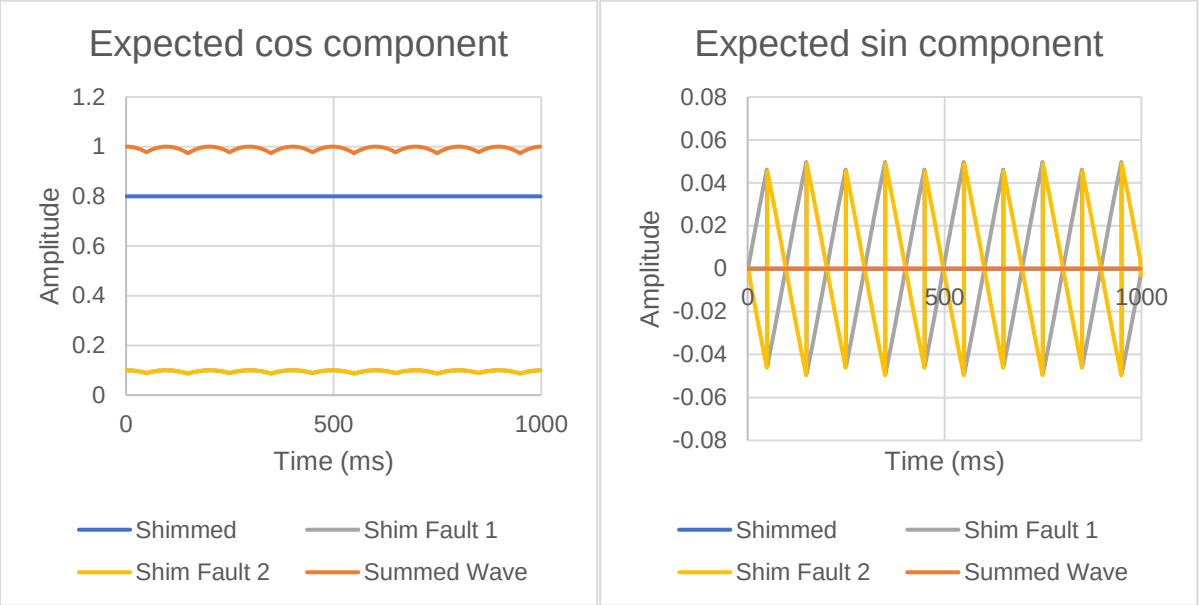

Figure 119: Model FIDs for an on-resonance SHARPER experiment with a symmetrical pair of shim faults. In the expected cos component both ±10 Hz frequencies overlap, so the shimming faults obscure each other. In the expected sin component the orange line showing the summed wave obscures the blue line showing the well shimmed component.

These model FIDs illustrate how partial phase cancellation can occur between different NMR signals when the transmitter offset is altered. This explains the phenomenon in SHARPER spectra that the optimum transmitter offset for signal-to-artefact ratio is not equivalent to the frequency of the peak maximum in a 1D ^{1}H spectrum. It also explains why the optimum transmitter offset is altered by both the duration of Δ and shimming conditions. Unfortunately, it does not explain the effects of the flip angle of the initial pulse on the optimal transmitter offset for signal-to-artefact ratio, so the optimum transmitter offset for SHARPER cannot currently be determined *apriori* from analysis of a 1D ^{1}H spectrum.

However, the mobile-SHARPER macro provides a fast and robust experimental method to determine the optimal transmitter offset. Thus, it may prove useful even when examining resonances with a static frequency for optimisation purposes.

5.6 Mobile-MR-SHARPER

We now move to demonstrate the combination of the mobile-SHARPER approach discussed in this Chapter with the MR-SHARPER experiment previously discussed in Chapter 4, in order to allow for simultaneous tracking of multiple resonances with changing frequencies. However, this necessitates a substantially more complex macro and brings the complication that parameters beyond just the transmitter offset will differ from spectrum to spectrum.

5.6.1 Mobile-MR-SHARPER Macro

Much like mobile-SHARPER a Topspin 3 macro is required to interact with the spectrometer and process the spectra, whilst all analysis and determination of new parameters is done by a Python 2.7 script (both provided in Appendix 8.5.8). The arrays used by MR-SHARPER are also needed (described in more detail in Section 4.2). The basic workflow is outlined in Figure 120. The scripts presented here can only track two resonances at a time, though in principle similar methodology could be applied to three or more resonances.

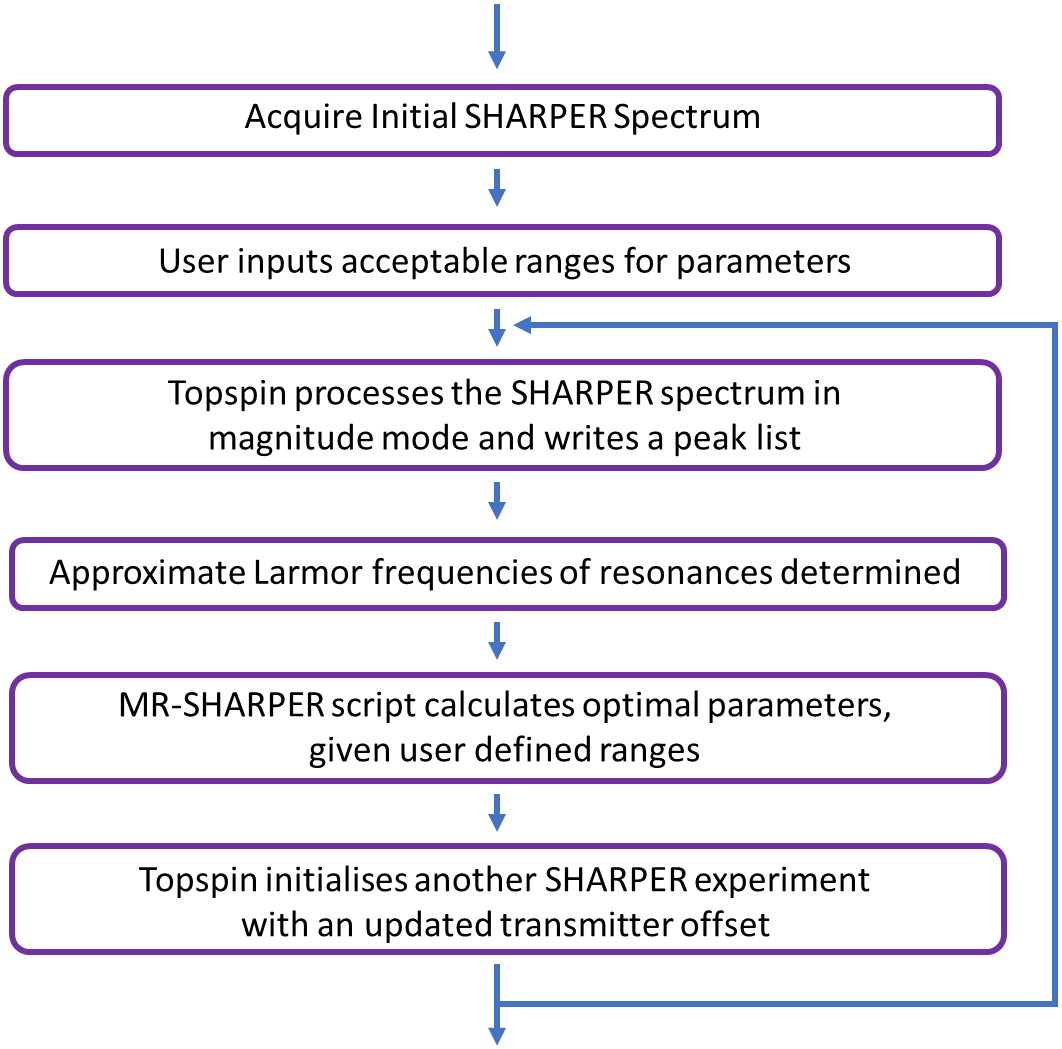

Figure 120: A flowchart showing the workflow of the mobile-MR-SHARPER macro.

The user is required to run an initial SHARPER spectrum, with experimental parameters set by the MR-SHARPER scripts (described in Section 4.2). This spectrum provides a starting point and defines experimental parameters not later adjusted.

The Topspin 3 macro then requests several parameters from the user, including the desired length of each FID, initial chemical shifts of the resonances of interest and acceptable ranges for both spectral width and dwell time. Magnitude mode processing is then applied to the spectrum and a peak list produced. This peak list, along with the parameters input by the user and the duration of Δ in the acquired SHARPER spectrum are passed to a Python 2.7 script.

The Python script then locates the most intense signal within 250 Hz or $2*(2\Delta)^{-1}$ Hz (whichever is greater) of the initial chemical shifts of the two resonances of interest. This value is arbitrary but allows the macro to distinguish between peaks relating to either resonance. The most intense sideband artefact adjacent to both of these peaks is then determined (which will be $(2\Delta)^{-1}$ Hz away). If no peak is found within 2 Hz of this location (though this is arbitrary and can be changed by the user) the chemical shift of the resonance is assumed to have remained the same.

If sideband artefacts have been located for at least one of the resonances these are used to calculate an intensity-weighted average frequency for that resonance, as per Equation 13, which is used as an updated chemical shift for that resonance.

A new transmitter offset is then determined, which is a simple average of the chemical shifts of the two resonances. Both resonances will thus have the same frequency, ωoff. The MR-SHARPER script (described in Section 4.2) then determines the dwell time and datapoints per chunk required to determine the optimal experimentally available value of Δ within user defined ranges for both spectral width and total duration. In the case that multiple values of Δ are found to be equally suitable for ωoff the one with the shortest duration is used.

Once the number of points per data chunk and dwell time have been calculated these are used to determine the number of data chunks required to produce an FID of the desired duration. These new parameters are passed back to the Topspin 3 macro, along with the updated chemical shifts of the resonances of interest. A new SHARPER experiment with the discussed parameters updated is then acquired. The macro can run any number of SHARPER experiments in succession, as defined by the user.

5.6.2 Mobile-MR-SHARPER on Resonances with Changing Frequencies

In order to provide a suitable test system with two resonances which changed in frequency variable temperature NMR was used on a sample of CD_3OD with an HDO impurity. A temperature change from 45 ºC to 15 ºC gives a 0.53 Hz and 146.79 Hz change in frequency for the residual CH_3OD and HDO resonances respectively. Using our spectrometer this takes 120 seconds, according to the thermostat. The sample was equilibrated for 10 minutes at 45 ºC before initiating the temperature change and acquiring SHARPER spectra.

Control MR-SHARPER experiments used a fixed offset and Δ duration of 4.4304 ms (42.6 µs dwell time, 104 datapoints per chunk). These values were determined to be suitable for the initial frequencies of both resonances at 45 ºC. FIDs were 9.48 s long and used a 20 s relaxation delay. A modified version of the mobile-MR-SHARPER macro was used to run successive experiments. This carried out all calculations relevant to mobile-MR-SHARPER as described in the previous Section but did not update any parameters. This ensures any additional time between scans due to use of the macro will be equal in the control experiment.

The SHARPER experiments acquired using the mobile-MR-SHARPER macro were initiated with the same parameters but allowed to vary the dwell time to give spectral widths of 10-25 ppm, with 4 ms < Δ < 8 ms duration. Spectra were as close to 9.50 s long as feasible and a selection of the spectra recorded are shown in Figure 121.

As there is only minimal change in the frequency of the CH_3OD resonance at ~3.3 ppm (+0.5 Hz) it consistently provides a single intense and sharp peak associated with it in both sets of spectra. However, the significant change in frequency of the HDO resonance results in significant sideband artefacts around HDO in the control MR-SHARPER spectra, rather than a single sharp peak.

In the spectra run using the mobile-MR-SHARPER macro the sideband artefacts generated around the HDO resonance are initially almost intense as in the control SHARPER experiments. However, by 90 seconds spectral quality can already be seen to be improved by the macro and after the temperature change is completed the spectra are consistently excellent with respect to the presence of significant sideband artefacts (*i.e.* there is only one intense peak around the frequency of each of the two resonances). The CH_3OD resonance also retains a consistently high signal-to-artefact ratio. It is worth mentioning that whilst its absolute frequency does not change its frequency relative to the offset changes in the mobile-MR-SHARPER spectra, as the transmitter offset is dynamically updated to adjust for the changing frequency of the HDO resonance.

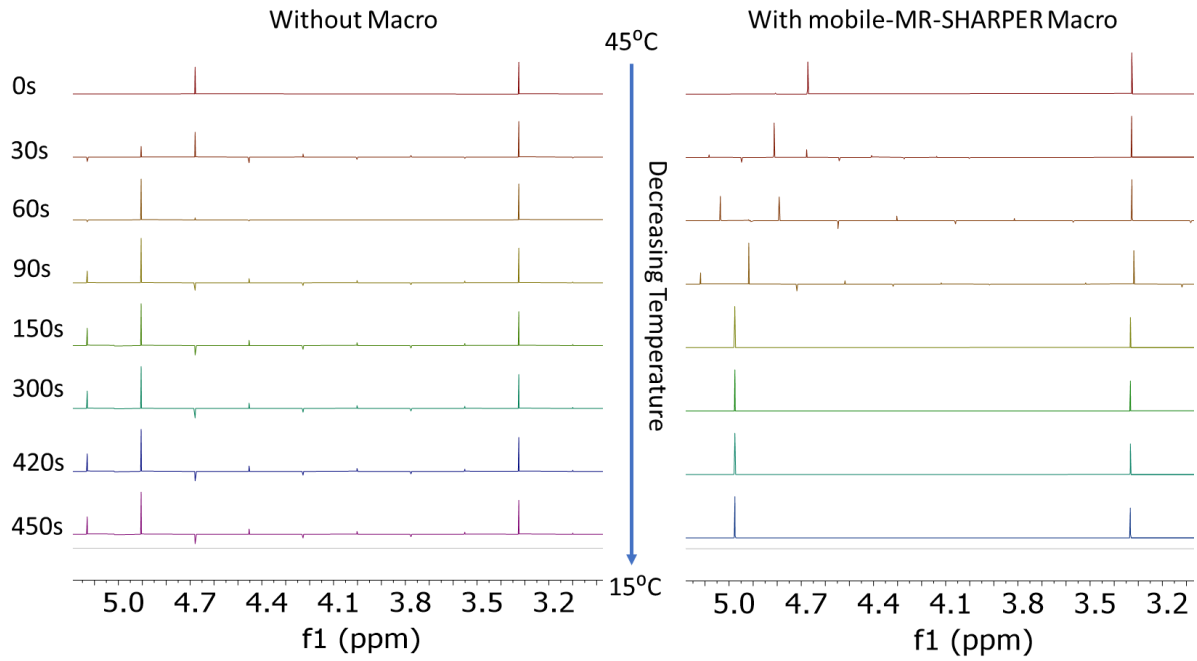

Figure 121: A selection of spectra acquired during a temperature reduction from 45 ºC to 15 ºC using the mobile-MR-SHARPER macro or with a fixed set of MR-SHARPER parameters.

SHARPER spectra were processed with 0.1 Hz Gaussian apodisation, 1st order polynomial baseline correction and zero-filled to 1024 K. The most intense peak in the region of the HDO (~5.0 ppm) and CH_3OD (~3.3 ppm) resonances was then integrated. The ratio of these integrals is shown in Figure 122. The yellow line indicates the correct ratio of integrals, as determined from a 1D ^1H spectrum run at 45 ºC. This spectrum was baseline corrected in the same fashion, but not zero-filled or apodised. The first spectrum acquired using both MR-SHARPER and mobile-MR-SHARPER gave the expected ratio of integrals. Spectra acquired during the temperature decrease gave an incorrect ratio of integrals in both sets of data, consistently underreporting the integral of the HDO, as integral is lost to sideband artefacts. However, the spectra recorded with the mobile-MR-SHARPER macro gave the expected ratio of integrals after the temperature change was completed and parameters had been updated to compensate for the change in frequency of the HDO resonance.

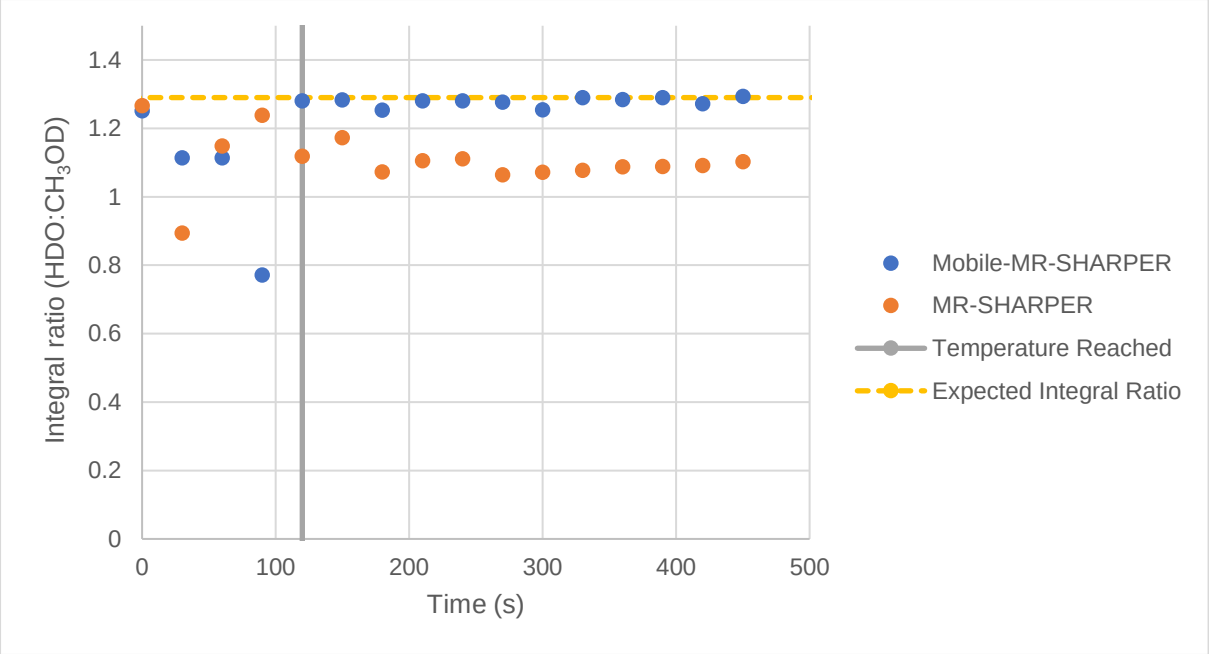

Figure 122: The ratio of the integrals of signals in a mobile-MR-SHARPER experiment and a MR-SHARPER experiment with fixed parameters.

The actual absolute integrals vary substantially when the mobile-MR-SHARPER macro is used, shown in Figure 123, as HDO changes by ±20% whilst CH_3OD changes by ±15%. The significant outliers relate to SHARPER experiments acquired at the start of the temperature decrease, where changes in parameters were not able to fully compensate for the rapidly changing frequency of the HDO peak. The rest of the datapoints correlate reasonably well. Of the 16 SHARPER spectra run, 14 different sets of parameters were used, with dwell times ranging from 40.113 µs to 58.667 µs and values of Δ ranging from 4.0922 ms to 7.3000 ms. As absolute integral has already been shown to be affected by choice of parameters (Chapter 4, Figure 88) it seems likely they are the cause of the behaviour in absolute integrals observed.

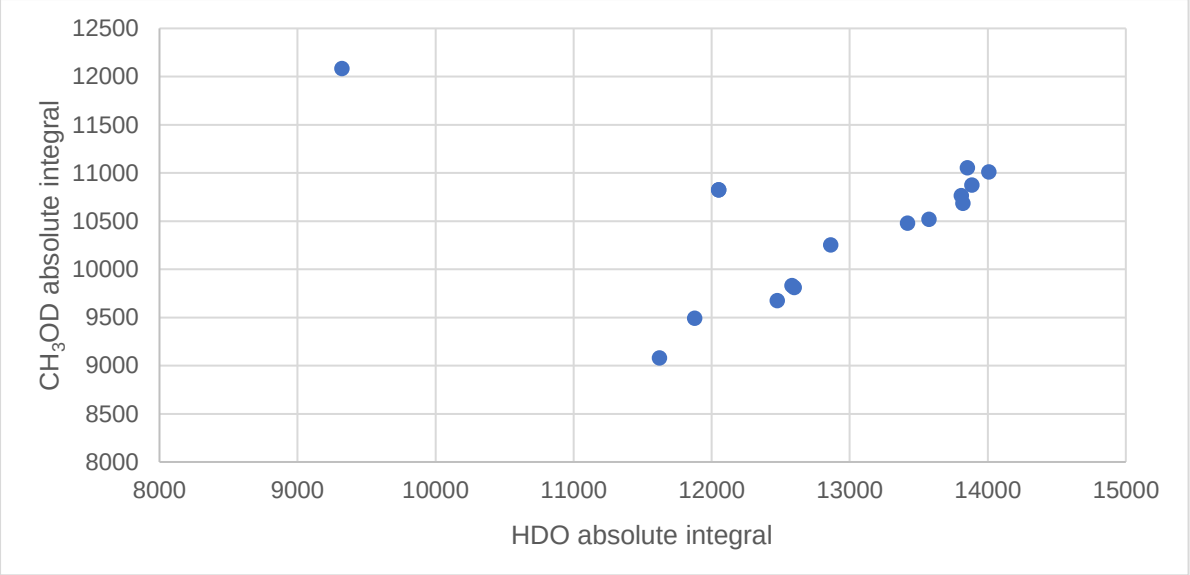

Figure 123: Absolute integrals from a set of spectra acquired using the mobile-MR-SHARPER macro.

As updating these parameters is essential for the function of mobile-MR-SHARPER any comparison between absolute integrals of different spectra acquired using the macro is impractical. *i.e.* one could not compare the HDO concentration in two spectra run at different time points. However, mobile-MR-SHARPER provides a reliable comparison between resonances in the *same* spectrum, and one could compare the ratio of concentrations of the two resonances of interest between different time points. This may prove sufficient for practical applications such as reaction monitoring.

6 Conclusion – Improvements to SHARPER

The SHARPER NMR experiment, as originally published[36] is a powerful, but in many ways limited experiment. The study of sideband artefacts produced by SHARPER when spectra were acquired off-resonance in Chapter 3 laid the groundwork for methodologies to alleviate these limitations.

Chapter 4 demonstrated that by use of highly precise timings which are both sample and spectrometer specific SHARPER can be used to simultaneously monitor multiple resonances. This greatly helps with what is primarily a reaction monitoring experiment, where there will always be two or more signals of interest – at the very least, a product and a reactant. This has been demonstrated on up to three resonances, though in principle the methodology could be extended to more resonances than this. However, as fewer values of Δ will be theoretically valid this will make finding a suitable experimentally accessible value of Δ more challenging.

It is worth noting that all SHARPER experiments presented here were conducted in fields of approximately 500 MHz. As it is the chemical shift difference *in Hertz* that determines the timings used a higher field spectrometer will yield shorter wave periods for the same sample, which may make finding an experimentally accessible Δ value for a large number of resonances more practical. Conversely, the reverse is also true, and MR-SHARPER can be expected to be less effective when used with lower field spectrometers, such as benchtop instruments.

This logic also applies when considering nuclei with a broader range of chemical shifts than ^{1}H, which has been primarily examined in this thesis. Examination of solvents and impurities provided spectra with low numbers of resonances as would be typical of NMR spectra of sparse heteronuclei, such as ^{19}F, ^{31}P and ^{11}B, which are frequently used for reaction monitoring. In particular ^{19}F has a broad chemical shift range and high gyromagnetic ratio[78] so any two resonances of interest are likely to have a greater frequency difference between them. Thus, extension of MR-SHARPER to many resonances at a time may be easier to implement on ^{19}F.

Retention of many of the desirable properties of the parent sequence, such as insensitivity to magnetic field inhomogeneity and removal of heterocoupling without requiring pulsing on additional channels has been demonstrated. It has not been demonstrated that the ability to compensate for what was described by A.B. Jones *et al*. as “dynamic” magnetic field inhomogeneity is retained off-resonance[36] – that being transient disruption to the homogeneity of the magnetic field whilst a scan is being conducted. However, as

MR-SHARPER's behaviour regarding static magnetic field inhomogeneity appears identical to the parent SHARPER experiment it seems likely that MR-SHARPER will be able to overcome this if required.

Chapter 5 demonstrated a method to alleviate SHARPER's requirement for a resonance with a fixed frequency, such that can remain on-resonance whilst SHARPER spectra with a fixed transmitter offset are acquired. Whilst it is possible to retain quantitation in such a case by integration of sideband artefacts[36] this introduces issues with decreased intensity (thus signal-to-noise) and integration of increasing amounts of the baseline. The mobile-SHARPER approach does not suffer from these issues, as it continually updates the transmitter offset to compensate for changes in the frequency of the resonance of interest.

This method also allowed exploration of the phenomenon that SHARPER spectra are not necessarily best run *exactly* on-resonance. Thus, the method used in the original SHARPER paper for setting the transmitter offset – analysing a 1D spectrum,[36] will not provide optimal results. This gives the mobile-SHARPER macro utility even when examining stationary frequencies as a rapid means of determining the optimum transmitter offset for SHARPER. It also provides the ability to determine this parameter without need for human interpretation of spectra. This could allow analysis using SHARPER of samples under automation or with only a single resonance present but where acquiring an initially well shimmed spectrum was impossible, such that the user could not provide a transmitter offset.

The two approaches were combined at the end of Chapter 5 in the mobile-MR-SHARPER approach. This combines their benefits, though is currently limited to examining only two resonances at a time. Unfortunately, because it necessitates changes between spectra of parameters which alter absolute integral the concentration of a given resonance cannot be reliably compared to the same resonance at a prior timepoint. However, the ability to extract ratios of the concentrations of molecules during a chemical reaction may still yield useful information in circumstances where no other experimental setup could provide it. An alternative use of this experiment may be to optimise starting parameters *i.e*. mobile-MR-SHARPER is run prior to the reaction, and the parameters it uses are kept fixed throughout the chemical reaction.

These extensions to the utility of the original SHARPER experiment should hopefully allow wider usage in solving challenging reaction monitoring problems.

7 Experimental

7.1 NMR Samples Used

Various NMR samples were used and relevant characteristics mentioned where appropriate throughout this thesis. Some details, such as specific concentrations and manufacturer were omitted, so they are included below for completeness:

- Strychnine (Acros Organics) 25 mg (107 mM) in 700 µl $CDCl_3$ (Sigma)
- Streptomycin (provided by C4X Discoveries) 20 mg (49.12 mM) in 700 µl D_2O at pH 6
- Estradiol (Sigma) 20 mg (105 mM) in CD_3OD
- Quinine (Fluka Chemica) 25 mg (88 mM) in $CDCl_3$ (Sigma)
- Neat D_2O (Sigma)
- Neat CD_3OD (Sigma)
- Neat $CDCl_3$ (Sigma)
- $CHCl_3$ (Sigma) added to CD_3OD (Sigma) both with an HDO Impurity

All samples were made up to 0.7 mL in 500 MHz rated 5 mm NMR tubes without degassing.

7.2 NMR Data Acquisition

The MSE pure shift sequence, and those related to it, are all based on Varian's PS1D sequence, pre-installed with VNMRJ 4.2A,[101] with appropriate modifications (Appendix 8.1.1). All MSE pure shift and related experiments were acquired using two 500 MHz Varian spectrometers, one equipped with a One NMR probe and the other an AutoX_DB_9070 probe. Selective pulse calibration was done automatically by PBox with a 100 Hz bandwidth, unless otherwise mentioned. These were applied simultaneously to a 1.5 G/cm field gradient. PSYCHE spectra acquired for comparative purposes utilised the original, non-TSE PSYCHE sequence.[52] Parameters were matched as closely as possible to the MSE pure shift experiments and are described in the text. The CHIRP pulses had a 6.0° flip angle were applied simultaneously to a 0.714 G/cm field gradient.

SHARPER experiments were primarily conducted using a 500 MHz Bruker Spectrometer equipped with a DCH Cryoprobe with a small number of experiments (those in Section 4.3) having been carried out on a 500MHz Varian spectrometer equipped with a One NMR probe. All acquisition used a half-length data chunk at the start (diagrammatic pulse sequence in Figure 68, full Bruker Topspin 3.6.1 code in Appendix 8.5.1) unless expressly indicated otherwise. Unless specified otherwise all NMR experiments were carried out at 298 K, with 800 µs delays for field gradient stabilisation and a 1 second relaxation delay.

7.3 NMR Data Processing

MSE Pure shift experiments were run as 2D spectra (pseudo-2D). Individual FIDs were extracted into a plain text format using the “writefid” command on openVNMRJ 4.2. A Python script (Appendix 8.1.2), was used to process the FIDs collected in each increment into several FIDs with a continuous sense of chemical shift evolution and no significant homocoupling, representing a standard pure shift FID and FIDs after a given number of refocussing cycles (this process is explained in more detail in Section 2.6.1). FIDs were then reimported into openVNMRJ 4.2 using the “makefid” command, before baseline correction, phasing, summation and signal-to-noise measurement in MestreNova V14.1.1. FIDs were apodised with a 1.5 Hz Gaussian before measurement of signal-to-noise.

All SHARPER spectra were zero-filled after acquisition to an appropriate number of datapoints – typically 1024 K or 2048 K depending on peak widths. Despite extreme acquisition times most spectra required apodisation to remove truncation artefacts, with an appropriate Gaussian window function having been applied in most cases. Any automated analysis of spectra was carried out using Topspin 3.6.1, whilst MestreNova V14.1.1 was used for all offline processing.

7.4 Calculations and Scripts

All scripts used in this thesis require Python 2.7[102] with the NumPy and SciPy modules. MR-SHARPER scripts can be found in Appendix 8.5.3 and 8.5.4. Mobile-SHARPER scripts and the Topspin 3 macro can be found in Appendix 8.5.7 and 8.5.8. The comparison between Bruker (AVIII HD, Topspin 3.6.1) and Varian (VNMRS, VNMRJ 4.2A) was performed by modification of the MR-SHARPER script to take a 1D array of 5000 random frequencies as input and print a measure of the expected spectrum quality, percentage of final rotation completed, to a text file. Calculations were run on a desktop workstation (i7-6700 CPU @ 370 GHz, 4 cores, 16 GB RAM), and took approximately 10 hours wall time. (See Appendix 8.5.5 and 8.5.6 for the script and frequency list respectively).

The Bruker dwell time list used by the MR-SHARPER scripts was produced empirically using Topspin 3.6.1 on an offline workstation and was found to be valid for both our 500 MHz Bruker system (mentioned previously) and two 400 MHz AVIII HD equipped systems, one at the University of Bristol, the other at the University of Edinburgh. Calculation of SHARPER FIDs in Section 5.5.4 used Microsoft’s Excel with the data solver package. Optimisation of the effective transmitter offset was done using the GRG non-linear method.

8 Appendix

8.1 MSE Pure Shift

8.1.1 MSE Pure Shift Pulse Sequence (Varian)

```
/*   PS1D - Pure shift 1D experiment
#include <standard.h>
#include <chempack.h>

static int ph1[4] = {0,1,2,3},
                        ph2[32] = {0,0,0,0,0,0,0,0,1,1,1,1,1,1,1,1,
                                   2,2,2,2,2,2,2,2,3,3,3,3,3,3,3,3},
                        ph3[8] = {0,0,1,1,2,2,3,3},
                        ph4[16] = {0,1,0,1,0,1,0,1,2,3,2,3,2,3,2,3},

                        ph22[8] = {0,1,2,3}; /*Phase of the pulses in the real time elements*/

pulsesequence()
{

   double    cycles = getval("cycles"),
                        gtE = getval("gtE"),
                        gzlvlE=getval("gzlvlE"),
                        selpwrPS = getval("selpwrPS"),
                        selpwPS = getval("selpwPS"),
                        gzlvlPS = getval("gzlvlPS"),
                        droppts=getval("droppts"),
                        gstab = getval("gstab"),
                        rte = getval("rte"); /*Runs a given number of reat time elements before acquisition*/


   int                  prgcycle=(int)(getval("prgcycle")+0.5);
   char                 selshapePS[MAXSTR];
                       initval(cycles,v20);
//synchronize gradients to srate for probetype='nano'
//   Preserve gradient "area"
       gtE = syncGradTime("gtE","gzlvlE",1.0);
       gzlvlE = syncGradLvl("gtE","gzlvlE",1.0);

   getstr("selshapePS",selshapePS);

  assign(ct,v17);
  assign(zero,v18);
  assign(zero,v19);

  if (getflag("prgflg") && (satmode[0] == 'y') && (prgcycle > 1.5))
    {
       hlv(ct,v17);
       mod2(ct,v18); dbl(v18,v18);
       if (prgcycle > 2.5)
         {
            hlv(v17,v17);
            hlv(ct,v19); mod2(v19,v19); dbl(v19,v19);
         }
    }

   settable(t1,4,ph1);
   settable(t2,32,ph2);
   settable(t3,8,ph3);
   settable(t4,16,ph4);
   settable(t22,4,ph22);

   getelem(t1,v17,v1);
   getelem(t2,v17,v2);
```

```
  getelem(t3,v17,v3);
  getelem(t4,v17,v4);
  assign(v4,oph);

  assign(v1,v6);
  add(oph,v18,oph);
  add(oph,v19,oph);

// BEGIN THE ACTUAL PULSE SEQUENCE
  status(A);
    obspower(tpwr);

  delay(5.0e-5);
  if (getflag("sspul"))
      steadystate();

  if (satmode[0] == 'y')
   {
      if ((d1-satdly) > 0.02)
            delay(d1-satdly);
      else
            delay(0.02);
      if (getflag("slpsat"))
        {
            shaped_satpulse("relaxD",satdly,v6);
            if (getflag("prgflg"))
              shaped_purge(v1,v6,v18,v19);
        }
      else
        {
            satpulse(satdly,v6,rof1,rof1);
            if (getflag("prgflg"))
              purge(v1,v6,v18,v19);
        }
   }
  else
      delay(d1);

  if (getflag("wet"))
    wet4(zero,one);


  status(B);
    obspower(tpwr);
    rgpulse(pw, v1, rof1, rof2);
          setacqmode(WACQ|NZ); //Windowed Acquisition On

          delay(d2/2.0);

          delay((0.25/sw1) - gtE - gstab - 2*pw/PI - rof2 - 2*GRADIENT_DELAY);
          zgradpulse(gzlvlE,gtE);
          delay(gstab);
          rgpulse(2*pw,v2,rof1,rof1);
          delay(0.25/sw1);

          delay(gstab);
          zgradpulse(-1.0*gzlvlE,gtE);
          delay(gstab);
          obspower(selpwrPS);
          rgradient('z',gzlvlPS);
          shaped_pulse(selshapePS,selpwPS,v3,rof1,rof1);
          rgradient('z',0.0);
          obspower(tpwr);
          delay(gstab);
          zgradpulse(-2.0*gzlvlE,gtE);
          delay(gstab - droppts/sw);
```

```
        delay(d2/2.0);

        acquire(((2/sw1)/(1/sw)),1/sw);
        //delay(0.016);

//Begin Inversion for TR-CC
getelem(t22,v17,v22);
//x2
starthardloop(v20);
                        rcvroff();
        obspower(selpwrPS);
        delay(gstab);
        rgradient('z',gzlvlPS);
        shaped_pulse(selshapePS,selpwPS,v22,rof1,rof1);
        rgradient('z',0.0);
        delay((gstab-2e-6)/2);
        rcvron();
        delay((gstab-2e-6)/2);
        acquire(((2/sw1)/(1/sw)),1/sw);
endhardloop(v20);
                incr(v20);
rcvroff();
acquire(np-(((2/sw1)/(1/sw))*(cycles+1)),1/sw);//Collect end datapoints to avoid errors

}
```

8.1.2 MSE Pure Shift Reconstruction Scripts

```
#!/usr/bin/python
#For producing a standard pureshift FIDs and a TRCC FIDs from pureshift FIDs
#Requires sequential FIDs in VNMRJ text format, i.e. X Component Y Component with titles “1, 2, … n”

import math
import numpy as np
from scipy import special

###Start of Parameters User May Need to Change###
name = "XXX" #nameforFIDsToSaveAs
c = 160 #datapoints per chunk (complex points)
y= 51 #total number of chunks
###End of Parameters User May Need to Change###
i=0 #iterator for increments
n = 0 #iterator for datapoints

for delta in range(y):
	n = 0
	i=i+1
	fidtoprint= ""+str(i)
	print fidtoprint
	fid = np.genfromtxt(fidtoprint,delimiter="  ")
	fidcc=fid*[-1,1]

	while n!=c:
		x1=fid[n]
		x2=fidcc[c*2-n-1]
		x3=fid[c*2+n]
		x4=fidcc[c*4-n-1]
		x5=fid[c*4+n]
		x6=fidcc[c*6-n-1]



		text_file = open("X1"+name+".txt", "a")
		text_file.write(str(x1).replace('[','').replace(']','').replace(' ','  ') + '\n')
		text_file.close()

		text_file = open("X2"+name+".txt", "a")
		text_file.write(str(x2).replace('[','').replace(']','').replace(' ','  ') + '\n')
		text_file.close()

		text_file = open("X3"+name+".txt", "a")
		text_file.write(str(x3).replace('[','').replace(']','').replace(' ','  ') + '\n')
		text_file.close()

		text_file = open("X4"+name+".txt", "a")
		text_file.write(str(x4).replace('[','').replace(']','').replace(' ','  ') + '\n')
		text_file.close()

		text_file = open("X5"+name+".txt", "a")
		text_file.write(str(x5).replace('[','').replace(']','').replace(' ','  ') + '\n')
		text_file.close()

		text_file = open("X6"+name+".txt", "a")
		text_file.write(str(x6).replace('[','').replace(']','').replace(' ','  ') + '\n')
		text_file.close()

		n=n+1
```

8.2 Signal-to-Noise for Individual Peaks Using MSE Pure Shift Estradiol

Selective Pulse	iSNOB2		SEDUCE		rSNOB		Gauss180°		g3 Cascade	
Chemical Shift (ppm)	SNR Pre-Refocussing	SNR Incorporating one refocussing cycle	SNR Pre-Refocussing	SNR Incorporating one refocussing cycle	SNR Pre-Refocussing	SNR Incorporating one refocussing cycle	SNR Pre-Refocussing	SNR Incorporating one refocussing cycle	SNR Pre-Refocussing	SNR Incorporating one refocussing cycle
7.06	22.7	37.0	66.8	69.4	48.7	55.7	62.1	73.8	14.7	25.0
6.53	8.9	11.1	19.1	18.9	12.8	12.9	17.2	19.4	3.3	4.2
6.47	8.2	12.3	19.2	17.4	12.6	12.2	18.2	18.6	4.0	10.5
3.64	16.9	28.4	49.6	53.1	37.0	41.6	48.9	57.6	11.3	30.2
3.3	4.4	6.3	10.2	10.2	8.0	8.7	11.7	12.5	0.0	7.6
2.27	23.7	30.1	40.0	40.4	37.4	40.6	39.4	42.6	9.6	20.8
2.1	14.7	20.5	25.7	25.0	23.7	25.8	23.0	26.4	0.0	11.8
2.02	21.2	34.9	52.7	55.2	42.5	47.9	51.8	59.8	8.6	16.1
1.94	22.8	38.6	56.1	59.9	44.4	50.3	53.9	63.8	5.6	16.9
1.84	19.3	32.7	50.1	52.0	37.1	40.9	48.4	56.7	9.5	21.4
1.68	20.9	27.8	26.0	25.8	32.5	36.4	23.9	26.4	0.0	0.0
1.41	17.2	22.6	31.4	28.6	28.4	29.2	29.9	30.4	0.0	8.6
1.24	19.9	24.8	35.6	34.2	32.7	34.1	31.3	34.8	5.8	13.4
0.75	67.0	120.2	208.6	215.7	150.5	168.2	201.2	232.0	26.9	111.3

Quinine

Selective Pulse	g3 Cascade		rSNOB		iSNOB2	
Chemical Shift (ppm)	SNR Pre-Refocussing	SNR Incorporating one refocussing cycle	SNR Pre-Refocussing	SNR Incorporating one refocussing cycle	SNR Pre-Refocussing	SNR Incorporating one refocussing cycle
8.50	6.0	4.3	9.3	14.5	6.9	12.7
7.90	6.4	5.4	10.0	13.7	7.2	9.6
7.45	8.9	6.8	10.6	21.1	9.8	18.5
5.71	6.7	5.2	12.8	17.8	8.0	13.2
5.48	11.0	8.9	17.3	29.0	12.8	23.3
4.94	8.6	6.6	13.9	20.4	7.9	15.3
4.89	8.0	5.8	12.1	19.5	9.4	15.8
3.42	9.6	5.9	16.6	29.8	15.3	25.7
3.09	9.2	5.9	12.3	22.9	13.2	20.8
3.04	10.1	6.0	16.0	18.4	16.9	17.4
2.24	8.6	4.7	10.7	16.9	9.4	14.1

Streptomcyin

Selective Pulse	iBURP2		g3 Cascade	
Chemical Shift (ppm)	SNR Pre-Refocussing	SNR Incorporating one refocussing cycle	SNR Pre-Refocussing	SNR Incorporating one refocussing cycle
5.44	3.9	11.37	4.93	14.4
5.16	4.09	11.6	4.1	15.3
4.92	4.75	12.58	5.47	13.51
4.3	3.85	8.47	3.87	12.15
4.26	5.02	12.4	0	14.37
3.81	3.48	8.54	3.91	13.08
3.79	3.48	4.07	0	4.02
3.38	2.72	5.99	0	5.72
3.18	3.81	9.23	0	12.15
2.73	13.38	31.58	13.09	43.57
1.11	12.8	31.64	12.6	43.32

Strychnine

Selective Pulse	SEDUCE		Gauss180		iSNOB2		iBURP2	
Chemical Shift (ppm)	SNR Pre-Refocussing	SNR Incorporating one refocussing cycle	SNR Pre-Refocussing	SNR Incorporating one refocussing cycle	SNR Pre-Refocussing	SNR Incorporating one refocussing cycle	SNR Pre-Refocussing	SNR Incorporating one refocussing cycle
8.07	26.7	29.5	27.3	31.6	3.9	6.0	7.6	14.6
5.87	40.7	46.1	41.4	48.7	6.8	8.4	11.6	22.2
4.26	61.2	66.3	59.6	67.8	9.0	11.0	16.1	29.8
3.91	53.5	60.2	53.8	64.0	8.2	10.8	13.9	20.9
3.83	54.6	58.3	54.7	60.7	7.9	10.2	16.2	27.1
3.68	70.7	73.6	67.5	76.0	11.1	14.3	19.3	35.4
3.16	46.8	49.0	45.9	49.8	6.9	9.6	17.1	26.7
3.11	74.9	79.9	74.3	85.2	11.1	15.8	19.5	36.5
2.84	47.9	53.5	45.5	53.1	8.4	11.8	21.3	30.9
2.70	72.2	80.1	65.1	77.9	12.2	15.3	20.4	35.4
2.65	63.4	68.2	63.2	71.1	9.8	12.9	18.4	33.9
2.33	72.3	77.1	72.5	82.9	10.1	13.6	19.0	33.3
1.86	112.7	118.3	111.7	124.1	16.3	20.9	31.2	51.2
1.43	73.7	79.6	72.5	84.4	11.9	15.3	24.6	37.9
1.25	51.77	55.78	55.95	61.77	8.08	11.74	15.85	27.54

8.3 Signal-to-Noise for Individual Peaks Using PSYCHE

Quinine			Estradiol			Strychnine			Streptomycin	
Chemical Shift (ppm)	SNR		Chemical Shift (ppm)	SNR		Chemical Shift (ppm)	SNR		Chemical Shift (ppm)	SNR
8.50	70.46		7.06	165.43		8.07	59.86		5.44	84.95
7.90	75.35		6.53	95.68		5.87	93.57		5.16	85.28
7.45	105.30		6.47	102.85		4.26	130.96		4.92	78.87
5.71	69.81		3.64	113.89		3.91	129.79		4.30	57.28
5.48	104.79		3.30	21.12		3.83	121.82		4.26	86.33
4.94	93.73		2.27	144.19		3.68	161.65		3.81	53.68
4.89	93.99		2.10	93.62		3.16	131.81		3.79	83.90
3.42	82.57		2.02	112.17		3.11	141.89		3.38	77.05
3.09	83.22		1.94	137.97		2.84	130.85		3.18	62.08
3.04	112.80		1.84	109.80		2.70	162.78		2.73	234.31
2.24	70.00		1.68	121.34		2.65	145.06		1.11	203.26
-	-		1.41	115.55		2.33	145.14		-	-
-	-		1.24	127.81		1.86	246.20		-	-
-	-		0.75	450.17		1.43	148.78		-	-
-	-		-	-		1.25	108.78		-	-

8.4 Strychnine Assignment, T_1 and T_2 Values

Assignment	Chemical Shift (ppm)	T_2 (s)	T_1 (s)
H13	1.25	0.72	1.18
H15a	1.45	0.5	0.53
H17A/B	1.88	0.43	0.66
H15B	2.34	0.5	0.51
H11B	2.65	0.56	0.86
H20B	2.70	0.54	0.64
H18B	2.85	0.43	0.54
H11A	3.11	-	-
H14	3.12	-	-
H18A	3.17	0.46	0.7
H20A	3.69	0.54	0.66
H8	3.84	0.74	1.35
H16	3.93	0.68	1.28
H23A	4.05	-	-
H23B	4.13	-	-
H12	4.27	0.61	1.09
H22	5.87	0.65	1.74
H2	7.08	-	-
H1	7.15	-	-
H3	7.24	-	-
H4	8.08	1.16	3.84

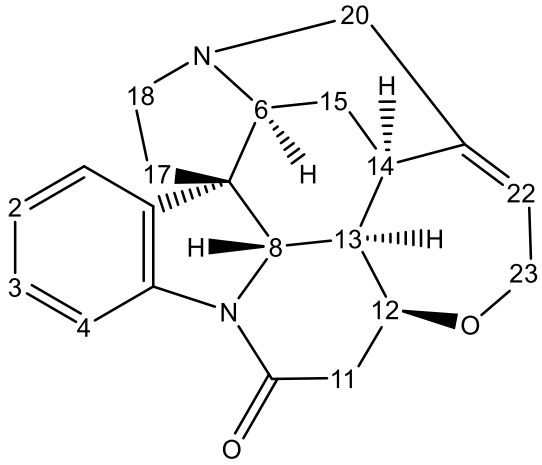

8.5 SHARPER

8.5.1 SHARPER Pulse Sequence (Bruker)

```
#include <Avance.incl>
#include <De.incl>
dwellmode explicit
define loopcounter ChunkPoints
define loopcounter Cycles

"acqt0=-p1*0.66/PI"

"ChunkPoints = cnst1"
"Cycles = cnst2 -1"
"anavpt = 1"
"d2=((2*ChunkPoints*(dw)))" ;Timing for Chunks
"d3 = ((ChunkPoints*(dw)))"
1 ze
d1 ;execute relaxation delay
p1 ph1 ;30 degree pulse

ACQ_START1(ph30, ph31) ; now start acquisition
(1u REC_UNBLK):f1 ; unblank receiver path
d3 DWL_CLK_ON ; turn dwell on
0.1u DWL_CLK_OFF ; turn dwell clock off
1u REC_BLK ; blank receiver path
100u ;needed delay to avoid errors from ringdown. Could possibly be pushed lower if needed for sensitivity
p1*2 ph2;execute 180 90deg out of phase
100.1u

5 (1u REC_UNBLK):f1 ; unblank receiver path

4 d2 DWL_CLK_ON ; turn dwell on
0.1u DWL_CLK_OFF ; turn dwell clock off

1u REC_BLK ; blank receiver path
100u ;needed delay to avoid errors from ringdown. Could possibly be pushed lower if needed for sensitivity
p1*2 ph2;execute 180 90deg out of phase
100.1u
lo to 5 times Cycles

100u eoscnp ; end of scan
; OK, FID has been acquired
10m wr #0 ; write fid down to disk
lo to 1 times ns
exit
ph1=0
ph2=1
ph30=0
ph31=0

;cnst1 : Number of Complex Points To Acquire Per Chunk
;cnst2 :Number of Chunks to Acquire Per FID
;d1 : relaxation delay; 1-5 * T1
;ns: Number of scans
```

8.5.2 Offsets Used for Off-Resonance SHARPER

Frequency Difference (Hz)	O1 (Hz)	Frequency Difference (Hz)	O1 (Hz)	Frequency Difference (Hz)	O1 (Hz)
-50	2301.95	120	2471.95	2480	4831.95
-40	2311.95	130	2481.95	2490	4841.95
-30	2321.95	140	2491.95	2495	4846.95
-20	2331.95	950	3301.95	2496	4847.95
-10	2341.95	960	3311.95	2497	4848.95
-5	2346.95	970	3321.95	2498	4849.95
-4	2347.95	980	3331.95	2499	4850.95
-3	2348.95	990	3341.95	2500	4851.95
-2	2349.95	1000	3351.95	2501	4852.95
-1	2350.95	1010	3361.95	2502	4853.95
0	2351.95	1020	3371.95	2503	4854.95
1	2352.95	1030	3381.95	2504	4855.95
2	2353.95	1040	3391.95	2505	4856.95
3	2354.95	1050	3401.95	2510	4861.95
4	2355.95	1060	3411.95	2520	4871.95
5	2356.95	1070	3421.95	2530	4881.95
10	2361.95	1080	3431.95	2540	4891.95
20	2371.95	1090	3441.95	2550	4901.95
30	2381.95	1100	3451.95	2570	4921.95
40	2391.95	1110	3461.95	2580	4931.95
50	2401.95	1120	3471.95	2610	4961.95
60	2411.95	1130	3481.95	2620	4971.95
70	2421.95	1140	3491.95	2630	4981.95
80	2431.95	1150	3501.95	2640	4991.95
90	2441.95	2450	4801.95	2650	5001.95
100	2451.95	2460	4811.95		
110	2461.95	2470	4821.95		

A table of offsets used and their relative distance from actual peak location in off-resonance SHARPER experiments. Frequency difference refers to how offset the spectrum was from the frequency of the HDO signal, based on the peak maximum in a 1D ^{1}H spectrum. O1 refers to the actual offset parameter used. Data used in Figure 69, Figure 70, Figure 71 and Figure 72.

Frequency Difference (Hz)	O1 (Hz)	Delta (ms)	Artefact Separation (Hz)		Frequency Difference (Hz)	O1 (Hz)	Delta (ms)	Artefact Separation (Hz)
-2628.04	-276.4	10	50.07		-1135.04	1216.6	7.5	66.69
-1884.04	467.6	10	49.99		-389.04	1962.6	7.5	66.61
-1140.04	1211.6	10	50		356.96	2708.6	7.5	66.66
-396.04	1955.6	10	50.19		1102.96	3454.6	7.5	66.68
347.96	2699.6	10	50.07		1848.96	4200.6	7.5	66.71
-768.04	1583.6	20	24.97		2221.96	4573.6	16.5	30.29
-24.04	2327.6	20	25.07		-2627.04	-275.4	16.5	30.33
719.96	3071.6	20	24.98		-1881.04	470.6	16.5	30.32
1463.96	3815.6	20	25		-1135.04	1216.6	16.5	30.31
2207.96	4559.6	20	25.01		-389.04	1962.6	16.5	30.36
2207.96	4559.6	5	99.92		-762.04	1589.6	12.5	39.97
-3000.04	-648.4	5	100.24		-16.04	2335.6	12.5	40.02
-2254.04	97.6	5	100.03		729.96	3081.6	12.5	40.02
-1508.04	843.6	5	99.99		1475.96	3827.6	12.5	40.04
-762.04	1589.6	5	100.02		2221.96	4573.6	12.5	39.98
-1881.04	470.6	6.25	80.07		2207.96	4559.6	2.5	200.16
-1135.04	1216.6	6.25	79.99		-2627.04	-275.4	2.5	200.22
-389.04	1962.6	6.25	80.02		-1881.04	470.6	2.5	199.95
356.96	2708.6	6.25	80.19		-1135.04	1216.6	2.5	199.97
1102.96	3454.6	6.25	80.01		-389.04	1962.6	2.5	200.05

A table of offsets used and their relative distance from actual peak location in off-resonance SHARPER experiments. Frequency difference refers to how offset the spectrum was from the frequency of the HDO signal, based on the peak maximum in a 1D ^{1}H spectrum. O1 refers to the actual offset parameter used. Data used in Figure 73, Figure 74 and Figure 75.

Frequency Difference (Hz)	O1 (Hz)		Frequency Difference (Hz)	O1 (Hz)
-0.01	2351.86		-1.76	2350.11
0.99	2352.86		-2.76	2349.11
1.99	2353.86		-3.76	2348.11
2.99	2354.86		-4.76	2347.11
3.99	2355.86		-0.26	2351.61
-1.01	2350.86		0.74	2352.61
-2.01	2349.86		1.74	2353.61
-3.01	2348.86		2.74	2354.61
-4.01	2347.86		3.74	2355.61
0.49	2352.36		-1.26	2350.61
1.49	2353.36		-2.26	2349.61
2.49	2354.36		-3.26	2348.61
3.49	2355.36		-4.26	2347.61
-1.51	2350.36		-0.01	2351.86
-2.51	2349.36		0.99	2352.86
-3.51	2348.36		1.99	2353.86
-4.51	2347.36		2.99	2354.86
-0.76	2351.11		3.99	2355.86
0.24	2352.11		-1.01	2350.86
1.24	2353.11		-2.01	2349.86
2.24	2354.11		-3.01	2348.86
3.24	2355.11		-4.01	2347.86

A table of offsets used and their relative distance from actual peak location in off-resonance SHARPER experiments. Frequency difference refers to how offset the spectrum was from the frequency of the HDO signal, based on the peak maximum in a 1D ^{1}H spectrum. O1 refers to the actual offset parameter used. Data used in Figure 94 and Figure 95.

8.5.3 MR-SHARPER Script (One Frequency)

```
#!/usr/bin/python
#For calculating timings required in multiple resonance SHARPER experiments with two signals
#Suitable for two off-resonance peaks with different |Frequency|
#Calculates a timing for a spectral width and refocussing period within user given bound
#Bounds set to provide nice spectra with adequate decoupling and T2* - > T2
#Wider bounds will improve average spectral quality
#N.B. FutureWarnings are harmless, but may render this way of performing the calcuations obsolete in the future

##N.B. This script calculates the value of "Delta" for multiple resonance SHARPER which is the half chunk
duration, not the full chunk duration

import math
import numpy as np
import warnings
from scipy import special
warnings.filterwarnings("ignore", category=FutureWarning) #This ignores a depreciation warning that is currently
irrelevant

#####Start of parameters the user should change#####

#Frequency of NMR signal (Hz)
f1 = 907.9690
#Spectrometer operating Frequency (for the nucleus of interest!)
Spectrometer_Frequency = 369.0 #This is in MHz, for the nucleus of interest
#Allowable Spectral Width
ppm_upper  = 375.0
ppm_lower = 330.0 #Around 60ppm spectral width seems to be the limit with 19F at 400MHz proton
#Allowable chunk timings in milliseconds (enter as a decimal, needs to be a float)
longest_timing = 100.0
shortest_timing = 0.000005

#####End of parameters the user should change#####

#Calculate the period of the NMR signal
p1 = 1.0/f1
#Convert to Hz limits
hz_upper=(ppm_upper*Spectrometer_Frequency)
hz_lower=(ppm_lower*Spectrometer_Frequency)

#Calculate the lowest allowed dwell time
dwell_lower=(1e6*(0.5/hz_upper))
#Calculate the maximum allowed dwell time
dwell_upper=(1e6*(0.5/hz_lower))

#Fetch Array Files
t_ar = np.genfromtxt("TimingArray",delimiter=",")
dwell_ar = np.genfromtxt("Dwellarray",delimiter=",")
cp_ar = np.genfromtxt("ChunkPointarray",delimiter=",")

#Produces a boolean mask for suitable dwell times
b = ((dwell_upper>dwell_ar)&(dwell_ar>dwell_lower))

#Produce arrays modified by first boolean mask with only suitable dwell times
dwell_arb = dwell_ar[b]
cp_arb = cp_ar[b]
t_arb = t_ar[b]

#Produce a second boolean mask based on timings
c = (((shortest_timing/1000)<t_arb)&(t_arb<(longest_timing/1000)))

#Produce arrays modified by second boolean mask with only suitable dwell times
dwell_arbc = dwell_arb[c]
cp_arbc = cp_arb[c]
t_arbc = t_arb[c]
```

```
#runs a modulo operation on the timing array with boolean mask applied
mod_arf1 = np.mod(t_arbc, p1)

#turn into a spectral quality array
mod_sqp1 = np.divide(mod_arf1, p1/100)

#Modify arrays to allow incomplete rotations
sub50ind = [(50.00<mod_sqp1)*(mod_sqp1<75.00)]
mod_sqp1[sub50ind] -= 50.0

subfrom50ind = [(25.00<mod_sqp1)*(mod_sqp1<50.00)]
mod_sqp1[subfrom50ind] -= 50.0

subfrom100ind = [(75.00<mod_sqp1)*(mod_sqp1<100.00)]
mod_sqp1[subfrom100ind] -= 100.0

mod_sqp1 = np.absolute(mod_sqp1)

#Troubleshooting line to print arrays
#np.savetxt('fname.txt',mod_sqp1)

#Find minimum element in modulo array
minElement = np.amin(mod_sqp1)
index = np.where(mod_sqp1 == np.amin(mod_sqp1))

#N.B. In the case multiple experimental viable timings are equally close to theoretically valid timings it will report
them all

#Fetch the corresponding Chunkpoints and dwell time
print "OptimalDwellTime =", dwell_arbc[index]
print "ChunkpointsMultiple =", cp_arbc[index]
#print index

sq1 = mod_sqp1[index]

#Spectral Quality Prediction - Percentage of final rotation completed
#If this number is not close to 0 or 100 the spectra can be expected to be of poor quality (S/A ratio)
Spectral_Quality_f1 = (sq1)
print 'Percentage of final rotation completed =', Spectral_Quality_f1,'%'
```

8.5.4 MR-SHARPER Script (Two Frequencies)

```
#!/usr/bin/python
#For calculating timings required in multiple peak SHARPER experiments with two frequency differences
#Suitable for two off resonance peaks with different |Frequency|
#Calculates a timing for a spectral width and refocussing period within user given bound
#Bounds set to provide nice spectra with adequate decoupling and T2* - > T2
#Wider bounds will improve average spectral quality

import math
import numpy as np
from scipy import special

#Frequency of NMR signal (Hz)
f1 = 2657.37
f2 = 2130.43

#Calculate the period of the NMR signal
p1 = 1.0/f1
p2 = 1.0/f2
#Spectrometer operating Frequency (for the nucleus of interest!)
Spectrometer_Frequency = 500 #This is in MHz

#Read in allowable spectral width (ppm)
ppm_upper  = 40.0
ppm_lower = 25.0

#Convert to Hz limits
hz_upper=(ppm_upper*Spectrometer_Frequency)
hz_lower=(ppm_lower*Spectrometer_Frequency)

#Calculate the lowest allowed dwell time
dwell_lower=(1e6*(0.5/hz_upper))

#Calculate the maximum allowed dwell time
dwell_upper=(1e6*(0.5/hz_lower))

#Read_in_timings - in ms, MUST USE A DECIMAL (needs to be a float)
longest_timing = 8.0/1000
shortest_timing = 5.0/1000

#Fetch Array Files
t_ar = np.genfromtxt("TimingArray",delimiter=",")
dwell_ar = np.genfromtxt("Dwellarray",delimiter=",")
cp_ar = np.genfromtxt("ChunkPointarray",delimiter=",")

#Produces a boolean mask for suitable dwell times
b = ((dwell_upper>dwell_ar)&(dwell_ar>dwell_lower))

#Produce arrays modified by first boolean mask with only suitable dwell times
dwell_arb = dwell_ar[b]
cp_arb = cp_ar[b]
t_arb = t_ar[b]

#Produce a second boolean mask based on timings
c = (((shortest_timing)<t_arb)&(t_arb<(longest_timing)))

#Produce arrays modified by second boolean mask with only suitable dwell times
dwell_arbc = dwell_arb[c]
cp_arbc = cp_arb[c]
t_arbc = t_arb[c]

#runs a modulo operation on the timing array with boolean mask applied
mod_arf1 = np.mod(t_arbc, p1)
mod_arf2 = np.mod(t_arbc, p2)
```

```
print mod_arf1

mod_sqp1 = np.divide(mod_arf1, p1)
mod_sqp2 = np.divide(mod_arf2, p2)

print mod_sqp1

#print mod_arf1.shape
#print mod_arf2.shape

#if True == np.array_equal(mod_arf1, mod_arf2):
#		print "identical"
#else:
#		print "non-identical"

mod_sq = np.add(mod_sqp1,mod_sqp2)
#print mod_arf1f2

#Find minimum element in modulo array
minElement = np.amin(mod_sq)
index = np.where(mod_sq == np.amin(mod_sq))

#Fetch the corresponding Chunkpoints and Dwell Time
print ("OptimalDwellTime", dwell_arbc[index])
print ("ChunkpointsMultiple", cp_arbc[index])
print index

sq1 = mod_sqp1[index]
sq2 = mod_sqp2[index]

#Spectral Quality Prediction - Percentage of final rotation completed
#If this number is not close to 0 or 100 the spectra can be expected to be of poor quality (S/A ratio)
Spectral_Quality_f1 = (sq1*100)
print ('Percentage of final rotation completed =', Spectral_Quality_f1,'%')
Spectral_Quality_f2 = (sq2*100)
print ('Percentage of final rotation completed =', Spectral_Quality_f2,'%')
```

8.5.5 MR-SHARPER Script for Evaluation

```
#!/usr/bin/python
#Reads an array of frequencies (NumbersList.csv) and provides a measure of expected spectrum quality
#Suitable for two off resonance peaks with different Frequency
#Calculates a timing for a spectral width and refocussing period within user given bound
#Bounds set to provide nice spectra with adequate decoupling and T2* - > T2
#Wider bounds will improve average spectral quality

import math
import numpy as np
from scipy import special

f1_ar = np.genfromtxt("NumbersList.csv",delimiter=",")

#Frequency of NMR signal (Hz)
for x in f1_ar:

        #Calculate the period of the NMR signal
        p1 = 1.0/x
        #Spectrometer operating Frequency (for the nucleus of interest!)
        Spectrometer_Frequency = 500 #This is in MHz

        #Read in allowable spectral width (ppm)
        ppm_upper  = 25.0
        ppm_lower = 10.0

        #Convert to Hz limits
        hz_upper=(ppm_upper*Spectrometer_Frequency)
        hz_lower=(ppm_lower*Spectrometer_Frequency)

        #Calculate the lowest allowed dwell time
        dwell_lower=(1e6*(0.5/hz_upper))

        #Calculate the maximum allowed dwell time
        dwell_upper=(1e6*(0.5/hz_lower))

        #Read_in_timings - in ms, MUST USE A DECIMAL (needs to be a float)
        longest_timing = 25.0/1000
        shortest_timing = 10.0/1000

        #Fetch Array Files
        t_ar = np.genfromtxt("TimingForVarian",delimiter=",")
        dwell_ar = np.genfromtxt("DwellForVarian",delimiter=",")
        cp_ar = np.genfromtxt("ChunksForVarian",delimiter=",")

        #Produces a boolean mask for suitable dwell times
        b = ((dwell_upper>dwell_ar)&(dwell_ar>dwell_lower))

        #Produce arrays modified by first boolean mask with only suitable dwell times
        dwell_arb = dwell_ar[b]
        cp_arb = cp_ar[b]
        t_arb = t_ar[b]

        #Produce a second boolean mask based on timings
        c = (((shortest_timing)<t_arb)&(t_arb<(longest_timing)))

        #Produce arrays modified by second boolean mask with only suitable dwell times
        dwell_arbc = dwell_arb[c]
        cp_arbc = cp_arb[c]
        t_arbc = t_arb[c]

        #runs a modulo operation on the timing array with boolean mask applied
        mod_arf1 = np.mod(t_arbc, p1)
```

```
#turn into a spectral quality array
mod_sqp1 = np.divide(mod_arf1, p1/100)

#Set of operations to get the other "almost made it" rotations
sub50ind = [(50.00<mod_sqp1)*(mod_sqp1<75.00)]
mod_sqp1[sub50ind] -= 50.0

subfrom50ind = [(25.00<mod_sqp1)*(mod_sqp1<50.00)]
mod_sqp1[subfrom50ind] -= 50.0

subfrom100ind = [(75.00<mod_sqp1)*(mod_sqp1<100.00)]
mod_sqp1[subfrom100ind] -= 100.0

mod_sqp1 = np.absolute(mod_sqp1)

#Troubleshooting line to print arrays
#np.savetxt('fname.txt',mod_sqp1)

#Find minimum element in modulo array
minElement = np.amin(mod_sqp1)
index = np.where(mod_sqp1 == np.amin(mod_sqp1))



#Fetch the corresponding Chunkpoints and Dwell Time
print ("OptimalDwellTime", dwell_arbc[index])
print ("ChunkpointsMultiple", cp_arbc[index])
print index

sq1 = mod_sqp1[index]

#Spectral Quality Prediction - Percentage of final rotation completed
#If this number is not close to 0 or 100 the spectra can be expected to be of poor quality (S/A ratio)
Spectral_Quality_f1 = (sq1)
print ('Percentage of final rotation completed =', Spectral_Quality_f1,'%')

Spectral_Quality = ((minElement))
text_file = open("Output.txt", "a")
text_file.write(str(Spectral_Quality)+ '\n')
text_file.close()
```

8.5.6 Random Frequencies for Comparison of NMR Spectrometers

Shown graphically in Figure 81 and Figure 82.

0.02; 0.25; 0.42; 0.44; 0.52; 0.56; 0.58; 0.6; 0.64; 0.9; 0.9; 1; 1.01; 1.45; 1.69; 1.86; 1.97; 1.98; 2; 2.14; 2.33; 2.4; 2.53; 2.66; 2.77; 2.87; 3; 3.11; 3.22; 3.36; 3.47; 4; 4.27; 4.6; 5; 5.24; 5.47; 5.54; 5.57; 5.73; 5.84; 5.96; 6; 6.13; 6.16; 6.17; 6.63; 6.79; 6.98; 7; 7.34; 7.37; 8; 8.34; 8.37; 8.39; 8.43; 8.44; 8.67; 8.89; 8.93; 9; 9.05; 9.06; 9.39; 9.42; 9.83; 9.84; 9.84; 9.87; 10; 10.04; 10.5; 10.64; 10.64; 11.04; 11.06; 11.28; 11.59; 11.65; 11.72; 11.89; 11.92; 11.98; 12.19; 12.38; 12.51; 12.57; 12.76; 12.86; 12.93; 13.24; 13.46; 13.58; 13.77; 14.07; 14.1; 14.34; 14.38; 14.38; 14.44; 14.5; 14.81; 14.88; 15.06; 15.18; 15.28; 15.36; 15.37; 15.43; 15.53; 15.6; 15.65; 15.73; 15.77; 15.9; 16.13; 16.18; 16.22; 16.31; 16.39; 16.4; 16.66; 16.67; 17.15; 17.2; 17.44; 17.69; 17.74; 17.8; 17.97; 17.97; 17.99; 18.28; 18.92; 18.96; 19.1; 19.13; 19.29; 19.39; 19.48; 19.49; 19.74; 20; 20.03; 20.14; 20.2; 20.42; 20.59; 20.76; 20.79; 20.82; 21.09; 21.15; 21.35; 21.68; 21.72; 22.09; 22.3; 22.51; 22.56; 22.68; 22.71; 22.93; 23.08; 23.43; 23.43; 23.45; 23.56; 23.75; 23.79; 24.23; 24.65; 24.83; 25.1; 25.63; 25.7; 25.84; 25.89; 26.07; 26.08; 26.25; 26.26; 26.37; 26.38; 26.38; 26.85; 26.95; 27.29; 27.31; 27.36; 27.5; 28.13; 28.51; 28.98; 29.27; 29.28; 29.41; 29.5; 29.55; 29.66; 29.87; 29.92; 29.93; 30; 30.1; 30.22; 30.25; 30.37; 30.67; 30.7; 32.24; 32.65; 32.93; 33.2; 33.8; 34.23; 34.34; 34.98; 34.99; 35.28; 35.62; 35.93; 36.03; 37.35; 37.47; 38.18; 38.74; 38.78; 39.01; 39.95; 40; 40.22; 40.98; 41.56; 41.66; 43.29; 44; 46.22; 46.38; 46.9; 47.24; 47.31; 47.34; 47.36; 47.39; 50; 52.18; 53.34; 53.89; 53.99; 54.65; 55.15; 55.54; 56.57; 56.98; 57.06; 57.93; 59.06; 59.95; 60; 61.19; 63.75; 63.89; 64.13; 65.24; 65.86; 66.34; 66.59; 66.82; 66.88; 67.43; 69.17; 69.35; 70; 70.78; 71.33; 71.71; 72.25; 72.36; 74.59; 75.56; 75.59; 76.15; 77.2; 77.49; 77.83; 78.19; 80; 80.96; 80.99; 81.29; 81.37; 81.88; 84.48; 85.5; 85.81; 86.67; 87.75; 88.59; 89.77; 90; 90.13; 90.15; 90.5; 90.95; 91.03; 91.95; 94.93; 95.85; 96.04; 97.16; 97.98; 99.21; 99.41; 99.84; 99.87; 100; 100.77; 100.94; 101.24; 103.24; 104.3; 107.09; 107.84; 107.93; 107.94; 111.31; 112.04; 112.32; 115.5; 115.82; 116.8; 117.87; 118.52; 118.59; 118.75; 119.18; 119.81; 120.59; 120.8; 121.05; 121.24; 121.25; 121.69; 123.79; 124.22; 124.3; 124.71; 124.89; 126.1; 127.42; 128.48; 132.03; 132.62; 132.72; 135.79; 136.21; 139.34; 141.53; 144.56; 144.63; 144.65; 145.26; 146.49; 147.67; 148.59; 149.74; 152.5; 155.29; 165.33; 166.38; 167.47; 167.98; 168.34; 169.52; 170.04; 172.28; 173.16; 174.36; 175.19; 175.82; 176.02; 176.49; 178; 180.22; 182.1; 182.44; 182.94; 184.8; 186.92; 188; 190.6; 191.64; 192.05; 195.98; 197.58; 198.01; 198.64; 200; 200.12; 200.51; 200.68; 200.73; 201.15; 202.33; 202.52; 202.78; 204.98; 207.14; 207.36; 209.16; 209.21; 215.52; 215.75; 216.45; 216.61; 217.18; 217.61; 218.13; 221.6; 222.91; 223.24; 224.5; 224.72; 226.22; 227.37; 227.73; 228.31; 229.84; 230.35; 235.47; 241.43; 241.67; 241.73; 242.88; 243.4; 243.71; 244.85; 245.04; 245.21; 245.8; 249.1; 249.49; 250.43; 252.08; 252.87; 254.8; 255.63; 255.94; 256.21; 256.26; 256.27; 256.72; 258.19; 258.82; 258.86; 261.03; 263.08; 263.17; 265.56; 266.09; 266.56; 266.59; 270.74; 271.04; 273.13; 276.06; 276.25; 276.62; 277.5; 278.72; 280.03; 280.32; 280.41; 280.68; 281.2; 281.98; 284.6; 285.87; 286.26; 286.42; 288.06; 288.52; 288.97; 289.35; 290.6; 290.82; 291.12; 292.46; 292.47; 292.69; 292.75; 294.2; 295.49; 296.3; 296.39; 297.95; 298.31; 298.42; 299.11; 300; 300.54; 303.63; 303.86; 304.46; 306.52; 307.32; 309.06; 311.09; 316.86; 318.07; 318.16; 318.18; 318.79; 320.38; 320.55; 321.51; 321.61; 321.97; 322.3; 322.9; 326.88; 326.93; 326.94; 327.27; 327.66; 329; 329.06; 330.05; 331.21; 332.32; 334.78; 335.01; 336.05; 336.24; 336.99; 337.6; 339.68; 341.23; 341.77; 345.56; 346.55; 347.34; 349.03; 349.73; 350.46; 354.01; 355.8; 357.06; 357.15; 360.65; 360.99; 361; 362.76; 363.11; 364.94; 365.52; 366.21; 368; 369.09; 369.5; 373.64; 375.15; 376.16; 376.51; 376.75; 376.85; 377.62; 378.03; 378.12; 379.63; 379.95; 380.11; 380.69; 380.9; 380.94; 382.12; 383.73; 384.95; 386.06; 386.08; 387.09; 388.61; 389.56; 391.16; 392.02; 392.49; 396.74; 397.65; 398; 398.86; 399.54; 399.65; 400; 400.85; 401.21; 401.62; 402.76; 404.19; 404.2; 404.73; 405.22; 408.82;

409.69; 411.26; 411.29; 412.97; 414.92; 415.85; 417.32; 418.35; 420.04; 423.09; 423.23; 423.79; 428.88; 429.8; 430.31; 430.57; 431.57; 431.83; 432.52; 432.64; 434.66; 436.84; 438.86; 439.68; 439.71; 441.3; 443.1; 443.34; 444.67; 446.87; 448.36; 448.57; 448.72; 449.03; 451.72; 452.51; 453.07; 454.62; 456.02; 456.41; 456.75; 458.13; 458.51; 458.78; 459.12; 462.28; 466.15; 466.59; 466.94; 469.55; 470.71; 473.32; 473.65; 475.28; 475.55; 476.04; 476.18; 476.24; 476.54; 476.84; 477.71; 478.36; 478.41; 480.41; 480.77; 480.83; 481.82; 482.1; 483.18; 484.29; 492.02; 492.83; 493.38; 495.69; 496.4; 496.69; 497.59; 498.88; 499.03; 499.07; 499.31; 500; 500.92; 501.1; 502.25; 503.15; 503.69; 505.42; 505.93; 506.49; 508.98; 510.49; 516.31; 518.01; 519.36; 519.71; 520.55; 524.01; 525.24; 525.98; 526.23; 526.75; 526.78; 530.17; 530.99; 531.29; 531.32; 534.37; 536.9; 537.04; 537.3; 540.97; 542.14; 542.43; 543.94; 544.68; 545.15; 545.16; 548.05; 548.13; 548.96; 551.7; 552.23; 554.13; 555.26; 556.27; 558.28; 558.37; 559.66; 560.14; 561.24; 564.39; 564.77; 564.8; 565.34; 565.65; 565.75; 568.58; 568.59; 569.17; 569.76; 569.87; 570.47; 571.53; 573.03; 573.43; 574.51; 574.8; 577.45; 580.81; 585.41; 587.44; 589.82; 590.44; 592.42; 596.89; 597.62; 598.63; 598.91; 600; 600.66; 601.46; 603.47; 603.95; 604.53; 605.82; 606.12; 606.15; 606.77; 607.01; 608.4; 611.55; 613.73; 613.87; 616.44; 617.97; 618.98; 620.48; 624.2; 624.93; 624.98; 625.82; 626.5; 626.73; 627.21; 629.25; 629.26; 629.77; 629.9; 630.26; 631.34; 631.38; 631.77; 632.93; 632.99; 635.06; 635.64; 638.38; 638.93; 638.99; 639.23; 639.61; 639.71; 640.92; 641.92; 642.44; 643; 645.03; 645.28; 652.23; 652.45; 654.04; 654.32; 654.82; 656.73; 657.62; 657.68; 663.44; 663.76; 664.92; 665.35; 665.41; 665.45; 666.09; 667.67; 667.97; 670.17; 671.2; 671.91; 672.44; 673.28; 674.59; 674.93; 675.56; 675.76; 675.9; 676.31; 676.76; 681.33; 681.43; 681.73; 684.02; 687.51; 687.61; 688.26; 689.31; 690.79; 692.39; 692.51; 692.98; 693.13; 693.28; 693.96; 694.97; 696.95; 697.61; 698.81; 700; 701.32; 702.08; 702.18; 702.38; 703.94; 705.71; 706.14; 711.27; 712.85; 713.44; 713.57; 714.86; 717.68; 717.76; 717.79; 718.83; 719.28; 722.28; 723.27; 723.93; 724.28; 724.63; 724.8; 725.14; 725.64; 726.99; 728.43; 728.84; 733.15; 733.95; 734.23; 734.65; 735.51; 736.81; 737.73; 738.07; 738.24; 738.25; 738.62; 739.16; 741.01; 741.33; 741.46; 741.57; 743.69; 744.11; 744.72; 745.36; 745.5; 748.39; 749.14; 749.26; 750.58; 750.67; 750.81; 756.53; 757.93; 759.79; 760.82; 761.38; 762.71; 763.63; 763.74; 763.91; 765.2; 765.81; 766.16; 766.74; 767; 768.79; 769.27; 769.81; 771.58; 771.66; 771.99; 772.15; 774.48; 775.33; 775.35; 776.26; 777.6; 777.87; 778.4; 779.25; 779.85; 781.2; 781.62; 782.19; 783.63; 784.49; 786.06; 787.32; 787.39; 790.22; 790.94; 793.88; 794.09; 795.15; 796.15; 796.79; 797.95; 798.01; 799.59; 800; 800.87; 801.34; 801.8; 802.31; 803.04; 803.43; 803.46; 804.52; 804.77; 805.3; 809.67; 810.97; 811.02; 813.17; 816.89; 818.01; 818.97; 819.87; 820.43; 821.11; 822.26; 822.9; 822.92; 823.75; 824.15; 824.22; 824.38; 825.43; 825.44; 827; 829; 834.13; 835.47; 836.09; 836.13; 836.73; 837.09; 837.53; 839.32; 839.87; 840.29; 844.54; 846.5; 850.57; 850.64; 850.77; 851.56; 851.89; 852.4; 852.82; 853.64; 853.93; 855.37; 858.16; 858.17; 858.26; 859.02; 859.19; 863.34; 864.63; 866.57; 867.05; 867.06; 868.1; 868.88; 869.57; 872.82; 873.47; 877.45; 878.27; 878.97; 879.75; 880.99; 881.47; 881.6; 883.27; 884.07; 884.49; 885.21; 887.21; 890.35; 892.43; 892.74; 894.28; 894.31; 894.44; 896.3; 898.79; 899.4; 899.98; 900; 901.21; 902.47; 906.73; 908.97; 909.3; 909.71; 912.78; 913.31; 916.19; 917.53; 918.81; 918.89; 919.6; 919.61; 919.94; 921.47; 921.57; 921.89; 923; 923.45; 924.94; 926.45; 928.18; 928.25; 929.8; 930.02; 930.03; 933.03; 935.38; 936.05; 936.88; 937.08; 938.07; 938.15; 939.27; 939.87; 941.38; 941.72; 943.35; 943.58; 944.07; 947.01; 947.36; 947.87; 952.89; 953.91; 954.81; 956.71; 958.49; 959.02; 959.85; 961.28; 962.95; 964.76; 965.01; 967.61; 968.57; 974; 974.42; 975.04; 980.19; 981.78; 983.33; 984.71; 985.38; 986.69; 988.15; 988.53; 989.13; 990; 990.5; 990.65; 990.89; 994.67; 994.68; 995.65; 998.3; 1000; 1002.24; 1004.67; 1004.8; 1006.09; 1006.64; 1007.03; 1007.77; 1008.25; 1010.15; 1011.07; 1011.9; 1014.55; 1014.76; 1014.94; 1015.02; 1015.23; 1015.81; 1016.72; 1016.84; 1017.34; 1017.56; 1018.39; 1021.74; 1022.11; 1025.4; 1025.73; 1027.71; 1027.78; 1027.83; 1028.63;

1028.79; 1028.93; 1029.36; 1030.04; 1030.94; 1032.35; 1034.44; 1035.26; 1035.81; 1036.6; 1036.7; 1038.03; 1039.27; 1039.59; 1041.92; 1043.59; 1044.22; 1045.62; 1046.01; 1047; 1047.76; 1048.18; 1049.09; 1051.25; 1051.28; 1051.88; 1052.65; 1052.98; 1055.64; 1056.26; 1056.4; 1056.85; 1057.01; 1057.32; 1058.4; 1059; 1059.35; 1060.51; 1061.18; 1061.25; 1061.61; 1063.47; 1064.85; 1064.86; 1065.06; 1065.38; 1067.22; 1067.93; 1067.96; 1069.17; 1069.37; 1071.44; 1072.47; 1073.36; 1073.78; 1074.37; 1077.13; 1078.27; 1078.34; 1078.93; 1079.08; 1080.06; 1082.94; 1082.96; 1082.99; 1083.38; 1086.34; 1087.89; 1089.15; 1090.08; 1092.09; 1095.31; 1097.1; 1098.02; 1100; 1100.58; 1101.83; 1102.22; 1102.83; 1103.36; 1103.43; 1103.9; 1103.95; 1104.53; 1106.46; 1106.64; 1109.34; 1112.26; 1112.62; 1115.96; 1119.97; 1120.77; 1121.72; 1122.44; 1122.69; 1123.27; 1123.62; 1124.15; 1124.83; 1125.87; 1129.92; 1130.5; 1133.73; 1134.69; 1137.67; 1140.19; 1144.46; 1145.01; 1145.95; 1149.43; 1150.42; 1150.86; 1151.39; 1155.9; 1157.68; 1157.89; 1158.27; 1159.67; 1160; 1161.41; 1161.57; 1161.6; 1162.39; 1163.37; 1163.8; 1165.37; 1165.8; 1165.88; 1166.51; 1167.02; 1168.88; 1169.2; 1170.27; 1171.37; 1171.5; 1171.9; 1176.45; 1176.64; 1179.3; 1180.24; 1180.36; 1182.84; 1183.46; 1183.66; 1183.92; 1185.34; 1186.69; 1188.46; 1189; 1189.52; 1189.94; 1190.02; 1190.24; 1193.15; 1196.32; 1197.45; 1200; 1200.13; 1202.86; 1203.08; 1204.1; 1204.37; 1204.62; 1208.94; 1209; 1209.43; 1209.61; 1210; 1210.14; 1210.52; 1212.48; 1213.72; 1214.34; 1214.44; 1215.34; 1216.33; 1216.6; 1217.24; 1218.58; 1219.19; 1219.29; 1219.73; 1220; 1220.12; 1221.11; 1221.82; 1226.04; 1228.9; 1229.16; 1230; 1231.5; 1231.54; 1232.63; 1233.78; 1235.87; 1236.53; 1237; 1237.14; 1237.53; 1238.89; 1239.41; 1240; 1240.58; 1240.95; 1241.26; 1241.44; 1241.46; 1241.5; 1241.93; 1242; 1242.19; 1242.35; 1243.66; 1246; 1246.38; 1246.76; 1247.03; 1249.37; 1250; 1251; 1251.72; 1252; 1252.02; 1252.18; 1252.3; 1253; 1253.51; 1254; 1254.01; 1254.1; 1254.2; 1254.3; 1254.31; 1254.32; 1254.33; 1254.34; 1254.35; 1254.36; 1254.37; 1254.38; 1254.39; 1254.4; 1254.5; 1254.6; 1254.7; 1254.8; 1254.9; 1254.94; 1255; 1255.25; 1255.36; 1255.47; 1256; 1256.19; 1257; 1257.6; 1258; 1258.06; 1258.08; 1258.15; 1258.19; 1258.27; 1259; 1260; 1261.48; 1261.49; 1263.39; 1264.05; 1264.41; 1265.1; 1265.48; 1265.68; 1266.58; 1267.47; 1269.41; 1270; 1270.35; 1270.92; 1275.63; 1276; 1276.35; 1277.97; 1280; 1280.19; 1280.37; 1280.83; 1280.85; 1282.04; 1282.11; 1282.5; 1282.58; 1283.04; 1283.88; 1284.49; 1284.68; 1289.44; 1290; 1290.19; 1295.09; 1296.28; 1296.77; 1298.18; 1299.1; 1300; 1300.19; 1301.21; 1301.49; 1302.96; 1303.62; 1303.67; 1304.59; 1305.99; 1308.49; 1308.5; 1309.21; 1310.08; 1310.88; 1311.05; 1311.16; 1311.59; 1313.55; 1314; 1314.15; 1315.13; 1318.76; 1320.15; 1320.32; 1320.82; 1321.61; 1322.17; 1324.52; 1326; 1326.36; 1327.15; 1327.66; 1328.91; 1329.73; 1329.81; 1332.53; 1332.62; 1333.05; 1334.08; 1334.11; 1334.85; 1335.49; 1338.05; 1338.26; 1338.46; 1343.23; 1343.4; 1344.33; 1344.91; 1345.8; 1346.61; 1347.58; 1349.65; 1352.66; 1354.07; 1357.18; 1357.26; 1358.1; 1358.35; 1360.2; 1360.44; 1360.73; 1362.3; 1362.77; 1363.23; 1363.4; 1363.69; 1365.49; 1368.56; 1369.78; 1369.84; 1370.46; 1373.09; 1374.63; 1376.09; 1378.21; 1378.29; 1378.76; 1385.26; 1386.08; 1387.05; 1391.03; 1391.92; 1393.07; 1393.64; 1396.59; 1396.62; 1397.88; 1400; 1400.35; 1400.69; 1400.72; 1400.85; 1402.6; 1403.73; 1404.89; 1406.79; 1407.74; 1408.77; 1409.08; 1409.23; 1409.51; 1409.58; 1410.22; 1410.74; 1411.45; 1413.14; 1414.13; 1417.07; 1417.42; 1417.69; 1418.49; 1420.62; 1421.16; 1422.5; 1424.95; 1425.96; 1427.57; 1427.94; 1428.12; 1428.49; 1430; 1434.06; 1434.14; 1434.22; 1434.25; 1436.87; 1438.91; 1439.23; 1440.84; 1441.32; 1441.46; 1443.27; 1445.21; 1446.43; 1447.84; 1448.08; 1448.53; 1448.81; 1448.87; 1450.79; 1451.32; 1451.56; 1451.82; 1452.39; 1454.14; 1455.81; 1455.97; 1458.77; 1460.07; 1460.21; 1460.62; 1461.59; 1462.65; 1463.53; 1464.78; 1465.42; 1466.84; 1467.61; 1468.52; 1468.67; 1471.76; 1474.76; 1475.53; 1475.8; 1476.7; 1476.73; 1476.97; 1477.45; 1479.53; 1481.02; 1484.35; 1484.41; 1484.66; 1487.61; 1487.79; 1488.72; 1490.98; 1491.53; 1494.25; 1496.08; 1497.91; 1498.03; 1500; 1500.19; 1501.06; 1502.02; 1502.34; 1504.78; 1505.29; 1505.47; 1506.83; 1507.94; 1508.23; 1508.48; 1509.28;

1509.92; 1514.44; 1516.31; 1516.53; 1519.89; 1522.21; 1524.2; 1526.14; 1528.21; 1531.25; 1531.45; 1532.94; 1534.26; 1535.83; 1537.89; 1539.81; 1541.76; 1542.75; 1542.88; 1543.77; 1545.47; 1546.11; 1548.2; 1548.41; 1548.82; 1549.78; 1551; 1551.16; 1554.14; 1554.78; 1555.25; 1555.39; 1556.25; 1557.52; 1559.02; 1563.56; 1564.19; 1564.32; 1565.57; 1566.31; 1570.38; 1571.06; 1571.24; 1571.68; 1572.28; 1573.08; 1573.15; 1573.84; 1576.78; 1578.27; 1578.66; 1579.6; 1579.63; 1580.14; 1580.71; 1582.45; 1585.63; 1587.12; 1589.06; 1589.62; 1590.72; 1590.82; 1591.32; 1592.79; 1595.11; 1596.38; 1596.62; 1598.69; 1599.94; 1600; 1600.64; 1601.07; 1601.58; 1601.78; 1603.12; 1603.16; 1604.84; 1606.93; 1607.3; 1608.83; 1608.99; 1611.86; 1612.38; 1612.51; 1613.15; 1613.91; 1614.81; 1615.15; 1619.2; 1619.45; 1620.71; 1622.57; 1623.96; 1625.78; 1625.92; 1626.59; 1626.73; 1627.21; 1627.54; 1628.9; 1629.5; 1630.08; 1630.82; 1631.4; 1632.06; 1633.17; 1633.68; 1634.22; 1635.08; 1635.45; 1636.4; 1636.99; 1638.42; 1642.27; 1642.36; 1642.49; 1642.58; 1642.94; 1645.01; 1645.41; 1649.1; 1649.26; 1649.77; 1650.16; 1652.6; 1654.85; 1655.11; 1656.35; 1657; 1657.63; 1659.66; 1661.26; 1662.48; 1662.63; 1664.66; 1664.67; 1665.18; 1666; 1666.39; 1668.69; 1671.65; 1674.88; 1677.41; 1681.85; 1682.8; 1684.28; 1685.56; 1686.06; 1688.01; 1688.84; 1689.46; 1689.75; 1690.1; 1692.21; 1692.25; 1693.23; 1693.65; 1694.47; 1695.88; 1696.83; 1697.2; 1697.7; 1700; 1701.67; 1701.83; 1704.21; 1706.56; 1709.77; 1709.98; 1710.16; 1711.81; 1712.14; 1712.93; 1713.24; 1713.42; 1716.55; 1717.78; 1718.26; 1719.44; 1719.98; 1721.02; 1721.75; 1721.91; 1721.96; 1722.89; 1724.15; 1724.79; 1725.15; 1725.18; 1726.1; 1727.18; 1727.64; 1728.4; 1728.79; 1729.41; 1729.88; 1731.59; 1731.6; 1731.71; 1735.95; 1736.32; 1736.8; 1738.15; 1738.54; 1738.75; 1739.71; 1741.39; 1741.44; 1742.87; 1745.73; 1746.85; 1747.06; 1748.18; 1751.28; 1751.31; 1751.39; 1751.5; 1753.17; 1753.29; 1753.84; 1754.26; 1754.37; 1755.09; 1756.36; 1756.62; 1756.65; 1756.69; 1756.79; 1759.18; 1760.55; 1760.74; 1761.39; 1761.79; 1764.06; 1764.31; 1765.09; 1766.73; 1766.85; 1767.73; 1768.02; 1769.71; 1769.78; 1771.52; 1775.28; 1776.47; 1777.14; 1778.28; 1781.09; 1782.47; 1782.9; 1784.36; 1784.66; 1784.91; 1784.99; 1785.03; 1785.15; 1785.18; 1785.55; 1789.47; 1789.7; 1790.23; 1790.82; 1791.28; 1792.98; 1798.7; 1800; 1800.3; 1800.39; 1800.54; 1801.4; 1801.73; 1804.36; 1805.41; 1805.89; 1806.59; 1807.2; 1807.89; 1808.44; 1810.6; 1813.35; 1814.13; 1815.1; 1816.61; 1820.44; 1821.45; 1822.22; 1822.51; 1823.09; 1823.84; 1825.73; 1826.11; 1826.19; 1826.64; 1826.77; 1828.17; 1828.22; 1828.28; 1828.87; 1829.16; 1830.83; 1833.37; 1833.47; 1834.09; 1836.46; 1836.98; 1839.06; 1840.45; 1841.27; 1842.47; 1843.38; 1844.01; 1845.08; 1845.32; 1848.63; 1852.17; 1853.62; 1854.92; 1856.09; 1858.87; 1859.55; 1859.99; 1862.46; 1862.98; 1863.21; 1864.27; 1865.25; 1866.37; 1866.6; 1868.04; 1868.09; 1871.25; 1872.17; 1872.28; 1872.37; 1872.49; 1873.34; 1873.66; 1873.77; 1874.46; 1876.16; 1877.05; 1879.5; 1880.84; 1881.6; 1881.68; 1882.31; 1882.58; 1882.59; 1883.52; 1883.55; 1884.16; 1885.08; 1887.29; 1887.78; 1889.16; 1889.88; 1890.23; 1890.66; 1895.11; 1895.26; 1897.58; 1900; 1900.27; 1900.28; 1900.54; 1902.32; 1903.22; 1906.06; 1906.38; 1908.95; 1909.57; 1910.13; 1910.88; 1911.82; 1912.6; 1912.94; 1918.33; 1920.95; 1922.43; 1924.19; 1924.31; 1924.63; 1925.39; 1925.55; 1927.73; 1927.82; 1928.15; 1928.57; 1928.66; 1929.27; 1929.91; 1934.38; 1935.13; 1935.68; 1936.25; 1937.37; 1937.95; 1938.09; 1938.76; 1938.79; 1939.36; 1940.77; 1942.26; 1944.71; 1946.69; 1946.77; 1946.92; 1947.74; 1949.8; 1950.34; 1953; 1953.78; 1954.8; 1955.36; 1955.57; 1956.69; 1959.11; 1960.96; 1961.19; 1963.46; 1964.04; 1964.8; 1967.06; 1967.41; 1967.56; 1967.84; 1968.34; 1970.15; 1972.23; 1972.37; 1973.15; 1976.59; 1977.73; 1978.28; 1978.39; 1979.26; 1980.57; 1980.87; 1982.09; 1982.78; 1984.06; 1985.2; 1986.06; 1986.15; 1986.28; 1986.35; 1987.36; 1987.9; 1988.17; 1989.16; 1991.85; 1991.95; 1992.17; 1992.74; 1994.53; 1995.07; 1995.45; 1995.61; 1996; 1996.75; 1997.73; 1999.25; 2000; 2001.2; 2001.7; 2002.2; 2002.75; 2003.43; 2004.68; 2005.73; 2007.04; 2009.19; 2010.45; 2012.12; 2013.84; 2014.68; 2017.39; 2017.99; 2018.06; 2018.5; 2018.77; 2018.91; 2019.55; 2019.81; 2022.73; 2023.01; 2026.8; 2028.12; 2029.19; 2031.73; 2031.79; 2032.21;

2034.61; 2036.43; 2037.2; 2038.07; 2040.25; 2040.29; 2040.39; 2040.78; 2041.38; 2042.14; 2045.92; 2049.52; 2051.1; 2051.13; 2052.21; 2053.3; 2054.51; 2055.75; 2058.44; 2058.54; 2061.98; 2062.15; 2062.49; 2064.36; 2064.6; 2064.87; 2066.36; 2066.45; 2067.9; 2069.07; 2070.97; 2072.16; 2072.89; 2073.77; 2073.98; 2075.32; 2076.09; 2079.17; 2079.77; 2079.94; 2081.08; 2082.06; 2082.78; 2083.23; 2083.24; 2083.32; 2083.91; 2084.21; 2084.23; 2086.65; 2086.72; 2087.58; 2088.68; 2088.7; 2089.46; 2089.89; 2090.32; 2090.54; 2091.53; 2092.26; 2093.2; 2093.29; 2093.31; 2093.48; 2094.13; 2096.06; 2096.67; 2096.73; 2097.62; 2098.6; 2099.12; 2101.27; 2101.73; 2103.59; 2103.91; 2104.39; 2107.76; 2109.26; 2109.47; 2110.12; 2111.41; 2111.5; 2112.12; 2115.12; 2115.24; 2117.4; 2120.13; 2121.57; 2121.65; 2121.68; 2122.64; 2122.74; 2123.22; 2124.22; 2124.61; 2126.01; 2127.01; 2127.78; 2127.87; 2130.43; 2132.26; 2133.53; 2133.75; 2136.95; 2138.23; 2138.71; 2138.75; 2139.3; 2140.5; 2141.46; 2141.99; 2142.37; 2142.59; 2142.75; 2143.22; 2143.46; 2143.88; 2144.01; 2147.52; 2148.77; 2149.25; 2149.94; 2152.67; 2152.78; 2153.46; 2153.68; 2155.11; 2155.5; 2156.32; 2156.34; 2156.76; 2157.57; 2157.77; 2158.53; 2160.19; 2160.92; 2161.01; 2167.09; 2167.59; 2168.75; 2170.78; 2171.25; 2172.28; 2174.54; 2174.93; 2175.12; 2177.12; 2177.72; 2179.19; 2181.35; 2181.75; 2182.17; 2183.57; 2183.59; 2183.86; 2184.85; 2187.51; 2190.6; 2191.24; 2191.49; 2192.16; 2194.48; 2196.79; 2197.12; 2197.52; 2197.62; 2198.01; 2198.65; 2199.39; 2199.79; 2199.82; 2199.9; 2200.04; 2201.48; 2201.7; 2201.74; 2201.97; 2203.58; 2204.14; 2204.2; 2204.58; 2204.71; 2206.51; 2206.61; 2207.68; 2212.26; 2212.29; 2212.99; 2213.66; 2213.99; 2215.83; 2217.13; 2218.79; 2220.14; 2223.57; 2225.75; 2226.17; 2226.34; 2227.11; 2227.81; 2229.98; 2230.97; 2234.22; 2235.15; 2235.56; 2236.06; 2236.71; 2238.06; 2238.8; 2240.2; 2240.78; 2240.95; 2243.83; 2244.22; 2244.49; 2245.52; 2245.84; 2248.89; 2249.13; 2249.17; 2250; 2251.56; 2251.91; 2255.17; 2257.21; 2257.38; 2257.67; 2257.77; 2258.07; 2258.29; 2259.89; 2261; 2262.84; 2263.17; 2263.44; 2263.48; 2263.67; 2266.18; 2268.13; 2268.96; 2269.36; 2270.54; 2271.6; 2271.72; 2272.28; 2273.26; 2273.41; 2274.22; 2274.39; 2276; 2277.68; 2278.88; 2281.99; 2282.42; 2283.76; 2284.12; 2289.57; 2291.23; 2291.72; 2292.81; 2294.6; 2294.93; 2296.78; 2297.13; 2300.36; 2300.82; 2302.51; 2303.28; 2305.03; 2305.71; 2306.38; 2306.89; 2306.9; 2306.94; 2309.97; 2310.32; 2311; 2311.63; 2314.51; 2318.84; 2319.43; 2319.75; 2321.98; 2325.36; 2325.69; 2327.5; 2330.39; 2334.19; 2334.37; 2335.43; 2336.33; 2336.74; 2338.6; 2340.16; 2340.21; 2344.93; 2346.72; 2348.9; 2352.41; 2353.53; 2353.95; 2354.02; 2354.82; 2356.41; 2357.08; 2357.25; 2358.27; 2359.17; 2360.66; 2362.27; 2362.87; 2363.3; 2363.87; 2363.98; 2364.04; 2366.6; 2368.74; 2369.57; 2369.96; 2373.62; 2374.92; 2375.5; 2375.71; 2375.73; 2376.11; 2376.41; 2377.87; 2379.3; 2379.42; 2383.31; 2384.01; 2384.76; 2385.37; 2385.38; 2386.32; 2386.93; 2387.85; 2387.98; 2389.03; 2391.2; 2391.97; 2392.49; 2394.42; 2396.66; 2398.26; 2398.53; 2398.78; 2401.17; 2401.36; 2402.51; 2405.79; 2406.43; 2406.8; 2407.49; 2407.61; 2408.41; 2409.05; 2410.9; 2412.04; 2412.12; 2412.47; 2412.58; 2412.62; 2413.94; 2414.12; 2416.68; 2416.93; 2417.4; 2421.47; 2421.53; 2421.93; 2422.57; 2423.56; 2423.88; 2423.89; 2424.19; 2424.52; 2427.71; 2429.89; 2430.3; 2431.71; 2432.01; 2432.31; 2433.88; 2437.03; 2437.53; 2438.25; 2438.45; 2439.26; 2444.73; 2445.64; 2445.86; 2446.7; 2447.06; 2447.88; 2448.04; 2448.08; 2448.51; 2451.41; 2453.37; 2455.12; 2455.26; 2455.99; 2456.38; 2456.87; 2457.3; 2459.83; 2460.27; 2460.99; 2462.8; 2464.09; 2467.52; 2468.07; 2469.49; 2471.95; 2472.16; 2472.52; 2473.23; 2473.86; 2474.12; 2475.87; 2476.01; 2476.37; 2478.1; 2479.89; 2479.92; 2480.37; 2481.69; 2483.15; 2484.16; 2484.2; 2484.87; 2486.07; 2486.44; 2487.36; 2489.83; 2489.87; 2490.98; 2491.33; 2491.49; 2492; 2496.56; 2496.57; 2496.73; 2497.5; 2498.28; 2498.53; 2500; 2502.06; 2502.1; 2504.73; 2505.36; 2505.38; 2506.53; 2506.72; 2507.16; 2507.99; 2508.19; 2508.78; 2508.87; 2509.26; 2510.34; 2511.19; 2511.62; 2512.25; 2514.19; 2516.86; 2517.53; 2519.39; 2519.89; 2521.35; 2521.9; 2522.04; 2522.26; 2524.68; 2524.92; 2526.3; 2527.19; 2529.16; 2529.18; 2530.14; 2533.58; 2534; 2534.53; 2536.45; 2537.12; 2539.22; 2539.29; 2539.86; 2539.93; 2540.7; 2540.87; 2545.67; 2548.94; 2553.51; 2557.48;

2557.7; 2558.28; 2560.77; 2560.83; 2561.04; 2561.85; 2562.08; 2563.61; 2563.64; 2563.87; 2565; 2565.55; 2566.87; 2569.94; 2570.08; 2570.3; 2571.6; 2571.93; 2572.18; 2572.59; 2574.04; 2574.91; 2576.63; 2578.55; 2581.99; 2583.87; 2585.1; 2585.74; 2586.15; 2588.53; 2590.19; 2592.01; 2594.59; 2594.77; 2596.37; 2601.44; 2602.09; 2602.27; 2602.52; 2602.84; 2604.15; 2605.72; 2606.09; 2609.33; 2612.85; 2613.77; 2615.07; 2615.96; 2616.39; 2617.65; 2619.78; 2620.69; 2621.1; 2621.22; 2622.38; 2625.05; 2626.38; 2627.3; 2631.72; 2632.18; 2636.69; 2638.32; 2640.83; 2640.85; 2641.12; 2641.9; 2642.17; 2647.07; 2650.52; 2652.42; 2652.75; 2653; 2655.46; 2656.43; 2658.3; 2660.59; 2662.24; 2662.74; 2663.22; 2663.62; 2664.17; 2666.04; 2666.43; 2667.47; 2668.39; 2669.07; 2671.01; 2672.2; 2672.21; 2674.07; 2675.06; 2676.22; 2676.41; 2676.84; 2677.19; 2678.41; 2681.72; 2681.91; 2682.17; 2685.97; 2688.31; 2688.65; 2691.23; 2691.72; 2692.53; 2692.75; 2694.72; 2694.94; 2696.08; 2696.63; 2699.17; 2700.34; 2700.36; 2702.05; 2702.23; 2703.53; 2707.16; 2710.14; 2711.15; 2712.02; 2712.35; 2714.4; 2720.02; 2720.89; 2721.34; 2722.62; 2723.03; 2727.72; 2728.36; 2729.68; 2731.47; 2731.8; 2732.06; 2732.15; 2732.34; 2736.34; 2738.63; 2739.43; 2740.8; 2741.77; 2741.79; 2741.83; 2742.57; 2742.58; 2742.97; 2749.41; 2750; 2750.25; 2750.96; 2751.04; 2751.85; 2752.12; 2754.35; 2755.54; 2757.21; 2757.5; 2758.12; 2760.62; 2760.73; 2761.31; 2763; 2764.93; 2767.61; 2767.73; 2767.97; 2769.7; 2769.71; 2771.36; 2772.25; 2772.52; 2773.75; 2773.81; 2774.46; 2774.64; 2779.13; 2779.82; 2779.85; 2780.61; 2780.69; 2783.58; 2783.76; 2784.24; 2786.96; 2788.31; 2788.34; 2790.14; 2790.54; 2791.32; 2791.33; 2791.83; 2792.1; 2794.75; 2794.96; 2800.56; 2801.13; 2801.25; 2802.54; 2804.42; 2804.82; 2804.92; 2805; 2805.89; 2809.01; 2809.95; 2810.57; 2811.07; 2812.78; 2814.08; 2814.66; 2814.78; 2814.96; 2817.28; 2817.83; 2818.77; 2819.29; 2821.7; 2821.74; 2823.23; 2823.45; 2825.22; 2829.19; 2830.07; 2830.82; 2831.12; 2833.01; 2834.5; 2835; 2836.27; 2837; 2837.43; 2837.94; 2838.83; 2839.99; 2841.29; 2841.31; 2841.97; 2842.58; 2842.6; 2842.9; 2843.9; 2844.31; 2846.59; 2848.17; 2848.64; 2850.44; 2851.73; 2852.01; 2852.44; 2852.63; 2854.57; 2855.86; 2855.97; 2857.18; 2857.52; 2857.92; 2858.16; 2858.29; 2858.58; 2859.55; 2861.59; 2863.88; 2864.25; 2865.31; 2868.09; 2869.23; 2870.76; 2871.58; 2871.67; 2872.63; 2875.07; 2876.33; 2876.97; 2883.19; 2883.6; 2885.76; 2887.91; 2888.26; 2888.43; 2889.99; 2890.08; 2892.65; 2892.82; 2893.57; 2893.77; 2894.73; 2895.77; 2896.15; 2896.39; 2897.24; 2897.88; 2898.38; 2898.45; 2898.69; 2898.72; 2902.12; 2902.13; 2902.15; 2902.3; 2902.51; 2902.9; 2904.53; 2907.11; 2907.32; 2907.75; 2907.78; 2911.39; 2912.58; 2913.09; 2913.25; 2916.08; 2917.43; 2918.51; 2918.9; 2919.68; 2922.75; 2925.28; 2926.11; 2926.47; 2926.59; 2928.85; 2929.15; 2930.34; 2931.86; 2933.32; 2934.02; 2934.09; 2936.01; 2938.25; 2938.69; 2939; 2939.13; 2941.01; 2941.39; 2941.62; 2942.04; 2943.03; 2943.44; 2944.21; 2945.56; 2947.34; 2948.01; 2948.61; 2949.19; 2951.25; 2951.66; 2952.77; 2953.7; 2954.05; 2954.08; 2954.21; 2955.68; 2958.06; 2961.98; 2963; 2963.03; 2963.23; 2965.35; 2965.88; 2967.45; 2967.99; 2968.27; 2968.43; 2970.01; 2970.25; 2970.95; 2971.91; 2971.95; 2972.25; 2976.42; 2979.05; 2979.33; 2980.27; 2983.5; 2985; 2987.22; 2988.45; 2989.95; 2992.04; 2993.43; 2996.91; 2996.97; 2998.99; 2999.15; 2999.3; 2999.85; 3000; 3000.08; 3001.6; 3001.98; 3002.11; 3002.62; 3003.01; 3005.47; 3006.02; 3007.21; 3007.46; 3008.71; 3008.87; 3009.96; 3011.4; 3012.11; 3012.89; 3013.73; 3014.65; 3014.79; 3015.24; 3015.75; 3018.28; 3019.97; 3020.15; 3020.47; 3021.08; 3022.89; 3025.22; 3026.01; 3026.6; 3035.01; 3037.04; 3038.62; 3038.84; 3040.85; 3042.65; 3042.89; 3043.76; 3043.83; 3043.98; 3045.01; 3046.35; 3047.84; 3051.81; 3052.05; 3054.38; 3055.73; 3056.78; 3056.81; 3057.25; 3057.71; 3057.85; 3057.87; 3058.18; 3058.32; 3060.47; 3061.09; 3062.02; 3064.69; 3064.85; 3065.07; 3065.2; 3065.38; 3066.65; 3066.81; 3067.54; 3069.26; 3070.38; 3070.52; 3070.8; 3070.96; 3075.16; 3077.12; 3077.68; 3078.33; 3079.53; 3079.59; 3079.76; 3080.49; 3080.99; 3082.27; 3082.72; 3082.97; 3085.12; 3085.13; 3085.23; 3087.54; 3087.67; 3088.55; 3088.94; 3089.17; 3090.88; 3091.2; 3092.14; 3092.43; 3092.59; 3094.53; 3095.97; 3096.59; 3098.2; 3098.3; 3098.86; 3099.56; 3099.71; 3101.96; 3102.83; 3107.92;

3108.15; 3108.19; 3110.72; 3111.4; 3112.03; 3113.84; 3116.44; 3116.59; 3117.1; 3118.14; 3118.38; 3119.01; 3119.98; 3121.56; 3121.81; 3122.75; 3123.17; 3126.36; 3126.55; 3126.76; 3127.86; 3128.52; 3129.82; 3130.52; 3132.85; 3133.95; 3134.33; 3136.89; 3137.27; 3137.51; 3138.55; 3139.01; 3139.21; 3140.09; 3141.53; 3141.66; 3143.07; 3144.28; 3145.03; 3146.78; 3149.18; 3149.58; 3150.1; 3153.28; 3153.84; 3155.16; 3155.51; 3155.53; 3156.47; 3156.52; 3156.77; 3158.07; 3158.27; 3160.51; 3164.43; 3165.43; 3165.49; 3166.68; 3169.36; 3170.42; 3171.3; 3171.61; 3172.99; 3173.04; 3173.06; 3173.33; 3174.4; 3174.46; 3174.65; 3176.45; 3178.02; 3183.12; 3183.59; 3184.53; 3184.87; 3186.86; 3188.17; 3188.48; 3190.05; 3190.33; 3191.93; 3192.09; 3192.18; 3194.17; 3197.2; 3197.38; 3198.07; 3199.69; 3200.6; 3200.93; 3201.6; 3201.97; 3202.67; 3203.72; 3205.85; 3205.87; 3207.24; 3207.58; 3207.88; 3208.39; 3209.2; 3209.58; 3210.68; 3211.62; 3213.15; 3215; 3215.86; 3215.95; 3216.58; 3217.74; 3217.85; 3217.91; 3219.55; 3220; 3220.37; 3224.11; 3226.03; 3227.2; 3228.5; 3228.61; 3229.09; 3231.42; 3231.64; 3232.74; 3233.78; 3234.6; 3235.7; 3235.73; 3236.27; 3236.38; 3236.39; 3238.29; 3238.92; 3240; 3241.49; 3241.53; 3243.02; 3245.22; 3245.7; 3246.57; 3246.71; 3248.04; 3249.5; 3249.64; 3250; 3253.26; 3254.67; 3255.02; 3255.22; 3256.24; 3256.76; 3257.98; 3258.37; 3258.79; 3258.99; 3261.62; 3267.11; 3267.46; 3267.76; 3268.82; 3271.03; 3271.04; 3272.49; 3275.01; 3276.09; 3277.41; 3278.09; 3278.88; 3279.64; 3281.43; 3282.91; 3283.13; 3283.2; 3283.78; 3284.08; 3284.95; 3285.57; 3286.17; 3287.77; 3288.52; 3289.85; 3290.17; 3291.12; 3292.03; 3293.45; 3294.39; 3294.46; 3294.55; 3298.71; 3299.93; 3300.04; 3301.08; 3308.07; 3308.19; 3309.2; 3309.38; 3309.87; 3310.61; 3310.86; 3311; 3311.24; 3313.82; 3314; 3315.27; 3316.02; 3316.12; 3318.56; 3318.59; 3319.89; 3321.22; 3321.46; 3326.18; 3326.68; 3326.94; 3327.06; 3327.17; 3327.21; 3328.81; 3329.41; 3330.66; 3331.03; 3331.31; 3332.78; 3333.98; 3335.99; 3336.65; 3336.73; 3336.86; 3337.47; 3338.29; 3339.02; 3340.95; 3342.42; 3342.68; 3343.48; 3345.07; 3347.94; 3348.59; 3349.08; 3349.9; 3350.08; 3351.5; 3351.57; 3353.2; 3356.44; 3356.8; 3357.14; 3362.38; 3364.45; 3364.68; 3365.53; 3369.66; 3371.02; 3372.62; 3373.94; 3374.32; 3375.11; 3375.19; 3375.43; 3376.59; 3379.01; 3384.37; 3384.43; 3385.75; 3387.08; 3388.35; 3389.33; 3390.59; 3390.77; 3390.86; 3391.46; 3391.97; 3392.23; 3392.29; 3392.44; 3392.5; 3392.61; 3392.92; 3393.22; 3394.76; 3395.52; 3397.71; 3398.91; 3398.96; 3399.04; 3401.26; 3401.6; 3401.63; 3401.65; 3401.79; 3404.64; 3406.3; 3407; 3409.39; 3409.61; 3410.06; 3411.51; 3412.43; 3413.08; 3413.59; 3415.33; 3415.98; 3416.26; 3417.79; 3418.34; 3418.7; 3420.6; 3420.95; 3423.43; 3425.35; 3425.97; 3427.82; 3427.98; 3428.59; 3428.78; 3429.96; 3430.77; 3431.52; 3432.4; 3434.27; 3434.48; 3435.54; 3436.23; 3437.58; 3437.61; 3437.98; 3438.84; 3440.09; 3441.21; 3441.27; 3442.68; 3442.74; 3443.52; 3444.42; 3444.51; 3444.82; 3446; 3446.22; 3451.61; 3454.19; 3456.25; 3457.21; 3457.51; 3458.15; 3458.63; 3462; 3462.05; 3462.57; 3462.91; 3463.06; 3464.1; 3466.12; 3467; 3467.04; 3467.21; 3468.82; 3471.02; 3471.73; 3473.53; 3474.8; 3475.06; 3476.27; 3477.29; 3481.28; 3481.95; 3482.52; 3483.86; 3484.72; 3485.61; 3485.95; 3487.2; 3487.49; 3488.38; 3491.08; 3491.23; 3494.63; 3494.96; 3496.65; 3496.74; 3497.1; 3497.15; 3498.14; 3498.21; 3499.24; 3500; 3501.91; 3502.58; 3504.62; 3506.66; 3507.68; 3509.13; 3510.98; 3512.77; 3513.6; 3517.66; 3519.57; 3520.42; 3520.89; 3521.9; 3526.05; 3530.17; 3530.37; 3531.37; 3532.12; 3532.16; 3532.81; 3535; 3537.51; 3538.66; 3538.87; 3540.12; 3543.32; 3544; 3545.15; 3549.49; 3549.69; 3550.62; 3552.15; 3553.17; 3553.28; 3554.54; 3554.58; 3554.82; 3555.77; 3556.51; 3556.71; 3557.13; 3559.56; 3559.91; 3560.06; 3562.78; 3565.06; 3565.75; 3565.92; 3566.58; 3566.83; 3567.12; 3568.42; 3568.52; 3568.94; 3569.08; 3570.77; 3570.79; 3570.96; 3571.12; 3571.66; 3573.2; 3575.68; 3577.15; 3579.3; 3580.19; 3581.6; 3582.18; 3582.5; 3584.87; 3585.13; 3585.51; 3586.53; 3587.16; 3587.65; 3587.8; 3588.53; 3589.17; 3589.63; 3590.74; 3591.06; 3593.04; 3593.5; 3594.59; 3595.11; 3595.86; 3600.17; 3601.05; 3601.53; 3602.2; 3603.13; 3604.11; 3604.47; 3605.04; 3605.06; 3606.51; 3606.58; 3606.78; 3607.59; 3609.73; 3609.95; 3611.94; 3613.06; 3613.49; 3613.64; 3614.62; 3615.28; 3615.86;

3616.29; 3617.02; 3620.78; 3621.05; 3622.14; 3622.28; 3622.47; 3624.39; 3626.46; 3627.73; 3627.91; 3628.21; 3629.57; 3630.19; 3630.95; 3633.49; 3633.71; 3634.63; 3636.71; 3638.42; 3638.89; 3638.96; 3639.03; 3639.91; 3640; 3640.47; 3642.78; 3644.25; 3644.29; 3644.48; 3645.25; 3646.62; 3646.78; 3647.27; 3648.5; 3648.77; 3649.18; 3649.93; 3650.14; 3650.73; 3651.93; 3652.8; 3654.15; 3654.29; 3654.78; 3656.68; 3657.66; 3657.75; 3658.91; 3660.25; 3661.2; 3661.58; 3661.91; 3662.47; 3662.56; 3662.8; 3665.36; 3667.71; 3667.78; 3669.27; 3671.97; 3673.45; 3674.58; 3674.86; 3675.97; 3676.25; 3676.77; 3678.45; 3681.19; 3681.73; 3684.47; 3687.47; 3687.88; 3688.03; 3688.14; 3688.37; 3688.7; 3689.78; 3690.52; 3692.98; 3693.93; 3694.84; 3694.86; 3695.16; 3696.44; 3697.3; 3699.28; 3700.35; 3700.76; 3701.34; 3702.64; 3703.55; 3703.88; 3704.84; 3705.08; 3706.82; 3708.17; 3708.27; 3710.51; 3712.05; 3712.3; 3714.38; 3714.47; 3714.55; 3714.84; 3716.58; 3717.7; 3718.09; 3718.5; 3718.93; 3719.89; 3720.25; 3720.39; 3721.95; 3722.28; 3722.9; 3723.1; 3724.84; 3725; 3726.09; 3727.64; 3727.93; 3728; 3730.14; 3730.38; 3730.43; 3730.58; 3731.08; 3731.27; 3733.66; 3736.04; 3736.74; 3737.72; 3737.86; 3738.81; 3743.53; 3745.28; 3745.33; 3747.19; 3748.26; 3748.83; 3749.32; 3750; 3751.77; 3752.24; 3758.14; 3758.35; 3758.39; 3758.77; 3760.9; 3761.24; 3762.78; 3764.52; 3765.26; 3766.23; 3767.16; 3767.19; 3768.92; 3769.85; 3773.11; 3774.02; 3774.65; 3777.16; 3779.5; 3780.22; 3780.27; 3782.38; 3782.59; 3786.05; 3787.96; 3788.87; 3791.86; 3791.94; 3792; 3792.6; 3793.47; 3796.44; 3797.5; 3798; 3799.61; 3799.93; 3800.04; 3801.04; 3803.55; 3804; 3804.05; 3805.3; 3805.9; 3808.59; 3809.3; 3810.65; 3810.94; 3812.02; 3813.07; 3814.05; 3814.75; 3815.12; 3816.32; 3819.03; 3819.2; 3820.41; 3820.54; 3822.19; 3822.26; 3824.45; 3825.46; 3826.61; 3827.75; 3829.21; 3830.07; 3830.51; 3830.74; 3831.21; 3833.6; 3836.53; 3837.38; 3840.12; 3843.34; 3844.1; 3845.44; 3849.57; 3850.12; 3852.47; 3852.97; 3853.37; 3854.05; 3854.88; 3855.24; 3856.25; 3857.6; 3858.48; 3859.01; 3860.15; 3860.51; 3860.69; 3860.87; 3860.99; 3862.46; 3862.9; 3863.56; 3867.26; 3868.6; 3869.68; 3872.68; 3874.1; 3877.01; 3877.83; 3878.52; 3879.96; 3880.15; 3880.35; 3882.03; 3883.65; 3884.66; 3885.2; 3885.47; 3886.64; 3887.11; 3887.6; 3888.48; 3889.34; 3890; 3890.49; 3890.89; 3891.03; 3891.78; 3894.58; 3895.35; 3896.96; 3897.27; 3897.31; 3899.28; 3899.37; 3900.85; 3901.04; 3902.54; 3902.59; 3902.66; 3904.86; 3905.1; 3906.07; 3906.14; 3906.42; 3906.56; 3907.13; 3907.58; 3908.33; 3909.91; 3913.02; 3913.1; 3913.76; 3914.01; 3914.49; 3915.87; 3916.29; 3919.79; 3922.46; 3922.99; 3923.7; 3924.9; 3925.3; 3926.97; 3927.88; 3928.13; 3930.48; 3930.7; 3931.93; 3932.35; 3932.4; 3933.53; 3934.68; 3937.64; 3937.73; 3942.66; 3942.68; 3947.09; 3947.91; 3948.16; 3948.23; 3948.43; 3948.83; 3948.87; 3949.55; 3954.3; 3954.39; 3954.45; 3955.08; 3955.31; 3956.15; 3956.96; 3957.05; 3957.75; 3961.36; 3961.46; 3963.84; 3965.67; 3968.88; 3968.9; 3969.77; 3970.72; 3971.81; 3973.12; 3973.19; 3973.9; 3973.94; 3975.86; 3976.77; 3978.01; 3979.79; 3979.89; 3981.48; 3982.24; 3982.96; 3984.97; 3985.59; 3986.71; 3987.4; 3988.15; 3989.8; 3990.85; 3991.17; 3991.29; 3992.25; 3992.38; 3993.49; 3993.96; 3995.96; 3996.23; 3997.53; 3998.86; 3998.88; 4000; 4000.38; 4001.55; 4002.34; 4003.81; 4008.56; 4009.28; 4010.08; 4010.19; 4014.25; 4016.22; 4016.26; 4016.71; 4017.9; 4020; 4020.01; 4021.21; 4021.47; 4023.35; 4023.47; 4025.62; 4025.86; 4026.74; 4027.15; 4029.44; 4030.05; 4032.87; 4033.91; 4034.66; 4035.75; 4036.45; 4036.85; 4038.14; 4038.4; 4038.68; 4039.35; 4040.15; 4043.77; 4044.77; 4045.33; 4047.1; 4050.03; 4050.25; 4052.78; 4052.99; 4055.53; 4056.21; 4056.89; 4056.95; 4057.94; 4057.99; 4058.01; 4058.06; 4058.08; 4059.26; 4061.16; 4061.72; 4064.21; 4066.87; 4066.9; 4067.48; 4069.32; 4070.26; 4071.12; 4071.34; 4071.82; 4072.15; 4072.76; 4072.84; 4077.71; 4079.29; 4079.33; 4079.75; 4081.24; 4081.97; 4082.38; 4082.68; 4083.55; 4087.08; 4087.35; 4087.69; 4088.19; 4088.68; 4089.38; 4092.14; 4092.63; 4096.8; 4097.1; 4098.2; 4098.55; 4100.05; 4100.3; 4101.96; 4102.26; 4102.34; 4102.36; 4105.73; 4106.54; 4107.33; 4107.99; 4108.08; 4108.49; 4109.16; 4110.88; 4112.14; 4112.56; 4112.76; 4113.84; 4114.2; 4114.71; 4115.08; 4115.47; 4119.44; 4119.93; 4123.96; 4124.34; 4124.69; 4124.75; 4124.8; 4125.85; 4126.95; 4126.97; 4127.35; 4129.43; 4130; 4131.92; 4133.42;

4133.55; 4134.5; 4134.55; 4134.67; 4135.66; 4136.23; 4138.43; 4138.9; 4141.39; 4141.54; 4142.02; 4143.95; 4144.7; 4147.47; 4147.73; 4148.24; 4150.65; 4151.04; 4151.9; 4151.95; 4152.65; 4152.71; 4152.79; 4154.14; 4155.26; 4155.72; 4156.6; 4157.08; 4159.05; 4160.66; 4161.5; 4163.19; 4163.22; 4163.27; 4164.62; 4164.64; 4164.9; 4166.89; 4168.02; 4170.73; 4173.1; 4173.17; 4173.46; 4174.5; 4175.93; 4176.7; 4177.43; 4177.76; 4177.96; 4178.4; 4178.5; 4179.18; 4179.59; 4180.15; 4180.69; 4185.7; 4186.22; 4187.64; 4187.73; 4191.8; 4192.2; 4192.79; 4193.35; 4193.36; 4194.43; 4195.09; 4197.08; 4198.38; 4200.54; 4202.71; 4203.87; 4206.13; 4206.23; 4208.14; 4208.32; 4208.37; 4209.09; 4211.33; 4212.51; 4214.42; 4215.73; 4217.86; 4218.78; 4219.47; 4220.63; 4221.54; 4222.52; 4223.37; 4225.88; 4226.71; 4228.98; 4229.36; 4232.13; 4232.14; 4234.08; 4234.7; 4235.79; 4238.72; 4240.58; 4240.63; 4241.47; 4241.72; 4242.24; 4243.74; 4246.01; 4246.83; 4248.43; 4248.84; 4250; 4250.59; 4253.36; 4253.88; 4256.29; 4256.58; 4259.09; 4261.13; 4263.44; 4264.58; 4266.93; 4267.16; 4267.72; 4267.97; 4268.2; 4268.47; 4268.58; 4271.87; 4272.16; 4273.91; 4274.54; 4274.69; 4275.36; 4276.49; 4277.76; 4277.86; 4277.91; 4281.06; 4281.73; 4282.61; 4284.41; 4284.47; 4284.79; 4288.83; 4289.1; 4289.33; 4290.64; 4290.67; 4291.32; 4292.2; 4292.66; 4294.66; 4294.72; 4295.19; 4297.85; 4297.99; 4298.43; 4298.5; 4299.72; 4300.34; 4302.59; 4303.57; 4303.83; 4304.12; 4307.84; 4310.04; 4310.33; 4311.01; 4312.26; 4312.82; 4312.94; 4313.72; 4315.53; 4318.29; 4320.01; 4320.09; 4320.12; 4320.24; 4320.33; 4321.25; 4321.75; 4322.17; 4322.38; 4322.6; 4323.14; 4325.72; 4325.86; 4326.72; 4328.67; 4330.16; 4330.24; 4330.28; 4333.01; 4333.02; 4334.44; 4339.66; 4340.66; 4340.84; 4340.85; 4341.21; 4341.51; 4342.28; 4344.75; 4344.97; 4347.22; 4349.12; 4350.71; 4351.01; 4351.42; 4352.12; 4353.64; 4354.01; 4354.72; 4354.85; 4355.08; 4357.02; 4358.67; 4359.35; 4359.95; 4360.27; 4360.8; 4361.27; 4361.36; 4362.19; 4362.75; 4362.99; 4363.09; 4365.84; 4366.44; 4366.78; 4368.51; 4368.57; 4368.88; 4369.99; 4370.58; 4373.63; 4374.47; 4374.62; 4377.26; 4378.07; 4378.28; 4378.47; 4378.48; 4378.85; 4379.23; 4380.19; 4382.02; 4382.7; 4382.86; 4383.19; 4386.99; 4387.73; 4388; 4389.88; 4392.42; 4396.52; 4397.13; 4397.34; 4397.56; 4400.61; 4402.42; 4404.3; 4405.4; 4407.52; 4410.62; 4411.79; 4412.04; 4412.67; 4413.68; 4414.9; 4416.22; 4420.53; 4421.36; 4422.06; 4422.32; 4423.03; 4423.34; 4424.02; 4424.17; 4424.32; 4424.98; 4427.07; 4427.16; 4428.12; 4430.49; 4432.83; 4433.53; 4435.39; 4436.01; 4437.03; 4437.47; 4438.86; 4439.06; 4439.91; 4440.39; 4441.43; 4441.74; 4443.99; 4444.75; 4450.36; 4450.55; 4451.6; 4452.91; 4454.36; 4455.48; 4456.33; 4457.79; 4458.07; 4458.56; 4458.61; 4458.93; 4459.01; 4460.58; 4461.11; 4461.79; 4461.93; 4461.99; 4462.31; 4463; 4463.6; 4463.7; 4464.25; 4464.38; 4466.51; 4466.89; 4467.5; 4468.29; 4470.57; 4471.33; 4472.3; 4472.67; 4474.99; 4475.07; 4475.74; 4476.37; 4476.61; 4481.65; 4482.66; 4483.75; 4484; 4484.18; 4484.24; 4485.21; 4485.46; 4485.93; 4486.69; 4486.88; 4488.09; 4488.95; 4492.09; 4493.94; 4495.35; 4496; 4496.06; 4497.83; 4498.58; 4500; 4501.38; 4501.8; 4503.06; 4507.4; 4508.64; 4508.72; 4509.42; 4510.21; 4510.88; 4511.6; 4512.07; 4512.3; 4513.72; 4513.78; 4516.08; 4517.07; 4518.23; 4521.59; 4522.28; 4522.52; 4522.7; 4524.9; 4526.69; 4528.2; 4528.74; 4531.85; 4532.25; 4533.78; 4534.65; 4534.84; 4538.01; 4538.39; 4538.79; 4541.77; 4541.85; 4542.32; 4542.44; 4543.98; 4544.05; 4545.07; 4546.1; 4547.05; 4547.49; 4548.58; 4548.96; 4549.78; 4549.85; 4550.14; 4552.76; 4552.85; 4556.36; 4557.71; 4560.02; 4560.18; 4560.67; 4564.96; 4566.14; 4567.21; 4567.28; 4569.18; 4571.11; 4573.72; 4575.87; 4577.16; 4578.92; 4581.77; 4581.99; 4582.55; 4582.6; 4584.74; 4586.05; 4586.75; 4587.45; 4587.8; 4590.59; 4590.85; 4591.59; 4592.5; 4593.72; 4594.4; 4594.68; 4595.44; 4595.91; 4596.1; 4596.39; 4599.12; 4600.02; 4600.38; 4601.76; 4601.84; 4601.99; 4602.08; 4602.89; 4603.29; 4604.42; 4604.55; 4606.13; 4606.61; 4608.91; 4610.12; 4612.01; 4612.29; 4612.66; 4616.23; 4617.29; 4621.03; 4623.29; 4623.71; 4625.07; 4625.39; 4626.21; 4626.47; 4627.41; 4630.94; 4631.38; 4631.74; 4631.85; 4632.03; 4634.61; 4634.87; 4635.45; 4635.47; 4635.56; 4635.99; 4636.66; 4637.3; 4643.42; 4644.48; 4645.13; 4645.35; 4648.08; 4649.1; 4649.61;

4649.63; 4650.11; 4653; 4654.3; 4654.85; 4655.87; 4658.62; 4660.71; 4660.95; 4661.14; 4663.63; 4665.41; 4665.65; 4665.87; 4666.82; 4670.46; 4671.05; 4671.63; 4671.68; 4671.99; 4672.31; 4674.02; 4674.76; 4675.74; 4677.57; 4680.36; 4680.65; 4681.52; 4683.9; 4684.98; 4687.01; 4687.53; 4687.71; 4689.2; 4690.9; 4691.92; 4693.91; 4695.82; 4696.07; 4696.69; 4697.22; 4697.95; 4698; 4699.64; 4702.49; 4702.61; 4704.3; 4705.25; 4705.4; 4706; 4707.72; 4709.45; 4709.76; 4713.73; 4715.49; 4715.74; 4717.01; 4717.57; 4717.95; 4718.3; 4719.32; 4721.41; 4722.59; 4724.78; 4724.99; 4726.61; 4726.94; 4727.15; 4727.23; 4727.9; 4728.82; 4732.45; 4733.25; 4733.79; 4734.28; 4734.63; 4734.84; 4738.81; 4739.26; 4741.12; 4741.71; 4742.77; 4743.21; 4744.6; 4745.5; 4748.03; 4750; 4751.24; 4752.33; 4754.32; 4754.65; 4755.12; 4755.85; 4758.3; 4758.62; 4758.85; 4759.72; 4761.58; 4761.69; 4763.41; 4765.68; 4765.78; 4765.82; 4766.35; 4767.39; 4768.1; 4768.24; 4768.7; 4768.97; 4770.12; 4770.7; 4771.72; 4771.91; 4773.12; 4773.75; 4773.82; 4775.17; 4775.72; 4775.93; 4776.11; 4780.33; 4780.61; 4780.98; 4781.2; 4783.07; 4783.15; 4784.17; 4784.27; 4787.82; 4788.03; 4788.38; 4789.58; 4789.65; 4790.87; 4791.26; 4792.45; 4792.76; 4794.12; 4794.73; 4794.83; 4795.57; 4796.48; 4798.13; 4802.44; 4802.66; 4804.53; 4804.73; 4805.88; 4806.3; 4807.03; 4807.74; 4809.04; 4809.14; 4809.24; 4809.9; 4810.14; 4811.69; 4811.88; 4815.28; 4816.67; 4816.89; 4816.97; 4819.92; 4820.01; 4822.61; 4823.43; 4824.75; 4824.78; 4825.81; 4825.82; 4826.91; 4826.95; 4827.85; 4829.7; 4830.65; 4830.67; 4830.89; 4831.93; 4834.68; 4836.69; 4836.99; 4837.33; 4837.77; 4839.11; 4840.56; 4840.63; 4841.55; 4842.08; 4842.11; 4842.28; 4844.73; 4845.22; 4851.5; 4852.65; 4853.11; 4855.54; 4855.7; 4855.98; 4856.72; 4857.16; 4858.48; 4858.69; 4859.86; 4861.68; 4862.95; 4863.14; 4863.31; 4863.89; 4864.81; 4864.83; 4865.17; 4866.52; 4869.37; 4869.43; 4871.06; 4871.75; 4872.48; 4872.8; 4873.09; 4873.1; 4874.32; 4875.27; 4876.97; 4879.04; 4879.23; 4880.45; 4881.52; 4882.12; 4882.67; 4883.46; 4883.64; 4883.65; 4883.77; 4884.35; 4885.42; 4885.98; 4886.69; 4887.52; 4888.61; 4888.99; 4889.01; 4890; 4891.1; 4892.31; 4892.89; 4893.16; 4894.36; 4895.07; 4895.5; 4896.05; 4896.25; 4896.41; 4898.15; 4898.86; 4902.39; 4905.42; 4906.51; 4908.29; 4913.16; 4914.14; 4914.41; 4914.62; 4915.85; 4920.95; 4920.98; 4921.31; 4923.74; 4924.02; 4925.76; 4926.28; 4927.44; 4927.83; 4928.43; 4929.69; 4929.87; 4929.88; 4931.08; 4932.03; 4934.23; 4934.49; 4934.79; 4934.97; 4935.28; 4935.36; 4935.56; 4936.77; 4938.21; 4938.34; 4939.23; 4939.85; 4940.53; 4940.98; 4945.4; 4945.73; 4946.3; 4946.46; 4947.71; 4947.83; 4951.64; 4951.94; 4951.95; 4952.71; 4953.28; 4953.72; 4954.43; 4955.38; 4957.33; 4957.72; 4958.21; 4960.29; 4960.45; 4962.75; 4962.97; 4964; 4965.06; 4965.57; 4966.76; 4967.16; 4969.01; 4969.68; 4970.18; 4970.67; 4970.7; 4970.93; 4971.39; 4971.69; 4972.87; 4973.77; 4974.42; 4975.15; 4976.12; 4976.88; 4978.72; 4978.99; 4979.86; 4980.99; 4982.81; 4983.78; 4983.82; 4985.57; 4986.01; 4986.31; 4987.36; 4987.49; 4989.23; 4990.56; 4992; 4992.39; 4993.87; 4996.63; 4996.74; 4998.32; 5000; 5000.86

8.5.7 Mobile-SHARPER Scripts

Bruker AU Macro

```
/*** ^^A -*-C++-*- ********************************************/
/*  mobile-SHARPER                                            */
/************************************************************/
/*  Short Description :                                       */
/*  Peak Tracking For SHARPER                                 */
/************************************************************/
/*  Keywords :                                                */
/*  zg, SHARPER                                               */
/************************************************************/
/*  Description/Usage :                                       */
/*  Requires a suitable external Python environment (with numpy)*/
/*  Run a standard SHARPER experiment. Then call this macro.    */
/*  It will repeat the spectrum a user defined number of times  */
/*  but each time adjust the offset based on the previously run  */
/*  spectrum in order to try and track a moving peak.           */
/*  ALL DATA ANALYSIS IS HANDLED BY THE COMPANION PYTHON SCRIPT */
/************************************************************/
/*  Author(s) :                                               */
/*  Name    : Matthew Davy                                    */
/*  Organisation  : Bristol   University                      */
/*  Contact: md17346@bristol.ac.uk or mjdavy@btinternet.com     */
/************************************************************/


//***Instructions***/
//Run a standard SHARPER experiment. Then initialise this macro. It will proceed to repeat the spectrum a user defined number of times each time using the previous SHARPER spectrum for offset adjustment to try and track a moving peak

//define your Python command here
//NB numpy and scipy must be installed with pip beforehand
//#define PYTHON_PATH "python" //even if on the path, not recognised by TopSpin
#define PYTHON_PATH "C:/Python27/python.exe" //for vanilla python 2.7
#define PYTHON_SCRIPT "C:/Python27/Scripts/mobile-SHARPER/mobile-SHARPERV2.py"

//input/output files for the Python script (ACQUPATH)
#define PYTHON_PARAMETERS "parameters.txt"

AUERR = local_au(curdat);
QUIT
int local_au(const char* curdat)

{
  /* declare variables */
  //general variables
  char text[PATH_MAX], py_cmd[PATH_MAX] = PYTHON_PATH;
  char disk_save[PATH_MAX], user_save[PATH_MAX], name_save[PATH_MAX];
  char peaklist[PATH_MAX];
  char source_peaklist[PATH_MAX], destination_parameters_name[PATH_MAX] = PYTHON_PARAMETERS,
destination_parameters[PATH_MAX];
  int expno_save = expno, procno_save = procno, prep_digmod, PH_mod_status = -1, FT_mod_status = -1;

  //for preparation experiment
  int i, numPeaks, numFreq, parmode;
  float lb_status, prep_offset, prep_HZpPT, prep_PPMpPT, prep_aq, prep_swh, prep_swh1, ideal_offset;
  float leftLimit, rightLimit, ppmFromLeft, multipletCentre, pointsfromLeft, peakArea, ChunkDur;
  double prep_grpdly, prep_sf, prep_sw_p, f1p, f2p, old_offset;
  int ExperimentNo, ExpNoMAX;
  //quick check for existing of Python files - pointless if they don't exist!
  //https://stackoverflow.com/questions/230062/whats-the-best-way-to-check-if-a-file-exists-in-c
  if(access(PYTHON_PATH, F_OK) == -1)
    STOPMSG("Could not locate Python exe.")
```

```
 if(access(PYTHON_SCRIPT, R_OK) == -1)
   STOPMSG("Could not locate Python script.")


GETINT("Please enter the number of times you would like to repeat this spectrum",ExpNoMAX);
GETFLOAT("Please enter the duration of a full datachunk in milliseconds",ChunkDur);

for (ExperimentNo = 0; ExperimentNo < ExpNoMAX; ++ExperimentNo)
{

SETCURDATA
  //save parameters for current dataset
strcpy(disk_save, disk);
strcpy(user_save, user);
strcpy(name_save, name);

  //THIS bit does the peak picking!

  {


    /* setup parameters for peak picking */
    /* define the plot region as big as the complete acquisition region */
    // necessary because the AU program "PP" actually behaves more like ppf does when used at the command-
line
    FETCHPARS("OFFSET", &prep_offset)
    FETCHPARS("SW_p" ,&prep_sw_p)
    FETCHPARS("SF", &prep_sf)
    f1p = prep_offset;
    f2p = f1p - prep_sw_p / prep_sf;
    STOREPAR("F1P", f1p)
    STOREPAR("F2P", f2p)

    //standard values
    STOREPAR("CY", 15.0) //defined intensity of largest peak
    STOREPAR("MAXI", 10000.0)
    STOREPAR("PC", 1.0) //S/N threshold for peak-picking (criterion never invoked if MI > 0)
    STOREPAR("PSIGN", 2) //Does the sign of the peak - may want 2, which should allow picking of both positive
and negative peaks
    STOREPAR("PSCAL", 4) //MI criterion is relative to non-solvent peaks, and will peak pick solvent peaks too

printf("float = %f\n", f1p);
printf("float = %f\n", f2p);

    //key values to get it working nicely for this application
    //threshold to ignore peaks i.e. peaks smaller than MI/CY are ignored
    STOREPAR("MI", 0.8)

    //pick peaks - CRITICAL
          FMC//Fourier transforms and magnitude instead of phase. APK often struggles to phase SHARPER
spectra well, leading to errors in peak picking
          //APK //Phase correction - not needed due to magnitude
    PP
    PPP
    XWP_PP
          XCMD("sendgui convertpeaklist txt")//Create a peaklist with intensity and Hz frequency in ASCII for easy
handling by python - https://qa.nmrwiki.org/question/502/topspin-peak-list-file-format
  }

//***CopyExperiment and set it as current whilst preparing python commands***//
strcpy(source_peaklist, PROCPATH("peak.txt"));
WRA(expno+1);
IEXPNO
DATASET(name_save, expno, 1, disk_save, user_save)
strcpy(destination_parameters, ACQUPATH(destination_parameters_name));
```

```
  //***prepare the command to send it off to python***//
    sprintf(py_cmd, "%s %s %s %s %f",
                PYTHON_PATH, PYTHON_SCRIPT, destination_parameters, source_peaklist, ChunkDur);
  //requires external python enviroment due to hard requirment for numpy support
system(py_cmd);

 //printf(py_cmd); //Simple check it's giving the right commands to python

//***Obtain Python Generated Parameters and Update Spectrum With them***//
FILE *stream;
stream = fopen(destination_parameters, "r");
fscanf(stream,"%f",&ideal_offset);
//printf("float = %f\n", ideal_offset);
printf("\n");
fclose(destination_parameters);
STOREPAR("o1",ideal_offset);

//***Runs spectrum***//
   XAU("au_zg", "")
   GETCURDATA
   ZG

}
}
```

Python Script

```
#/*** ^^A -*-Python 2.7++-*- ************************************/
#/*  mobile-SHARPER companion python script                      */
#/*****************************************************************/
#/*  Short Description :                                         */
#/*  Data analysis to allow Peak Tracking For SHARPER */
#/*****************************************************************/
#/*  Keywords :                                                  */
#/*  zg, SHARPER                                                 */
#/*****************************************************************/
#/*  Description/Usage :                                         */
#/*  Should be called automatically by the bruker AU script      */
#/*  thus needing no end user interaction                        */
#/*****************************************************************/
#/*  Author(s) :                                                 */
#/*  Name    : Matthew Davy                                      */
#/*  Organisation  : Bristol   University                        */
#/*  Contact: md17346@bristol.ac.uk or mjdavy@btinternet.com     */
#/*****************************************************************/
#/*****************************************************************/
#/*  To Do                                                       */
#/*  Only detect a peak if it's within a certain range of the offset - preventing tracking of impurities early/late in a
reaction when the peak of interest is small */

#!/usr/bin/python

#Python script for calculating the needed offset for SHARPER experiments on the fly from a Bruker provided
peak list

import math
import numpy as np
import os
import itertools
import sys
import time

error = 2 #This is the Hz error it allows when searching for the secondary artefact. Higher values risk picking
incorrect peaks

#import scipy
from scipy import special

dataset_folder = os.getcwd();

# arguments
   # sys.argv[0] = name of (this) script
   # sys.argv[1] = source of multiplet list (also destination folder for NUS schedule)

parameters_file = os.path.abspath(sys.argv[1]);  #Eventual file to save parameters to after manipulations
dataset_folder = os.path.dirname(parameters_file)

peaklist = os.path.abspath(sys.argv[2]); #Input peaklist
dataset_folder = os.path.dirname(peaklist)

ChunkDur = float(sys.argv[3]); #Input chunk duration - could be automated in future and will need to be for multi
resonance SHARPER
ArtSep = (1.0/(ChunkDur / 1000.0)) #Calculates the expected separation of artefacts

nuslist_destination = os.path.join(dataset_folder, 'best_sampling.txt')

open(peaklist);
peakarray = np.genfromtxt(peaklist,names="Peak_No,Address,Hz,PPM,Intensity",skip_header=4)
peakarray_sort = np.sort(peakarray,order='Intensity')
x = len(peakarray)
y= np.ndim(peakarray)
```

```
IntensityArrPrep=peakarray_sort['Intensity']
IntensityArr = np.absolute(IntensityArrPrep)
LocationsArr=peakarray_sort['Hz']

PrimaryArtefactIntensity = IntensityArr[x-1]
PrimaryArtefactLocation = LocationsArr[x-1]

if x > 1: #Conditional that deals with cases of only identifying a single peak
	HzUpperPrep = LocationsArr-PrimaryArtefactLocation+ ArtSep
	HzUpper = np.absolute(HzUpperPrep)
	UpfieldPeakIndex = np.argmin(HzUpper)
	UpfieldCandidateIntensity = IntensityArr[UpfieldPeakIndex]
	UpfieldCandidateLocation = LocationsArr[UpfieldPeakIndex]

	HzLowerPrep = LocationsArr-PrimaryArtefactLocation- ArtSep
	HzLower = np.absolute(HzLowerPrep)
	DownfieldPeakIndex = np.argmin(HzLower)

	DownfieldCandidateIntensity = IntensityArr[DownfieldPeakIndex]
	DownfieldCandidateLocation = LocationsArr[DownfieldPeakIndex]

	if UpfieldCandidateIntensity > DownfieldCandidateIntensity:
			SecondaryArtefactIntensity = UpfieldCandidateIntensity
			SecondaryArtefactLocation = UpfieldCandidateLocation

	else:
		SecondaryArtefactIntensity = DownfieldCandidateIntensity
		SecondaryArtefactLocation = DownfieldCandidateLocation

	#The below determines if something has gone wrong in terms of peak picking (or the experimental
parameters are perfect!). If this seems probable it just repeats the offset
	if abs(PrimaryArtefactLocation +ArtSep - SecondaryArtefactLocation) > error:
		NewOffset =
(((PrimaryArtefactLocation*PrimaryArtefactIntensity)+(SecondaryArtefactLocation*SecondaryArtefactIntensity))/(
PrimaryArtefactIntensity+SecondaryArtefactIntensity))
	elif abs(PrimaryArtefactLocation -ArtSep - SecondaryArtefactLocation) > error:
		NewOffset =
(((PrimaryArtefactLocation*PrimaryArtefactIntensity)+(SecondaryArtefactLocation*SecondaryArtefactIntensity))/(
PrimaryArtefactIntensity+SecondaryArtefactIntensity))
	else:
		NewOffset = PrimaryArtefactLocation
else:
	NewOffset = PrimaryArtefactLocation

#Use two decimal places because that's the input topspin takes
np.savetxt(parameters_file, [NewOffset], fmt='%1.2f')
```

8.5.8 Mobile-MR-SHARPER Scripts

Bruker AU Macro

```
/*** ^^A -*-C++-*- *********************************************/
/*  mobileSHARPER                                              */
/*************************************************************/
/*  Short Description :                                        */
/*  Peak Tracking For SHARPER                                  */
/*************************************************************/
/*  Keywords :                                                 */
/*  zg, SHARPER                                                */
/*************************************************************/
/*  Description/Usage :                                        */
/*  Requires a suitable external Python environment (with numpy)*/
/*  Run a standard SHARPER experiment. Then call this macro.    */
/*  It will repeat the spectrum a user defined number of times  */
/*  but each time adjust the offset based on the previosly run  */
/*  spectrum in order to try and track a moving peak.           */
/*  ALL DATA ANALYSIS IS HANDLED BY THE COMPANION PYTHON SCRIPT */
/*************************************************************/
/*  Author(s) :                                                */
/*  Name    : Matthew Davy                                     */
/*  Organisation  : Bristol   University                       */
/*  Contact: md17346@bristol.ac.uk or mjdavy@btinternet.com     */
/*************************************************************/
/*************************************************************/
/*  To Do                                                      */
/*  Pass chunk duration off to python automatically - though this ties it to a specific pulse sequence */


//***Instructions***/
//Run a standard SHARPER experiment. Then initialise this macro. It will proceed to repeat the spectrum a user defined number of times each time using the previous SHARPER spectrum for offset adjustment to try and track a moving peak

//define your Python command here
//NB numpy and scipy must be installed with pip beforehand
//#define PYTHON_PATH "python" //even if on the path, not recognised by TopSpin
#define PYTHON_PATH "C:/Python27/python.exe" //for vanilla python 2.7
#define PYTHON_SCRIPT "C:/Python27/Scripts/mobileMRSHARPER.py"

//input/output files for the Python script (ACQUPATH)
#define PYTHON_PARAMETERS "parameters.txt"



AUERR = local_au(curdat);
QUIT
int local_au(const char* curdat)

{
  /* declare variables */
  //general variables
  char text[PATH_MAX], py_cmd[PATH_MAX] = PYTHON_PATH;
  char disk_save[PATH_MAX], user_save[PATH_MAX], name_save[PATH_MAX];
  char peaklist[PATH_MAX];
  char source_peaklist[PATH_MAX], destination_parameters_name[PATH_MAX] = PYTHON_PARAMETERS,
destination_parameters[PATH_MAX];
  int expno_save = expno, procno_save = procno, prep_digmod, PH_mod_status = -1, FT_mod_status = -1;

  //for preparation experiment
  int i, numPeaks, numFreq, parmode;
  float lb_status, prep_offset, prep_HZpPT, prep_PPMpPT, prep_aq, prep_swh, prep_swh1, ideal_offset,
Dwell_Time, Chunkpoints, ChunkNumber, Peak1, Peak2, Peak1_prep, Peak2_prep, SpectrometerFreq;
```

```
  float leftLimit, rightLimit, ppmFromLeft, multipletCentre, pointsfromLeft, peakArea, SpectrumDuration,
ppm_upper, ppm_lower, longest_timing, shortest_timing;
  double prep_grpdly, prep_sf, prep_sw_p, f1p, f2p, old_offset;
  int ExperimentNo, ExpNoMAX, Datapoint_Number;
  //quick check for existing of Python files - pointless if they don't exist!
  //https://stackoverflow.com/questions/230062/whats-the-best-way-to-check-if-a-file-exists-in-c
  if(access(PYTHON_PATH, F_OK) == -1)
    STOPMSG("Could not locate Python exe.")

  if(access(PYTHON_SCRIPT, R_OK) == -1)
    STOPMSG("Could not locate Python script.")

GETINT("Please enter the number of times you would like to repeat this spectrum",ExpNoMAX);
GETFLOAT("Please enter the desired duration of the SHARPER spectra (in seconds)",SpectrumDuration);
GETFLOAT("Please enter the position of 1st peak",Peak1_prep);
GETFLOAT("Please enter the position of 2nd peak",Peak2_prep);
GETFLOAT("Upper bound for spectral width - ppm",ppm_upper);
GETFLOAT("Lower bound for spectral width - ppm",ppm_lower);
GETFLOAT("Longest timing allowable - milliseconds",longest_timing);
GETFLOAT("Shortest timing allowable - milliseconds",shortest_timing);
STOREPAR("CNST3", Peak1_prep);
STOREPAR("CNST4", Peak2_prep);


for (ExperimentNo = 0; ExperimentNo < ExpNoMAX; ++ExperimentNo)
{

SETCURDATA
  //save parameters for current dataset
strcpy(disk_save, disk);
strcpy(user_save, user);
strcpy(name_save, name);

  //THIS bit does the peak picking!

  {
    /* setupp parameters for peak picking */
    /* define the plot region as big as the complete acquisition region */
    // necessary because the AU program "PP" actually behaves more like ppf does when used at the command-
line
    FETCHPARS("OFFSET", &prep_offset)
    FETCHPARS("SW_p" ,&prep_sw_p)
    FETCHPARS("SF", &prep_sf)
    f1p = prep_offset;
    f2p = f1p - prep_sw_p / prep_sf;
    STOREPAR("F1P", f1p)
    STOREPAR("F2P", f2p)

    //standard values
    STOREPAR("CY", 15.0) //defined intensity of largest peak
    STOREPAR("MAXI", 1000.0)
    STOREPAR("PC", 0.5) //S/N threshold for peak-picking (criterion never invoked if MI > 0)
    STOREPAR("PSIGN", 2) //Does the sign of the peak - may want 2, which should allow picking of both positive
and negative peaks
    STOREPAR("PSCAL", 4) //MI criterion is relative to non-solvent peaks, and will peak pick solvent peaks too

    //CRITICAL - threshold to ignore peaks i.e. peaks smaller than MI/CY are ignored
    STOREPAR("MI", 0.01)

    //pick peaks - CRITICAL
            FMC//Fourier transforms and magnitude instead of phase. APK often struggles to phase SHARPER
spectra well, leading to errors in peak picking
            //APK //Phase correction - not needed due to magnitude mode phasing
    PP
    PPP
    XWP_PP
```

```
            XCMD("sendgui convertpeaklist txt")//Create a peaklist with intensity and Hz frequency in ASCII for
easy handling by python - https://qa.nmrwiki.org/question/502/topspin-peak-list-file-format
  }



//***CopyExperiment and set it as current whilst preparing python commands***//
strcpy(source_peaklist, PROCPATH("peak.txt"));
FETCHPAR("DW", &Dwell_Time);
FETCHPAR("CNST1", &Chunkpoints);
FETCHPAR("CNST2", &ChunkNumber);
FETCHPAR("CNST3", &Peak1);
FETCHPAR("CNST4", &Peak2);

WRA(expno+1);
IEXPNO
DATASET(name_save, expno, 1, disk_save, user_save)
strcpy(destination_parameters, ACQUPATH(destination_parameters_name));



  //***prepare the command to send it off to python***//
    sprintf(py_cmd, "%s %s %s %s %f %f %f %f %f %f %f %f %f",
              PYTHON_PATH, PYTHON_SCRIPT, destination_parameters, source_peaklist, SpectrumDuration,
Dwell_Time, Chunkpoints, ChunkNumber, Peak1, Peak2, ppm_upper, ppm_lower, longest_timing,
shortest_timing);
  //requires external python enviroment due to hard requirment for numpy support
system(py_cmd);

 //printf(py_cmd); //Simple check it's giving the right commands to python
 printf("%f \n",Peak1);
 printf("%f \n",Peak2);

//***Obtain Python Generated Parameters and Update Spectrum With them***//
FILE *stream;
stream = fopen(destination_parameters, "r");
fscanf(stream,"%f %f %f %f %f %f %i",&ideal_offset, &ChunkNumber, &Chunkpoints, &Dwell_Time, &Peak1,
&Peak2, &Datapoint_Number);

fclose(destination_parameters);
STOREPAR("o1",ideal_offset);
STOREPAR("CNST2",ChunkNumber);
STOREPAR("CNST1",Chunkpoints);
STOREPAR("DW",Dwell_Time);
STOREPAR("CNST3", Peak1);
STOREPAR("CNST4", Peak2);
STOREPAR("TD", Datapoint_Number);

//***Runs spectrum***// Commented out for debugging
   // XAU("au_zg", "")
   GETCURDATA
   ZG

}
}
```

Python Script

```
#/*** ^^A -*-Python 2.7++-*- ***********************************/
#/*  mobileSHARPER companion python script                      */
#/*****************************************************************/
#/*  Short Description :                                        */
#/*  Data analysis to allow Peak Tracking For MR-SHARPER        */
#/*****************************************************************/
#/*  Keywords :                                                 */
#/*  zg, MRSHARPER                                              */
#/*****************************************************************/
#/*  Description/Usage :                                        */
#/*  Should be called automatically by the bruker AU script     */
#/*  thus needing no end user interaction                       */
#/*****************************************************************/
#/*  Author(s) :                                                */
#/*  Name    : Matthew Davy                                     */
#/*  Organisation  : Bristol   University                       */
#/*  Contact: md17346@bristol.ac.uk or mjdavy@btinternet.com    */
#/*****************************************************************/
#/*****************************************************************/
#/*  To Do                                                      */

#!/usr/bin/python

###Parameters the user may wish to change
AllowedMove = 100 #This is the Hz movement per scan peaks can make that the macro will effectivley track. Note that if ArtSep*2 is greater for any given scan that value will be used instead.
error = 2 #This is the Hz error it allows when searching for the secondary artefact. Higher values risk picking incorrect peaks
Spectrometer_Frequency = 500 #Put spectrometer frequency in MHz - can be approximate. The nucleus you're using matters, not what it's rated for proton!!!
import math
import numpy as np
import os
import itertools
import sys
import time
import warnings
warnings.filterwarnings("ignore", category=FutureWarning) #This ignores a depreciation warning that is currently irrelevant



#import scipy
from scipy import special

#dataset_folder = os.getcwd();

# arguments
   # sys.argv[0] = name of (this) script
   # sys.argv[1] = source of multiplet list (also destination folder for NUS schedule)

parameters_file_precleanup = os.path.abspath(sys.argv[1]);  #Eventual file to save parameters to after manipulations
#dataset_folder = os.path.dirname(parameters_file)
parameters_file = parameters_file_precleanup.replace("\\","/") #Cleanup because of bruker's backslash forward slash issue


peaklist_precleanup = os.path.abspath(sys.argv[2]); #Input peaklist
#dataset_folder = os.path.dirname(peaklist)
peaklist = peaklist_precleanup.replace("\\","/")


SpectrumDur = float(sys.argv[3]); #Desired length of SHARPER spectra
```

```
Dwell_Time = float(sys.argv[4]); #Input_Dwell_Time
Chunkpoints = float(sys.argv[5]); #Input_Chunkpoints
ChunkDur = Chunkpoints*Dwell_Time*0.000002 #Convert so seconds, find full chunk length
ArtSep = (1.0/(ChunkDur)) #Calculates the expected separation of artefacts
Peak1 = float(sys.argv[7]); #1st Peak approximate position based on previous spectrum
Peak2 = float(sys.argv[8]); #2nd Peak approximate position based on previous spectrum
ppm_upper = float(sys.argv[9]); #upper bound for ppm
ppm_lower = float(sys.argv[10]); #lower bound for ppm
longest_timing = float(sys.argv[11]); #longest_allowable_timing_milliseconds
shortest_timing = float(sys.argv[12]); #shortest_allowable_timing_milliseconds


####Determine allowance for peak movement
if ArtSep*2 > AllowedMove:
        PeakMove = AllowedMove
else:
        PeakMove = ArtSep*2

####Do the peak analysis here ####
open(peaklist)
peakarray = np.genfromtxt(peaklist,names="Peak_No,Address,Hz,PPM,Intensity",skip_header=4)
peakarray_sort = np.sort(peakarray,order='Intensity')
x = len(peakarray)
y= np.ndim(peakarray)

IntensityArrPrep=peakarray_sort['Intensity']
IntensityArr = np.absolute(IntensityArrPrep)
LocationsArr=peakarray_sort['Hz']

PrimaryArtefactIntensity = IntensityArr[x-1]
PrimaryArtefactLocation = LocationsArr[x-1]

####Find peak one location ####
PeakOneBoolean = ((Peak1-PeakMove<peakarray['Hz'])&(peakarray['Hz']<Peak1+PeakMove))

PeakOneIntensities = (peakarray['Intensity'])[PeakOneBoolean]
PeakOneLocations = (peakarray['Hz'])[PeakOneBoolean]

PeakOnePrimaryArtefactIntensity = np.amax(PeakOneIntensities)
PeakOnePrimaryArtefactIndex = np.argmax(PeakOneIntensities)
PeakOnePrimaryArtefactLocation = PeakOneLocations[PeakOnePrimaryArtefactIndex]

PeakOneHzUpperPrep = LocationsArr-PeakOnePrimaryArtefactLocation+ArtSep
PeakOneHzUpper = np.absolute(PeakOneHzUpperPrep)
PeakOneUpfieldPeakIndex = np.argmin(PeakOneHzUpper)
PeakOneUpfieldCandidateIntensity = IntensityArr[PeakOneUpfieldPeakIndex]
PeakOneUpfieldCandidateLocation = LocationsArr[PeakOneUpfieldPeakIndex]

PeakOneHzLowerPrep = LocationsArr-PeakOnePrimaryArtefactLocation-ArtSep
PeakOneHzLower = np.absolute(PeakOneHzLowerPrep)
PeakOneDownfieldPeakIndex = np.argmin(PeakOneHzLower)

PeakOneDownfieldCandidateIntensity = IntensityArr[PeakOneDownfieldPeakIndex]
PeakOneDownfieldCandidateLocation = LocationsArr[PeakOneDownfieldPeakIndex]

if PeakOneUpfieldCandidateIntensity > PeakOneDownfieldCandidateIntensity:
                PeakOneSecondaryArtefactIntensity = PeakOneUpfieldCandidateIntensity
                PeakOneSecondaryArtefactLocation = PeakOneUpfieldCandidateLocation
else:
        PeakOneSecondaryArtefactIntensity = PeakOneDownfieldCandidateIntensity
        PeakOneSecondaryArtefactLocation = PeakOneDownfieldCandidateLocation

#The below determines if something has gone wrong in terms of peak picking (or the experimental parameters
are perfect!). If this seems probable it just repeats the offset
if abs(PeakOnePrimaryArtefactLocation +ArtSep - PeakOneSecondaryArtefactLocation) > error:
```

```
                PeakOneCurrentLocation =
(((PeakOnePrimaryArtefactLocation*PeakOnePrimaryArtefactIntensity)+(PeakOneSecondaryArtefactLocation*Pe
akOneSecondaryArtefactIntensity))/(PeakOnePrimaryArtefactIntensity+PeakOneSecondaryArtefactIntensity))
elif abs(PeakOnePrimaryArtefactLocation -ArtSep - PeakOneSecondaryArtefactLocation) > error:
                PeakOneCurrentLocation =
(((PeakOnePrimaryArtefactLocation*PeakOnePrimaryArtefactIntensity)+(PeakOneSecondaryArtefactLocation*Pe
akOneSecondaryArtefactIntensity))/(PeakOnePrimaryArtefactIntensity+PeakOneSecondaryArtefactIntensity))
else:
        PeakOneCurrentLocation = Peak1

####Find peak Two location ####
PeakTwoBoolean = ((Peak2-ArtSep*2<peakarray['Hz'])&(peakarray['Hz']<Peak2+ArtSep*2))

PeakTwoIntensities = (peakarray['Intensity'])[PeakTwoBoolean]
PeakTwoLocations = (peakarray['Hz'])[PeakTwoBoolean]

PeakTwoPrimaryArtefactIntensity = np.amax(PeakTwoIntensities)
PeakTwoPrimaryArtefactIndex = np.argmax(PeakTwoIntensities)
PeakTwoPrimaryArtefactLocation = PeakTwoLocations[PeakTwoPrimaryArtefactIndex]

PeakTwoHzUpperPrep = LocationsArr-PeakTwoPrimaryArtefactLocation+ArtSep
PeakTwoHzUpper = np.absolute(PeakTwoHzUpperPrep)
PeakTwoUpfieldPeakIndex = np.argmin(PeakTwoHzUpper)
PeakTwoUpfieldCandidateIntensity = IntensityArr[PeakTwoUpfieldPeakIndex]
PeakTwoUpfieldCandidateLocation = LocationsArr[PeakTwoUpfieldPeakIndex]

PeakTwoHzLowerPrep = LocationsArr-PeakTwoPrimaryArtefactLocation-ArtSep
PeakTwoHzLower = np.absolute(PeakTwoHzLowerPrep)
PeakTwoDownfieldPeakIndex = np.argmin(PeakTwoHzLower)

PeakTwoDownfieldCandidateIntensity = IntensityArr[PeakTwoDownfieldPeakIndex]
PeakTwoDownfieldCandidateLocation = LocationsArr[PeakTwoDownfieldPeakIndex]

if PeakTwoUpfieldCandidateIntensity > PeakTwoDownfieldCandidateIntensity:
                PeakTwoSecondaryArtefactIntensity = PeakTwoUpfieldCandidateIntensity
                PeakTwoSecondaryArtefactLocation = PeakTwoUpfieldCandidateLocation
else:
        PeakTwoSecondaryArtefactIntensity = PeakTwoDownfieldCandidateIntensity
        PeakTwoSecondaryArtefactLocation = PeakTwoDownfieldCandidateLocation

#The below determines if something has gTwo wrong in terms of peak picking (or the experimental parameters
are perfect!). If this seems probable it just repeats the offset
if abs(PeakTwoPrimaryArtefactLocation +ArtSep - PeakTwoSecondaryArtefactLocation) > error:
                PeakTwoCurrentLocation =
(((PeakTwoPrimaryArtefactLocation*PeakTwoPrimaryArtefactIntensity)+(PeakTwoSecondaryArtefactLocation*Pe
akTwoSecondaryArtefactIntensity))/(PeakTwoPrimaryArtefactIntensity+PeakTwoSecondaryArtefactIntensity))
elif abs(PeakTwoPrimaryArtefactLocation -ArtSep - PeakTwoSecondaryArtefactLocation) > error:
                PeakTwoCurrentLocation =
(((PeakTwoPrimaryArtefactLocation*PeakTwoPrimaryArtefactIntensity)+(PeakTwoSecondaryArtefactLocation*Pe
akTwoSecondaryArtefactIntensity))/(PeakTwoPrimaryArtefactIntensity+PeakTwoSecondaryArtefactIntensity))
else:
        PeakTwoCurrentLocation = Peak2

NewOffset = (PeakOneCurrentLocation+PeakTwoCurrentLocation)/2



###Run Modified Multiple Peak SHARPER Script
#Frequency of NMR signal (Hz) and calculate wave period
f1 = abs(PeakOneCurrentLocation - PeakTwoCurrentLocation)/2
p1 = 1.0/f1

#Convert to Hz limits
hz_upper=(ppm_upper*Spectrometer_Frequency)
hz_lower=(ppm_lower*Spectrometer_Frequency)

#Calculate the lowest allowed dwell time
```

```
dwell_lower=(1e6*(0.5/hz_upper))
#Calculate the maximum allowed dwell time
dwell_upper=(1e6*(0.5/hz_lower))

#Fetch Array Files
target_path_1 = os.path.join(os.path.dirname(__file__), 'TimingArray')
t_ar = np.genfromtxt(target_path_1,delimiter=",")
target_path_2 = os.path.join(os.path.dirname(__file__), 'Dwellarray')
dwell_ar = np.genfromtxt(target_path_2,delimiter=",")
target_path_3 = os.path.join(os.path.dirname(__file__), 'ChunkPointarray')
cp_ar = np.genfromtxt(target_path_3,delimiter=",")

#Cut down arrays with boolean masks
b = ((dwell_upper>dwell_ar)&(dwell_ar>dwell_lower))
dwell_arb = dwell_ar[b]
cp_arb = cp_ar[b]
t_arb = t_ar[b]
c = (((shortest_timing/1000)<t_arb)&(t_arb<(longest_timing/1000)))
dwell_arbc = dwell_arb[c]
cp_arbc = cp_arb[c]
t_arbc = t_arb[c]

#runs a modulo operation on the timing array with boolean mask applied
mod_arf1 = np.mod(t_arbc, p1)

#turn into a spectral quality array
mod_sqp1 = np.divide(mod_arf1, p1/100)

#Modify arrays to allow incomplete rotations
sub50ind = [(50.00<mod_sqp1)*(mod_sqp1<75.00)]
mod_sqp1[sub50ind] -= 50.0
subfrom50ind = [(25.00<mod_sqp1)*(mod_sqp1<50.00)]
mod_sqp1[subfrom50ind] -= 50.0
subfrom100ind = [(75.00<mod_sqp1)*(mod_sqp1<100.00)]
mod_sqp1[subfrom100ind] -= 100.0
mod_sqp1 = np.absolute(mod_sqp1)

#Find minimum element in modulo array
minElement = np.amin(mod_sqp1)
index = np.where(mod_sqp1 == np.amin(mod_sqp1))

#Fetch the corresponding Chunkpoints and Dwell Time
finaltar = t_arbc[index]
finaldwellar = dwell_arbc[index]
finalcpar = cp_arbc[index]

minTiming = np.amin(finaltar)
finalindex = np.where(finaltar == np.amin(finaltar))

lastdwellcheck = finaldwellar[finalindex]
lastcpcheck = finalcpar[finalindex]

#The below lines are needed because multiple dwell time/cp combinations can have identical timing - this just
picks one arbitrarilly!
newdwell = lastdwellcheck[0]
newcp = lastcpcheck[0]

#Calculate number of chunks in spectrum and how many datapoints it should have
ChunkNoPreRound = (SpectrumDur*1000000)/(newdwell*newcp)
ChunkNo = round(ChunkNoPreRound)
Datapoints = ChunkNo*newcp-ChunkNo/2

sq1 = mod_sqp1[index]

#Spectral Quality Prediction - Percentage of final rotation completed
#If this number is not close to 0 or 100 the spectra can be expected to be of poor quality (S/A ratio)
Spectral_Quality_f1 = (sq1)
```

```
#Write a text file with the needed parameters
#Lets bruker do the rounding this time! - May be a mistake
np.savetxt(parameters_file, ([NewOffset], [ChunkNo], [newcp], [newdwell], [PeakOneCurrentLocation],
[PeakTwoCurrentLocation], [Datapoints] ), fmt='%1.2f')
```

8.5.9 Dwell Times available on a Varian, with OpenVNMRJ 4.2 in µs

17.6	49.6
18.4	50.4
19.2	51.2
20	52
20.8	52.8
21.6	53.6
22.4	54.4
23.2	55.2
24	56
24.8	56.8
25.6	57.6
26.4	58.4
27.2	59.2
28	60
28.8	60.8
29.6	61.6
30.4	62.4
31.2	63.2
32	64
32.8	64.8
33.6	65.6
34.4	66.4
35.2	67.2
36	68
36.8	68.8
37.6	69.6
38.4	70.4
39.2	71.2
40	72
40.8	72.8
41.6	73.6
42.4	74.4
43.2	75.2
44	76
44.8	76.8
45.6	77.6
46.4	78.4
47.2	79.2
48	80
48.8	

8.5.10 Dwell Times on a Bruker with Topspin 3.6.1 and an AVIII HD in µs

0.05	5	10.4	16.2	22.5	28.4	33.6	39.1	44.4	49.8
0.1	5.067	10.5	16.4	22.533	28.5	33.8	39.2	44.5	49.867
0.15	5.1	10.667	16.5	22.667	28.6	34	39.333	44.667	50
0.2	5.2	10.8	16.533	22.8	28.667	34.1	39.467	44.8	50.133
0.25	5.333	11	16.667	23	28.7	34.133	39.5	45	50.267
0.3	5.4	11.2	16.8	23.1	28.8	34.2	39.6	45.067	50.4
0.35	5.5	11.333	16.9	23.2	28.9	34.3	39.867	45.1	50.5
0.4	5.6	11.4	17	23.333	28.933	34.4	40	45.2	50.6
0.5	5.7	11.6	17.067	23.4	29	34.5	40.133	45.333	50.7
0.533	5.867	11.7	17.1	23.5	29.2	34.533	40.2	45.6	50.8
0.6	6	11.733	17.2	23.6	29.4	34.667	40.3	45.733	51
0.7	6.133	11.9	17.333	23.8	29.467	34.8	40.4	45.867	51.1
0.8	6.3	12	17.733	24	29.5	35	40.5	45.9	51.2
1	6.4	12.1	18	24.2	29.6	35.1	40.533	46	51.3
1.067	6.5	12.133	18.2	24.3	29.7	35.2	40.6	46.2	51.333
1.2	6.533	12.267	18.4	24.4	29.9	35.4	40.667	46.4	51.5
1.33	6.6	12.4	18.5	24.5	30	35.467	40.7	46.5	51.6
1.4	6.667	12.5	18.6	24.6	30.1	35.5	40.8	46.667	51.7
1.5	6.8	12.6	18.7	24.7	30.4	35.6	41	46.8	51.8
1.6	6.9	12.667	18.8	24.8	30.5	35.7	41.133	46.9	52
1.8	7	12.8	18.9	25	30.6	35.733	41.333	46.933	52.2
1.867	7	13	19	25.067	30.667	36	41.4	47	52.267
2	7.2	13.067	19.067	25.2	30.8	36.1	41.5	47.2	52.4
2.1	7.333	13.2	19.2	25.3	30.933	36.267	41.6	47.3	52.5
2.133	7.467	13.3	19.33	25.333	31	36.3	41.8	47.333	52.7
2.2	7.5	13.333	19.5	25.5	31.2	36.4	42	47.4	52.8
2.4	7.6	13.5	19.6	25.6	31.333	36.5	42.3	47.467	52.9
2.5	7.7	13.6	19.733	25.8	31.467	36.6	42.4	47.5	53
2.6	7.8	13.8	19.8	25.9	31.5	36.667	42.5	47.6	53.1
2.667	8	13.867	20	26	31.6	36.8	42.533	47.7	53.2
2.7	8.1	14	20.267	26.1	31.733	36.9	42.6	48	53.3
2.8	8.4	14.3	20.3	26.133	31.8	36.9	42.667	48.1	53.4
2.933	8.5	14.4	20.4	26.4	31.9	37	42.7	48.133	53.5
3	8.533	14.5	20.5	26.5	32	37.1	42.8	48.3	53.6
3.2	8.667	14.667	20.533	26.6	32.2	37.2	42.9	48.4	53.733
3.3	8.8	14.7	20.667	26.667	32.267	37.4	42.933	48.5	53.9
3.4	9	14.8	20.7	26.8	32.3	37.5	43	48.533	54
3.5	9.067	14.933	20.8	27	32.4	37.6	43.067	48.6	54.133
3.6	9.1	15	20.9	27.067	32.5	37.8	43.2	48.667	54.267
3.8	9.2	15.2	21	27.2	32.533	37.867	43.333	48.8	54.4
3.9	9.333	15.3	21.2	27.3	32.667	38	43.4	49	54.5
4	9.5	15.333	21.333	27.333	32.8	38.133	43.5	49.067	54.6
4.2	9.6	15.4	21.5	27.5	32.9	38.267	43.6	49.2	54.667
4.267	9.7	15.467	21.6	27.6	32.933	38.4	43.7	49.3	54.8
4.4	9.8	15.5	21.7	27.733	33	38.5	43.8	49.333	54.9
4.5	9.9	15.6	21.867	27.867	33.067	38.533	43.867	49.4	55
4.6	10	15.867	22	27.9	33.2	38.7	44	49.467	55.1
4.667	10.133	16	22.1	28	33.3	38.8	44.1	49.5	55.2
4.8	10.2	16.1	22.2	28.2	33.333	38.933	44.2	49.6	55.3

60.9	66.3	71.1	76.5
61	66.4	71.2	76.533
61.1	66.5	71.3	76.7
61.2	66.6	71.333	76.8
61.333	66.667	71.4	77
61.5	66.7	71.467	77.067
61.6	66.8	71.5	77.2
61.8	67	71.6	77.4
61.867	67.1	71.867	77.5
62	67.2	72	77.6
62.1	67.333	72.2	77.7
62.3	67.467	72.4	77.733
62.4	67.5	72.5	77.867
62.5	67.6	72.533	77.9
62.533	67.733	72.6	78
62.667	67.8	72.667	78.1
62.7	67.9	72.8	78.2
62.8	68	72.9	78.3
62.9	68.133	73	78.4
63	68.2	73.067	78.5
63.067	68.267	73.1	78.6
63.2	68.4	73.2	78.667
63.333	68.5	73.333	78.8
63.5	68.6	73.467	78.933
63.6	68.667	73.5	79
63.7	68.8	73.6	79.1
63.8	68.9	73.7	79.2
63.9	68.933	73.733	79.3
64	69	73.8	79.333
64.133	69.067	74	79.467
64.2	69.2	74.1	79.5
64.4	69.3	74.133	79.6
64.5	69.333	74.2	79.733
64.6	69.5	74.4	79.8
64.667	69.6	74.5	79.9
64.8	69.7	74.533	80
64.9	69.867	74.7	
65	70	74.8	
65.067	70.2	74.9	
65.1	70.267	75	
65.2	70.3	75.2	
65.4	70.4	75.4	
65.5	70.5	75.5	
65.6	70.533	75.6	
65.7	70.667	75.733	
65.733	70.7	75.9	
65.8	70.8	76	
65.867	70.933	76.2	
66	71	76.3	
66.133	71.067	76.4	

9 References

[1] *Resonance absorption by nuclear magnetic moments in a solid.* Purcell, E.M., Torrey, H.C. and Pound, R.V. *Physical Review*, 1945, 69, 37.

[2] Press Release for 1991 Prize in Chemistry, https://www.nobelprize.org/nobel_prizes/chemistry/laureates/1991/press.html, (accessed 09/02/2021)

[3] Bharti, S.K. and Roy, R., 2012. Quantitative 1H NMR spectroscopy. *TrAC Trends in Analytical Chemistry*, *35*, pp.5-26.

[4] Moskau, D., 2002. Application of real time digital filters in NMR spectroscopy. *Concepts in Magnetic Resonance: An Educational Journal*, *15*(2), pp.164-176.

[5] Liu, Y., Green, M.D., Marques, R., Pereira, T., Helmy, R., Williamson, R.T., Bermel, W. and Martin, G.E., 2014. Using pure shift HSQC to characterize microgram samples of drug metabolites. *Tetrahedron Letters*, *55*(40), pp.5450-5453.

[6] Hore, P.J., 2015. *Nuclear magnetic resonance*. Oxford University Press, USA.

[7] Aue, W.P., Bartholdi, E. and Ernst, R.R., 1976. Two-dimensional spectroscopy. Application to nuclear magnetic resonance. *The Journal of Chemical Physics*, *64*(5), pp.2229-2246.

[8] Nagayama, K., Kumar, A., Wüthrich, K. and Ernst, R.R., 1980. Experimental techniques of two-dimensional correlated spectroscopy. *Journal of Magnetic Resonance (1969)*, *40*(2), pp.321-334.

[9] Dickson, C.L., Blundell, C.D., Butts, C.P., Felton, A., Jeffreys, A. and Takacs, Z., 2017. Accurate measurement of long range proton–carbon scalar coupling constants. *Analyst*, *142*(4), pp.621-633.

[10] Hu, H. and Krishnamurthy, K., 2006. Revisiting the initial rate approximation in kinetic NOE measurements. *Journal of Magnetic Resonance*, *182*(1), pp.173-177.

[11] Bax, A., Freeman, R. and Frenkiel, T.A., 1981. An NMR technique for tracing out the carbon skeleton of an organic molecule. *Journal of the American Chemical Society*, *103*(8), pp.2102-2104.

[12] Kupče, Ē. and Claridge, T.D., 2017. NOAH: NMR supersequences for small molecule analysis and structure elucidation. *Angewandte Chemie International Edition*, *56*(39), pp.11779-11783.

[13] Kupče, Ē. and Claridge, T.D., 2018. Molecular structure from a single NMR supersequence. *Chemical Communications*, *54*(52), pp.7139-7142.

[14] Butts, C.P., Jones, C.R. and Harvey, J.N., 2011. High precision NOEs as a probe for low level conformers—a second conformation of strychnine. *Chemical Communications*, *47*(4), pp.1193-1195.

[15] Wu, J., Lorenzo, P., Zhong, S., Ali, M., Butts, C.P., Myers, E.L. and Aggarwal, V.K., 2017. Synergy of synthesis, computation and NMR reveals correct baulamycin structures. *Nature*, *547*(7664), pp.436-440.

[16] Lorenzo, P., Butts, C.P., Myers, E.L. and Aggarwal, V.K., 2017. The Story behind "Synergy of Synthesis, Computation, and NMR Reveals Correct Baulamycin Structures".

[17] Wei, R., Hall, A.M., Behrens, R., Pritchard, M.S., King, E.J. and Lloyd-Jones, G.C., 2021. Stopped-Flow 19F NMR Spectroscopic Analysis of a Protodeboronation Proceeding at the Sub-Second Time-Scale. *European Journal of Organic Chemistry*, *2021*(17), pp.2331-2342.

[18] Huo, R., Wehrens, R., Van Duynhoven, J. and Buydens, L.M.C., 2003. Assessment of techniques for DOSY NMR data processing. *Analytica chimica acta*, *490*(1-2), pp.231-251.

[19] Hu, H., Bradley, S.A. and Krishnamurthy, K., 2004. Extending the limits of the selective 1D NOESY experiment with an improved selective TOCSY edited preparation function. *Journal of Magnetic Resonance*, *171*(2), pp.201-206.

[20] Duncan, S.J., Lewis, R., Bernstein, M.A. and Sandor, P., 2007. Selective excitation of overlapping multiplets; the application of doubly selective and chemical shift filter experiments to complex NMR spectra. *Magnetic Resonance in Chemistry*, *45*(4), pp.283-288.

[21] Ernst, R.R. and Primas, H., 1963. Nuclear magnetic resonance with stochastic high-frequency fields. *Helvetica Physica Acta (Switzerland)*, *36*.

[22] Waugh, J.S., 1982. Theory of broadband spin decoupling. *Journal of Magnetic Resonance (1969)*, *50*(1), pp.30-49.

[23] Suter, D., Schenker, K.V. and Pines, A., 1987. Theory of broadband heteronuclear decoupling in multispin systems. *Journal of Magnetic Resonance (1969)*, *73*(1), pp.90-98.

[24] Freeman, R., Kempsell, S.P. and Levitt, M.H., 1979. Broadband decoupling and scaling of heteronuclear spin-spin interactions in high-resolution NMR. *Journal of Magnetic Resonance (1969)*, *35*(3), pp.447-450.

[25] Shaka, A.J. and Keeler, J., 1987. Broadband spin decoupling in isotropic-liquids. *Progress in nuclear magnetic resonance spectroscopy*, *19*(1), pp.47-129.

[26] Levitt, M.H., Freeman, R. and Frenkiel, T., 1982. Supercycles for broadband heteronuclear decoupling. *Journal of Magnetic Resonance (1969)*, *50*(1), pp.157-160.

[27] Jesson, J.P., Meakin, P. and Kneissel, G., 1973. Homonuclear decoupling and peak elimination in Fourier transform nuclear magnetic resonance. *Journal of the American Chemical Society*, *95*(2), pp.618-620.

[28] Rachineni, K., Kakita, V.M.R., Dayaka, S., Vemulapalli, S.P.B. and Bharatam, J., 2015. Precise determination of enantiomeric excess by a sensitivity enhanced two-dimensional band-selective pure-shift NMR. *Analytical chemistry*, *87*(14), pp.7258-7266.

[29] Aue, W.P., Karhan, J. and Ernst, R.R., 1976. Homonuclear broad band decoupling and two-dimensional J-resolved NMR spectroscopy. *The Journal of Chemical Physics*, *64*(10), pp.4226-4227.

[30] Pell, A.J., Edden, R.A. and Keeler, J., 2007. Broadband proton-decoupled proton spectra. *Magnetic Resonance in Chemistry*, *45*(4), pp.296-316.

[31] Bax, A., Mehlkopf, A.F. and Smidt, J., 1979. Homonuclear broadband-decoupled absorption spectra, with linewidths which are independent of the transverse relaxation rate. *Journal of Magnetic Resonance (1969)*, *35*(1), pp.167-169.

[32] Castañar, L., Nolis, P., Virgili, A. and Parella, T., 2013. Full sensitivity and enhanced resolution in homodecoupled band-selective NMR experiments. *Chem. Eur. J*, *19*(51), pp.17283-17286.

[33] Castañar, L., 2017. Pure shift 1H NMR: what is next? *Magnetic Resonance in Chemistry*, *55*(1), pp.47-53.

[34] Kiraly, P., Adams, R.W., Paudel, L., Foroozandeh, M., Aguilar, J.A., Timári, I., Cliff, M.J., Nilsson, M., Sándor, P., Batta, G. and Waltho, J.P., 2015. Real-time pure shift 15 N HSQC of proteins: a real improvement in resolution and sensitivity. *Journal of biomolecular NMR*, *62*(1), pp.43-52.

[35] Garbow, J.R., Weitekamp, D.P. and Pines, A., 1982. Bilinear rotation decoupling of homonuclear scalar interactions. *Chemical Physics Letters*, *93*(5), pp.504-509.

[36] Jones, A.B., Lloyd-Jones, G.C. and Uhrín, D., 2017. SHARPER Reaction Monitoring: Generation of a Narrow Linewidth NMR Singlet, without X-Pulses, in an Inhomogeneous Magnetic Field. *Analytical chemistry*, *89*(18), pp.10013-10021.

[37] Aue, W.P., Karhan, J. and Ernst, R.R., 1976. Homonuclear broad band decoupling and two-dimensional J-resolved NMR spectroscopy. *The Journal of Chemical Physics*, *64*(10), pp.4226-4227.

[38] Kiraly, P., Foroozandeh, M., Nilsson, M. and Morris, G.A., 2017. Anatomising proton NMR spectra with pure shift 2D J-spectroscopy: A cautionary tale. *Chemical Physics Letters*, *683*, pp.398-403.

[39] Keeler, J., 2004, "Understanding NMR Spectroscopy, Chapter 7." http://www-keeler.ch.cam.ac.uk/lectures/understanding/chapter_7.pdf Accessed 12/03/2021.

[40] Pell, A.J. and Keeler, J., 2007. Two-dimensional J-spectra with absorption-mode lineshapes. *Journal of Magnetic Resonance*, *189*(2), pp.293-299.

[41] Bax, A., Freeman, R. and Morris, G.A., 1981. A simple method for suppressing dispersion-mode contributions in NMR spectra: The "pseudo echo". *Journal of Magnetic Resonance (1969)*, *43*(2), pp.333-338.

[42] Zangger, K., 2015. Pure shift NMR. *Progress in nuclear magnetic resonance spectroscopy*, *86*, pp.1-20.

[43] Adams, R.W, 2014 Pure Shift NMR Spectroscopy. *eMagRes, 3(4)*.

[44] Kaltschnee, L., Knoll, K., Schmidts, V., Adams, R.W., Nilsson, M., Morris, G.A. and Thiele, C.M., 2016. Extraction of distance restraints from pure shift NOE experiments. *Journal of Magnetic Resonance*, *271*, pp.99-109.

[45] Foroozandeh, M., Adams, R.W., Nilsson, M. and Morris, G.A., 2014. Ultrahigh-resolution total correlation NMR spectroscopy. *Journal of the American Chemical Society*, *136*(34), pp.11867-11869.

[46] Nilsson, M. and Morris, G.A., 2007. Pure shift proton DOSY: diffusion-ordered 1 H spectra without multiplet structure. *Chemical communications*, (9), pp.933-935.

[47] Aguilar, J.A., Morris, G.A. and Kenwright, A.M., 2014. "Pure shift" 1 H NMR, a robust method for revealing heteronuclear couplings in complex spectra. *RSC Advances*, *4*(16), pp.8278-8282.

[48] Kaltschnee, L., Kolmer, A., Timári, I., Schmidts, V., Adams, R.W., Nilsson, M., Kövér, K.E., Morris, G.A. and Thiele, C.M., 2014. "Perfecting" pure shift HSQC: full homodecoupling for accurate and precise determination of heteronuclear couplings. *Chemical Communications*, *50*(99), pp.15702-15705.

[49] Zangger, K. and Sterk, H., 1997. Homonuclear broadband-decoupled NMR spectra. *Journal of Magnetic Resonance*, *124*(2), pp.486-489.

[50] Castañar, L., Nolis, P., Virgili, A. and Parella, T., 2013. Simultaneous multi-slice excitation in spatially encoded NMR experiments. *Chem Eur J*, *19*, pp.15472-15475.

[51] Mauhart, J., Glanzer, S., Sakhaii, P., Bermel, W. and Zangger, K., 2015. Faster and cleaner real-time pure shift NMR experiments. *Journal of Magnetic Resonance*, *259*, pp.207-215.

[52] Foroozandeh, M., Adams, R.W., Meharry, N.J., Jeannerat, D., Nilsson, M. and Morris, G.A., 2014. Ultrahigh-resolution NMR spectroscopy. *Angewandte Chemie International Edition*, *53*(27), pp.6990-6992.

[53] Supporting information, Figure S6 *Ultrahigh-Resolution NMR Spectroscopy. Foroozandeh, M., Adams, R.W., Meharry, N.J., Jeannerat, D., Nilsson, M. and Morris, G.A. Angewandte Chemie International Edition,* 2014, 53, 6990-6992.

[54] Anderson, W.A. and Freeman, R., 1962. Influence of a second radiofrequency field on high-resolution nuclear magnetic resonance spectra. *The Journal of Chemical Physics*, *37*(1), pp.85-103.

[55] Levitt, M.H., Freeman, R. and Frenkiel, T., 1982. Supercycles for broadband heteronuclear decoupling. *Journal of Magnetic Resonance (1969)*, *50*(1), pp.157-160.

[56] Basus, V.J., Ellis, P.D., Hill, H.D. and Waugh, J.S., 1979. Utilization of chirp frequency modulation with 180°-phase modulation for heteronuclear spin decoupling. *Journal of Magnetic Resonance (1969)*, *35*(1), pp.19-37.

[57] Kupce, Ē., Freeman, R., Wider, G. and Wüthrich, K., 1996. Suppression of cycling sidebands using bi-level adiabatic decoupling. *Journal of Magnetic Resonance, Series A*, *122*(1), pp.81-84.

[58] Kupče, Ē., 2020. Perspectives of adiabatic decoupling in liquids. *Journal of Magnetic Resonance*, *318*, p.106799.

[59] Lupulescu, A., Olsen, G.L. and Frydman, L., 2012. Toward single-shot pure-shift solution 1H NMR by trains of BIRD-based homonuclear decoupling. *Journal of Magnetic Resonance*, *218*, pp.141-146.

[60] Kaltschnee, L., Kolmer, A., Timári, I., Schmidts, V., Adams, R.W., Nilsson, M., Kövér, K.E., Morris, G.A. and Thiele, C.M., 2014. "Perfecting" pure shift HSQC: full homodecoupling for accurate and precise determination of heteronuclear couplings. *Chemical Communications*, *50*(99), pp.15702-15705.

[61] Lopez, J.M., Cabrera, R. and Maruenda, H., 2019. Ultra-Clean Pure Shift 1 H-NMR applied to metabolomics profiling. *Scientific reports*, *9*(1), pp.1-8.

[62] Ndukwe, I.E., Shchukina, A., Zorin, V., Cobas, C., Kazimierczuk, K. and Butts, C.P., 2017. Enabling Fast Pseudo-2D NMR Spectral Acquisition for Broadband Homonuclear Decoupling: The EXACT NMR Approach. *ChemPhysChem*, *18*(15), pp.2081-2087.

[63] Shchukina, A., Kaźmierczak, M., Kasprzak, P., Davy, M., Akien, G.R., Butts, C.P. and Kazimierczuk, K., 2019. Accelerated acquisition in pure-shift spectra based on prior knowledge from 1 H NMR. *Chemical Communications*, *55*(64), pp.9563-9566.

[64]Dickson, C. 2016. Second Year Progress Report "Improving NMR Methods to Solve 3D Molecular Structure In Solution", pp 63.

[65] Bax, A., Mehlkopf, A.F. and Smidt, J., 1979. Absorption spectra from phase-modulated spin echoes. *Journal of Magnetic Resonance (1969)*, *35*(3), pp.373-377.

[66] Allerhand, A. and Cochran, D.W., 1970. Carbon-13 Fourier-transform nuclear magnetic resonance. I. Comparison of a simple spin-echo procedure with other methods. *Journal of the American Chemical Society*, *92*(14), pp.4482-4484.

[67] Bocan, J., Pileio, G. and Levitt, M.H., 2012. Sensitivity enhancement and low-field spin relaxation in singlet NMR. *Physical Chemistry Chemical Physics*, *14*(46), pp.16032-16040.

[68] Hu, J.Z. and Wind, R.A., 2003. Sensitivity-enhanced phase-corrected ultra-slow magic angle turning using multiple-echo data acquisition. *Journal of Magnetic Resonance*, *163*(1), pp.149-162.

[69] Agilent VnmrJ 4.2 Spectroscopy User Guide, Revision A, 2014, Aglient, pp140.

[70] Claridge, T.D., 2016. *High-resolution NMR techniques in organic chemistry, 2nd Edition* (Vol. 27), Elsevier.

[71] Reinsperger, T. and Luy, B., 2014. Homonuclear BIRD-decoupled spectra for measuring one-bond couplings with highest resolution: CLIP/CLAP-RESET and constant-time-CLIP/CLAP-RESET. *Journal of Magnetic Resonance*, *239*, pp.110-120.

[72] Koos, M.R., Kummerlöwe, G., Kaltschnee, L., Thiele, C.M. and Luy, B., 2016. CLIP-COSY: A clean in-phase experiment for the rapid acquisition of COSY-type correlations. *Angewandte Chemie International Edition*, *55*(27), pp.7655-7659.

[73] Timári, I., Kaltschnee, L., Kolmer, A., Adams, R.W., Nilsson, M., Thiele, C.M., Morris, G.A. and Kövér, K.E., 2014. Accurate determination of one-bond heteronuclear coupling constants with "pure shift" broadband proton-decoupled CLIP/CLAP-HSQC experiments. *Journal of Magnetic Resonance*, *239*, pp.130-138.

[74] Kiraly, P., Private Email Communication, January 2018.

[75] Glanzer, S. and Zangger, K., 2015. Visualizing unresolved scalar couplings by real-time J-upscaled NMR. *Journal of the American Chemical Society*, *137*(15), pp.5163-5169.

[76] Glanzer, S. and Zangger, K., 2015. Uniform Reduction of Scalar Coupling by Real-Time Homonuclear J-Downscaled NMR. *ChemPhysChem*, *16*(15), pp.3313-3317.

[77] Hall, A.M., Chouler, J.C., Codina, A., Gierth, P.T., Lowe, J.P. and Hintermair, U., 2016. Practical aspects of real-time reaction monitoring using multi-nuclear high resolution FlowNMR spectroscopy. *Catalysis Science & Technology*, *6*(24), pp.8406-8417.

[78] Levitt, M.H., 2013. *Spin dynamics: basics of nuclear magnetic resonance*, John Wiley & Sons.

[79] Kind, J. and Thiele, C.M., 2015. Still shimming or already measuring?–Quantitative reaction monitoring for small molecules on the sub minute timescale by NMR. *Journal of Magnetic Resonance*, *260*, pp.109-115.

[80] Gomez, M.V. and de la Hoz, A., 2017. NMR reaction monitoring in flow synthesis. *Beilstein journal of organic chemistry*, *13*(1), pp.285-300.

[81] Howe, P.W., 2020. Recent developments in the use of fluorine NMR in synthesis and characterisation. *Progress in Nuclear Magnetic Resonance Spectroscopy*, *118*, pp.1-9.

[82] Edwards, J.C., 2016. The emergence of benchtop NMR systems and the exciting future of the technology. *Magnetic Resonance in Chemistry*, *54*(6), pp.492-493.

[83] Grootveld, M., Percival, B., Gibson, M., Osman, Y., Edgar, M., Molinari, M., Mather, M.L., Casanova, F. and Wilson, P.B., 2019. Progress in low-field benchtop NMR spectroscopy in chemical and biochemical analysis. *Analytica chimica acta*, *1067*, pp.11-30.

[84] Richardson, P.M., Parrott, A.J., Semenova, O., Nordon, A., Duckett, S.B. and Halse, M.E., 2018. SABRE hyperpolarization enables high-sensitivity 1 H and 13 C benchtop NMR spectroscopy. *Analyst*, *143*(14), pp.3442-3450.

[85] Semenova, O., Richardson, P.M., Parrott, A.J., Nordon, A., Halse, M.E. and Duckett, S.B., 2019. Reaction monitoring using SABRE-hyperpolarized benchtop (1 T) NMR spectroscopy. *Analytical chemistry*, *91*(10), pp.6695-6701.

[86] Matviychuk, Y., Steimers, E., von Harbou, E. and Holland, D.J., 2020. Bayesian approach for automated quantitative analysis of benchtop NMR data. *Journal of Magnetic Resonance*, *319*, p.106814.

[87] Jeol Royal HFX Probe Overview https://jeolusa.s3.amazonaws.com/resources_ai/JEOL%20ROYAL%20HFX%20NMR%20Probe%20Overview.pdf?AWSAccessKeyId=AKIAQJOI4KIAZPDULHNL&Expires=2145934800&Signature=Djv5dWpuuiAPBRqnM02rb4%2FUxYI%3D – Accessed 11/02/2021.

[88] Zientek, N., Laurain, C., Meyer, K., Kraume, M., Guthausen, G. and Maiwald, M., 2014. Simultaneous $^{19}F - {}^{1}H$ medium resolution NMR spectroscopy for online reaction monitoring. *Journal of Magnetic Resonance*, *249*, pp.53-62.

[89] Claridge, T.D., 2016. *High-resolution NMR techniques in organic chemistry, 1st Edition* (Vol. 27), Elsevier.

[90] Hoye, T.R., Eklov, B.M., Ryba, T.D., Voloshin, M. and Yao, L.J., 2004. No-D NMR (no-deuterium proton NMR) spectroscopy: A simple yet powerful method for analyzing reaction and reagent solutions. *Organic letters*, *6*(6), pp.953-956.

[91] Feldmeier, C., Bartling, H., Riedle, E. and Gschwind, R.M., 2013. LED based NMR illumination device for mechanistic studies on photochemical reactions–Versatile and simple, yet surprisingly powerful. *Journal of Magnetic Resonance*, *232*, pp.39-44.

[92] Gomez, M.V., Juan, A., Jiménez-Márquez, F., De La Hoz, A. and Velders, A.H., 2018. Illumination of Nanoliter-NMR Spectroscopy Chips for Real-Time Photochemical Reaction Monitoring. *Analytical chemistry*, *90*(3), pp.1542-1546.

[93] Bliumkin, L., Dutta Majumdar, R., Soong, R., Adamo, A., Abbatt, J.P., Zhao, R., Reiner, E. and Simpson, A.J., 2016. Development of an in situ NMR photoreactor to study environmental photochemistry. *Environmental science & technology*, *50*(11), pp.5506-5516.

[94] Huang, Y., Cao, S., Yang, Y., Cai, S., Zhan, H., Tan, C., Lin, L., Zhang, Z. and Chen, Z., 2017. Ultrahigh-resolution NMR spectroscopy for rapid chemical and biological applications in inhomogeneous magnetic fields. *Analytical Chemistry*, *89*(13), pp.7115-7122.

[95] Topgaard, D., Martin, R.W., Sakellariou, D., Meriles, C.A. and Pines, A., 2004. “Shim pulses” for NMR spectroscopy and imaging. *Proceedings of the National Academy of Sciences*, *101*(51), pp.17576-17581.

[96] Supporting Information, Jones, A.B., Lloyd-Jones, G.C. and Uhrín, D., 2017. SHARPER Reaction Monitoring: Generation of a Narrow Linewidth NMR Singlet, without X-Pulses, in an Inhomogeneous Magnetic Field. *Analytical chemistry*, *89*(18), pp.10013-10021.

[97] NMR Software Department, 2016, Introduction to Bruker NMR Pulse Programming User Manual Version 2, Bruker Corporation.

[98] Agilent Technologies, 2013, VnmrJ 4 User Programming Reference Guide Revision A, Agilent.

[99] Dickson, C., Private Email Communication, October 2020.

[100] G. Larry Bretthorst 2018, Bayesian Data-Analysis ToolboxRelease 4.23, Manual Version 3, page 163-166.

[101] Krishnamurthy, K., PS1D, VNMRJ-4.2A, 2012.

[102] Python Software Foundation. Python Language Reference, version 2.7. Available at http://www.python.org